Universität Konstanz

Roles of the GPI-anchored proteins Thy-1 and PrP and the myelin- and ER-associated protein RTN4b in axon growth and regeneration

Dissertation

zur Erlangung des akademischen Grades

des Doktors der Naturwissenschaften (Dr. rer. nat.)

an der Universität Konstanz Mathematisch-Naturwissenschaftliche

Sektion Fachbereich Biologie

vorgelegt von

Sarah Engel

Tag der mündlichen Prüfung: 09.06.2021

Referent/in: Prof. Dr. Elisa May

Referent/in: Prof. Dr. Catherine G. Becker

Referent/in: Prof. Dr. Marcel Leist

Konstanz, 2021

Abstract

The ability of fish to regenerate injured central nervous system (CNS) axons fascinates neuroscientists for a long time, particularly because mammals seem to have lost this potential. Efforts to understand the basis of this evolutionary difference focus on two key aspects of axon regeneration: 1) neuron-intrinsic properties required to initiate the growth machinery upon lesion, and 2) extrinsic factors that render the cellular environment growth-permissive or inhibitory. In mammals a glial scar forms and inhibitory molecules are expressed at the injury site, creating a physical and biochemical barrier for axon regrowth. In contrast, the injury site in fish provides a regeneration-supportive environment and neurons readily upregulate growth-promoting molecules.

PART I of this thesis focuses on Thy-1 and PrP, two GPI-linked proteins highly abundant in the mammalian CNS and implicated in formation and maintenance of neuronal structures like visual system development and synaptic plasticity of the brain. Given their association with proteins that become upregulated in fish regenerating axons, we asked whether and how Thy-1 and PrP contribute to axonal growth. To achieve this goal, one fundamental approach of this work was to establish and verify zebrafish-specific antibodies for Thy-1 and PrP, required for my research.

Interestingly, PrP and Thy-1 became up-regulated in zebrafish retina ganglion cells (RGCs) upon optic nerve lesion, suggesting that these proteins support axon regeneration. To clarify this finding, I analyzed the localization and expression of Thy-1 and PrP in the zebrafish retina, and performed gain- and loss-of-function experiments in zebrafish and mouse neurons. Here I provide evidence that both molecules are key players during axon regeneration in zebrafish RGCs and also in mouse hippocampal neurons. Thus, morpholino- and siRNA-mediated knockdown of Thy-1 and PrP resulted in zebrafish and mouse neurons with diminished axon growth *in vitro* and impaired the regeneration capacity of the fish optic nerve *in vivo*. Conversely, Thy-1 and PrP overexpression led to improved axonal outgrowth in cultured mouse hippocampal neurons. In addition, these manipulations identified Src family kinases (SFKs) as downstream effectors of PrP-altered signaling in fish RGCs, suggesting that the disregulation of tyrosine phosphorylation targets contributes to the disturbed actin cytoskeleton of these neurons and their diminished axon growth.

PART II of this study investigates the neuronal role of the myelin-associated protein Nogo-A (Reticulon-4, RTN4), best known as perhaps the most potent inhibitor of axon regeneration in

mammals. Because fish myelin has been reported to be permissive for neurite growth, it was proposed that the absence of Nogo-A would account for the ability of zebrafish CNS neurons to regenerate. In line with this notion, RTN4a, one of the duplicated zebrafish orthologues of mammalian Nogo-A was found to be non-inhibitory to fish and mammalian neurons. While a similar result was expected for the second zebrafish orthologue, RTN4b, its effect on axon growth had not been investigated so far. Intriguingly, a sequence homologous to the NSR (Nogo-A-specific region), the key inhibitory domain of mammalian Nogo-A, was recently identified in RTN4b. Therefore, I investigated whether RTN4b has a yet unexplored inhibitory activity. Surprisingly, I found that when offered as a substrate *in vitro*, recombinant fish RTN4b strongly impairs the growth of fish and mammalian neurons, similar to its mammalian counterpart. Moreover, I show that the mutation of four integrin-binding motifs (M1-4) in the NSR of mammalian Nogo-A is sufficient to abolish its inhibitory activity. When localized intracellular, Nogo-A is associated with the tubular endoplasmic reticulum (ER) and has been proposed to support the regeneration of mouse RGC axons upon optic nerve injury. Interestingly, using our newly established antibody against zebrafish RTN4b, I found that it is upregulated in RGCs upon optic nerve injury and that its knockdown leads to impaired regeneration. Besides challenging current notions about the absence of key axon growth inhibitors in fish, these findings highlight the opposing roles of Nogo-A, dependent on its subcellular localization.

Taken together, these results provide new insights into the molecular and cellular mechanisms behind the remarkable regenerative potential of fish axons. From my work, Thy-1, PrP and RTN4b emerge as key modulators of the different regenerative outcomes observed in fish and mammalian neurons.

Zusammenfassung

Die Fähigkeit der Fische nach einer Verletzungen des zentralen Nervensystems (ZNS) erfolgreich Axone zu regenerieren fasziniert Neurowissenschaftler seit langem, vor allem da Säugetiere diese Fähigkeit scheinbar verloren haben. Bestrebungen, die Grundlagen dieser evolutionären Unterschiede zu verstehen, konzentrieren sich hauptsächlich auf zwei zentrale Aspekte: 1) intrinsische Eigenschaften der Neurone, die benötigt werden um die Wachstumsmaschinerie in Gang zu setzen, und 2) extrinsische Faktoren der zellulären Umgebung, welche Wachstum erlauben, fördern oder hemmen. Bei Säugern bildet sich an der verletzten Stelle Glianarbengewebe und es werden inhibitorische Moleküle freigesetzt, was eine physikalische und biochemische Wachstumsbarriere darstellt. Im Gegensatz dazu existiert in Fischen ein regenerations-begünstigendes Umfeld und betroffene Neurone regulieren wachstumsfördernde Moleküle hoch.

PART I meiner Dissertation konzentriert sich auf Thy-1 und PrP, zwei GPI-verankerte Proteine, welche reichlich im ZNS der Säugetiere vorkommen und an der Bildung und Aufrechterhaltung neuronaler Strukturen, wie beispielsweise der Entwicklung des visuellen Systems oder der synaptischen Plastizität des Gehirns, beteiligt sind. Da sie mit Proteinen assoziiert sind, welche in regenerierenden Axonen hochreguliert werden, war die Fragestellung, ob und wie Thy-1 und PrP zum axonalen Wachstum beitragen. Um dies zu untersuchen, war vorab die Herstellung spezifischer Zebrafisch-Antikörper gegen Thy-1 und PrP erforderlich.

Interessanterweise wurden Thy-1 und PrP nach Läsion des Sehnervs in Zebrafisch-Retinaganglienzellen (RGZ) hochreguliert, was impliziert, dass beide Proteine die Regeneration von Axonen unterstützen. Daher erörterte ich zunächst die Lokalisierung und Expression von Thy-1 und PrP in retinalen zebrafisch Ganglienzellen und führte funktionelle Gewinn- und Verlustexperimente in Zebrafisch- und Mäuseneuronen durch. In dieser Arbeit erbringe ich den Nachweis, dass Thy-1 und PrP Schlüsselmoleküle der Axonregeneration retinaler Zebrafisch Ganglienzellen und hippocampaler Mäuseneurone sind. Morpholino- und siRNA-vermittelter Knockdown von Thy-1 und PrP führten zu vermindertem Axonwachstum in Zebrafisch- und Mausneuronen *in vitro* und beeinträchtigte die Regenerationsfähigkeit des Fischsehnervs *in vivo*. Umgekehrt führte die Überexpression von Thy-1 und PrP *in vitro* zu gesteigertem Axonwachstum in hippocampalen Mäuseneuronen. Des Weiteren identifizierte ich die Kinasen der Src-Familie (SFKs) als nachgeschaltete Effektoren der manipulierten PrP-Signalgebung in Fisch-RGZs. Dies legt nahe, dass die Disregulierung betroffener Tyrosin-

Phosphorylierungsziele zu einer Störung des Aktin-Zytoskeletts und daher zu vermindertem Axonwachstum führt.

PART II dieser Studie untersucht die neuronale Rolle des Myelin-assoziierten Proteins Nogo-A (Reticulon-4, RTN4), welches als einer der stärksten Regenerationsinhibitoren in Säugetieren bekannt ist. Da berichtet wurde, dass Fischmyelin sich nicht hemmend auf neuronalen Wachstum auswirkt, wurde angenommen, dass die Abwesenheit von inhibitorischem Nogo-A diese Regenerationsfähigkeit erklären könnte. Damit einhergehend wurde berichtet, dass RTN4a, eines der duplizierten Zebrafisch-Orthologe des Säuger-Nogo-As, nicht wachstumshemmend für Fisch- und Säugertierneurone sei. Dasselbe wurde auch für das zweite Zebrafisch-Ortholog -RTN4b- angenommen, dessen Effekt auf das Wachstum von Neuriten jedoch noch nicht untersucht wurde. Vor kurzem wurde die homologe Sequenz zur NSR (Nogo-A spezifischen Region) in RTN4b identifiziert, der inhibitorischen Schlüsseldomäne von Säuger-Nogo-A. Uns interessierte, ob RTN4b eine potentielle, bisher unbekannte, wachstumshemmende Aktivität besitzt. Überraschenderweise beeinträchtigte rekombinantes RTN4b als Substrat das Wachstum von Fisch- und Säugerneuronen ebenso stark, wie sein Säugertier-Pendant. Darüber hinaus führte eine Mutation innerhalb der vier Integrin-Bindedomänen (M1-4) der NSR des Säuger-Nogo-As zum völligen Verlust von dessen hemmender Aktivität, was die inhibitorischen Bereiche des Moleküls identifiziert.

Andererseits wurde gezeigt, dass intrazelluläres Nogo-A wiederum, welches vorwiegend mit dem Endoplasmatischen Retikulum (ER) assoziiert ist, die Regeneration von Mäuse-RGZ-Axonen fördert. Interessanterweise beobachtete ich mit unserem neu etablierten Antikörper gegen Zebrafisch-RTN4b, dass RTN4b nach einer Läsion des Sehnervs in RGZ hochreguliert wird und, dass ein Knockdown zu verminderter Regeneration führt. Zum einen stellt dies die derzeitige Hypothese zur Abwesenheit Axonwachstum-inhibierender Schlüsselkomponenten in Fischen infrage, zum anderen werden die gegensätzlichen Rollen von Nogo-A, abhängig von dessen subzellulärer Lokalisierung, aufgezeigt.

Diese Ergebnisse liefern neue Erkenntnisse über die molekularen und zellulären Regenerationsprozesse und zeigen, dass Thy-1, PrP und RTN4b wichtige Schlüsselmodulatoren bezüglich der unterschiedlichen Regenerationskapazität von Fisch- und Säugerneuronen darstellen.

List of abbreviations

aa	amino acid
α-actin	alpha actin
AKR	aldo-keto reductase
ALS	amyotrophic lateral sclerosis
AMV	avian myeloblastosis virus
Asn	asparagine
BSE	bovine spongiform encephalopathy
c	cellular
Ca^{2+}	calcium
CAD	cath.-a-differentiated
cAMP	cyclic adenosinemonophosphat
CAP	catabolite activator protein
CD 90	cluster of differentiation 90
cDNA	complementary DNA
CJD	Creutzfeld Jakob disease
CNS	central nervous system
CREB	cAMP response element-binding protein
CSPG	chondroitin sulfate proteoglycan
CST	corticospinal tract
Cu^{2+}	copper
DEPC	diethylpyrocarbonate
DNA	deoxyribonucleic acid
DRG	dorsal root ganglion
DRM	detergent resistant membrane
DTT	dithiothreitol
EAE	experimental autoimmune encephalomyelitis
ECM	extracellular matrix
EDTA	ethylendiamintetraacetate
EF1α	elongation factor 1 alpha
EGFP	enhanced green fluorescent protein
EGFR	epidermal growth factor receptor
ER	endoplasmic reticulum
F-actin	filamentous actin
FCS	fetal calf serum
GABA	gamma aminobutyric acid
GPI	glycosylphosphatidylinositol
GSS	Gerstmann-Sträussler-Scheinker syndrome
GTP	guanosine-5`-triphosphate
HD	hydrophobic domain
HEPES	2-(4-(2-Hydroxyethyl)-1-piperazinyl)-ethansulfonacid
ICC	immunocytochemistry
Ig	immunoglobulin
IgSF	immunoglobulin super family
IHC	immunohistochemistry
IPTG	Isopropyl-β-D-thiogalactopyranoside
Kb	kilobase
kDa	kilodalton
KLF	krüppel-like factor
KO	knockout
LN	laminin
LTP	long term potentiation
M	molar
mAb	monoclonal antibody
MAG	myelin associated glycoprotein
MAP	mitogen associated protein
MBP	myelin basic protein
MEKK	MAP kinase kinase kinase
MO	morpholino
mRNA	messenger RNA
MS	multiple sclerosis
NCAM	neuronal cell adhesion molecule
NCAN	neurocan
NGF	nerve growth factor
NgR	Nogo receptor
NMDAR	N-Methyl-D-aspartate receptor
NP40	nonyl phenoxypolyethoxylethanol
NS	nervous system
NSR	Nogo specific region
OMgp	oligodendrocyte-myelin glycoprotein
ONL	optic nerve lesion
ONS	optic nerve section
ORF	open reading frame
pAb	polyclonal antibody
PCR	polymerase chain reaction
PI3K	phosphoinositide-3-kinase
PirB	paired-immunoglobulin-like receptor
PKA	protein kinase A
PLC	phosphatidylinositol-specific phospholipase C
PLL	poly-L-lysine
PNGase	Peptide-N-Glycosydase F
PNS	peripheral nervous system
PrP	prion protein
PSD 95	post synaptic density protein 95
PTEN	phosphatase and tensin homolog
rel	relative
RGC	retinal ganglion cell
RHD	reticulon homology domain
RIPA	radioimmunoprecipitation assay
RLS	restless legs syndrome
RNA	ribonucleic acid
ROCK	rho-associated protein kinase
Rpl13α	ribosomal protein L13 alpha
rpm	revolutions per minute
RT	room temperature
RTN	reticulon
S1PR2	sphingosine-1-phosphate receptor 2
sc	scrapie
SDS-PAGE	sodiumdodecylsulfate-polyacrylamide gel electrophorese
SFK	src family kinase
Sho	shadoo
siRNA	small interfering RNA
SOCS3	suppressor of cytokine signaling 3
SP	signal peptide
Src	sarcoma
STI 1	stress inducible protein 1
TAG1	transient axonal glycoprotein-1
TCA	trichloro-acetic acid
TEMED	N,N,N',N'-Tetramethylethylendiamine
Thy-1	thymocyte antigen-1
TROY	tumor necrosis factor receptor superfamily, member 19
TSE	transmissible spongiform encephalopathy
U	unit
UTR	untranslated region
VGCC	voltage-gated calcium channel
WB	Western blot
WT	wild type
ZF	zebrafish

Table of contents

Abstract……3

Zusammenfassung……5

List of Abbreviations……7

Table of contents……8

1. Introduction……14

1.1. MECHANISMS OF AXON REGENERATION……14

PART I Specific Introduction: The GPI-anchored proteins Thy-1 and PrP……16

1.2. Thy-1……17

Discovery, general expression and function……17

Structural features……17

Knockout mice and links to pathophysiology……19

Thy-1 in the neuronal context……20

1.3. PrP……23

Discovery, general expression and function……23

Structural features……25

Knockout mice and links to pathophysiology……28

PrP in the neuronal context……29

PART II Specific Introduction: The myelin- and ER-associated protein Nogo-A/RTN4……32

1.4. Nogo-A/RTN4……32

Discovery, general expression & function……32

Cell surface Nogo-A……32

Intracellular, ER-associated Nogo-A……34

Structural features……34

Nogo-A in the the neuronal context……36

Clinical significance, axon regeneration in mammals and fish……37

2. Working hypothesis and aims of this study……39

2.1. PART I: Investigating the roles of neuronal Thy-1 and PrP in axon growth and regeneration……39

2.2. PART II: Investigating the role of the myelin- and ER-associated protein Nogo-A/RTN4b in axon growth and regeneration……40

3. Materials……41

3.1. Organisms, cell lines and cell culture media……41

3.2. Morpholino antisense oligonucleotides (Gene Tools, LLC)……42

3.3. Solutions and buffers……42

3.4. Kits……45

3.5. Enzymes……45

3.6. Antibodies and dyes……46

3.7. List of primer oligonucleotides for molecular cloning, ISH and qRT-PCR……47

3.8. List of DNA vectors and siRNAs……47

3.9. List of reagents and chemicals……48

3.10. Protein purification materials……49

3.11. Laboratory devices and microscopes……49

3.12. Software and databases……49

4. Methods……50

4.1. Animal models……50

4.2. Optic nerve lesion in adult fish……50

4.3. *In vivo* morpholino application to the zebrafish optic nerve……50

4.4. Morpholino microinjection of zebrafish embryos……51

4.5. Fish retina preparation……51

4.6. Preparation of Poly-L-Lysine (PLL) coated coverslips for cell culture……51

4.7. Single zebrafish RGC primary cultures……52

4.7.1. Zebrafish RGC culture……52

4.7.2. Morpholino transfection of single zebrafish RGCs *in vitro*, outgrowth assay……52

4.7.3. Single zebrafish RGCs cultured with Thy-1-GST as soluble substrate, outgrowth assay…53

4.7.4. Single zebrafish RGCs cultured on different Nogo substrates, outgrowth assay……53

4.8. Zebrafish retinal explant cultures……54

4.8.1. Morpholino-transfection of retinal explants, outgrowth assay……54

4.8.2. Retinal explants cultured on different Nogo substrates, outgrowth assay……54

4.9. *In vivo* regeneration studies in zebrafish RGCs……55

4.10. Single mouse hippocampal neurons primary culture, siRNA-mediated protein knockdown, overexpression of proteins, co-localization assays……56

4.10.1. Primary hippocampal culture……56

4.10.2. Transfection of hippocampal cells with siRNA Thy-1/PrP and EGFP-Thy-1/EGFP-R1……56

4.10.2.1. Outgrowth studies……57
4.10.2.2. Co-localization studies……57
4.11. PC 12 cells on different Nogo substrates, spreading assay……58
4.12. Molecular cloning……58
4.12.1. Photometric DNA / RNA concentration measurement……60
4.12.2. Cloning of zebrafish Thy-1 into the pGEX-KG- / pIgPlus- / pEGFP-C1-vector and bacterial expression of GST- / FC- / EGFP-Thy-1……60
4.12.3. Cloning and expression of rat and fish Nogo-A M1-4 specific region and mutation of the conserved functional motifs M1-4……61
4.12.4. Verification of the mouse EGFP-Thy-1 vector……62
4.13. *In situ* hybridization (ISH) against zebrafish Thy-1 in whole mount retinae……62
4.13.1. Total RNA extraction……63
4.13.2. Reverse transcription / cDNA synthesis……63
4.13.3. Hybridization probe synthesis……63
4.13.4. Zebrafish retina whole mount ISH……64
4.14. Relative quantitative Realtime PCR (qRT PCR) of Thy-1 mRNA levels in zebrafish retinae and embryos……65
4.14.1. Total RNA extraction and reverse transcription / cDNA synthesis……66
4.14.2. Relative qRT PCR……66
4.14.3. Quantification and statistical analysis for qRT PCR……67
4.15. Biochemical assays, Immunohisto-/cytochemistry (IHC, ICC)……67
4.15.1. Protein extraction from tissues (brain, retina), zebrafish embryos or cell lines……67
4.15.2. Purification of recombinant GST-tagged proteins……68
4.15.3. Antigen-specific affinity purification of antibodies……68
4.15.4. IgG purification of antibodies……69
4.15.5. Protein concentration measurement……69
4.15.6. Immunoprecipitation assay from tissue or cell lysates ……70
4.15.7. Deglycosylation assay with PNGase F (Peptide-N-Glycosidase F)……70
4.15.8. SDS-PAGE……70
4.15.9. Western blotting……71
4.15.10. Immunohistochemistry, Immunocytochemistry (IHC, ICC)……71
4.16. Generation of pAbs specific for zebrafish Thy-1, PrP-2, RTN4b……73
4.17. Generation of a mAb specific for zebrafish Thy-1……73

5. Results……75

PART I Thy-1……75

5.1. Expression pattern of Thy-1 in zebrafish RGCs……75

5.1.1. Characterization of a pAb specific for zebrafish Thy-1……75

5.1.2. Generation of a Thy-1-specific zebrafish mAb and analysis of the Thy-1 expression pattern in the retina……79

5.1.3. Expression pattern of Thy-1 in cultured single zebrafish RGCs……82

5.1.4. Knockdown of Thy-1 in zebrafish RGCs……83

5.1.5. Expression and knockdown of Thy-1 in the zebrafish embryo……86

5.1.6. The monoclonal zebrafish Thy-1 antibody 89/9 in the goldfish……89

5.2. The neuronal function of Thy-1……92

5.2.1. Thy-1-GST promotes, knockdown of Thy-1 impairs differentiation and growth of zebrafish RGCs *in vitro*……92

5.2.2. Knockdown of Thy-1 in zebrafish RGCs *in vivo* impairs neurite outgrowth and optic nerve regeneration ……96

5.2.3. Thy-1 overexpression enhances, Thy-1 knockdown impairs neurite outgrowth of mouse hippocampal neurons *in vitro*……99

5.2.4. Thy-1 loss-of-function effect in mouse hippocampal neurons is rescued by Thy-1 overexpression *in vitro*……100

PART I PrP……102

5.3. Expression pattern of PrP-2 in zebrafish RGCs, characterization of a specific pAb……102

5.3.1. Characterization of PrP-2 in zebrafish RGCs……103

5.3.2. Knockdown of PrP-2 in zebrafish RGCs……105

5.4. The neuronal role of PrP-2……107

5.4.1. Knockdown of PrP-2 in zebrafish RGCs *in vitro* and *in vivo* impairs neurite outgrowth……107

5.4.2. Knockdown of PrP-2 in zebrafish RGCs impairs Src kinase signaling……110

5.5. Potential interactions of Thy-1 and PrP in hippocampal neurons……112

5.6. Thy-1, PrP and flotillin-2 in the neuronal mouse CAD cell line……114

PART II RTN4b……115

5.7. Expression of RTN4b in zebrafish RGCs and its role in axon regeneration……117

5.7.1. Expression of RTN4b in zebrafish RGCs……117

5.7.2. Knockdown of RTN4b in zebrafish RGCs *in vivo* impairs neurite outgrowth……120

5.7.3. Expression pattern of CLIMP-63 in zebrafish RGCs……121

5.8. Nogo-A (RTN4b) M1-4 peptides as substrates for axonal growth, tested on zebrafish and mammalian neurons……123

5.8.1. Rat and zebrafish RTN4b inhibit and mutated rat M1-4 D/A permits outgrowth of zebrafish RGCs *in vitro* ……123

5.8.2. Effects of M1-4 peptides on the growth ability of rat PC12 cells……127

6. Discussion……128

PART I Thymocyte antigen 1 (Thy-1) and the Prion Protein (PrP)……128

6.1. Thy-1 in zebrafish RGCs, its lesion-induced expression and biological relevance….128

6.2. Thy-1 expression in early zebrafish embryos ……131

6.3. Role of Thy-1 in neuronal function……132

6.4. Thy-1-associated signaling partners in neurons……134

6.5. Specificity and validation of antibodies used in research ……139

6.5.1. Validation of the polyclonal and monoclonal Abs specific for zebrafish Thy-1 used in this research……142

6.6. PrP-2 in zebrafish retinal ganglion cells, its lesion-induced expression and validation of the pAb 981……148

6.7. Role of PrP in neuronal function and its biological relevance……149

6.8. PrP-associated signaling partners in neurons……151

6.9. Functional similarities and differences between Thy-1 and PrP……153

PART II Reticulon-4 (RTN4b)……155

6.10. RTN4b/Nogo-A in zebrafish RGCs, its lesion-induced expression and endogenous neuronal function ……155

6.11. Substrate properties of fish and mammalian RTN4b/Nogo-A, identification of its four inhibitory motifs……156

7. Conclusions and outlook……160

PART I Thy-1 and PrP……160

PART II RTN4b……161

8. References……162

9. Supplementary data and statistics……192

PART I Thy-1 and PrP……192

9.1. Chapter 5.1.2: Verification of the specificity of the mAb 89/9 raised against zebrafish Thy-1……192

9.2. Chapter 5.1.2: Analysis of Thy-1 expression upon ONS in zebrafish RGCs……..192

9.3. Chapter 5.1.4: MO-mediated knockdown of Thy-1, quantification of protein levels in zebrafish RGCs and embryos ……..197

9.4. Chapter 5.1.6: Characterization of the zebrafish Thy-1 mAb 89/9 in the goldfish…..201

9.5. Chapter 5.2: The neuronal role of Thy-1……201

9.6. Chapter 5.3.1: Specificity of the zebrafish PrP-2 pAb 981……212

9.7. Chapter 5.3.1: Analysis of PrP-2 expression upon ONS in zebrafish RGCs……213

9.8. Chapter 5.3.2: MO-mediated knockdown of PrP-2, quantification of protein levels in zebrafish RGCs……216

9.9. Chapter 5.4.1: The neuronal role of PrP-2……218

9.10. Chapter 5.5: Potential interactions of Thy-1 and PrP in hippocampal neurons……223

PART II RTN4b……225

9.11. Chapter 5.7: Expression of RTN4b in zebrafish RGCs, specificity of the pAb RTN4b K1121……225

9.12. Chapter 5.7.1: Analysis of RTN4b expression upon ONL in zebrafish RGCs……226

9.13. Chapter 5.7.2 B: Knockdown of RTN4b impairs axonal outgrowth of zebrafish retinal explants *in vitro* ……230

9.14. Chapter 5.8.1 & 5.8.2: Inhibitory substrate properties of different Nogo-A (RTN4b) M1-4 peptides, tested on zebrafish and mammalian neurons ……232

Record of contributions……237

Acknowledgements……238

1. Introduction

1.1. MECHANISMS OF AXON REGENERATION: intrinsic and extrinsic factors, the difference between lower vertebrates and mammals

The poor capacity of the CNS of higher vertebrates to regenerate their axons after damage to the brain, spinal cord or optic nerve has challenged neuroscientists for a long time. Substantial progress has been made since the beginning of the 19th century when Ramon y Cajal visualized the anatomy of the brain and other neuronal structures. He was a pioneer in modern neuroscience and introduced a concept called "neuron doctrine". By using Camillo Golgi`s silver nitrate stain method he found that the nervous system is built up of basic units, the individual neurons, that are polarized, have dendrites and axons with dendritic spines and growth cones (Cajal, 1928; López-Muñoz et al., 2006). This fundamental knowledge about the anatomy of neurons enabled scientists and physicians to understand the mechanisms of regeneration in the nervous system.

To this day the mechanisms underlying neurite outgrowth and regeneration remain the focus of intensive research aimed at finding therapeutic targets which support functional recovery. The ultimate goal will be to cure the human CNS after paraplegia, stroke, multiple sclerosis or other neurological diseases.

Primitive vertebrates like fish and amphibians are able to regenerate CNS neurons after injury and even recover complete functional limbs and organs. What is their "secret"? And what are molecular mechanisms underlying successful regeneration?

The vertebrate nervous system comprises the central (CNS; brain and spinal cord) and the peripheral (PNS; motor and sensory neurons, autonomic and enteric system) subdivisions. While axons in the mammalian PNS regenerate to a significant extent, injured neurons of the brain and spinal cord fail to do so after embryonic differentiation is completed. The degenerating proximal axon forms a dystrophic retraction bulb, whereas the distal end undergoes "Wallerian degeneration", followed by disassembly of the myelin sheath and invasion of macrophages (Waller, 1850). One groundbreaking early study done by Albert J. Aguayo and colleagues found that rat CNS axons are able to extend when placed on a substrate made of transplanted PNS glia (Schwann cells) (David & Aguayo, 1981). Furthermore, neurons with axons in both the CNS and PNS, such as dorsal root ganglia (DRG), can only regenerate their peripheral processes (Yiu & He, 2006). These data point to

differences between CNS and PNS in terms of their growth/inhibitory molecules and axon guidance cues (extrinsic factors) as well as the ability of their neurons to re-express molecules and receptors that stimulate or prevent outgrowth (intrinsic factors).

Extrinsic factors:

After damage, the scar forming tissue contains reactive astrocytes expressing growth-inhibitory chondroitin-sulfate proteoglycans (CSPGs). In addition, the accruing myelin debris releases strong neurite outgrowth inhibitors like Nogo-A (reticulon-4), the myelin-associated glycoprotein (MAG) and the oligodendrocyte myelin glycoprotein (OMgp) (Vajn et al., 2013). Earlier studies showed that the regeneration of goldfish axons is inhibited by oligodendrocytes and myelin from the rat but not by optic nerve tract oligodendrocytes or CNS myelin from the goldfish (Bastmeyer et al., 1991; 1993). Moreover, the spinal cord injury of zebrafish differs markedly from the mammalian one: reactive astrocytes have not been observed there but instead ependymoradial glial cells proliferate and extend across the lesion site thereby forming a bridge between the spinal cord stumps (Vajn et al., 2013; Goldshmit et al., 2012). In a comparative study about the response to spinal cord injury it was further found that, in contrast to mammals, zebrafish radial glia cells serve as neuronal progenitors and Schwann cells, which express little or no Nogo-A/reticulon-4 (Rtn4) and MAG, proliferate and re-myelinate CNS axons (Hui et al., 2010). This cell replacement phenomenon was only observed in zebrafish in addition to the existence of a growth permissive environment. Functional differences included the absence or clearance of myelin debris, the presence of supportive Schwann cells and the absence of a detrimental inflammatory response (Hui et al., 2010). In goldfish optic nerves, injury sites are invaded by fibroblasts, suggesting a physical and molecular supportive role for this type of cells during fish axonal regeneration (Hirsch et al., 1995).

Intrinsic factors:

Interestingly, not all neurons in zebrafish are able to regenerate. Moreover, only certain mammalian CNS neurons are able to do so when they are given a permissive growth substrate (like peripheral or embryonic nerve grafts) (Rossi et al., 1995). This implies the existence of key neuron intrinsic molecules that enable an axon to regrow after traumatic damage or disease. Accordingly, multiple transcription factors (e.g. krüppel-like family, KLFs), second messengers (e.g. Ca^{2+} and cAMP), signaling and cell adhesion molecules, neurotrophins and their corresponding guidance receptors have been found to be involved in axon regeneration

in mammals and zebrafish (Moore & Goldberg, 2011; Bashaw & Klein, 2010). Further examples include regeneration promoting molecules like the growth-associated protein-43 (GAP-43), the L1 cell adhesion molecule (L1 CAM), the transient axonal glycoprotein (TAG-1/Contactin-2) or the suppressor of cytokine signaling 3 (SOCS3). Among growth preventing molecules, the inhibitor of the PI3K/AKT/mTOR pathway named PTEN (phosphatase and tensin homolog) is an important example (Vajn et al., 2013; Liu et al., 2011). Notably, most pathways converge at the regulation of cytoskeleton dynamics and the influence on Rho-GTPase signaling and actin turnover, which modulate the direction and speed of growth cone motility and is essential for proper axon elongation and navigation (Gordon-Weeks & Fournier, 2014; Vitriol & Zheng, 2012). The zebrafish is able to upregulate a set of many gene transcripts upon CNS lesion, a phenomenon that was analyzed in a wide screening study performed with quantitative realtime PCR and microarray analysis in zebrafish RGCs after optic nerve lesion to identify important key players which are involved in successful CNS regeneration (McCurley & Callard, 2010).

PART I

Specific Introduction: The GPI-anchored proteins Thy-1 and PrP

During the search for axon regeneration factors in fish and amphibians, the membrane microdomain proteins flotillin-1 (also named reggie-2) and flotillin-2 (reggie-1) were found to be up-regulated and important for effective regeneration after optic nerve lesion in zebrafish and in rats (Munderloh et al., 2009; Schulte et al., 1997; Koch et al., 2013). Further work showed that flotillins mark signaling platforms within plasma membrane microdomains (lipid rafts) to which growth-associated, cell-surface proteins like Thy-1 and PrP anchor via their glycosylphosphatydylinositol (GPI) tails (Simons & Ikonen, 1997; Stuermer et al. 2001; Stuermer & Plattner, 2005b; Stuermer et al. 2004). When stimulated by antibody-mediated-crosslinking, GPI-anchored proteins can trigger cytoskeletal rearrangements and signal transduction via Src tyrosine and mitogen-activated protein (MAP) kinases (Head et al., 2014; Stuermer 2011). Preliminary experiments in our laboratory showed that Thy-1 and PrP were up-regulated in RGCs after optic nerve lesion. Therefore, we hypothesized that these two GPI-anchored proteins influence re-growth of fish and possibly mouse axons in collaboration with flotillin microdomains.

1.2. THY-1

Discovery, general expression & function:

Thy-1 (thymocyte differentiation antigen 1), also known as CD90 (cluster of differentiation 90), is a small, heavily glycosylated (~25-37 kDa) GPI-anchored protein. It was originally identified during a molecular screen for leukemia specific antigens in mouse thymocytes (Reif & Allen, 1964). 20 years later, the human homologue was isolated and after another 20 year, a zebrafish counterpart was characterized (Ades et al., 1980; Deininger et al., 2003; Reuter et al., 2004). Because it is the smallest member of the immunoglobulin superfamily (IgSF) -it contains a single V-like Ig domain- it was suggested that Thy-1 may represent a primordial Ig molecule, which evolved independently in the genome of tunicates, birds, fish, amphibians, rodents and humans (Williams & Gagnon, 1982; Leyton & Hagood, 2014).

The variable spatiotemporal expression of Thy-1 across diverse cell types and tissues suggests that is has a context-dependent biological role. Thy-1 is expressed in T-cells, thymocytes, fibroblasts, in cells of endothelial, mesangial, hematopoetic or mesenchymal origin and, most important for the scope of this thesis, throughout the nervous system. Neurons in the CNS and PNS express it strongly but also some glial cells seem to produce it (Kemshead et al., 1982). As an interaction partner of the extracellular matrix (ECM), Thy-1 plays a role in cell-cell interaction, cell adhesion and migration, which are essential aspects of nervous system development and regeneration, as well as of metastasis formation, inflammation, fibrosis, apoptosis and cancer (Rege & Hagood, 2006). Despite these advances, the physiological role of this molecule and the cellular mechanisms involved remain largely unknown.

Structural features:

The *thy-1* gene exhibits a conserved structural organization in all species, with an open reading frame (ORF) spanning three out of four exons. The first one encodes the majority of the N-terminal signal peptide (aa 1-19), which is necessary for the transport of Thy-1 to the endoplasmic reticulum (ER) and is then cleaved. The second one encompasses the Thy-1 core Ig-like V-type domain (aa 20-130) and the third one encodes the GPI-anchor signal sequence, which is cleaved post-translationally from the immature polypeptide and replaced by a GPI-anchor (aa 131-161).

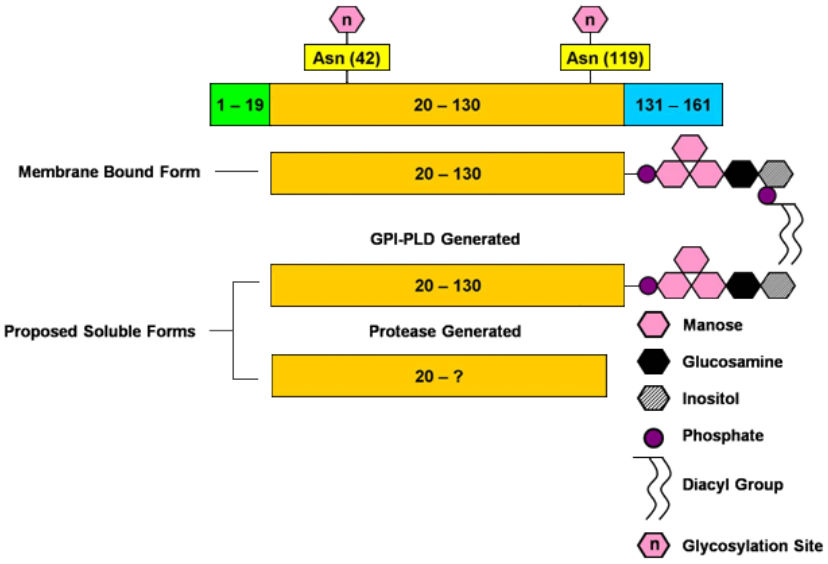

Figure 1.2.1 Thy-1 molecule and proposed soluble forms. Thy-1 is initially generated as a 161 aa immature form. The N-terminal 19 aa signal peptide is removed, and the C-terminal 31 aa are replaced with a GPI anchor, generating the mature form, which is anchored to the outer leaflet of the cell membrane by the diacyl group of the GPI anchor. N-linked glycosylations depict conserved asparagines within murine Thy-1. Soluble Thy-1 could be generated either by cleavage of the GPI anchor by PI-PLC, or by undefined proteases acting at as yet undetermined cleavage sites. Figure and caption taken from atlasgeneticsoncology.org.

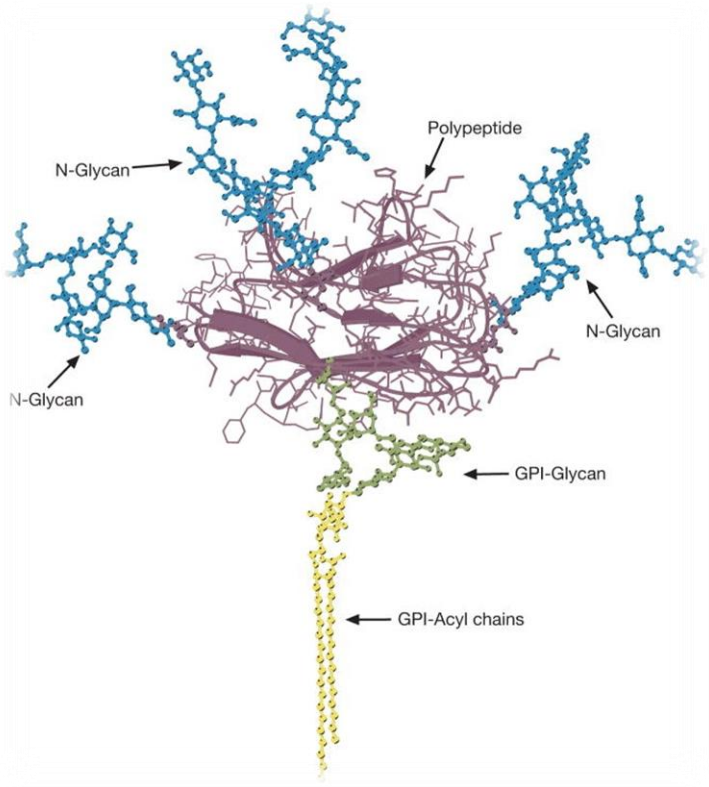

Figure 1.2.2 Schematic representation of the Thy-1 glycoprotein including the three N-glycans (*blue*) and a glycosylphosphatidylinositol (GPI- glycan, *green*) lipid anchor whose acyl chains (*yellow*) would normally be embedded in the membrane bilayer. Note that the polypeptide (*purple*) represents only a relatively small portion of the total mass of the protein. Figure and caption: Original art courtesy of Mark Wormald and Raymond Dwek, Oxford Glycobiology Institute.

Mature, non-glycosylated Thy-1 is about 18 kDa size and shows varying degrees of glycosylation among species (Haeryfar & Hoskin, 2004). For instance, rodent and human Thy-1 have three and two N-confirmed glycosylation sites, respectively, whereas three potential N-glycosylation sites have been identified in fish Thy-1 (T. Seki et al., 1985; Reuter et al., 2004).

Moreover, the number, degree or type of glycosylation is variable among different tissues and subject to developmental regulation (Haeryfar & Hoskin, 2004). The *thy-1* gene of mice is located on chromosome 9 and occurs in two allotypic forms; Thy-1.1 (only AKR and PL mouse strains) and Thy-1.2 (in Balb/c and other strains), characterized by either arginine or glutamine at amino acid residue 89, respectively (Giguére et al., 1985). In humans, *thy-1* is located on chromosome 11 and in fish it is harbored by chromosome 5 (Reuter et al., 2004). The GPI-anchorage of Thy-1 is common to all species and locates it to lipid rafts, but a human soluble form of Thy-1 has also been described (Saalbach et al., 1999). Interestingly, Thy-1 possesses a binding motif, the Arg-Leu-Asp (RLD) tripeptide, that specifically binds to transmembrane integrin receptors and another one that recognizes the heparin-binding domain (REKRK) of syndecan-4, a transmembrane proteoglycan (Hermosilla et al., 2009; Avalos et al., 2009). These motifs represent identified structural domains relevant to the functional interaction of Thy-1 with the ECM. Of note in this context, Thy-1 is also able to undergo homophilic interactions and to multimerize *in vivo* or *in vitro* (Mahanthappa & Patterson, 1992b).

Knockout mice and links to pathophysiology:

Generation of Thy-1 null mice by R. Morris and his colleagues did not provide clear conclusions about the enigmatic function of Thy-1 (Mayeux-Portas et al., 2000). These mice were normal and showed only “mild” phenotypes, like impairment of hippocampal long-term potentiation (LTP) and of other mechanisms involved in learning and memory (Nosten-Bertrand et al., 1996; Mayeux-Portas et al., 2000). Although Thy-1 has long been suspected to play a crucial role in neuronal progression and growth, the brains and spinal cords of knockout mutants seemed to develop and behave rather normally (Barlow et al., 2002). Thy-1 has also been observed in synaptic vesicles and it was suggested to play a regulatory role in the vesicular release of neurotransmitters at the synapse (Jeng et al., 1998). Possibly related to this specialized function, lower levels of iron and Thy-1 have been detected in the substantia nigra of patients with primary Restless Legs syndrome (RLS), suggesting impaired dopaminergic transmission (Wang et al., 2004). Beside these neurological phenotypes, Thy-1 null mice show an impaired cutaneous immune response and display a more severe course of lung fibrosis in histopathological analysis (Hagood et al., 2005). Additionally, Thy-1 knockdown delayed skin wound repair in mice by affecting cell migration into the wound and TGF-ß induced inflammation (Lee, Shin, & Jung, 2013). In thymocytes, Thy-1 has been reported to induce apoptosis and to contribute to the development of glomerulonephritis by inducing mesangial

cell death (Fujita et al., 1996; Mosley et al., 2000). The influence of Thy-1 on cell-cycle proliferation and cell migration has further been connected to tumor suppression in ovarian cancer and nasopharyngeal carcinoma but the precise molecular mechanisms have not been solved yet (Abeysinghe et al., 2003; Lung et al., 2005). To summarize, Thy-1 has been implicated in many diverse cellular and molecular functions during diseases like cancer or immunological deficits. Particularly relevant to this thesis is the increasing experimental evidence supporting a physiological role of Thy-1 as key player in neuronal function and dysfunction.

Thy-1 in the neuronal context:

Thy-1 is abundantly expressed in the vertebrate nervous system, predominantly in adult neurons where it serves as a neuron-specific marker. It is most highly concentrated in the striatum, followed by the hippocampus, neocortex, cerebellum, spinal cord, retina and optic nerve (Seki et al., 2002). In the retina (or the brain) Thy-1 is cumulatively expressed, concurrent with synaptogenesis and therefore, Thy-1 is thought to play a role in synaptogenesis during nervous tissues development (Liu et al., 1996). The importance of Thy-1 for neurons is underscored by its remarkable abundance in these cells. For instance the average amount of Thy-1 on retina ganglion cell (RGC) axons has been estimated to about 500 molecules per square micron (Beech et al., 1983). In line with this, Thy-1 was found to be critical for normal retinal development, as the inner nuclear, inner plexiform, ganglion cell and outer segment/pigment epithelium layers of Thy-1 knockout mice retinae were thinner than those of wild type animals (Simon et al., 1999). Moreover, RGCs isolated from mice lacking Thy-1 showed significantly reduced neurite outgrowth compared to control animals (Simon et al., 1999). The function of Thy-1 in neuronal outgrowth is still a controversial issue, because it was reported to inhibit the growth of neurons when they were cultured over a monolayer of astrocytes, but not when co-cultured over Schwann cells or embryonic glial cells (Tiveron et al., 1992). This effect has been attributed to the specific binding of astrocytic αVß3-integrin to Thy-1, leading to its clustering in neurons, the restriction of growth and the retraction of already existing processes in the CAD cells and primary neurons (Herrera-Molina et al., 2012). Cell signaling in this experimental model was bidirectional and induced migration of astrocytes through the engagement of αVß3 intergrin and syndecan-4 (Herrera-Molina et al., 2012). These publications suggest that Thy-1 is an inhibitory molecule, capable to stabilize neuronal circuits and block neuronal repair in astrocyte-rich regions of the brain and CNS (Herrera-

Molina et al., 2012). Nevertheless, this statement was questioned by the finding that corticospinal tracts or thalamocortical axons failed to regenerate *in vivo* in Thy-1$^{-/-}$ mice (Barlow et al., 2002). Intriguingly, monoclonal antibodies specific for Thy-1 induce neurite outgrowth and sprouting in cultured PC12 cells (Mahanthappa & Patterson, 1992a). Similarly, an earlier study with primary rat RGCs, grown on a substrate of monoclonal antibodies against Thy-1, showed enhanced process regeneration (Leifer et al., 1984). These findings were interpreted in terms of antibody-mediated "blockage" of the assumed inhibitory function of Thy-1 and lend credit to the hypothesis that that the molecule has a negative impact on neurite outgrowth (Leifer et al., 1984; Mahanthappa & Patterson, 1992a). Later on, since only certain monoclonal antibodies were able to promote neurite outgrowth, these data were shown to be caused by selective interactions of the antibody in question with one or more active sites for Thy-1 (Lipton et al., 1992). In other studies, several antibodies against Thy-1 neither inhibited nor stimulated neurite outgrowth of PC12 cells. The effects were again dependent on the epitopes recognized by the antibodies employed in each case (Kuroiwa et al., 2012). Stimulation of neurite growth in neuronal PC12 cells was induced with a rat Thy-1 monoclonal antibody in solution, requiring an influx of calcium via N- and L-type calcium channels (Doherty et al., 1993). The effect was suggested to involve clustering of Thy-1 and the activation of second messenger pathways via cell adhesion molecules like NCAM, N-Cadherin or L1 rather than via integrins (Doherty et al., 1993). Notably, treatment of DRG neurons with anti-Thy-1 monoclonal antibodies not only stimulated neurite outgrowth but also increased branching complexity and induced activation of the PKA-MEKK-CREB and the c-Src kinase-MEK-CREB pathways (Chen et al., 2007; Yang et al., 2008). Altogether, whether Thy-1`s effects on neurite outgrowth are due to the inhibition or stimulation of the protein remains largely a matter of interpretation.

In neuronal rat PC12 cells, activated Thy-1 co-localizes with flotillin microdomains and both proteins could be co-immunoprecipitated in rat brains, PC12s and DRGs (Lang et al., 1998). Importantly, flotillins support axon regeneration in the zebrafish optic nerve and differentiation of mouse hippocampal and N2a neurons (Munderloh et al., 2009). This is consistent with their putative roles in protein sorting and membrane trafficking, as well as in the coordination of signaling molecules at the plasma membrane mediating outside-inside cell responses (Banning et al., 2011). Specifically, flotillins interact with Src tyrosine kinases (Src, Fyn, Lck) as well as with Rho-family GTPases through the CAP-associated signaling complex

and affect actin cytoskeleton dynamics (Baumann et al., 2000; Kimura et al., 2001; Langhorst et al., 2007; Stuermer, 2010). The emerging view from all these findings is that upon stimulation GPI-molecules (like Thy-1) cluster in flotillin microdomains, which results in the recruitment and activation of various intracellular signaling molecules (Herrera-Molina et al., 2013) (Fig.1.2.3). Mechanistically, it is still not clear how this is achieved, since neither Thy-1 nor flotillins possess transmembrane domains through which they could interact with each other. Two scenarios are conceivable: 1) a classical transmembrane molecule is required to connect the extra- and intracellular proteins in question or, 2) clustering of cell surface proteins deforms the lipid bilayer, making it quite possible for them to reach the cell interior and interact directly with intracellular signaling partners as suggested by (Morozova et al., 2011).

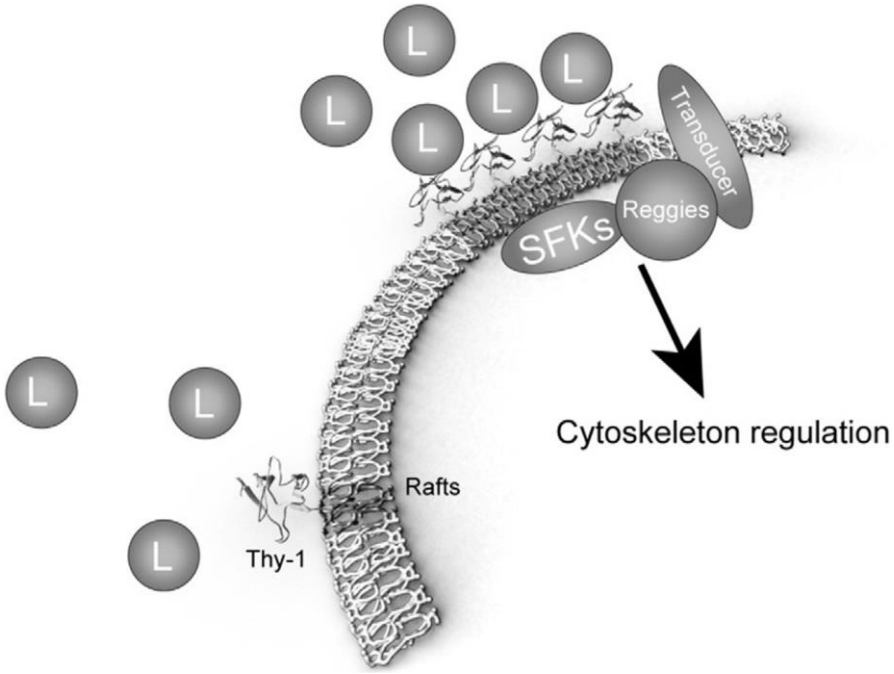

Figure 1.2.3 Signaling triggered by Thy-1 in *cis*. Thy-1 binds to its ligand (L) and undergoes molecular clustering at the plasma membrane. Aggregation of Thy-1 molecules recruits proteins such as flotillins and Src family kinases (SFKs). A transducer has been proposed to connect the intracellular proteins with aggregated Thy-1, transducing signals that lead to regulation of the cytoskeleton. Rafts in the plasma membrane are indicated as darker areas of the membrane. Figure and caption taken from (Herrera-Molina et al., 2013).

1.3. PrP

Discovery, general expression & function:

The prion protein (PrP) was identified 1982 by Stanley B. Prusiner, as the result of a long search for the causative agent of the Creutzfeldt-Jacob disease (CJD) in humans, bovine spongiform encephalopathy (BSE) in cattle and scrapie in sheep (Bolton et al., 1982). He named it prion protein after postulating it was the only component of the "proteinaceous infectious particles" (prions) that are responsible for the transmission of spongiform encephalopathies (TSE) in mammals. PrP is a small (~27-30 kDa in mammals), glycosylated, GPI-anchored membrane protein with rather puzzling physiological function (Requena & Wille, 2014). It is abundantly expressed already during vertebrate embryogenesis and in various adult organs and tissues but most prominently in the brain, spinal cord including associated glial cells (Manson et al., 1992; Harris et al., 1993; Malaga-Trillo et al., 2009; Moser et al., 1995). Peripheral tissues that integrate the body's immune defense and the neuroendocrine system, as well as neurons within the PNS and associated Schwann cells also express significant amounts of PrP (Ford et al., 2002). While these data suggest a role in nervous system development and maintenance, PrP has also been found in many non-neuronal cells like lymphoid and dendritic cells or tissues like the lung, heart, kidney, gastro-enteric tract and muscles, suggesting a more general cellular function of special importance to neurons (Horiuchi et al., 1995; Martínez del Hoyo et al., 2006). The fish orthologues of PrP have been characterized and found to have a similar wide tissue distribution as in mammals, with strong expression in the brain, retina, skin, heart, muscle and gills (Suzuki et al., 2002; Rivera-Milla et al., 2003). More in-depth studies found two duplicated PrP fish versions (termed PrP-1 and PrP-2), which were differentially expressed during embryonic development (Cotto et al., 2005; Rivera-Milla et al., 2006). While PrP-1 is expressed ubiquitously during blastula and gastrula stages, PrP-2 becomes up-regulated later during somatogenesis, predominantly in differentiating neuronal tissues. It was concluded that both PrPs serve different purposes during zebrafish embryogenesis, because knockdown of PrP-1 led to gastrulation arrest, whereas PrP-2 knockdown generated embryos with malformed heads and eyes (Malaga-Trillo et al., 2009). Notably, the PrP-1 knockdown phenotype could be cross-rescued even with mouse PrP, implying a strong functional conservation of the protein across species. This notion was further strengthened by the observation that homologous mutations in mouse and zebrafish PrPs similarly affected their subcellular localization patterns and their adhesive and signaling properties *in vitro* and *in vivo*,

using *Drosophila*, human and zebrafish embryonic cells (Solis et al., 2013). These results expanded previous data showing that PrP mediates cell-cell-contact formation and adhesion via homophilic trans-interactions that activate Src-related kinases and stabilize E-cadherin/ß-catenin adhesion complexes at the cell surface, as well as controlling actin-cytoskeleton dynamics and cell-matrix interactions (Malaga-Trillo et al., 2009; Schrock et al., 2009). In terms of its subcellular distribution, the GPI-linked PrP was mainly localized to detergent resistant membrane domains (DRMs or “lipid rafts”) that are rich in cholesterol and sphingolipids, but it was also present in compartments of the secretory and endocytic pathways (Naslavsky et al., 1997; Harris, 2003). Just as in the case of Thy-1, these specialized lipid raft environments also contained flotillin proteins and appear to provide signaling platforms for associated molecules that activate inward signaling cascades upon stimulation with ligands or receptors (Simons & Toomre, 2000).

Throughout decades of intensive research, the physiological role of PrP remains a complex question, as PrP was involved in mechanisms as diverse as nervous system development, neurotransmitter metabolism, immune cell activation, cell adhesion, signal transduction, copper metabolism, antioxidant activity and programmed cell death (Westergard et al., 2007; Linden et al., 2008; Zomosa-Signoret et al., 2008).

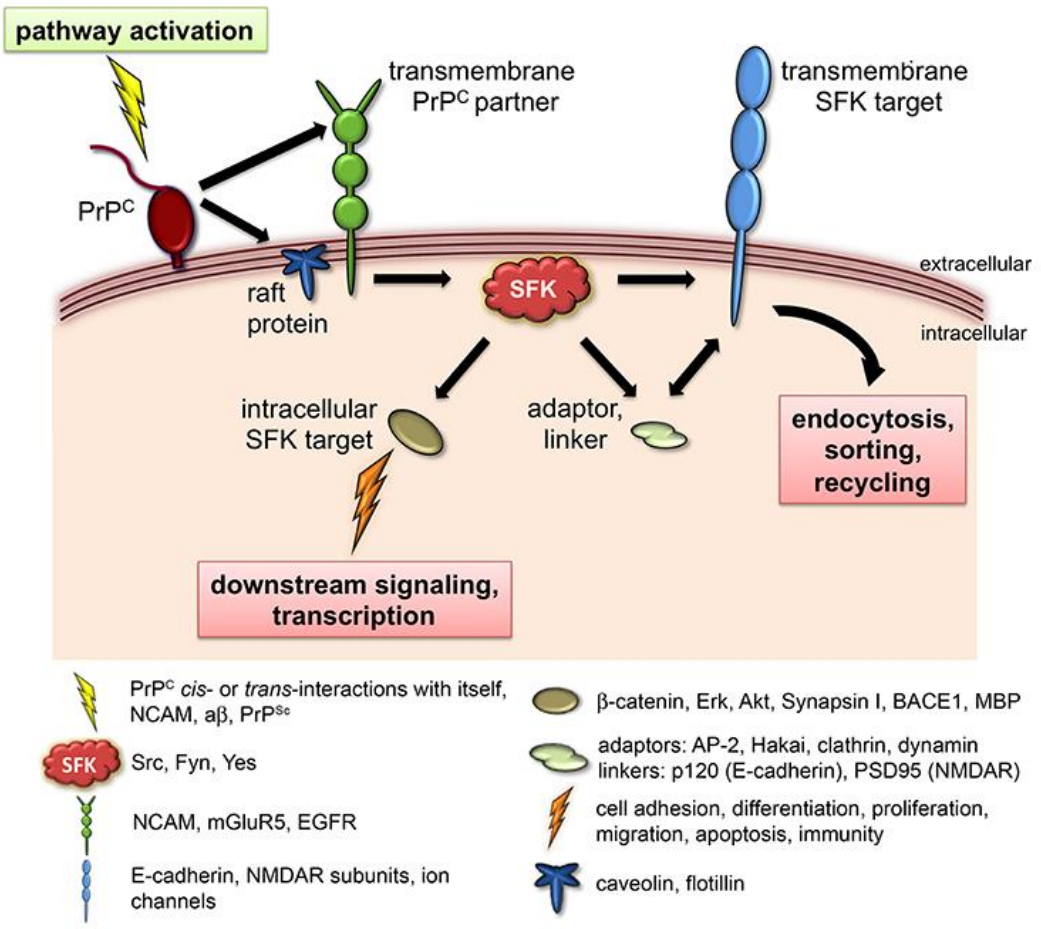

Figure 1.3 PrP^C signaling via SFKs (Src family kinases). Known physiological roles of PrP^C such as neurotransmission, embryonic cell adhesion, olfactory function, and myelination converge at the use of SFKs as intracellular signaling partners. In this model, engagement of PrP^C in various *cis*- or *trans*-interactions (depicted as "pathway activation") elicits the catalytic activity of SFKs, leading to the modulation of diverse downstream targets that include ion channels, adhesion complexes, and cytosolic signaling molecules. Phosphorylation of transmembrane SFK targets controls their cell surface expression and/or signaling properties, whereas phosphorylation of intracellular SFK targets regulates the activation of additional downstream pathways, gene transcription, and protein translation. The caption below provides concrete examples of documented components of this cascade. Figure and caption taken from (Ochs & Málaga-Trillo, 2014).

Structural features:

The gene and protein architecture of PrP is well characterized. The *Prnp* gene is composed of three (rat, mouse, bovine, sheep) or two exons (hamster, humans), where only the last exon encodes for the entire open reading frame (ORF) (Pastore & Zagari, 2007). The basic structure of the protein is highly conserved among all species. Like other extracellular GPI-anchored molecules, PrP contains an N-terminal signal peptide (aa 1-22) that targets it to the ER and a cleavable C-terminal signal peptide (aa 231-254) that serves for the attachment of a GPI-anchor (Pastore & Zagari, 2007). The N-terminus is a flexible domain, containing a repetitive structure with various Cu^{2+}-binding octarepeat sequences (aa 51-91) and is linked to the C-

terminus via a short and conserved hydrophobic stretch (aa 112-133) (Pastore & Zagari, 2007). The C-terminal domain is a stable, globularly structured region composed of three α-helices and two β-sheets and includes two N-glycosylation sites (Asn 181 and 197) (approximate amino acid positions from mouse PrP sequence adapted from (Linden et al., 2008)) (Donne et al., 1997). The degree of glycosylation (di-, mono- or non-glycosylated molecules) and the kind and complexity of the sugar residues (glycans) attached to the protein can be quite diverse, depending on the species, organs, tissues and cells considered (Tuzi et al., 2008; Russelakis-Carneiro et al., 2002).

PrP is highly conserved among mammals, especially within the hydrophobic stretch and the globular domain (>95%) (van Rheede et al., 2003). The sequence identity between birds or frogs and mammalian PrPs is much lower, although the protein domain composition stays the same in all species (Harrison et al., 2010; Rivera-Milla et al., 2006, 2003). Evolutionary analysis of fish PrPs indicate that fish PrP-1 and PrP-2 most probably arose during a fish-specific genome duplication (Rivera-Milla et al., 2006, 2003; Postlethwait et al., 1998; Amores et al., 1998). While both fish PrPs are considerably longer than their mammalian counterparts, fish PrP-1 is approximately 10% longer than PrP-2 and their average amino acid sequence similarity is about 40%, and much lower (~17%) with respect to fish and mammals (Rivera-Milla et al., 2006).

Two additional proteins have been generally pooled as being part of the "prion protein family": besides PrP (*Prnp*), there is a related protein named Doppel (*Prnd*) and possibly one more, called Shadoo (*Sprn*) (Ciric & Rezaei, 2015). All three proteins contain a C-terminal GPI-anchor but only PrP and Doppel have the typical PrP-like arrangement of three α-helices and two β-sheets plus two glycosylation-sites and a charged N-terminus (Ciric & Rezaei, 2015). PrP and Doppel also share the same chromosome locus, *Prnd* being ~20 kb downstream of *Prnp* (Ciric & Rezaei, 2015). As comparison, the lower sequence similarity between Shadoo and PrP is limited to the conserved hydrophobic stretch, a single N-glycosylation site and the presence of tetrarepeats. Furthermore, Shadoo is located to a different chromosome than Prnp and Prnd (Watts & Westaway, 2007). In contrast to PrP, which is predominantly produced in the nervous system, Doppel expression was most evident in adult testis (both somatic and germ cells) and its absence caused male sterility (Behrens et al., 2002). However, Doppel is also co-expressed with PrP in cells of the immune system (B-cells, neutrophils, dentritic cells) (Paltrinieri et al., 2006). Doppel expression in the brain is restricted to early stages of

embryogenesis; moreover, expression in neurons at a later stage appeared to be neurotoxic as shown in PrP knockout mice, where deletion of the ORF encoding PrP led to incidental overexpression of the downstream gene *doppel* as a chimeric protein under the control of the remaining PrP promoter (Rossi et al., 2001). On the other hand, Shadoo expression is restricted to the brain and retina and although its relationship to PrP is rather loose and its physiological function unknown, it has been proposed that Shadoo shares a common role with PrP in neuroprotection (Premzl et al., 2003; Watts & Westaway, 2007). All these three PrP family members seem to be widely conserved in nature because relatives are also present in fish, with two duplicated Doppel paralogs , called PrP-rel-1 and PrP-rel-2 (rel=relative) and possibly two likewise duplicated Shadoo homologues, Sho-1 and Sho-2 (Rivera-Milla et al., 2006; Premzl et al., 2004).

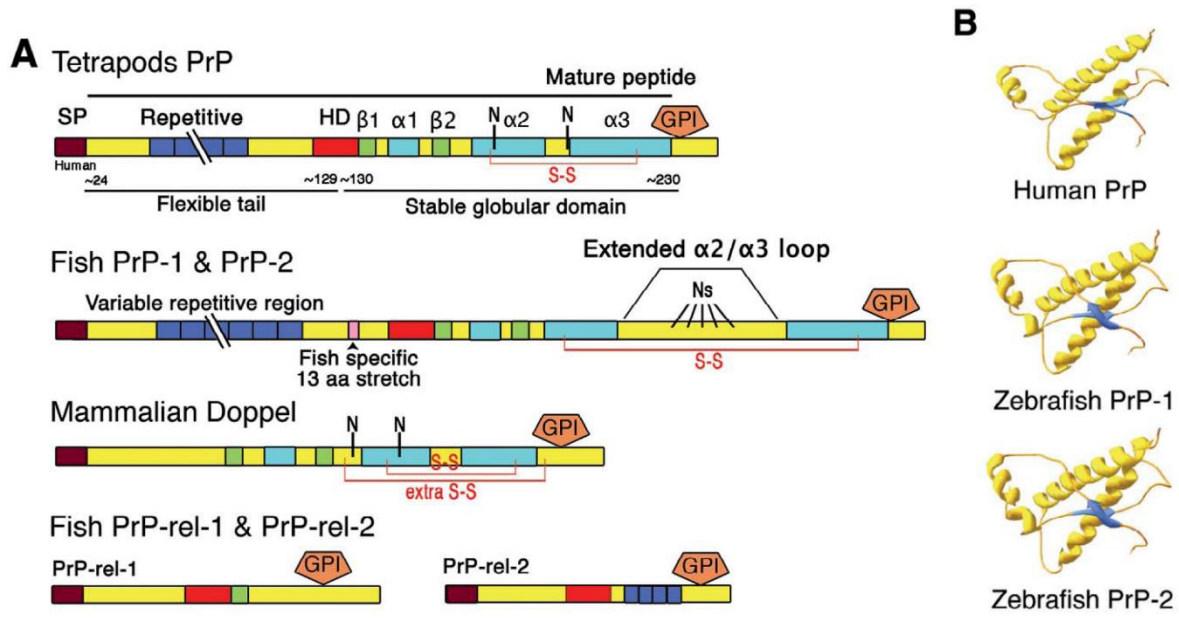

Figure 1.3.2 PrP structural diversity in vertebrates. A. Distribution of landmark motifs in PrP, Doppel, and PrP-rel proteins of tetrapods and teleost fish. Tandem repeats are shown in blue, hydrophobic domains (HD) in red, β-strands in green, α- helices in cyan, and the fish-specific 13 aa motif in pink. S*p* = signal peptide; orange pentagons = GPI-anchors; N = glycosylation sites; and S-S = disulfide bridges. Breakpoints in repetitive regions indicate length variation. **B.** 3-D structures of human (based on 1QLX.pdb model) and zebrafish (predicted) PrP-1 and -2 globular domains. Zebrafish loops α-1/β-2 and α-2/α-3, predicted to be unstructured, were shortened to the length of their human counterparts for comparative purposes. Figure and caption taken from (Rivera-Milla et al., 2006).

Knockout mice and links to pathophysiology:

The conversion of normal, cellular PrP (PrP^{c}) into a pathogenic conformation, called PrP^{sc} (for scrapie), is known since long as the molecular event leading to prion-induced neurodegeneration (Prusiner et al., 1988). During this process, the predominantly α-helical structure of PrP^{c} turns into a β-sheets-rich isoform that is resistant to proteinase K digestion and progressively accumulates within the brain (Pan et al., 1993). PrP^{c} has a half-life of 3-6 h at the cell surface, before it becomes internalized and degraded (Chakrabarti et al., 2009; Borchelt et al., 1990). Conversion into the pathogenic isoform PrP^{sc} leads to a stabilization of the protein with a prolonged half-life of >24 h which is thought to be one of the reasons behind the accumulation of prion amyloid fibrils in neurons (Ertmer et al., 2004). PrP^{c} is converted into PrP^{sc} at the plasma membrane or right after its endocytic internalization on the way to the lysosomal compartment, where it accumulates (Caughey, 1993). In a key discovery, it was shown that host PrP^{c} needs the GPI-anchorage and its physiological glycosylation for exogenous prions in order to induce brain disease (Chesebro et al., 2005; Tuzi et al., 2008). The question as to whether the neurotoxic effect of the PrP^{sc} isoform is due to a novel function, gained by conversion/aggregation, or to the loss of a normal PrP^{c} function is not fully resolved yet. In either case, PrP^{sc} constitutes the basis of the infectious particle that causes prion disease, and it is widely accepted that only PrP^{c} and PrP^{sc} are needed for successful transmission, without the requirement of additional viral or bacterial elements (Prusiner, 1982).

PrP knockout mice are relatively normal and show no obvious phenotypes, making it difficult to ascertain the physiological function of PrP (Büeler et al., 1992). Although genetic compensation and developmental plasticity may mask the real phenotype for PrP function in knockout mice, one “phenotype” is clear: these animals are resistant to prion infection and they do not develop prion disease or replicate prions, which demonstrates vividly that the host protein is indispensable for the disease to develop (Málaga-Trillo & Sempou, 2009; Steele et al., 2007; Büeler et al., 1993). More detailed analysis revealed sleep disturbances and altered circadian rhythm in PrP knockout mice, implicating PrP in sleep mechanisms and linking this function to a mutation in the *Prnp* gene which triggers a disease called fatal familial insomnia (Tobler et al., 1996; Lugaresi et al., 1998). Interestingly, CJD patients also develop sleeping disorders (Cohen et al., 2014). Unfortunately, the exact underlying molecular mechanisms are not clear and no cures are available for now.

PrP`s ability to bind Cu^{2+} initially led to the assumption that it is involved in defense mechanisms against oxidative stress (Milhavet et al., 2000). Indeed, increased levels of oxidative stress markers have been found in brains of mice devoid of PrP (Wong et al., 2001). PrP also seems to contribute to immune reactions during the uptake of foreign organisms, as PrP knockout animals resist infection with various pathogens, perhaps as a result of its role in T-cell activation (Steele et al., 2007; Ballerini et al., 2006). One report demonstrated that PrP is involved in stem/progenitor cell proliferation, because hematopoetic stem cells of PrP knockout mice were not able to self-renew and these mice had less proliferating neural precursors in the dentate gyrus of the hippocampus, whereas over-expression of PrP enhanced cell proliferation in the subventricular zone (Zhang et al., 2006; Steele et al., 2006). Although PrP is widely expressed in the nervous system, it seems to be dispensable there since $PrP^{-/-}$ mice did not show problems during development or maintenance of their CNS. Although underlying compensation mechanisms that could explain this mild knockout phenotype are very likely, the closely PrP-related Doppel protein does not account for them, since double knockouts lacked a severe neuronal phenotype as well (Paisley et al., 2004). In conclusion, the basic molecular functions of PrP keep challenging scientists in the field, aiming above all at identifying therapeutic targets that could serve to ameliorate prion-related diseases, no matter whether they have been inherited, occurred sporadically or have been transmitted via infection.

PrP in the neuronal context:

The prion protein is of enormous biomedical interest because of its ability to induce neurotoxicity upon misfolding/aggregation, thus being a central element in several mammalian neurodegenerative diseases including scrapie, BSE, CJD, Kuru and the Gerstmann-Straussler-Scheinker syndrome (GSS) (Imran & Mahmood, 2011). Better insights into the molecular mechanisms of PrP^{c} function will be required in order to explain its neurotoxic properties upon misfolding. For now, though, basic data on its cellular localization and physiological function in neurons can be quite informative. For instance, the involvement of PrP in synaptic function and maintenance is suggested by its predominant localization in the axon and foremost in presynaptic, but also postsynaptic, structures in normal brains (Moya et al., 2000; Haeberlé et al., 2000; Herms et al., 1999). Notably, addition of recombinant PrP to rat hippocampal neurons *in vitro* induces rapid polarization and fast development of synapses (Kanaani et al., 2005). In $PrP^{-/-}$ mice, it was long evident that important mechanisms of brain

plasticity were affected, such as short and long term memory retention and hippocampal-dependent spatial learning (Nishida, 1997; Criado et al., 2005). Two molecular interaction partners at the cell surface have been proposed to mediate a role of PrP in memory formation: stress inducible protein 1 (STI1) and Laminin (LN) (Coitinho et al., 2006, 2007). The PrP-LN interaction has additionally been identified as a putative mechanism for recombinant PrP-induced neurite outgrowth (Graner et al., 2000). Various other studies have shown that application of recombinant PrP promotes neurite outgrowth (Chen et al., 2003; Bodrikov et al., 2011). The situation is likely to be complex, because other interaction partners for PrP-mediated neurite outgrowth have been identified. On the one hand beside LN, vitronectin has been shown to elicit PrP-induced stimulation (Hajj et al., 2007); on the other hand, the neuronal receptor NCAM was found to enhance neurite outgrowth upon PrP-activated signaling (Santuccione et al., 2005).

The requirement of PrP for normal synaptic function is consistent with the early finding of impaired long term potentiation (LTP) and memory loss in PrP-null mice, an effect attributed to reduced $GABA_A$ receptor-mediated fast inhibition (Whittington et al., 1995). In this context it is noteworthy to mention that PrP, via its capability to bind copper (Cu^{2+}) within the N-terminal octarepeat, is most probably necessary to maintain fluent neuronal communication. In brain homogenates, PrP is found in highest concentration in synaptosomal fractions. Mice devoid of PrP ($PrP^{-/-}$ mice) show synaptosomal Cu^{2+} concentrations diminished by 50% as compared to normal mice (Westergard et al., 2007). Cu^{2+} gets released by nerve endings upon depolymerization where PrP may serve as a Cu^{2+} buffer and be responsible for the re-uptake into the presynapse (Kardos et al., 1989; Kretzschmar, 2000). Moreover, PrP was suggested to buffer Cu^{2+}, but also calcium Ca^{2+} levels at the synaptic cleft indirectly by reducing their influx via L-type VGCC channels (Vassallo & Herms, 2003; Fuhrmann et al., 2006). PrP`s capacity to bind Ca^{2+} is not only important for the function of synaptic ion channels, but also for Ca^{2+}-dependent cell adhesion events. The Ca^{2+}-dependent cell-cell adhesion molecule E-Cadherin has been shown to be modulated by PrP, being the underlying force of proper cell-cell-adhesion in zebrafish cells and embryos (Malaga-Trillo et al., 2009). In this context, PrP has also been implicated in N-cadherin trafficking in growth cones of hippocampal mouse neurons (Bodrikov et al., 2011). Another molecule whose endocytosis seems to be dependent on proper PrP-mediated signaling is the postsynaptic NMDA receptor its internalization is disturbed upon amyloid-β binding to PrP, leading to excessive NMDA receptor activity,

enhanced Ca^{2+} influx and neuronal excitotoxicity (Um et al., 2012). Additionally, PrP has been found to have a neuroprotective role by counteracting and rebalancing NMDA-excitotoxicity (Stys et al., 2012). PrP was also connected directly to increased resistance to seizures: knockout mice exhibited lower thresholds to induced seizures than normal mice, whereas strains overexpressing PrP appeared to be more resistant (Walz et al., 1999; Linden et al., 2008). Various cellular roles of PrP both -non-neuronal (proliferation, differentiation, migration, adhesion) and neuronal (synapse plasticity/density, myelination)- have been attributed to altered SFK-mediated cell signaling (Nygaard et al., 2014). Particularly in the context of neurotoxicity, PrP has been reported to be the upstream activator of SFKs (Src, Fyn, Yes) thereby influencing events like endocytosis of the NMDARs and of VGCCs or proper myelination of axons (Ochs & Málaga-Trillo, 2014). Accumulating evidence shows that PrP modulates neuronal excitability and synaptic activity, and it is becoming increasingly clear that PrP functions as an upstream regulator of cell-cell communication by modulating the endocytosis and activation of many signaling molecules in neurons (Zomosa-Signoret et al., 2008; Linden et al., 2008; Málaga-Trillo & Sempou, 2009).

PART II

Specific introduction: The myelin- and ER-associated protein Nogo-A/Reticulon-4 (RTN4)

1.4. Nogo-A/RTN4

Discovery, expression & function:

Nogo-A was discovered in the late 1980s, when M. Schwab and colleagues discovered that myelin isolated from CNS (but not PNS) was non-permissive for neurite growth and cell spreading, an effect which could be abolished by simple protease treatment (Caroni & Schwab, 1988). After size fractionation and growth-permissiveness tests of myelin protein fractions, a potent growth-inhibitory membrane protein of ~250 kDa was identified and later on named Nogo-A (Caroni & Schwab, 1988). Further research showed it to be a member of the reticulon (RTN) family (GrandPré et al., 2000).

In the adult CNS, Nogo-A is mainly expressed by oligodendrocyte cell bodies and processes, localized on the innermost adaxonal and outermost myelin membranes (Huber et al., 2002). It is also expressed in projecting neurons such as the cortex, the hippocampus, spinal motor neurons, dorsal root ganglia and Purkinje neurons (Huber et al., 2002; Peng et al., 2011). Various studies have been performed to analyze the cellular localization of Nogo-A in order to get more information about the molecular processes in which it might be involved. It became evident that Nogo-A is expressed extra-, as well as intracellularly and that its cellular roles depent on its localization.

Cell surface Nogo-A:

Although Nogo-A is retained mainly intracellularly (ER-associated), a small proportion (<10%) is expressed at the surface, as was shown in oligodendrocytes, fibroblasts and various types of neurons (Oertle et al., 2003; Dodd et al., 2005). It is an extracellular molecule that exerts its inhibitory effect on neurite outgrowth and cell spreading and initiates cytoskeletal remodeling via specific receptor complexes (Vincent Pernet & Schwab, 2012; Schwab, 2004).

Nogo-A comprises two inhibitory domains. The first one is the C-terminal “Nogo-66” domain which binds to a receptor complex consistent of NgR1/Lingo1/TROY(or p75) or to the receptor PirB (Fournier et al., 2001; Atwal et al., 2008). The second one is the stronger inhibitory N-terminal “delta-20” domain which binds to a recently discovered molecular complex that incorporates the G-protein-coupled receptor sphingosine 1-phosphate receptor 2 (S1PR2) and

engages integrins (Kempf et al., 2014; Hu & Strittmatter, 2008). Both receptor/Nogo-A interactions are known to activate the RhoA/ROCK pathway, which result in depolymerization and attenuated reorganization of the cytoskeleton, in increased actomyosin contraction, as well as in reduced stabilization of microtubules in axons and growth cones (Schmandke et al., 2014). In addition to the cytoskeleton-linked blockage of Nogo-A, it was demonstrated by M. Schwab`s group that a Pincher-dependent internalization of Nogo-A also takes place, which leads to decreased cAMP response element binding protein (CREB) phosphorylation and a repressed cellular growth program (Joset et al., 2010) (Fig. 1.4). Briefly summarized Nogo-A was shown to inhibit mechanisms like neurite outgrowth, growth cone size and motility as well as neurite fasciculation *in vitro* in dissociated DRG cells and explants (Montani et al., 2009; Petrinovic et al., 2010).

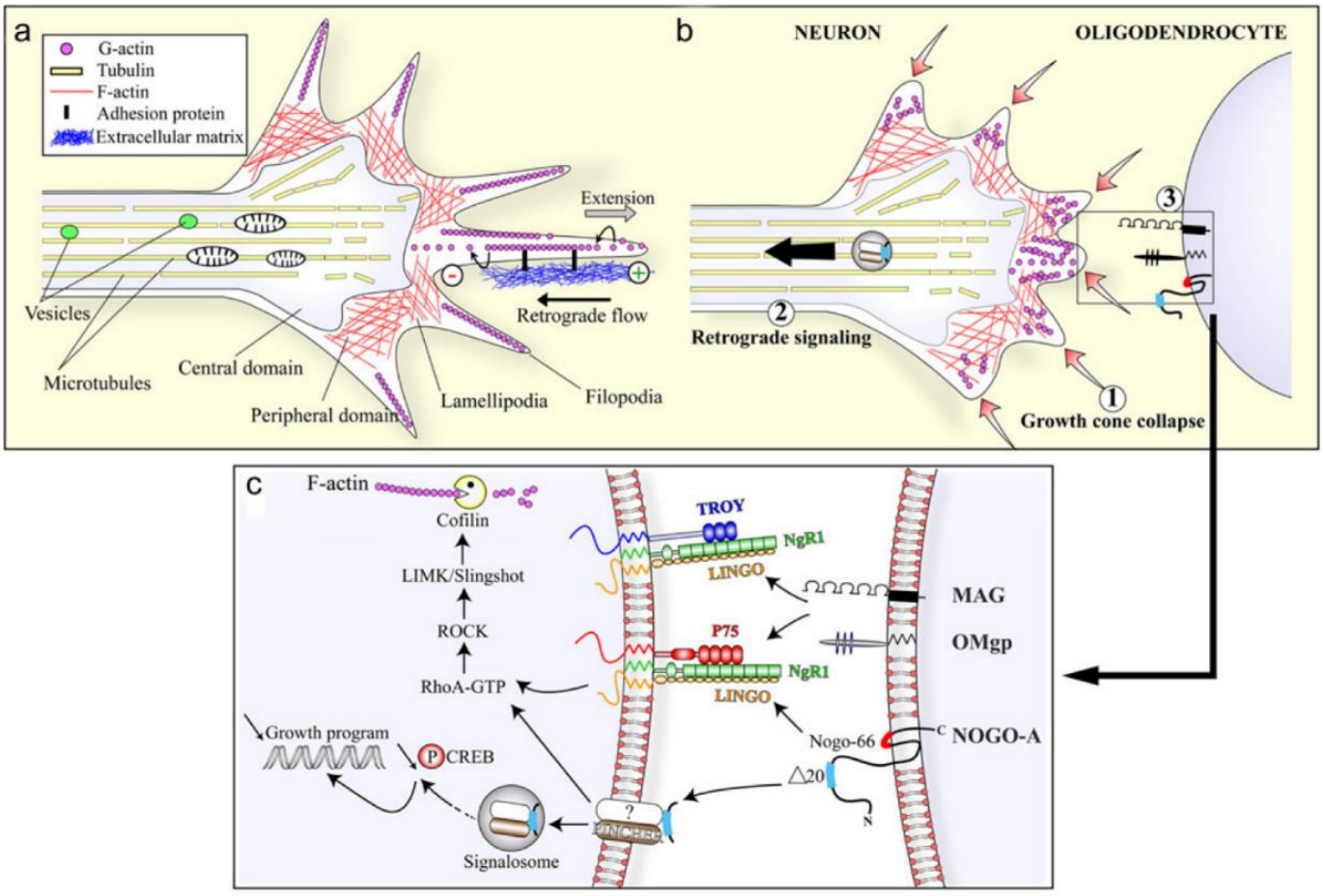

Figure 1.4.1 Molecular mechanisms of Nogo-A-mediated axonal growth inhibition. a. Organization of the growth cone. The growth cone is composed of a central domain containing the microtubules involved in the transport of organelles and of a peripheral domain in which actin filaments (F-actin) form a cytoskeleton meshwork in the lamellipodia and filopodia. The protrusion of the filopodia occurs at the plus end (+) of the actin filament and is required to allow the traction of the growth cone on the extracellular matrix. **b.** Growth cone inhibition. The contact of filopodial extensions with myelin-associated inhibitors such as Nogo-A (1) triggers the quick collapse of F-actin in the growth cone (2). The retrograde signaling is thought to mediate the long-term effects of Nogo-A on the repression of the neuronal growth program (3). **c.** Nogo-66 and other myelin inhibitors exhibited at the cell surface of oligodendrocytes bind to and stimulate a common neuronal receptor complex. The transduction of the signal passes through the intracellular activation of the RhoA/ROCK pathway and involves the actin-severing enzyme cofilin, a main effector in the disassembly of the growth cone cytoskeleton. Alternatively, the Nogo-A delta-20 region is internalized by an unknown receptor via a pincher-dependent mechanism. The uptake of Nogo-A delta-20 leads to the activation of the RhoA/ROCK/cofilin cascade. In addition, the resulting molecular complex can also be retrogradely transported in signalosomes to the neuronal cell body in which it activates RhoA, negatively regulates phospho-CREB and thereby attenuates the neuronal growth program. Figure and caption taken from (Vincent Pernet & Schwab, 2012).

Intracellular, ER-associated Nogo-A:

Being a member of the reticulon (RTN) protein family, most of Nogo-A/RTN4 is predominantly found intracellularly, associated to the membrane of the ER via hydrophobic transmembrane domains (Oertle & Schwab, 2003; GrandPré et al., 2000). Due to the special hairpin topology of the protein, Nogo-A is believed to be responsible for the tubular shaping of the ER; upon overexpression, the reticulons form high curvature membranes, whereas deletion leads to disruption of the tubular ER (Voeltz et al., 2006). Interestingly, intracellular neuronal Nogo-A was found to initiate neurite growth and branch formation *in vitro*, which implies two separate, opposing roles of Nogo-A depending on its subcellular localization (Kurowska et al., 2014). Nogo/RTN4 can inhibit neurite growth at the cell surface via specific receptors, whereas more general 'ancestral' RTN functions might relate to those of the endoplasmic reticulum, for example intracellular trafficking, cell division and apoptosis (Oertle & Schwab, 2003).

Structural features:

The RTN protein family comprises four members: RTN1, RTN2, RTN3 and RTN4/Nogo. The latter gives rise to three different proteins, Nogo-A/-B/-C, all of which share a conserved, carboxy-terminal ~200 aa reticulon homology domain (RHD) (Oertle et al., 2003). The RHD domain, also called “Nogo-66”, comprises two long hydrophobic stretches that are thought to target the reticulon proteins to the ER (Oertle et al., 2003). The N-terminal domain of RTN4/Nogo-A shares no homology with the other two isoforms and is therefore called Nogo-specific region (NSR) (Oertle et al., 2003). Both RTN4 domains inhibit neurite growth, each one acting via its own specific receptor (as described above).

Evolutionary analysis of protein sequences identified the zebrafish homologs of the inhibitory myelin-associated Nogo-A/Rtn4 protein as *rtn4a* and *rtn4b*, two isoforms resulting from the genome duplication that took place in a bony fish ancestor (Diekmann et al., 2005). Later work showed that Rtn4a is rather the closest homologue to the mammalian Nogo-B and Nogo-C isoforms (66% identity), containing only the C-terminal RHD (Nogo-66) of mammalian Nogo-A but not the NSR (delta-20) (Shypitsyna et al., 2011). Interestingly, the zebrafish RTN4b isoform turned out to be the closest homologue to mammalian Nogo-A in which the N-terminal, more potent inhibitory NSR/delta-20 domain is still present, despite sharing only ~18% identity at the amino acid sequence level (Shypitsyna et al., 2011). It had initially been thought that the growth-inhibiting properties of the NSR were either lost in fish or acquired in mammals, but then it became evident that an ancient Nogo-A homolog, including all inhibitory domains (Nogo-66 and delta-20), must have already existed in the last common ancestor of fish and tetrapods (Shypitsyna et al., 2011). This evolutionary study further showed that the NSR of Nogo-A contains four putative β-1 integrin binding motifs, called M1-M4 (Shypitsyna et al., 2011). These four motifs are highly conserved among all vertebrate species analyzed and were suggested to be the functional domains able to block various integrin complexes, thereby inhibiting cell adhesion and axonal outgrowth (Hu & Strittmatter, 2008). Of note, the NSR of Nogo-A shares substantial sequence relationship to another myelin-derived, glial scar-associated CSPG member of axon regeneration inhibitors named neurocan (NCAN), which is also known to inhibit neurite outgrowth via an integrin-dependent manner. These sequence similarities with NCAN suggest that Nogo-A originated via insertion of an NCAN-like sequence into the rtn4 gene of an early jawed vertebrate with myelinated axons (Li et al., 2000; Shypitsyna et al., 2011).

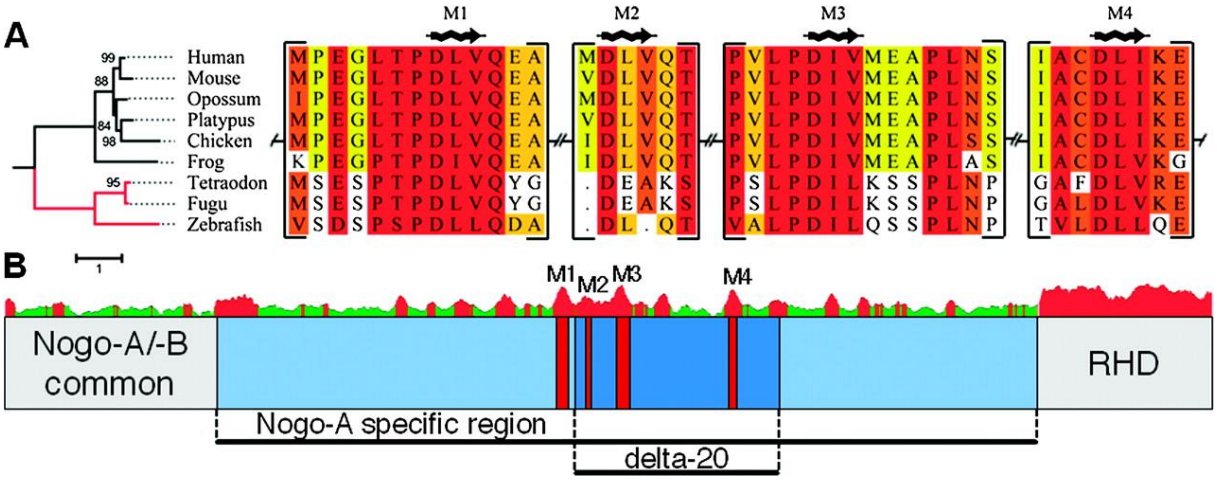

Figure 1.4.2 Nogo-A in vertebrates. (*A*) Left, phylogram showing the evolutionary relationships among vertebrate NSR amino acid sequences. The scale bar represents the number of exchanges per site. Right, multiple alignment of selected conserved clusters (in brackets) containing putative *β*1-integrin–binding motifs (M1–M4). The degree of sequence similarity is highlighted using the cyan-to-red color code. The location of the clusters along the Nogo-A polypeptide is indicated in (*B*). (*B*) Schematic representation of the entire Nogo-A alignment. Within the central NSR (light blue), the relative positions of delta-20 (dark blue) and the putative *β*1-integrin–binding motifs (red) are indicated. The percent identity plot above the scheme shows positions with identity scores higher than or lower than 50% in red and green, respectively. Figure and caption taken from (Shypitsyna et al., 2011).

Nogo-A in the neuronal context

The need to achieve better functional recovery and regeneration after CNS damage in higher vertebrates led to the generation of Nogo-A knockout mice in order to analyze their axon growth properties when the potent Nogo-A inhibitor is absent (Dimou et al., 2006). As expected, two studies reported an enhancement of corticospinal tract (CST) regeneration in the partially transected spinal cord of Nogo-A- and A/B-specific knockout mice (Kim et al., 2003; Simonen et al., 2003). Notably, this effect could not be observed by a third group, an inconsistency mainly attributed to differences in mouse strains used for the studies (Zheng et al., 2003). This problem was solved by back-crossing these Nogo-A knockout mice, which led to a consistent enhancement of regeneration *in vitro* and in transected CST axons in adult mouse spinal cords (Dimou et al., 2006). Additional microarray experiments in these mice revealed many differentially regulated genes that belonged to functional categories associated with neurite growth, synapse formation, and inflammation (Dimou et al., 2006). Interestingly, these knockout mice seemed to partially compensate the loss of Nogo-A by up-regulating other inhibitory guidance molecules in their spinal cord, like the Ephrin/Eph and Semaphorin/Plexin family members (Kempf et al., 2013). In an elegant conditional knockout model, Nogo-A was deleted either in oligodendrocytes or in RGCs during regeneration of the rat optic nerve. After cell-type specific gene ablation, only oligodendrocyte-specific knockout promoted regeneration, whereas regeneration potential was reduced upon RGC-restricted Nogo-A knockout (Vadja et al., 2015).

Cultured neurons derived from Nogo-A knockout mice displayed enlarged, more motile growth cones due to an increased activation of the Rho-GTP/LIMK1/cofilin pathway, thereby regulating the actin cytoskeleton (Montani et al., 2009). Additionally, postnatal Nogo-A knockout mice displayed more complex dendrites and stronger synaptic transmission, suggesting a negative role of Nogo-A in synaptogenesis and synaptic plasticity (Petrinovic et

al., 2013). This hypothesis is supported not only by knockout of Nogo-A but also by neutralization via Nogo-A specific antibodies, since the latter led to enhanced synaptic plasticity in rodents and the knockdown of the NgR1 resulted in increased synapse number in the developing mouse hippocampus (Zemmar et al., 2014; Zagrebelsky et al., 2010; Wills et al., 2012). All these data led to the conclusion that Nogo-A represses anatomical and functional plasticity of neurons in the CNS (Kempf & Schwab, 2013).

During embryonic development, Nogo-A seems to be important for oligodendrocyte maturation and myelination processes, as Nogo-$A^{-/-}$ mice displayed hypo-myelinated axons and delayed differentiated glia cells in optic nerves and cerebella (Pernet et al., 2008). In the developmental context, a pro-migratory effect of Nogo-A during migration of mouse embryonic cortex neurons was found, since Nogo-A deletion disturbed their tangential and radial migration patterns (Mathis et al., 2010).

In sum, Nogo-A regulates cell migration, neurite growth and myelination during CNS development, while with regard to CNS growth and plasticity in adulthood, it is thought to act as a “tonic brake”, thereby stabilizing neuronal circuits (Kempf & Schwab, 2013).

Clinical significance, axon regeneration in mammals and fish:

Neurons and surrounding glia cells upregulate Nogo-A in the spinal cord after acute injury, and after optic nerve lesion in adult rat and mice, as well as in pyramidal and interneurons after induced ischemic stroke in rats (Hunt et al., 2003; V Pernet et al., 2012; Cheatwood et al., 2008). Many attempts have been made to block the inhibitor under severe lesion conditions and indeed, function-blocking anti-Nogo-A antibodies were capable to improve regeneration and restore motor functions in spinal cord injury models in rat and primates (Liebscher et al., 2005; Freund et al., 2006). Based on the assumption that Nogo-A exerts its function via a negative modulation of the cytoskeleton blocking the Nogo-66 receptor NgR1, its associated protein Lingo-1 or the downstream signaling components RhoA all led to positive, growth-promoting effects (Li & Strittmatter, 2003; Fournier et al., 2003; Pernet & Schwab, 2012). Improved axon regeneration *in vivo* by blocking Nogo-A led to preclinical trials by the Schwab team in monkeys. The animals almost completely recovered dexterity of a paralyzed arm and hand after a cervical hemi-section when perfused with Nogo-A-specific antibodies (Freund et al., 2009). Successful therapeutic administration has been already performed in a Phase I clinical trial with 52 acutely-injured para- and tetraplegic patients (Abel et al. 2011). A placebo-controlled Phase II clinical trial is in progress (Pernet & Schwab, 2012).

Interestingly, Nogo-A has also been suggested as a potential therapeutic target against auto-immune mediated diseases associated with demyelination of axons, such as multiple sclerosis (MS) or amyotrophic lateral sclerosis (ALS). For instance, blocking Nogo-A with anti-Nogo IgGs effectively suppressed disease progression in an experimental autoimmune encephalomyelitis (EAE) paradigm, a mouse model of MS (Karnezis et al., 2004). The same improving effect was recently observed in a transgenic mouse model that shows a phenotype and pathology similar to those of human ALS patients. A monoclonal antibody specific for human Nogo-A, called Ozanezumab, has already been used in a randomized, first-in-human clinical trial (Bros-Facer et al., 2014; Meininger et al., 2014).

To understand the mechanisms behind the differences in neuronal regeneration ability between mammals and fish, the inhibitory properties of the zebrafish paralogs to Nogo-A were analyzed: interestingly, fish RTN4a (=RHD/Nogo-66) was reported to be non-inhibitory to zebrafish and mouse neurons (Abdesselem et al., 2009). In contrast, the mammalian Nogo-66 domain was inhibitory to fish and mammalian neurons, an effect shown to be mediated by the GPI-linked Nogo receptor (NgR) (Abdesselem et al., 2009). The NgR, surface expressed in both species, leads to downstream Cofilin activation which results further in actin filament disassembly (Abdesselem et al., 2009). Altogether, this study hypothesizes that fish express the cognate receptor for a fish and a mammalian ligand, despite the fish ligand being non-inhibitory (Abdesselem et al., 2009). Evolutionary sequence analyzes suggests that the Nogo-66/NgR1 induced signal transduction became inhibitory only after fish-tetrapod transition (Shypitsyna et al., 2011).

The role of the second, NSR-containing, RTN4b zebrafish protein and its inhibitory potential in fish and mammalian neurons has not been evaluated so far. Recent morpholino loss-of-function experiments indicate that both RTN4a and RTN4b play essential roles during zebrafish embryonic development and patterning of the nervous system (Pinzón-Olejua et al., 2014).

2. Working hypothesis and aims of this study

2.1. PART I: Investigating the roles of neuronal Thy-1 and PrP in axon growth and regeneration

The goal of my study was to investigate if the two GPI-anchored proteins, Thy-1 and PrP, are important for neurons to regrow after injury. To this end, we chose a model organism that is able to readily regenerate after CNS injury, the zebrafish, and one that does not, the mouse. Thy-1 and PrP are well-characterized cell-adhesion and signaling molecules, both highly abundant in neurons. In addition, they are known to cluster in membrane microdomains and elicit intracellular, cytoskeleton-modulating signaling via SFKs and Rho-family GTPases (Rege & Hagood, 2006b; Stuermer, 2011a). Flotillins have also been shown to modulate neuronal process formation and regeneration (Munderloh et al., 2009). Since Thy-1 and PrP are functionally associated to flotillin proteins, here we put forward the hypothesis that they are key components of the mechanism that allows neurons to orchestrate a proper growth machinery (Stuermer, 2012). At the beginning of this project, the intrinsic role of Thy-1 and PrP in the successful regeneration of fish neurons had not been analyzed yet but preliminary experiments revealed that their levels were increased after optic nerve lesion in the fish. Therefore, we asked at first how optic nerve injury affects the expression of Thy-1 and PrP in adult fish RGCs, and second by whether they are essential key players during axon growth and regeneration. Is there a functional difference of these proteins between mice and fish? Could lesion-induced re-expression of these two molecules explain, at least in part, why fish are able to regenerate in contrast to mammals? Is there any functional interaction between both proteins and could there be a connection to flotillins? We set out to provide answers to these questions by performing gain- and loss-of-function experiments in addition to functional outgrowth and co-localization studies. To accomplish this, reliable tools had to be developed, such as specific antibodies and effective translation-blocking antisense morpholinos. From these experiments, we hoped to gain more insight into basic cellular functions of the well-known proteins Thy-1 and PrP, two molecules that have been extensively studied but whose physiological role during neuronal axon growth and regeneration have remained puzzling and contradictory in the literature. Could they belong to the category of the neuron-intrinsic, growth-promoting molecules, which fish -but not mammals- are able to upregulate during axon regeneration?

2.2. PART II: Investigating the role of the myelin- and ER-associated protein Nogo-A/RTN4b in axon growth and regeneration

Another interesting topic regarding the different regeneration potentials of fish and mammals is the contribution of extrinsic factors, like the extracellular myelin-expressed and intracellular ER-associated protein Nogo-A/RTN4. It is one of the most potent known inhibitors during axon growth and regeneration in mammals and it exerts its effect via two distinct domains, the N-terminal RHD (reticulon homology domain) and the C-terminal NSR (Nogo-specific region). While mammals produce a hostile environment after CNS lesion, fish offer a more supportive substrate for growth (Bastmeyer et al., 1993). The Nogo-A/RTN4 protein was originally proposed to be one of the molecules making the difference between fish and mammals (Diekmann et al., 2005). Meanwhile we know that among the zebrafish duplicates (RTN4a and RTN4b), only RTN4b is the functional fish counterpart of mammalian Nogo-A (Shypitsyna et al., 2011). Since the shortened version RTN4a, comprising only the RHD of mammalian Nogo-A, was reported to be non-inhibitory, we asked whether the complete duplicate, RTN4b, encompassing RHD plus NSR, would exert an effect on growing neurons in culture (Abdesselem et al., 2009). To this end, we generated recombinant fish RTN4b protein and analyzed its effects on zebrafish and mammalian neurons *in vitro*. Furthermore, we wanted to characterize the expression pattern of the newly discovered fish RTN4b protein in the fish retina before and after optic nerve lesion, and find out if there are any intrinsic contributions of fish RTN4b during regeneration. Therefore, we generated a RTN4b antibody to analyze its expression and to control subsequent morpholino-mediated downregulation of the protein. Firstly, we monitored the growth potential of fish RGCs after knockdown of RTN4b in a retinal explant outgrowth study, analyzing the contribution of intracellular fish Nogo-A to axon regeneration. Secondly, we addressed the question as to whether the fish version of Nogo-A would be as inhibitory to neuronal growth as its myelin-associated mammalian counterpart. Furthermore, we were interested to determine whether the four conserved integrin-binding motifs (M 1-4) within the NSR are indeed mediating the C-terminal inhibitory function of mammalian Nogo-A. We investigated this aspect using the recombinant peptides as substrates to mouse and fish neurons in various outgrowth assays, thereby determining the inhibitory differences between Nogo-A in regenerating and non-regenerating species.

3. Materials

3.1. Organisms, cell lines and cell culture media

Organism		**Maintenance**
Mouse C56BL/6J; PrP knock-out (*prnp* $^{-/-}$)		Animal research facility University of Konstanz, purchased from Adriano Aguzzi (Clinical Trials Center Zürich, Switzerland)
Mouse C56BL/6J; wild type		Animal research facility University of Konstanz
Zebrafish; wild type		Animal research facility University of Konstanz
Primary culture		**Medium**
Mouse hippocampal neurons		Neurobasal-A medium (serum free, 1x B27 Supplement®, 10 µg/ml streptomycin, 10 U/ml penicillin, 0.1 mg/ml gentamycin, 25 µM L-glutamin, 5 ng/ml bFGF (10 µg/ml after 2 dic)
Zebrafish retinal mini explants		Leibovitz`s L-15 medium, 2.5 mM HEPES, 1% FCS, 10 U/ml penicillin, 10 mg/ml streptomycin and 0.1 mg/ml gentamycin, 5 ng/ml bFGF
Zebrafish retinal ganglion cells		L-15 medium, 2.5 mM HEPES (Sigma, US), 10% FCS, 10 µg/ml streptomycin, 10 U/ml penicillin, 0.1 mg/ml gentamycin and 25 µM L-glutamine, 5 ng/ml bFGF (10 ng/ml after 2 days)
Cell line	**Biological source**	**Medium**
CAD cells	Catecholaminergic neurons from mouse (CNS, semi-adherent)	50% DMEM, 50% F12 Nutrient Mixture (Ham), 2 mM L-glutamine, 10% FCS, 10 µg/ml streptomycin, 10 U/ml penicillin
CHO cells	Ovary from hamster (epithelial, adherent)	DMEM, 2 mM L-glutamine, 10% FCS, 10 µg/ml streptomycin, 10 U/ml penicillin, pyruvate
HEK-293 cells	Kidney, embryo from human (epithelial, adherent)	DMEM, 2 mM L-glutamine, 10% FCS, 10 µg/ml streptomycin, 10 U/ml penicillin
HeLa cells	Cervix from human (epithelial, adherent)	MEM, 2 mM L-glutamine, 10% FCS, 10 µg/ml streptomycin, 10 U/ml penicillin
HpL-3-4-PrP-deficient cells	Hippocampal neurons from mouse (adherent)	DMEM, 2mM L-glutamine, 10% FCS, 10 µg/ml streptomycin, 10 U/ml penicillin
Myeloma cells SP2/0	Spleen cells from mouse fused to mouse myeloma, HAT sensitive (suspension)	SP2/0 medium: DMEM+GlutaMAX, 10% FCS, 2mM L-glutamine, 10 µg/ml streptomycin, 10 U/ml penicillin HAT selection medium: DMEM+GlutaMAX (1x), 10% FCS, 10x HAT, 2mM L-glutamine, 10 µg/ml streptomycin, 10 U/ml penicillin in RPMI medium
PC 12 cells	Adrenal gland phaeochromocytoma from rat (adherent)	DMEM, 2 mM L-glutamine, 10% FCS, 10 µg/ml streptomycin, 10 U/ml penicillin, pyruvate

Bacteria	Medium
E. coli DH5 alpha TOP 10 BL21-CodonPlus (DE3)-RIPL (Stratagene)	Luria-Bertani (LB) medium: 1% (w/v) Bacto tryptone, 0.5% (w/v) Bacto yeast extract, 1% (w/v) NaCl, pH 7, autoclaved
	LB agar: 1% (w/v) Bacto tryptone, 0.5% (w/v) Bacto yeast extract, 1.5% (w/v) Bacto agar, 1% (w/v) NaCl, pH 7, autoclaved
	To obtain a selection medium Kanamycin or Ampicillin are added to a final concentration of 50 g/ml or 100 g/ml, respectively.

3.2. Morpholino antisense oligonucleotides (Gene Tools, LLC)

Morpholino	Sequence (3´-Lissamine)	Stock solution
PrP-2 MO1 (Málaga-Trillo et al., 2009)	5'-CCA AGG GAC AAC AAT CGC CCA AGA G-3'	1 mM
PrP-2 MO2 (see above)	5'-AGG ACT CGC TTA AAA CAG CCC GAA G-3'	1 mM
RTN-4b MO1 (Pinzón-Olejua, Welte, Abdesselem, Málaga-Trillo, & Stuermer, 2014)	5'-CCA CTG CGG GAG AAC TCA GAA CAG C-3'	1 mM
RTN-4b MO2 (see above)	5'-GCT CGT TCT GTG TCC TCC ATC GGG A-3'	1 mM
Standard control oligo	5´-CCT CTT ACC TCA GTT ACA ATT TAT A-3´	1 mM
Thy-1 MO1	5´-ATG CTA GAG ATG TTG CGT TAT AGA C-3´	1 mM
Thy-1 MO2	5´-ACG GTG CAC AGC AAA AAT CCT TCT T-3´	1 mM
Morpholino working solution	**Recipe**	
Gelfoam sponge administration	140 µM or 70 µM (0.425 µg/µl or 0.2125 µg/µl) in zebrafish Ringer`s solution	
Injection of zebrafish embryos	1 ng/nl morpholino and 0.125% (v/v) Phenol Red (Sigma) in 1x Danieau buffer	

3.3. Solutions and buffers

Zebrafish buffers	
50x Danieau buffer	2.9 M NaCl, 35 mM KCl, 20 mM MgSO4, 30 mM Ca(NO3)2, 250 mM HEPES pH 7.6, sterilized
60x E3 embryo medium	300 mM NaCl, 10.2 mM KCl, 19.8 mM CaCl2, 19.8 mM MgSO4, autoclaved
Zebrafish Ringer`s	116 mM NaCl, 2.9 mM KCl, 1.8 mM CaCl2, 5 mM HEPES, pH 7.2
Buffers for isolation of proteins from zebrafish embryos tissues	
Deyolking buffer	1/2 Ginzburg Fish Ringer without Calcium: 55 mM NaCl, 1.8 mM KCl, 1.25 mM NaHCO3
Lysis buffer	20 mM Tris-HCL pH 7.5, 2 mM EDTA, 100 mM NaCl, 5 mM MgCl2, 1% Triton™- X-100, 10% (v/v) glycerol, 1x Protease/Phosphatase inhibitor
Washing buffer	110 mM NaCL, 3.5 mM KCl, 2.7 mM CaCl2, 10 mM Tris-HCl pH 8.5

Buffers for isolation of proteins from brain and retina tissues	
RIPA lysis buffer	50 mM Tris-HCL pH 7.5, 150 mM NaCl, 1% SDS, 1% NP-40, 0.5% Deoxycholate, 1mM NaF, 1x protease inhibitors
Tissue homogenization buffer	50 mM Tris-HCl pH 7.4, 0.32 mM sucrose
Buffer for deglycosylation of proteins	
PNGase/N-Glycosidase F buffer	250 mM H2PO4, 50 mM EDTA, 0.5% SDS, 1% ß-mercaptoethanol added freshly
Buffers for purification of proteins from bacteria under denaturating conditions	
Elution buffer	100 mM Tris-HCL pH 8.0, 2 mM glutathione, 2 mM EDTA, 10 mM DTT
Lysis buffer	1x PBS, 2 mM EDTA, 5 mM DTT, 8 M Urea, 1x Protease inhibitors
Washing buffer	1x PBS, 2mM EDTA, 10 mM DTT
Buffers for purification of proteins from bacteria under native conditions	
Elution buffer	100 mM Tris-HCL pH 8.0, 2 mM glutathione, 2 mM EDTA, 10 mM DTT
Lysis buffer	1x PBS, 2 mM EDTA, 10 mM DTT, 1x Protease inhibitors
Washing buffer	1x PBS, 2mM EDTA, 10 mM DTT
Buffers for peptide affinity purification of antibodies	
10x coupling buffer	500 mM Tris, pH 8.5, 50 mM EDTA
Blocking buffer	50 mM cysteine, 50 mM Tris pH 8.5, 5 mM EDTA
Elution buffer/100 mM citrate buffer	1M citric acid monohydrate (pH 1.5) titrate to pH 3 with 1 M tri.Na-citrate-2 hydrate (pH 8.2) and dilute 1:10 with aqua bidest
High salt washing buffer	1 M NaCl
NET buffer	50 mM Tris pH 7.4, 150 mM NaCl, 5 mM EDTA
NET/Salt/Detergent	20 mM Tris pH 7.4, 0.5 M NaCl, 0.5% NP40
NET/Salt/Detergent/EDTA	20 mM Tris pH 7.4, 150 mM NaCl, 0.5% NP40, 5 mM EDTA
Neutralization buffer	1 M Tris-HCl pH 8.5-9
Storage buffer	1x PBS, 0.05% sodium azide (NaN3)
Buffers for IgG purification of antibodies	
Elution buffer	100 mM glycine pH 3
Neutralization buffer	1 M Tris-HCl pH 9
Washing buffer	20 mM Na3PO4

Buffers for SDS-PAGE and Western Blot	
1x PBS	137 mM NaCl, 2.7 mM KCl, 10 mM Na2HPO4, 2 mM KH2PO4. Adjusted to pH 7.4 with HCL
5x protein loading Läemmli buffer	2% (v/v) SDS, 40% (w/v) Glycerol, 0.00625% (w/v) Bromophenol blue, 5% (v/v) β-Mercaptoethanol
Blocking solution	3% milk powder or 3% BSA in 1x PBS
Blotting buffer	0.2 mM TRIS-Base, 150 mM Glycine, 25% (v/v) Methanol
Coomassie destain solution	40% MeOH, 7% acetic acid
Coomassie solution	1 g Coomassie Blue, 400 ml MeOh, 100 ml pure acetic acid, adjusted to 1 l H2O bidest, filtration
PBST	1x PBS, 0.05% Tween
Ponceau solution	0.1% Ponceau S (w/v), 5 % acetic acid (w/v)
SDS-PAGE running buffer	0.25 M TRIS-HCl, 2 M Glycine, 1% (w/v) SDS pH 8.3
Separating gel mix (50 ml)	50 ml 1,5 M Tris pH 8,8 (= 9.08 g) + 2 ml 10% SDS (= 0.4 % SDS, 1:25)
Stacking gel mix (40.5 ml)	37.5 ml 1 M Tris pH 6.8 + 3 ml 10% SDS (= 0.8% SDS, 1:12,5)
Stripping buffer	0.5 M NaCl solution, 0.04 M acetic acid
Buffers for IHC, ICC	
1x PBS	137 mM NaCl, 2.7 mM KCl, 10 mM Na2HPO4, 2 mM KH2PO4, adjust to pH 7.4
Blocking solution	3% BSA in 1x PBS, pH 7.3
Fixation soltution	4% (w/v) PFA in 1x PBS
Mounting solution for retinae and cells	Mowiol 4-88 in 1x PBS
Mounting solution for zebrafish embryos	25, 50, 75, 100% glycerol in 1x PBS
PBS-DT	1x PBS / 0.1% Triton™ X-100 / 1% DMSO
PBS-T	1x PBS / 0.1% Triton™ X-100
Permeabilization solution	0.25% Triton™ X-100 in 1x PBS
Buffers for molecular cloning, agarosegel elektrophorese	
50x Tris-acetate-EDTA (TAE) running buffer	2 M Tris acetate, 1 M Glacial acetic acid, 0.5 M EDTA
6x DNA loading buffer for agarose gels	0.25% (w/v) Bromophenol blue, 0.25% (w/v) Xylene cyanol FF, 15% (w/v) Ficoll (type 400) in water
Buffers for ISH	
BCL buffer (20 ml)	2 ml 1 M Tris-HCL pH 9.5, 1 ml 1 M MgCl2, 2 ml 1 M NaCl, 200 µl 10% Tween-20, 14.8 ml H2O
DEPC-H_2O	0.1% DEPC, stir overnight and autoclave
Hyb-buffer (50 ml)	25 ml formamide, 12.5 ml SSC 20x, 500 µl Tween-20 10% 25 mg torula yeast RNA, 50 µl heparin (50 mg/ml), adjust to 50 ml with H2O
NBT/BCIP/X-phosphate staining solution	4.5 µl NBT (50mg/ml), 3.5 µl in1 ml BCL buffer
SSCT (2x)	5 ml SSC (saline soudium citrate), 50 µl Tween-20 10%, adjust to 50 ml H2O
PBS and PBS-T prepared in DEPC H2O!	

3.4. Kits

Kit	Source
Bio-Rad Protein Assay Kit I	Bio-Rad, cat. no: 500-0001
Bradford Reagent	Sigma-Aldrich, cat. no: B6916
DIG RNA Labeling Kit (SP6/T7)	Roche, cat. no: 11175025910
GeneJET™ Plasmid Miniprep Kit	Fermentas, cat. no: K0502
GoScript™ Reverse Transcription System	Promega, cat. no: A5001
LightCycler® FastStart DNA Master SYBR Green I	Roche, cat. no: 12239264001
QIAquick Gel Extraction Kit	QIAGEN, cat. no: 28706
QIAquick PCR Purification Kit	QIAGEN, cat. no: 28106
ReliaPrep™ RNA Cell or Tissue Miniprep Systems	Promega, cat. no: Z6112
RNeasy Mini Kit	QIAGEN, cat. no: 74106
SuperScript™ First-Strand Synthesis System for RT-PCR	Invitrogen, cat. no: 11904-018
SuperSignal West Pico Chemiluminescent Substrate	Thermo Scientific, cat. no: 34080
TOPO® TA Dual Promoter Kit with pCR®II-TOPO® TA vector	Life Technologies, cat. no: K460040

3.5. Enzymes

Enzyme	Source
Avian Myeloblastosis Virus (AMV) Reverse Transcriptase	Promega, cat. no: M5101
Calf Intestinal Alkaline Phosphatase (CIAP)	New England BioLabs, cat. No: M0290S
Restriction enzymes	All from Fermentas
DNase I	Thermo Scientific, cat. no: EN0521
N-Glycosidase F	Roche, cat. no: 06538355103
Papain	Sigma-Aldrich, cat. no: P4762
Phusion™ High-Fidelity DNA polymerase	Finnzymes, cat. no: F-530S
Platinum®Taq polymerase	Invitrogen, cat. no: 10966018
Proteinase K	Roche, cat. no: 03115887001
Ribonuclease H (RNase H)	Invitrogen, cat. no: 18021-071
SP6/T7 polymerase	Roche, cat. no: 11175025910
SuperScript® II Reverse Transcriptase	Invitrogen, cat. no: 18064-014
T4 DNA Ligase	New England BioLabs, cat. no: M0202S
Topoisomerase I	Invitrogen, cat. no: 38042-024

3.6. Antibodies and dyes

Primary antibodies	**Source**
mAb mouse anti-GFP	Roche, cat. no: 11814460001
mAb mouse anti-human flotillin-2 (ESA-epidermal surface antigen)	BD Biosciences, cat. no: 610383
mAb mouse anti-zebrafish Thy-1 89/9	C. Stuermer laboratory (Germany)
mAb mouse anti-GST	Sigma, cat. no: G 1160
mAB rat anti-mouse THY-1 CD90.2	Thermo Scientific, cat. no: 14-0902-82
mAB rat anti-mouse THY-1 CD90.2	BD Pharmingen, cat. no: 553004
mAB rat anti-mouse Thy-1 (53-2.1)	Santa Cruz Biotechnology, cat. no: sc-18914
pAb goat polyclonal anti-alpha-actin	Santa Cruz Biotechnology, cat. no: sc-1615
pAb goat anti-GST	Amersham Biosciences, cat. no: 27-4577-01
pAb rabbit anti-mouse CLIMP-63	H. Farhan laboratory, BITg (Switzerland)
pAb rabbit anti-mouse phospho-Cofilin	Cell signaling, cat. no: 3311
pAb rabbit anti-alpha-tubulin	Abcam, cat. no: ab15246
pAb rabbit anti-human flotillin-2 (F1680)	Sigma, cat. no: F1680
pAb rabbit anti-human Thy-1	Cell Signaling, cat. no: 9798
pAb rabbit anti-mouse PrP	A. Aguzzi Laboratory (Italy)
pAb rabbit anti-zebrafish PrP-2 981	C. Stuermer laboratory (Germany)
pAb rabbit anti-zebrafish RTN4b K1121	C. Stuermer laboratory (Germany)
pAb rabbit anti-mouse phospho-Src (Tyr527)	Cell Signaling, cat. no: 2105
pAb rabbit anti-mouse phospho-Src (Tyr416)	Cell Signaling, cat. no: 2101
pAb rabbit anti-zebrafish Thy-1 4716	C. Stuermer laboratory (Germany)
Secondary antibodies	**Source**
Cy3-conjugated donkey anti-mouse IgG	Jackson ImmunoResearch, cat. no: 715-165-150
Cy3-conjugated donkey anti-rat IgG	Jackson ImmunoResearch, cat. no: 712-165-150
Cy5-conjugated goat anti-rabbit IgG	Jackson ImmunoResearch, cat. no: 111-165-144
Alexa488 goat anti-rabbit IgG	Invitrogen, cat. no: A-11034
Peroxidase-conjugated goat anti-rat IgG	Sigma-Aldrich, cat. no: A9037
Peroxidase-conjugated goat anti-mouse	Jackson ImmunoResearch, cat. no: 115-035-003
Peroxidase-conjugated goat anti-rabbit IgG	Jackson ImmunoResearch, cat. no: 111-035-144
Peroxidase-conjugated goat anti-rat IgG	Sigma-Aldrich, cat. no: A9037
Other dyes/labels/markers	**Source**
DAPI	Sigma-Aldrich, cat. no: D9542
Alexa Fluor® 488 Phalloidin	Invitrogen, cat. no: A12379
Alexa Fluor® 568 Phalloidin	Invitrogen, cat. no: A12380
Dextran, Alexa Fluor® 488	Molecular Probes, cat. no: D-22910
PageRuler™ Prestained Protein Ladder	Thermo Scientific, cat. no: 26616
Quick-Load® DNA Ladders (1 kb, 100 bp)	New England BioLabs, cat. no: N3232S, N0467S

3.7. List of primer oligonucleotides for molecular cloning, ISH and qRT-PCR

Primer name	Sequence 5´-3´	Source
Zebrafish Thy-1 GST primers:		
Thy1zf-BamH1-For	cGGATCCgcccagacatcccttaggattac	Eurofins
Thy-1zf-Xho1-Rev	gCTCGAGtcaggtctgaagcttactcttgtc	Eurofins
Zebrafish Thy-1-Fc primers:		
zfThy1-Xba	cTCTAGAatgttgtgctacaccgcctttgc	Eurofins
zfThy1-Bam	cGGATCCgtctgaagcttactcttgtcc	Eurofins
Zebrafish Thy-1-EGFP primers:		
Thy1zf-NheI-For	cGCTAGCatggcccagacatcccttaggattac	Eurofins
Thy1zf-XhoI-Rev	gCTCGAGtcaggtctgaagcttactcttgtc	Eurofins
Zebrafish RTN4b primers:		
Forward	GGGAATTCT-AGCCCGTCTCCAGACCTGCTCCAGGA-	Biomers
Reverse	GGGTCGACCTA-CTGCAGACCCTGGAGCAGCTCTGCC	Biomers
Mouse EGFP-Thy-1 primers:		
CMV_fwd_primer	CGCAAATGGGCGGTAGGCGTG	GATC
EGFP_C_primer	CATGGTCCTGCTGGAGTTCGT	GATC
In situ hybridization riboprobes:		
Thy1 5`UTR forw	GTCTATAACGCAACATCTCTAGCATTC	Biomers
Thy1 3`UTR rev1	GTTGTAAATGTGAACCAAATGCTTG	Biomers
Thy1 5`cds forw	CCTTTGCCACTCTCTTTTTACTTGG	Biomers
Thy1 3`UTR rev2	AGGTTGTGCTGATGTCAAACACTGT	Biomers
Realtime PCR:		
EF1α forward	CTGGAGGCCAGCTCAAACAT	Biomers
EF1α reverse	ATCAAGAAGAGTAGTACCGCTAGCATTAC	Biomers
Rpl13α forward	TCTGGAGGACTGTAAGAGGTATGC	Biomers
Rpl13α reverse	AGACGCACAATCTTGAGAGCAG	Biomers
ZFThy-1 A forward	TTCAAACTGTGGACAAGAGTAAGC	Biomers
ZFThy-1 A reverse	ACAGTCAGAAGACTTTGGATTTCAG	Biomers
ZFThy-1 B forward	TTGCCACTCTCTTTTTACTTGGTGT	Biomers
ZFThy-1 B reverse	GTCCACAGTTTGAATGATTGACAC	Biomers

3.8. List of DNA vectors and siRNAs

siRNA (GE Healthcare)	Target sequence 5´-3´
Control against firefly luciferase (GL2)	CGT ACG CGG AAT ACT TCG A
Mouse PrP	CTG ATT GAA GGC AAC AGG AAA (Schrock, Solis, & Stuermer, 2009)
Mouse Thy-1 SMARTpool	D-041986-01 GAG AAU AAC ACC AAG GAU A, D-041986-02 GGU CAA GUG UGG CGG CAU A, D-041986-03 GGA UGA GGG CGA CUA CUU U, D-041986-04 CCA ACC AGC CCU AUA UCA A

DNA Vector	Source / Description
pEGFP-C1	Clontech
pEGFP-mouse Thy-1	C. Stürmer laboratory, see 4.12.4.
pEGFP-mouse R1	C. Stürmer laboratory, see (Solis et al., 2007)
pCRII-TOPO	Invitrogen
pGEX-KG GST	GE Healthcare
pGEX-KG GST-zebrafish Thy-1	Cloning see 4.12.2.
pGEX-4 T-3 GST-rat RTN4b M1-4	Cloning see 4.12.3. (Shypitsyna et al., 2011)
pGEX-4 T-3 GST-rat RTN4b M1-4 D/A mutant	Cloning see 4.12.3. (Shypitsyna et al., 2011)
gGEX-4 T-3 GST-zebrafish RTN4b M1-4	Cloning see 4.12.3. (Pinzón-Olejua et al., 2014)
pIG plus-FC	Described in (Bodrikov et al., 2011)

3.9. List of reagents and chemicals

Acetic acid (Roth)
Acrylamid/Bisacrylamid 30 (Roth)
Agarose (Roth)
Ampicillin (Roth)
B 27 Supplement (Life technologies)
Bacto Agar (Becton Dickinson)
Bacto yeast extract (Becton Dickinson)
Bactotryptone (Becton Dickinson)
bFGF (Life technologies)
Bromophenol blue (Merck)
BSA, bovine serum albumine (Sigma-Aldrich)
Coomassie blue (Merck)
DMEM (Life technologies)
DMSO, dimethyl sulfoxide (Sigma-Aldrich)
DPBS (Life technologies)
EDTA (Roth)
Endo-Porter (GeneTools)
Ethidium bromide (Sigma-Aldrich)
F12 (Life technologies)
FCS (Life technologies)
Fuming nitric acid (Sigma-Aldrich)
Gentamycin (Life technologies)
Glycerol (VWR International)
Halt™ Protease Inhibitor Cocktail (EDTA free) (Thermo Scientific)
HEPES (Sigma-Aldrich)
IPTG/X-Gal (Peqlab)
Kanamycin (Roth)
L15 (Sigma-Aldrich)
Laminin (Sigma-Aldrich)
L-Glutamine (Life technologies)
Lipofectamine (Life technologies)
Lipofectamine 200 (Life technologies)
MEM (Life technologies)
Methanol (VWR International)
Mowiol 4-88 (Hoechst)
MS-222 (Sigma-Aldrich)
Neurobasal A (Life technologies)
NGF (Life technologies)
Otimem (Life technologies)
Penicillin (Life technologies)
Paraformaldehyde (Arcos Organic)
Phenol red (Sigma-Aldrich)
PLL (Culturex Trevigen)
Ponceau S (Sigma-Aldrich)
RNase Out (Life technologies)
RPMI (Life technologies)
Streptomycin (Life technologies)
Thimerosal (Sigma-Aldrich)
Tris (hydroxymethyl) aminometahne (Sigma-Aldrich)
Tris-acetate (Sigma-Aldrich)
TEMED (Roth)
TCA, trichloroacetic acid ((Merck)
Triton™ X-100 (Sigma-Aldrich)
Tween-20 (Sigma-Aldrich)
Xylene cyanol FF (Sigma-Aldrich)
Isopropanol (Fisher Scientific)

3.10. Protein purification materials

Glutathione Sepharose 4B beads (GE Healthcare)
Protein A Sepharose beads (GE, Healthcare)
Millipore Falkon (Amicon Ultra)
Protein A/G PLUS Agarose beads (Santa Cruz Biotechnology)
SulfoLink® Coupling resin Agarose beads (Thermo Scientific)

3.11. Laboratory devices and microscopes

Axioplan2 microscope (Zeiss)
Axiovert 200M microscope (Zeiss)
Confocal microscope LSM700 (Zeiss)
Lightcycler® II system (Roche)
NanoPhotometer (Implen)
Stemi 2000 stereo- microscope, Zeiss
Transjector 5246 Eppendorf
Zeiss Lumar.V12 stereomicroscope (Zeiss)

3.12. Software and databases

Addgene plasmid database (www.addgene.org)
Adobe Photoshop CS4
Alignment tool analysis:
(http://blast.ncbi.nlm.nih.gov/Blast.cgi) (http://www.genome.jp/tools/clustalw/)
Axiovision SE64 Rel. 4.9
Graphpad Prism 6, Graphpad software Inc.
ImageJ (National Institutes of Health)
Mendeley reference manager
Microsoft excel, word 2013
NCBI Reference Sequence database (http://www.ncbi.nlm.nih.gov/refseq/)
Restriction digest tool NEB cutter V2.0 @tools.neb.com
Roche Molecular Biochemicals LightCycler Software Version 3.5
Scion Image, Scion Cooperation
ZEISS ZEN 2011 SP2

4. Methods

4.1. Animal models

Wild type zebrafish (*Danio rerio*) or goldfish (*Carassius auratus*) were bred and maintained at 28°C or 23°C, respectively, at the animal facility of the University of Konstanz according to standard animal welfare proceedings.

To investigate the role of our proteins of interest (Thy-1, PrP-2, RTN4b) in neuronal growth and regeneration in the fish retina, protein expression was analyzed and morphological consequences after knockdown via antisense oligo morpholinos were checked. Biochemical studies were performed in retina, brain or embryo tissue lysates along with functional *in vitro* outgrowth assays in single RGCs, *semi-in vivo* in retinal explants or *in vivo* during optic nerve regeneration.

Wild type C57BL/6J inbred laboratory mice were also raised and maintained at the animal facility of the University of Konstanz appropriate to standard animal welfare procedures.

To investigate the roles of Thy-1 and PrP in growing mammalian neurons, loss- and gain-of-function experiments with primary hippocampal neurons of postnatal mice were analyzed in neurite outgrowth and co-localization assays. Biochemical experiments were done with entire brains of 1-3 days or 2 months old mice.

4.2. Optic nerve lesion in adult fish

Transection of the optic nerve in zebrafish was done according to the guidelines of the German Protection of Animals Act. Fish were anaesthetized in 0.03% MS-222 (Sigma, US) and operated under a dissecting microscope, body and gills covered with a wet tissue. The eye was pulled out of the orbit with bent forceps (Fine Science Tools, Heidelberg) and the optic nerve was carefully transected completely or partially from the ventral side without injuring blood vessels.

4.3. *In vivo* morpholino application to the zebrafish optic nerve

Initially, the dried lissamine-tagged antisense morpholino oligos (Gene Tools, LLC) were dissolved in distilled water to a final concentration of 1 mM. Stock solutions were kept at 4°C for short term, or as small aliquots at -20°C for long term storage. To solubilize precipitated/frozen morpholinos, they were thawed at room temperature (RT) and heated up to 55°C for 10 min in a water bath. Upon resuspension, working solutions (140 µM or 70 µM) were prepared in zebrafish Ringer`s solution and 2 µl (equates to 0.425 µg/µl or 0.2125 µg/µl,

respectively) were absorbed into a small gelfoam sponge (Pharmacia, Upjohn). For the preparation of zebrafish retinal mini-explants, a full optic nerve transection was performed (4.2.) and the morpholino-soaked sponge applied directly to the lesion site. Five days later, retinal mini-explants were prepared as described in section 4.8.1.. To study the *in vivo* regeneration potential of zebrafish optic nerves, the cut was made only partially from the ventral side, leaving a thin dorsal strand of nerve fibers intact. The morpholino-sponges were applied onto the orbit and the *in vivo* regeneration study proceeded as described in 4.9..

4.4. Morpholino microinjection of zebrafish embryos

To proof the specificity of our new antibodies via targeted protein knockdown, Western blots of morpholino-injected zebrafish embryos were performed.

Manual microinjections were carried out in early (one- to four-cell) embryo stages by means of a glass needle and micromanipulator coupled to a pneumatic transjector (Transjector 5246 Eppendorf) and monitored under a stereomicroscope (Stemi 2000 stereo- microscope, Zeiss). The injection solution contained 1 ng/nl morpholino and 0.125% (v/v) Phenol Red (Sigma) in 1x Danieau buffer and a total volume of 5 nl was injected into the yolk. Afterwards embryos were maintained in a 94 mm diameter petri dish in E3 medium at 28.5 °C and analyzed at different days post fertilization (Malaga-Trillo et al., 2009).

4.5. Fish retina preparation

After 30 min of dark adaption, adult fish were euthanized via an overdose of MS-222. To isolate the retina, the eye was transferred into a L-15- or 1x PBS-containing petri dish and all other components (lens, vitreous body, cornea, iris, pigmental cells) were carefully removed with forceps under a dissecting microscope. To remove the blood vessel layer -on top of the RGC layer- the retina was attached tightly to a black-dyed Hybond-N^+ filter (photoreceptors face down, RGCs face up) and the blood vessel carpet was carefully taken off. For all immunostaining procedures (4.15.10.1.), the retinae were incubated attached to this filter, subsequently detached and mounted with Mowiol onto a coverslip (Vielmetter & Stuermer 1989).

4.6. Preparation of Poly-L-Lysine (PLL) coated coverslips for cell culture

Glass coverslips were boiled for 30 min in fuming nitric acid (Sigma-Aldrich) for abrasion, washed, autoclaved and kept in distilled water at 4°C. Prior to use they were washed again once with distilled water and dried in multiwell plates (Greiner). Coverslips were coated with

PLL (Culturex 100µg/ml, Trevigen) for at least 1 h at RT, washed with distilled water and left to dry.

4.7. Single zebrafish RGC primary cultures

To study the morphological effects of protein knockdown (PrP-2, Thy-1) in re-growing single primary RCGs, cells were transfected *in vitro* with antisense morpholinos and neurite outgrowth was analyzed. Furthermore, we tested the effect of soluble Thy-1-GST added to the medium of RGCs in culture. Additionally, zebrafish RGCs were placed on different Nogo substrates to investigate axon-growth.

4.7.1. Zebrafish RGC culture

Fish retinae were isolated as described in 4.5. and transferred into a 15 ml Falkon tube into pre-warmed, sterile Leibovitz`s L-15 medium (Sigma, US) supplemented with 2.5 mM HEPES (Sigma, US), 10% FCS, 10 µg/ml streptomycin, 10 U/ml penicillin, 0.1 mg/ml gentamycin and 25 µM L-glutamine (all Invitrogen, CA) (~300 µl/retina). Single cells were obtained by mechanical dissociation with a P1000 micropipette, followed by a 10 min incubation to let debris settle down, and the RGCs-containing supernatant was transferred into a new Falkon tube containing 1 ml of fresh L-15 medium. Further chemical separation of cells was achieved by adding papain (Invitrogen, CA) (1:1000) and incubating for 10 min at 28°C. After a double volume dilution with L-15, the cell suspension was centrifuged for 5 min at 28°C at 800 rpm. The supernatant was discarded and the RCG-containing pellet thoroughly resuspended in fresh, 5 ng/ml bFGF (Invitrogen, CA)-containing L-15 medium (~200 µl/retina). 100 µl of cell suspension were dropped onto one coverslip (Ø 12 mm) and the RGCs let to settle down for 30 min before the medium was adjusted to 500 µl. Cells were maintained at 28°C. After 2 days, the medium was exchanged for a higher concentration of bFGF (10 ng/ml) and gentamycin was removed.

4.7.2. Morpholino transfection of single zebrafish RGCs *in vitro*, outgrowth assay

After three days in culture, when RGCs had started to develop protrusions, they were transfected into increasing concentrations of morpholinos (0.25/0.5/0.7/1/2 µM) to check for protein-specific, concentration-dependent loss-of-function effects. Efficient delivery of the antisense oligos was achieved with an amphiphilic peptide, called “Endo-Porter” provided by GeneTools. Its hydrophobic face attaches to the membrane and induces co-endocytosis of the Endo-Porter peptide together with the morpholinos. Natural acidification of the endosome

protonates the Endo-Porter that, in its ionic form, permeabilizes the endosome and releases the contents into the cytosol. First, morpholinos were diluted to the desired concentrations in fresh L-15 medium (containing 4 µg/ml bFGF) and applied to the cells. Next, the transfection reagent (Endo-Porter in DMSO, 1 mM stock solution) was applied in a final concentration of 6 µM and everything was well swirled to mix (Procedure and protocol described at http://www.gene-tools.com).

To analyze the cells via microscopy, coverslips were washed carefully three times with 1x PBS (to remove Endo-Porter precipitates), fixed 5 min with 4% PFA/1x PBS, washed three times with 1x PBS and incubated (in the dark) with Alexa-488-Phalloidin and Dapi (each 1:1000 in 3% BSA) for 4 h at RT. Cells were washed once with 1x PBS and coverslips were mounted with Mowiol onto cover glasses for epi-fluorescent analysis using a Plan-Apochromat 63x/1.4 objective and an Axioplan2 microscope (Zeiss, Jena). Cells containing the lissamine-tagged morpholino (red) in their cytoplasm (predominantly perinuclear) were chosen for measurement by means of the ImageJ software (National Institutes of Health, USA). The longest neurite -at least as long as one cell diameter- was quantified.

4.7.3. Single zebrafish RGCs cultured with Thy-1-GST as soluble substrate, outgrowth assay

RGCs were cultured for 1 day and different concentrations of Thy-1-GST were added (purification see 4.15.2.). To monitor a protein-specific, concentration-dependent effect on the neurite lengths of the neurons, concentrations of 2, 4, 6 and 8 µg/ml of the Thy-1-GST fusion protein were analyzed. Recombinant protein was diluted in L-15 medium and applied to the cells. As a control, GST was used at the highest concentration (8 µg/ml). After 3 days, cells were fixed and analyzed as described in 4.7.2..

4.7.4. Single zebrafish RGCs cultured on different Nogo substrates, outgrowth assay

Coverslips were prepared as described in 4.6., but additionally coated with 2 µg/ml of Laminin (Sigma). 200 nmol of the GST-tagged Nogo proteins (GST control, rat M 1-4-GST, M 1-4 D/A-GST, fish RTN4b-GST; protein purification see 4.15.2.) were applied either as stripes (with a silicone matrix) or to the entire coverslip, incubated for 1 h at RT, briefly washed with distilled water and dried shortly before cells and medium were added. Primary culture of retinal ganglion neurons was prepared as described in section 4.7.1.. After 3 days at 28°C, cells were fixed, stained and analyzed as described in 4.7.2..

4.8. Zebrafish retinal explant cultures

To study the potential of retinal axons to regrow after protein knockdown via morpholinos or on different Nogo substrates, outgrowth assays with cultured zebrafish retinal explants were performed (Munderloh et al., 2009; Abdesselem et al., 2009).

4.8.1. Morpholino-transfection of retinal explants, outgrowth assay

In vivo delivery of antisense oligo morpholinos (Thy-1, PrP-2, RTN4b) to retinal ganglion cells is explained in 4.3.. 5 days after the application of morpholinos to the optic nerve (time required for retrograde transport and protein knockdown), the retinae were extracted, cut into small (300x300 µm) squares with a scalpel under the dissecting microscope and kept in sterile L-15 medium. 48-Multi-Well-Plates were pre-coated with 100 µl PLL (100 µg/ml) for 1 h, washed with sterile water and dried. 1 ml of L-15 medium (2.5 mM HEPES, 1% FCS, 10 U/ml penicillin, 10 mg/ml streptomycin and 0.1 mg/ml gentamycin, 5 ng/ml bFGF) was added and the explants transferred into single wells (see Fig 4.8.1). After 24 and 48 h, live pictures of the explants were taken with a α-Plan Fluor 10x/1.45 objective on an Axiovert 200M microscope (Zeiss), coupled to a TIRF slider system. Numbers of emerging axons from the explants were measured and compared between groups, using ImageJ software (National Institutes of Health).

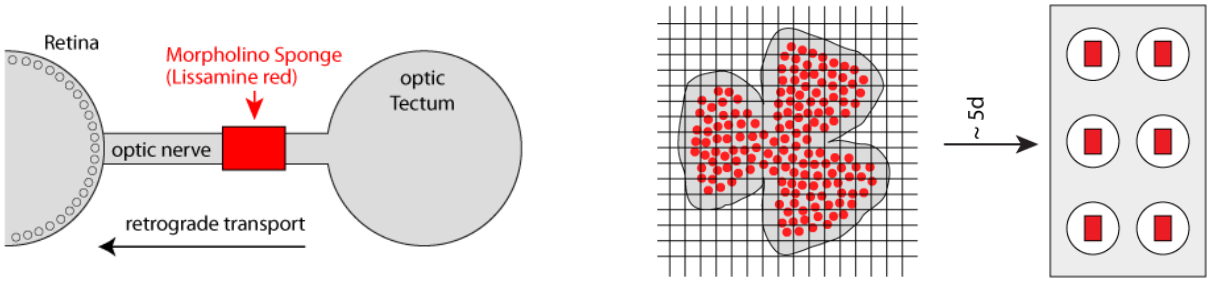

Figure 4.8.1. Preparation scheme of morpholino-treated retinal explants. The morpholino is applied to the transected optic nerve. After 5 days, retinae are cut into mini-explants in order to quantify the axonal outgrowth potential after protein knockdown.

4.8.2. Retina explants cultured on different Nogo substrates, outgrowth assay

Coverslips were coated with the recombinant GST-tagged Nogo proteins as described in 4.7.4.. Retinal explants were prepared as described previously and placed in a multi-well plate, containing 2 ml sterile, pre-warmed L-15 medium (2.5 mM HEPES, 1% FCS, 10 U/ml penicillin, 10 mg/ml streptomycin and 0.1 mg/ml gentamycin, 5 µg/ml FGF). Analysis after 24 or 48 h was performed according to 4.8.1..

4.9. *In vivo* regeneration study in zebrafish RGCs

To investigate the effect of Thy-1 knockdown on optic nerve regeneration *in vivo*, a previously established method was used (Becker et al., 2004; Veldman et al., 2007; Munderloh et al., 2009). Morpholino application to the injured optic nerve and the concentrations used are described in 4.3.. 7 days after the first cranial lesion (only dorsal part of the optic nerve) and simultaneous morpholino application, a second cut was made immediately behind (~ 2mm caudal) to measure the amount of regenerated RGC axons. During this second surgery a full optic nerve transection was carried out and a gelfoam sponge, soaked with 2 µl of Alexa488-labelled Dextran tracing solution (50 µg/µl, Invitrogen), was added. Three days later, retinae were fixed with 4% PFA and stained with antibodies or directly mounted for microscopic analysis as explained in 4.5., visualized with a Plan-Apochromat 63x/1.4 objective on a confocal microscope (LSM510 META, Zeiss). Green marked cells in the center region of the morpholino-labelled part of the retinae represented RCGs that had successfully regenerated their axons after the first ventral nerve lesion. To control that the second full optic nerve cut was indeed behind the first partial cut, only retinae that showed an exclusive green-colored belt at the periphery (= first time spared ventral nerve strand) were taken for analysis (see Fig. 4.9).

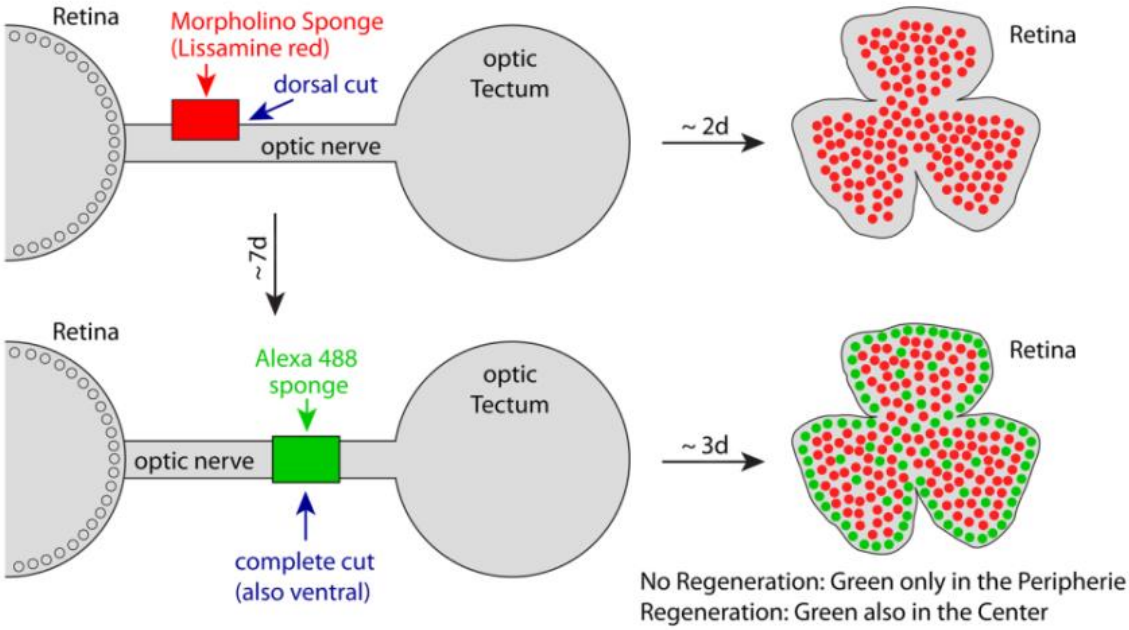

Figure 4.9 Experimental setup of the *in vivo* regeneration assay. Regeneration capacity of the transected zebrafish optic nerve after morpholino-mediated Thy-1 knockdown in RGCs is analyzed. RGCs labelled with the tracer dye Alexa488 Dextran successfully regenerated after the lesion.

4.10. Single mouse hippocampal neurons primary culture, siRNA-mediated protein knockdown, overexpression of proteins, co-localization assays

Studies of the roles of Thy-1 and PrP in mammalian neurons were performed in cultured, postnatal primary mouse hippocampal cells. Axon outgrowth potentials and co-localization assays upon protein knockdown or overexpression were analyzed (Niethammer et al., 2002; Bodrikov et al., 2008).

4.10.1. Primary hippocampal culture

Hippocampi were obtained from 1-3 days old neonatal C57BL/6J laboratory mice of either sex. Mice were killed by decapitation and the brain transferred into a small petri dish, containing sterile, pre-warmed Neurobasal-A medium (serum free, 1x B27 Supplement®, 10 µg/ml streptomycin, 10 U/ml penicillin, 0.1 mg/ml gentamycin, 25 µM L-glutamine; GIBCO). After sectioning the hemispheres, the hippocampi were isolated and carried over to a 15 ml Falkon with 1 ml of Neurobasal-A medium, 1 µl of papain was added, and mechanical and enzymatic dissociation was done with a P1000 micropipette and 10 min incubation at 37°C. Medium was adjusted to 5 ml, cells briefly resuspended again and the suspension centrifuged for 5 min at 37°C at 800 rpm. The pellet was resuspended in fresh medium (~ 1 ml/hippocampus) and 150 µl directly dropped onto PLL-coated (4.6.) coverslips. After 30 min incubation at 37°C, cells were attached to the bottom, medium was removed and replaced by 1 ml fresh Neurobasal-A medium supplemented with 5 ng/ml bFGF in a 12-Multi-Well-Plate. When the medium was exchanged after 2 days, the bFGF concentration was doubled. Cells were maintained in an incubator at 37°C and 5% CO_2.

4.10.2. Transfection of hippocampal cells with siRNA Thy-1/PrP and EGFP-Thy-1/EGFP-R1

Neurons *in vitro* were transfected with siRNA (100 pmol/ml) and DNA vectors (1 µg/ml) by means of the transfection reagent Lipofectamine 2000 (Invitrogen) according to the manufacturer`s instruction. In brief, siRNA/DNA was diluted in 100 µl of serum-free Optimem, Lipofectamine was diluted in 100 µl Optimem separately, and both were mixed and incubated for 20 min. Volume was adjusted to 300 µl with Optimem and transfection of the cells was perfomed for 2 h at 37°C. Afterwards, the transfection medium was removed and replaced by Neurobasal-A medium (1x B27 Supplement®, 10 µg/ml streptomycin, 10 U/ml penicillin, 10 ng/ml bFGF). We used siGENOME SMARTpool siRNA Thy-1 for RNA interference experiments with the target sequences: D-041986-01 5´-GAGAAUAACACCAAGGAUA-3´, D-041986-02 5´-

GGUCAAGUGUGGCGGCAUA-3´, D-041986-03 5´-GGAUGAGGGCGACUACUUU-3´, D-041986-04 5´-CCAACCAGCCCUAUAUCAA-3´. The target sequence for mouse PrP was: 5´-CTGATTGAAGGCAACAGGAAA-3´ (Schrock, Solis, & Stuermer, 2009). A commercial siRNA against firefly luciferase GL2 served as non-specific negative control (all GE Healthcare) and co-transfection with the pEGFP-C1 vector was used to label transfected cells.

4.10.2.1. Outgrowth studies

To analyze the outgrowth behavior of hippocampal neurons *in vitro*, non-confluent mouse hippocampal cells after days in culture were transfected with siRNAs plus EGFP-plasmids and fixed after two days. For visualization and further microscopic analysis the cells were fixed with 4% PFA and stained for F-actin with Phalloidin-AlexaFluor568 (1/500) and Dapi (1/1000) in 1% BSA for at least 4 h. Coverslips were mounted with Mowiol and analyzed using a Plan-Apochromat 63x/1.4 objective and an Axioplan2 microscope. Cells that were successfully co-transfected with EGFP were taken into measurements for the length of neurites with the ImageJ software (National Institutes of Health).

4.10.2.2. Co-localization studies

Putative physiological interactions between two molecules were analyzed via co-localization assay which can be used to detect the spatial overlap of different proteins of interest. After fixation, immunostaining and mounting, pictures of neurites were taken with a Plan-Apochromat 63x/1.4 objective on a confocal microscope (LSM510 META). The same microscopy settings were used for each protein dye within the different groups. For co-localization analysis, a protein cluster was defined as an accumulation of fluorescent antibody labeling with a mean intensity at least 30% higher than background. Protein clusters were automatically outlined using the threshold function of the Scion Image software (Scion Corporation). Within the outlined areas, mean intensities of the protein of interest labeling associated with another protein cluster were measured. The same threshold was used for all groups. To determine the total amount of proteins, neurites were manually outlined, and the total fluorescence along the neurite was measured (Leshchyns'ka et al., 2003; Bodrikov et al., 2005).

4.11. PC 12 cells on different Nogo substrates, spreading assay

Rat neuroendocrine PC12 cells were maintained in DMEM (10% FCS, 2 mM L-glutamine, 10 µg/ml streptomycin, 10 U/ml penicillin) at 37°C and 5% CO_2. For neuronal differentiation, cells were treated with 100 ng/ml NGF. To analyze spreading behavior, PC 12 cells were plated on 200 or 500 nmol of different recombinant Nogo-protein substrates (preparation see 4.7.4.). After 24 h in culture, the cells were stained for F-actin and prepared for microscopy as explained in 4.7.2.. Visualization was done with a Plan-Apochromat 63x/1.4 objective in an Axioplan2 microscope (Zeiss). Area or scope was measured using ImageJ (National Institutes of Health). The spreading assay was adopted from (Rubin et al., 1995; Oertle et al., 2003).

4.12. Molecular cloning

The general steps of molecular cloning encompass amplification of the target DNA (Insert) via PCR (thereby introducing the desired restriction sites), TOPO®-TA cloning (Invitrogen), ligation of the PCP product into the pCRII-Topo® vector (single 3`-A-overhangs of the insert ligated to single 3`-T-overhangs of the vector produced by terminal transferase activity of the TaqPolymerase, ligation via TopoisomeraseI) and subsequent transformation of *E. coli* bacteria. After selection, plasmid purification and sequencing, the insert was cut out of the pCRII-Topo vector (EcoRI, BamHI) and purified from the gel. Restriction digest of the insert and the vector which contains the favored tag, ligation of both, transformation of bacteria, selection of correct clones and transformation of expression bacteria strains was performed. Next, expression of recombinant proteins was induced and the product purified.

PCR setup:

Reaction batch		**Thermocycler PCR conditions**	
Template DNA	1 µl	Initial denaturation	95°C for 2 min
Primer (rev. & forw.) (10 pmol/µl)	0.6 µl each	30 cycles of: denaturation, annealing, elongation	95°C for 30 s 50-65°C for 1 min (depending on primer) 72°C for 30 s
dNTPs mixture (10 mM)	1 µl	Final elongation	72°C for 5 min
10x Taq buffer	2 µl	Cooling	4°C for ∞
RED TaqPolymerase (5U/µl)	1 µl		
Sterile H_2O	adjust to 20 µl		

Restriction digest setup:

Restriction enzyme (10 U/µl) (Fermentas)	0.5 µl each
DNA (vector or insert)	1 µg
10x reaction buffer (Fermentas)	4 µl (2x)
Total reaction volume	20 µl
Incubation time	1 h up to 16 h
Incubation temperature	depends on the enzyme, generally 37°C

Ligation setup:

Prior to ligation, the vector had to be dephosphorylated by 1 µl Calf Intestinal Alkaline Phosphatase (CIAP, 10 U/µl)) for ~1h at 37°C, to prevent self-ligation.

125 ng vector x insert length bp / Vector length bp = input insert ng	X µl insert + x µl vector (125 ng)
T4 Ligase buffer (10x, NEB)	2 µl (1x)
T4 Ligase (1 U/µl, NEB)	1 µl
Sterile H_2O	adjust to 20 µl
Incubation time	1 h
Incubation temperature	Room temperature

Production of chemically competent bacteria:

E. coli DHα5 bacteria were incubated in LB at 37°C until they reached a density of OD_{600}= 0.8. After centrifugation for 10 min at 4.000 rpm at 4°C, bacteria pellets were resuspended in 50 mM cold $CaCl_2$ and incubated for 30 min on ice. Following repeated centrifugation for 10 min at 4.000 rpm, bacteria were resuspended in cold 50 mM $CaCl_2$ + 86% glycerol (1:5 ratio) and stored at -80°C.

Transformation process:

Competent *E. coli* bacteria were thawed on ice. 50 µl of bacteria were mixed with 3 µl of ligation product and incubated for 30 min on ice. Transformation was performed by heat shock at 42°C for 1 min in a thermoblock. After chilling on ice, 500 µl of LB medium were added and the mix was shaken for 1 h at 37°C. 50 µl were spread on LB agar plates containing the corresponding antibiotic for selection and incubated overnight at 37°C. The next day, single positive colonies were picked, grown in LB medium with antibiotic, and plasmids were purified using the GeneJet Plasmid Miniprep Kit (Fermentas) and sent for sequencing (GATC, Köln). Selected colonies were grown in 6 ml of LB medium and shaken at 37°C until the OD_{600} reached 0.5. Then expression was induced with IPTG (1 mM) and shaking for another 2 h. Expression of the recombinant proteins was checked by SDS-PAGE and subsequent Coomassie staining or Western blot. Bacteria stocks were kept in 10% DMSO, or 70% glycerol at -80°C.

4.12.1. Photometric DNA / RNA concentration measurement

The photometric method is based on the Lambert-Beer's equation and utilizes the fact that the nitrogenous bases in nucleotides have a maximum absorption at approximately 260 nm. Concentrations of DNA or RNA were measured with a Nanophotometer (Implen) at a wavelength of 260 nm. An OD_{260}=1.0 corresponds to 50 µg/ml DNA or 40 µg/ml RNA and nucleic acid concentration is calculated by using the formula:

c [ng/µl] = OD_{260}nm x dilution factor x 40 (for RNA) or 50 (for DNA).

4.12.2. Cloning of zebrafish Thy-1 into the pGEX-KG- / pIgPlus- / pEGFP-C1-vector and bacterial expression of GST- / FC- / EGFP-Thy-1

The zebrafish *thy-1 cell surface antigen* (source: ZFIN ID: ZDB-GENE-030131-8561) cDNA was kindly provided by Dr. Alexander Reuter in a PCR2.1 TOPO vector (Invitrogen). The vector was sent for sequencing (GATC, Köln) and controlled for the proper insert.

To obtain recombinant, GST-tagged zebrafish Thy-1 protein as an antigen for immunization and future screening, the core protein (without leader and GPI) was amplified by PCR with the primers Thy1zf-BamH1-For cGGATCCgcccagacatcccttaggattac and Thy-1zf-Xho1-Rev gCTCGAGtcaggtctgaagcttactcttgtc (Eurofins), containing the BamH1 and Xho1 restriction sites and cloned in frame after the thrombin cleavage site of the pGEX-KG-vector (GE Healthcare). Accuracy of the insert was confirmed by sequencing (GATC, Köln) and subsequent alignment tool analysis (http://blast.ncbi.nlm.nih.gov/Blast.cgi) (http://www.genome.jp/tools/clustalw/). DHα5 bacteria were transformed and selected on ampicillin plates (Roth) supplemented with IPTG/X-GAL (Peqlab) for blue/white sorting. Positive clones were sequenced and the expression strain E. coli BL21-CodonPlus (DE3)-RIPL (Stratagene) was transformed with the plasmid carrying the correct sequence. After IPTG-induced expression, the GST-tagged proteins (~38 kDa) were purified via glutathione-Sepharose 4B beads according to the manufacturer's instructions (GE Healthcare).

For further monoclonal antibody screening and functional assays, the zebrafish Thy-1 protein (leader + IgG core, 390 bp) was introduced into the Fc-containing pIg plus vector after PCR-mutagenesis with forward primer zfThy1-Xba-5`cTCTAGAatgttgtgctacaccgcctttgc and reverse primer zfThy1-Bam-3' cGGATCCgtctgaagcttactcttgtcc. After PCR amplification and gel extraction (QIAquick Gel Extraction Kit, QIAgen) the purified PCR fragment (QIAquick PCR Purification Kit, QIAgen) was ligated into the PCR II- TOPO Vector (TOPO TA Cloning Kit, Invitrogen). DHα5 bacteria were transformed and selected with Kanamycin and IPTG/X-GAL

for blue/white sorting. With the positive clones containing the correct sequence plasmid, purification and further EcoR1 restriction digest and gel extraction were performed. After digesting the insert and pIg plus vector (CIAP dephosphorylated) with the engineered BamH1 and Xba1 sites and following ligation, bacteria were transformed and positive vectors purified for transfection. Since the leader sequence was still present in the protein, it was expected to be secreted and contained in the medium. Despite several transfections into different cell lines like HeLa, HEK, HPL-3 or CHO cells, none of them was able to produce the recombinant fish proteins.

The next approach was to introduce the core zebrafish Thy-1 protein into the pEGFP-C1 vector. This was done by amplification of the soluble core protein (without leader and GPI) and insertion of Nhe1 and Xho1 restriction sites using the primers Thy1zf-NheI-For cGCTAGCatggcccagacatcccttaggattac and Thy1zf-XhoI-Rev gCTCGAGtcaggtctgaagcttactcttgtc. After Topo®-TA cloning and positive selection, the insert and the pEGFP-C1 vector were treated with Nhe1 and Xho1 restriction enzymes, ligated and subsequently bacteria were transformed. After sequence analysis, the correct plasmid was transfected into various cells lines via Lipofectamine 2000 for expression (HeLa, HEK) but the expected fish Thy-1 protein was not expressed by the mammalian cell lines and could not be detected in Western blots.

4.12.3. Cloning and expression of rat and fish Nogo-A specific region and mutation of the conserved functional motifs M1-4

Zebrafish possess two isoforms of the mammalian Nogo-A paralogue (*rtn4* gene), called *rtn4a* and *rtn4b,* a result of a genome duplication. While RTN4a is lacking the most inhibitory part of the protein, the Nogo-A specific region (NSR), the fish RTN4b underwent divergent evolution and still retains the conserved *rtn4b-M1-M4* region (Shypitsyna et al., 2011). To analyze the inhibitory properties of this region and to compare between species, the four conserved putative functional motifs of the rat NSR were cloned into the pGEX-4T-3 GST expression vector and the most conserved single aspartic acid (D) within each motif was point mutated into Alanin (A). The rat M1-4 constructs were cloned and mutated by Dr. Aleksandra Shypitsyna based on her genomic survey (Shypitsyna et al., 2011). Transformed bacteria were obtained and GST-tagged proteins were expressed and purified according to the standard procedure (4.12.1.).

Production of a GST-tagged zebrafish paralogue of the Nogo-A Specific Region (NSR) was achieved in collaboration with Dr. Alejandro Pinzon-Olejua and Dr. Edward Malaga-Trillo

(Pinzón-Olejua et al., 2014). The purpose behind this was 1) to obtain an immunization antigen and 2) to use it as a substrate in functional outgrowth assays. The zebrafish *rtn4b-M1-M4* region (Shypitsyna et al., 2011) was amplified by PCR from a TOPO2.1 vector containing the *rtn4b* ORF (Pinzón-Olejua et al., 2014). Forward 5'-GGGAATTCT-AGCCCGTCTCCAGACCTGCTCCAGGA-3' and reverse 5'-GGGTCGACCTA-CTGCAGACCCTGGAGCAGCTCTGCC-3' primers containing EcoRI and SalI restriction sites were designed to amplify 490 base pairs including the M1 to M4 motifs. The PCR product was digested with EcoRI and SalI and cloned in frame after the thrombin cleavage site of the pGEX-4T-3 GST expression vector (GE Healthcare). All these PCR reactions were performed with the Phusion high-fidelity DNA polymerase (Finnzymes). Positive clones were sequenced and the expression strain E. coli BL21-CodonPlus (DE3)-RIPL (Stratagene) was transformed. After IPTG-induced expression, the GST-tagged protein (~48 kDa) was purified via glutathione-Sepharose 4B beads according to manufacturer's recommendations (GE Healthcare).

4.12.4. Verification of the mouse EGFP-Thy-1 vector

To investigate the effect of Thy-1 overexpression in primary mammalian neurons, cells were transfected with an EGFP-Thy-1 construct. At first, the vector had to be verified for whether the inserted *thy-1* DNA sequence would be correct. This was done by sequencing with the CMV_fwd_primer CGCAAATGGGCGGTAGGCGTG placed N-terminal of the multiple cloning site (MCS) and the EGFP_C_primer CATGGTCCTGCTGGAGTTCGT at the end of the tagged EGFP-sequence. The sequence analysis showed that the full length mouse *thy-1* (NCBI Reference Sequence: NM_009382.3) was cloned into the pEGFP-C1 vector with the leader ahead to the GFP-tag and the proximate core protein plus GPI sequence. Sequence alignment was performed using the Addgene vector database and the alignment tools mentioned above (4.12.1.).

4.13. *In situ* hybridization (ISH) against zebrafish Thy-1 in whole mount retinae

To detect the Thy-1 messenger RNA in the zebrafish retinae and to gain insight into the expression pattern before and after optic nerve transection, whole mount *in situ* hybridization (ISH) was performed. Technique adapted from guidelines of Westerfield (1995).

4.13.1. Total RNA extraction

Total RNA was isolated from zebrafish brains, using the RNeasy Mini Kit (QIAgen), according to the manual. To avoid degradation it was of great importance that everything was sterile and free of RNases and that all steps were performed on ice. RNA concentration and integrity were verified with a NanoPhotometer (Implen) and a 1% agarose gel. RNA was stored at -80°C.

4.13.2. Reverse transcription / cDNA synthesis

First strand cDNA of total zebrafish mRNA was synthesized with the SuperScript™ II First-Strand Synthesis System for RT PCR according to the protocol provided by Invitrogen. In brief, for denaturation and annealing RNA + Oligo(dT) primer + dNTPs were heated to 65°C for 5 min. After adding Reverse Transcription Buffer, $MgCl_2$, DTT, RNaseout and SuperScript®II Reverse Transcriptase enzyme, cDNA synthesis took place for 50 min at 50°C. The reaction was terminated by incubating for 5 min at 85°C and the remaining RNA was removed by adding RNaseH for 20 min at 37°C. First strand cDNA was stored at -20°C.

RNA	5 µl
Primer Oligo(dT) (0.5 µg/µl)	1 µl
dNTP mix (10 mM)	1 µl
Sterile, RNase-free H_2O	3 µl to a volume of 10 µl
10x Reverse Transcription buffer	2 µl
MgCl2 (25 mM)	4 µl
DTT (0.1 M)	2 µl
RNase Out	1 µl
SuperScript®II reverse transcriptase enzyme	1 µl final volume 20 µl

4.13.3. Hybridization probe synthesis

Specific double stranded zebrafish Thy-1 DNA was prepared by using two pairs of sequence specific primers (Thy1 5`UTR forw GTCTATAACGCAACATCTCTAGCATTC and Thy1 3`UTR rev1 GTTGTAAATGTGAACCAAATGCTTG, product size 751 bp. Thy1 5`cds forw CCTTTGCCACTCTCTTTTTACTTGG and Thy1 3`UTR rev2 AGGTTGTGCTGATGTCAAACACTGT, product size 609 bp). Thy-1 specific standard PCR was done by using the first strand cDNA as template and product quality was monitored with a 1% agarose gel. After purification of the insert (A-overhangs) with the PCR Purification Kit (QIAgen), ligation into the linearized pCRII vector (T-overhangs) was done by TOPO®-TA Cloning Kit-Dual Promotor (Invitrogen). DHα5 bacteria were transformed and selected via kanamycin and ampicillin resistance. After preparation of plasmids with the GeneJET Plasmid Miniprep Kit (Fermentas) they were

sequenced (GATC Biotech, Köln) and analyzed. The orientation of the plasmid was confirmed with the T7 promoter located upstream (control sense probe) and the SP6 promotor downstream (detection antisense probe). To synthesize the hybridization probes the plasmid had to be linearized with proper restriction enzymes that do not cut the insert (prior test with NEB cutter V2.0 @tools.neb.com), which were BamH1 for the sense and EcoRV for the antisense probe. After precipitation of the linearized DNA, homogenously labeled RNA probes were transcribed with the DIG RNA Labeling Kit (Roche) via the SP6 or T7 polymerase. The remaining DNA was digested with DNaseI and the sense and antisense RNA probes were cleaned up (RNeasy MiniKit, QIAgen) and checked in a 1% agarose gel.

4.13.4. Zebrafish retina whole mount ISH

Retinae were prepared as in 4.5., kept tightly fixed to the blackened filter. After fixation overnight at +4°C with 4% PFA, they were washed with 1x PBS prior to delipidation with 100% methanol for 30 min at -20°C (or kept for long term storage). Retinae were rehydrated in decreasing concentrations of methanol 75% / 50% / 25% in PBT for 5 min at RT and washed two times with PBT. The blood vessel layer was removed and Proteinase K (10 µg/ml) digest and postfixation with 4% PFA was performed for 15 min and 20 min, respectively. Next, tissues were put into Hyb-buffer for at least 2 h at 60°C as a pre-hybridization procedure and hybridization was done overnight with 100 ng of pre-warmed riboprobes in Hyb-buffer at 55°C in a water bath. At the next day, tissues were washed twice for 15 min with Hyb-buffer, twice with SSCT and transferred to PBT. DIG-labelled RNA probes that bound to cytoplasmic mRNA were detected with antibodies against digoxigenin and conjugated to alkaline phosphatase. Prior to this, retinae underwent a blocking step (0.5 % Blocking reagent in PBST) for 30 min, then antibody was applied overnight (1:100 in blocking solution). To equilibrate the tissues, BCL buffer was added 3 times for 5 min. The color reaction was achieved by incubation in coloration buffer (4.5 µl NBT + 3.5 µl BCIP/X-phosphate per ml of BCL buffer) in the dark at RT until a blue reaction product was visible. The color reaction was stopped with excess water. Too high background staining could be cleared with sequential ethanol washing steps (100%, 70%, 50%, 30%). After mounting the retinae with Mowiol, transcription patterns were visualized using an Axioplan 2 compound microscope (Zeiss) using Nomarski (differential interference contrast) optics.

4.14. Relative quantitative Realtime PCR (qRT PCR) of Thy-1 mRNA levels in zebrafish retinae and embryos

Quantitative Realtime PCR allows to determine the relative amount of mRNA transcripts (compared to a stable standard) by detecting the amplified dsDNA in "real time". Here we were interested in the *thy-1* gene expression profile in retinae before and after optic nerve lesion and in zebrafish embryos in a time course. Experiments were performed using the Lightcycler® SYBR GreenI system (Roche): a cyanine dye that binds to dsDNA, DNA-dye-complex emits green light and the fluorescence rises proportionally to the amount of DNA produced in each PCR cycle. By comparison to a stably expressed intern control, a housekeeping gene, a relative quantification can be done. For protocols and reviews see (Lan et al., 2009; Bustin et al., 2005; Bustin, 2002). The selection of a good reference gene that is not regulated by treatment, developmental stages or different conditions is an essential issue for normalization and quantification. Publications dealing with the validation and comparison of reference genes in D*anio rerio* are available and the two mainly recommended, most stable reference genes for developmental stages and tissue analysis in zebrafish established were chosen: **EF1α** (Elongation factor 1 alpha, α subunit of the EF1 complex) and **Rpl13α** (Ribosomal protein L13a, part of the 60s subunit). For validation of Rpl13α and EF1α as normalizer after optic nerve crush and during developmental stages in zebrafish see (McCurley & Callard, 2010; McCurley & Callard, 2008; Tang et al., 2007; Udvadia et al., 2001). Primers were ordered at Biomers according to these publications: EF1α forward CTGGAGGCCAGCTCAAACAT reverse ATCAAGAAGAGTAGTACCGCTAGCATTAC (product size 87 bp) and Rpl13α forward TCTGGAGGACTGTAAGAGGTATGC reverse AGACGCACAATCTTGAGAGCAG (product size 148 bp).

Thy-1 gene primers were designed according to common Realtime PCR primer design criteria, with one of them encompassing an intron exon boundary. Exon-intron borders were determined by aligning the genomic *thy-1* sequence in chromosome 5 (NCBI Reference Sequence: NC_007116.5) to the mRNA sequence (NCBI Reference Sequence: NM_198065.1). One primer pair was located between exon III and IV (ZFThy-1 A forward TTCAAACTGTGGACAAGAGTAAGC, reverse ACAGTCAGAAGACTTTGGATTTCAG, product size 225 bp) and one pair was between exon II and III (ZFThy-1 B forward TTGCCACTCTCTTTTTACTTGGTGT, reverse GTCCACAGTTTGAATGATTGACAC).

4.14.1. Total RNA extraction and reverse transcription / cDNA synthesis

Pooled retinae (at least 6 per group), either 5 days post optic nerve lesion or untreated, or embryos of different developmental stages (1 dpf, 3 dpf, 5 dpf, approximately 30 per group) were homogenized and total RNA was extracted under strict RNase-fee conditions following the instructions of the kit by Promega (ReliaPrep™ RNA Cell and Tissue Miniprep Systems). Subsequent treatment with DNaseI removed residues of genomic DNA. An aliquot of each extract was used for spectrophotometry to determine RNA quality and concentration. RNA with a 260/280 nm ratio between 1.95–2.2 and a 260/230 nm ratio >1 and <3 was used. 1 µg of each sample was electrophoresed on a 1% agarose gel to confirm quality. First strand cDNA was synthesized from total RNA (1 µg; 20 µl final reaction volume) with oligo(dT) priming using the GoScript™ Reverse Transcription kit (Promega) (see also 4.13.2.) according to the manufacturer's instructions in a thermocycler, including a control lacking AMV reverse transcriptase. The reaction mix was incubated for 1 h at 42°C with a subsequent 95°C step for five minutes and a cool down to 4°C.

$MgCl_2$ (25 mM)	4 µl
10x Reverse Transcription-buffer	2 µl
dNTPs (10 mM)	2 µl
Primer Oligo(dT) (0.5 µg/µl)	1 µl
RNasin	0.5 µl
AMV Reverse Transcriptase (25 U/ml)	0.6 µl
1 µg of total RNA	x µl
Sterile, RNase-free H_2O	y µl to a final volume of 20 µl

4.14.2. Relative qRT PCR

Realtime PCR reactions were performed with the reaction mix LightCycler® Fast Start Master SYBR Green I kit in a Lightcycler® II system (Roche) and monitored with a Roche Molecular Biochemicals LightCycler® Software Version 3.5. The temperature profile included: initial denaturation step at 95°C for 10 min, 40 cycles of amplification with melting at 95°C for 10 s / annealing at x°C dependent on the primers for 5 s / elongation at 72°C for 13 s and a final step at 65°C for 15 s. The 20 µl reaction batch contained:

$MgCl_2$ (25 mM)	2 µl
Primer forward (50 µM)	0.5 µl
Primer reverse (50 µM)	0.5 µl
SYBR GreenI Master Mix (incl. polymerase)	2 µl
CDNA template	2 µl
Sterile H_2O	12.6 µl to a final volume of 20 µl

4.14.3. Quantification and statistical analysis for qRT PCR

Quantification occurs at the Crossing Point (CP), at the beginning of the exponential phase, defined as the number of cycles needed for fluorescence to achieve a defined threshold level of detection which is inversely correlated with the amount of template in the reaction. The relative expression rate of the target gene was calculated via the threshold cycle difference the so called delta-delta CP ratio (Pfaffl et al., 2002):

$\delta CP = CP^{\text{target gene}} - CP^{\text{reference gene}}$

$\delta\delta\ CP = \delta CP^{\text{treatment}} - \delta CP^{\text{control}}$

Ratio = $2^{-\delta\delta\ CP} \rightarrow$ "x-times expression"

A standard error for each relative gene expression value was calculated as a measure of data variation. Student`s t-test was used to determine significant differences in mean $\delta\delta$CP values. Significance was set at $p \leq 0.05$.

4.15. Biochemical assays, Immunohisto-/cytochemistry (IHC, ICC)

4.15.1. Protein extraction from tissues (brain, retina), zebrafish embryos or cell lines

4.15.1.1. Fish or mouse brains and fish retinae

Brain and retina tissues were extracted and immediately put on ice or -20°C. The samples were homogenized in a small volume of tissue homogenization buffer and double volume of RIPA lysis buffer with the aid of a pestle and a 20-gauge needle. To prevent degradation, 1x Halt™ Protease Inhibitor Cocktail (EDTA-free) was added and lysis proceeded for ~1-2 h with rotation at 4°C. After 15 min centrifugation at 14.000 rpm at 4°C, the proteins were collected in the supernatant. Storage at -20°C.

4.15.1.2. Zebrafish embryos

Isolation of proteins from zebrafish embryos for further Western blot analysis was performed according to (Link et al., 2006). Embryos were analyzed for their Thy-1 expression in different developmental stages (1 dpf, 3dpf, 5dpf) to determine the right time-point for effective down-regulation after morpholino injection. About 30 embryos were taken per group, per stage and per treatment. After manual dechorionation under the stereomicroscope, embryos were transferred into a 2 ml tube, medium was removed, and 100 µl of deyolking buffer was added (4 µl/embryo). Deyolking was done manually by pipetting and gentle vortexing. After 30 s of centrifugation at 1.100 rpm, the supernatant was discarded and embryos were washed with

1 ml washing buffer. Washing buffer was removed by centrifugation, 30 s, 1100 rpm. Cold lysis buffer (containing 1x HALT™ Protease/Phosphatase inhibitor cocktail, EDTA-free, Thermo Scientific) was added with a volume of 50 µl (2 µl/embryo), and the tissue was homogenized with a pestle and lysed 10 min on ice. After 5 min of centrifugation at 14.000 rpm, the protein-containing supernatant was transferred into a clean reaction tube and protein concentration was measured (4.15.5.). Samples were used directly for Western blotting or stored at -20°C.

4.15.1.3. Cell lines

Lysates of any cell line (HEK, HeLa, CAD…) intended for Western blotting were prepared by washing the cells once with 1 ml of 1x PBS in the 12-Multi-Well-Plates and then adding 200 µl of cold lysis buffer (1x protease/phosphatase inhibitors). All steps of cell lysis were performed on ice. Cells were scratched from the bottom of the well, collected in a tube and disrupted thoroughly by a 20-gauge needle. Lysis occurred for at least 1 h under rotation at 4°C. After centrifugation for 15 min at 14.000 rpm at 4°C, protein concentration was determined (4.15.5.) and lysates were analyzed or stored at -20°C.

4.15.2. Purification of recombinant GST-tagged proteins

Bacteria expression strains were stored already in 10 ml of lysis buffer (buffer compositions see 3.9.) at -80°C. While thawing on ice, protease inhibitor cocktail (EDTA-free) was added. The column was equilibrated: 500 µl of glutathione-Sepharose beads (GE Healthcare) were washed 3 times by slow rotation 5 min in 10 ml of 1x PBS. Lysates were sonified 3 times 20 s, 5 cycles, max. output 60, 1 min rest on ice. After centrifugation for 30 min at 14.000 rpm at 4°C, the supernatant was added to the beads in the column. Proteins bound during slow rotation overnight at 4°C. The bead-containing solution was transferred into a dropping column and washed 3 times with 5 ml of washing buffer. Elution buffer had to be prepared fresh, and proteins were eluted slowly with 2 times 300 µl for 30 min.

4.15.3. Antigen-specific affinity purification of antibodies

Affinity-isolation of antibodies from animal sera was done with the SulfoLink® Coupling Resin (Thermo Scientific) system, were the sulfhydryl-containing antigen peptide is covalently immobilized at iodoacyl groups of the agarose resins (Fig 4.15.3). Column membranes were equilibrated with 5 ml of coupling buffer. The antigen peptide was dissolved in 50% glycine in 1x coupling buffer. 2 ml peptide solution was diluted in 5 ml 1x coupling buffer, 1 ml beads (for ~500 µg of peptide) were added and binding occurred 1 h rotating at RT. The solution was

eluted and the binding proven afterwards via SDS-PAGE plus Coomassie staining. Beads were washed with 10 ml 1x coupling buffer and then blocked for 1 h RT with blocking buffer. After washing the beads with 6 ml of high salt washing buffer (1 M NaCl) and additional 2 ml of storage buffer, binding of the antibody started. The pH of the serum was adjusted to 7.5. 2 ml of antibody-serum was applied and incubated rotating overnight at 4°C. The next day, serum was eluted and the beads washed with 10 ml NET/salt/detergent buffer and 5 ml high salt washing buffer. Antibodies were eluted in fractions with ~300 µl elution buffer, neutralized to pH 7.5 with ~800 µl of 1 M Tris-HCl (pH 8.5-9). Pooled eluates were concentrated in a Millipore Falkon tube (Amicon Ultra) with 30 kDa pore size and antibody concentration was determined. Sera were stored with thimerosal at 4°C or in glycerol at -20°C.

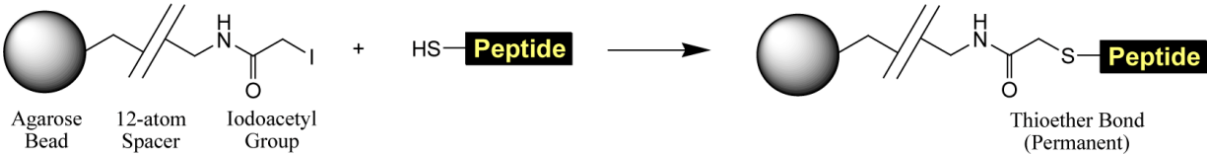

Figure 4.15.3 Scheme of the SulfoLink® Coupling Resin system. Figure taken from the instruction manual of Thermo Scientific.

4.15.4. IgG purification of antibodies

Isolation of antibodies was done by means of Protein A Sepharose beads (GE Healthcare), because bacterial protein A binds to the heavy chain of IgGs within the Fc region. 1 ml of beads was added to the column and washed with 100 ml of washing buffer. After adding 5 ml of serum, antibody binding occurred slowly rotating overnight at 4°C. The next day, the column was washed with 100 ml of washing buffer and fractions were collected with ~100 µl elution buffer into ~30 µl of neutralization buffer for a final pH of 7.5. Protein concentration was evaluated and the solution concentrated if desired (see also 4.15.3.).

4.15.5. Protein concentration measurement

4.15.5.1.1. Bio-Rad protein assay (Lowry)

The assay is based on the reaction of proteins with an alkaline copper tartrate solution and a Folin reagent. 20 µl of sample (1:10 diluted from the original) were added to 100 µl of Reagent A and 800 µl of Reagent B, vortexed, incubated for 15 min and measured at a maximum absorbance of 750 nm wavelength in a photometer. Protein concentration was determined with a BSA standard curve.

4.15.5.1.2. Sigma Bradford protein assay

The method is based on the complex formation between the dye Brilliant Blue G and proteins in solution which leads to a shift in absorbance upon binding. 500 µl of Bradford reagent (Sigma) were diluted in 500 µl of sterile H_2O and 2 µl of the sample were added. After vortexing and incubation for ~5-10 min, protein concentration was determined photometrically at the absorbance at 595 nm wavelength and compared to a BSA standard curve.

4.15.6. Immunoprecipitation assay from tissue or cell lysates

Selective isolation of proteins from tissues, bacteria or cell lysates: 1 mg of total protein in solution was applied to 1 µg of the specific antibody (or mouse/rabbit IgG control) and antigen binding proceeded rotating 4 h (or overnight) at 4°C. The next day, 30 µl of A/G agarose beads (Santa Cruz Biotechnology) were added and binding of the antibody-antigen-complex occurred 4 h (or overnight) at 4°C. The beads were washed two times with 500 µl of RIPA lysis buffer and once with 1x PBS. Immunoprecipitation was checked by SDS-PAGE in a Coomassie staining or a Western blot, as well as the putative co-immunoprecipitation components.

4.15.7. Deglycosylation assay with PNGase F (Peptide-N-Glycosidase F)

To demonstrate the glycosylation of proteins of interest (Thy-1 and PrP), the enzymatic cleavage of N-linked glyco-residues by peptide-N4-(N-acetyl-beta-glucosaminyl)asparagine amidase (N-Glycosidase F, Roche) was performed. Whole protein lysates were directly lysed in PNGase F buffer and 1 µl of PNGase F (1 U/µl) was added and incubated overnight at 37°C. After enrichment of proteins via immunoprecipitation, intended for deglycosylation, the 30 µl of A/G agarose beads were washed with 500 µl RIPA and 500 µl PNGase buffer. 12 µl of PNGase buffer (containing 1% fresh ß-mercaptoethanol) were added to the beads and boiled at 95°C while shaking. 9 µl of 3.4% NP40, 1x protease inhibitors and 1 U of PNGase F enzyme were added to the reaction and incubated overnight at 37°C. Efficient deglycosylation was verified by Western blot.

4.15.8. SDS-PAGE

For specific protein analysis, polypeptides were separated due to their molecular mass in an electric field via sodium dodecyl sulfate polyacrylamide gel electrophoresis (SDS-PAGE) according to (Laemmli, 1970**;** Sambrook & Russell, 2001, also known as "Maniatis")**.** For quantitative protein analysis, lysates containing 20 µg of protein were denatured in Läemmli buffer (1x final conc.) and boiled for 5 min at 95°C prior to separation. For simple protein

detection, cells or tissues were directly homogenized in an appropriate volume of 5x Läemmli buffer with a pestle and a 20-gauge-needle, underwent ultrasonic treatment (3 cycles, 10 s, output 30) and boiled for 5 min at 95°C before they were loaded onto the gel.

Component	Separating gel					Stacking gel
	6 %	8 %	10 %	12 %	15 %	5 %
H20	5.3	4.6	4.0	3.3	2.3	4.1
30 % Acryl-/Bisacrylamid	2.0	2.7	3.3	4.0	5.0	1.0
Sep. gel mix	2.6	2.6	2.6	2.6	2.6	-
Stack. gel mix	-	-	-	-	-	0.081
10 % APS	0.1	0.1	0.1	0.1	0.1	0.1
TEMED	0.008	0.006	0.004	0.004	0.004	0.006

4.15.9. Western blotting

After gel electrophoresis, the proteins were transferred to a nitrocellulose membrane by wet transfer at 90 V for 2 h (Towbin et al., 1979). Successful transfer was checked by 10 min Ponceau staining of the membrane. After decoloration of the Ponceau dye by washing in 1x PBS/ 0.05 % Tween (PBST), the membrane was blocked in 3% milk powder in 1x PBS for 45 min. The antibody was diluted in 3% BSA in 1x PBS in concentrations depending on the antibody and protein concentration (1:500 – 1:5.000). After removing the blocking solution, primary antibody incubation occurred overnight shaking at 4°C. The next day, after washing 3 times for 15 min in 1x PBST, the species-specific HRP-labelled secondary antibody diluted in 3% milk powder in 1x PBS (1:1000 – 1:40.000) was applied for 1.5 h RT. After washing in 1x PBST, the membranes were incubated in SuperSignal™ West Pico Stable Peroxide and Luminol/Enhancer Solution (Thermo Scientific) and developed on a High Performance Chemoluminescence film (GE Healthcare). Primary antibodies were stored at 4°C with addition of NaN_3 for reutilization and stained nitrocellulose membranes were frozen at -20°C.

4.15.10. Immunohistochemistry, Immunocytochemistry (IHC, ICC)

For expression and (co-) localization studies of proteins, cells and tissues were immunostained with specific antibodies against the proteins of interest and visualized using an Axioplan2 microscope or a confocal microscope LSM510 META (Zeiss).

4.15.10.1. Fish retina whole mount immunostainings

Fish retinae were prepared as described in 4.5.. For fixation in 4% PFA/1x PBS, tissues were incubated 10-15 min at RT and washed 3 times with 1x PBS. To stain intracellular proteins, the retinae were permeabilized for 5 min with 0.25% Triton™ X-100 in 1x PBS (Sigma). For fixation with methanol, the tissue was incubated in pure, ice-cold MeOH for 10-15 min on ice and permeabilization was omitted. Blocking was performed with 3% BSA/1x PBS for 45 min. Primary antibodies (dilution 1:100 – 1:1.000 in 3% BSA/1x PBS) were applied overnight at 4°C. Retinae were washed in 1x PBS and species-specific fluorescent-labelled secondary antibodies were added (1:1.000 in 3% BSA/1x PBS) for 1.5 h at RT in the dark. If DAPI staining was desired, the DAPI dye (1:1.000) was added to the secondary antibody solution. To detect physiological, membrane-bound proteins, the primary antibody was applied for a short time (10 min) on ice to avoid internalization (live staining). Tissues were fixed with 4% PFA/1x PBS and incubated with secondary antibodies as described previously. Mounting onto coverslips was performed under the stereomicroscope and coverslips were stored at 4°C in the dark.

4.15.10.2. Single fish RGCs and explant immunostainings

Retinal ganglion cells or explants were washed in the wells with warm 1x PBS prior to fixation with 4% PFA for 7 min at RT. Subsequently, they were washed with 1x PBS and blocked in 3% BSA/1x PBS for 40 min. If permeabilization was required, 2 min 0.25% Triton™ X-100 in 1x PBS was added and removed by washing before blocking. To stain live cells, they were blocked shortly for 15 min at RT and the antibodies were applied for short time on ice prior to fixation.

4.15.10.3. Zebrafish embryo immunostainings

Zebrafish embryos were fixed in 4% PFA/1x PBS overnight at 4°C and then washed three times in 1x PBS. After dechorionation they were washed three times in PBS-T (1x PBS/0.1% Triton™ X-100) and once in PBS-DT (1x PBS/0.1% Triton™ X-100/1% DMSO), each wash for 5 min with mild shaking at RT. Embryos were blocked in 1% goat serum (Sigma)/PBS-DT (blocking solution) for 2 h on a shaker at RT. Primary antibody was diluted (1:500) in blocking solution and incubated overnight at 4°C. Embryos were washed 3 times in PBS-DT, fluorescent secondary antibody was diluted (1:1.000) in blocking solution and applied overnight at 4°C

with mild shaking. Embryos were washed three times in PBS-T. For mounting, the yolk had to be removed with forceps under a stereomicroscope. Embryos were transferred gradually from 25, to 50 and finally 75% glycerol/1x PBS and then placed onto the coverslip in 100% glycerol for microscopic analysis. Fixed or mounted embryos were stored at 4°C.

4.15.10.4. Mouse hippocampal neurons

Primary hippocampal cells were fixed with 4% PFA/1x PBS for 10 min at RT, subsequently washed three times with 1x PBS and blocked in 3% BSA/1x PBS for 45 min at RT. If permeabilzation was required, cells were treated for 5 min with 0.25% Triton™ X-100/1x PBS prior to blocking. Antibody incubations and further steps were performed as described in 4.15.10.2..

4.15.10.5. CAD neuronal cell line

CAD cells in culture start to differentiate into neuron like cells, when deprived from serum. These cells were thought to serve as a model system for biochemical co-immunoprecipitation experiments to identify flotillin-dependent interaction partners for Thy-1 signaling. Since this cell line was new in the lab, it was firstly characterized by immunostaining and Western blot for all proteins of interest (Thy-1, PrP, flotillin…). Immunostainings on CAD cells were performed as described in 4.15.10.4..

4.16. Generation of pAbs specific for zebrafish Thy-1, PrP-2, RTN4b

Polyclonal antibodies against zebrafish Thy-1 were ordered at BIOTREND (Köln) and produced against a short peptide (15 aa, position 60-74), (N-)H-Cys-Leu-Ile-Gly-Ser-Thr-Asn-Ser-Ser-Ser-Thr-Pro-Asp-Ser-Thr-OH(-C). Two rabbit sera, called Thy-1 4716 and Thy-1 4717, were obtained and affinity purified according to 4.15.3..

Zebrafish PrP-2 polyclonal antibodies were raised against the globular domain of PrP-2 (recombinant GST-PrP-2glob) in the TFA of the University of Konstanz, affinity purified and called PrP-2 981.

The antibody against zebrafish RTN4b was generated against the recombinant protein of the conserved fish Nogo-A M1-M4 region, for cloning see 4.12.3.. After cleavage of the GST-tag with thrombin, rabbits were immunized and the serum was immuno-purified. The antibody was called K1121.

All antibodies were tested for specificity in Western blot and immunostaining with expressed recombinant proteins and after specific morpholino-mediated knockdown in zebrafish embryos and retinae.

4.17. Generation of a mAb specific for zebrafish Thy-1

The monoclonal antibody against zebrafish Thy-1 was produced against the recombinant, GST-tagged core of the Thy-1 protein (~12.6 kDa). For the cloning procedure of the antigen see 4.12.2.. Two mice were immunized against the Thy-1 antigen at the animal facility of the University of Konstanz. They were killed by cervical dislocation, B-lymphocytes were isolated from the spleen and fused to immortalized myeloma cells (cancerous B-lymphocytes, SP2/0 cells, kindly provided by Prof. Marcus Gröttrup, University of Konstanz). To select the evolved hybridoma cells, HAT medium (hypoxanthine-aminopterin-thymidine) was used, because only the fused hybridomas are able to evade the blockage of DNA synthesis by the drug aminopterin. Hybridomas are able to use hypoxanthine and thymidine to make purine nucleotides by using the HGPRT enzyme (hypoxanthine-guanine phosphoribosyltransferase). Single clones of hybridomas, which produce antibodies that recognize one specific epitope of the antigen, were achieved by sequential subcloning and screening steps. Antibodies were secreted into the medium, which was used for wide screenings in Western blots with recombinant Thy-1-GST and zebrafish embryo, brain or retina lysates. Supernatants that recognized one clean band at the expected molecular weight (~25 kDa in tissue lysate, ~38 kDa for the GST-Thy-1 fusion protein) were screened further by immunostainings of untreated and optic nerve lesioned zebrafish retinae (procedures see 4.15.9. and 4.15.10.1.). After screening all sera and hybridoma supernatants of both immunized mice for specific monoclonal antibodies, the most promising clone -89/9- was selected (see 4.15.4.). Hybridoma supernatants were tested with recombinant Thy-1, and for protein specific knockdown in Thy-1 morpholino-treated zebrafish retinae and embryo lysates by Western blots and immunostainings.

5. Results

PART I Thy-1

My aim was to analyze the expression of the GPI-anchored protein Thy-1 in zebrafish RGCs. Furthermore, I wanted to investigate its behavior upon optic nerve lesion and its role in regeneration. Mammalian Thy-1 is highly expressed in all neurons, representing up to 7.5% of all neuronal surface proteins (Reif & Allen, 1964; Beech et al., 1983). It is considered a ganglion cell marker for rodent retinae and being critical for normal retinal development (Barnstable & Drager, 1984; Simon et al., 1999). Studies evaluating its developmental expression detected Thy-1 in rat retinae already from birth, albeit at low levels, by immunohistochemistry and qRT-PCR (Liu et al., 1996).

5.1. Expression pattern of Thy-1 in zebrafish RGCs

To investigate the expression pattern of the Thy-1 glycoprotein in the zebrafish retina, a specific detection tool was needed. With an antibody specific for zebrafish Thy-1, I would be able to perform immunohistochemical analysis to validate the knockdown of Thy-1 in functional assays. For this purpose, a specific antibody (Ab) is the reagent of choice, since it can unequivocally ensure that the translation-blocking morpholino (MO) specifically recognizes its target. In this thesis, both polyclonal and monoclonal antibodies were evaluated in order to strengthen my conclusions.

5.1.1. Characterization of a pAb specific for zebrafish Thy-1

Two potentially reactive rabbit sera (nr. 4716 & 4717) were obtained by challenging the rabbits with a short peptide sequence of the Thy-1 core protein: 15 aa, position 60-74, (N-)H-Cys-Leu-Ile-Gly-Ser-Thr-Asn-Ser-Ser-Ser-Thr-Pro-Asp-Ser-Thr-OH(-C). This part of Thy-1 provides a well accessible epitope since the leader peptide is cleaved after processing and the outer leaflet of the membrane covers the GPI-anchor. We chose the animals after testing the pre-immunization blood for unspecific reactivity in zebrafish retina whole mount immunostainings. After antigen-specific affinity purification, I used both sera for Western blots and immunostainings of zebrafish brain and retina lysates and tissues (see methods 4.16.). The serum of rabbit number 4716 gave a more specific signal and was used in all further experiments. Western blots with recombinant Thy-1-GST expressing bacteria lysates showed

the expected ~38 kDa band of the Thy-1-GST-fusion protein, only after IPTG-induced expression (Fig. 5.1.1.1 A). Notably, analysis of zebrafish retina lysates obtained 5 days after ONS showed a strong increase of the Thy-1-specific protein bands in Western blots (WB) (Fig.5.1.1.1 D).

In single RGCs, Thy-1 was localized particularly at the cell membrane and on axons, including growth cones, and displayed a dotted and clustered pattern (Fig. 5.1.1.1 E). Interestingly, the strongly labeled Thy-1 protein clusters in the whole retinae appeared to be even larger and reorganized after ONS (Fig. 5.1.1.1 B and C). Since Thy-1 is a GPI-linked membrane protein, and therefore localizes and redistributes to specialized lipid rafts, we expected a dotted and clustered staining pattern, which is reminiscent of microdomains (Lemansky et al., 1990).

In order to verify the specificity of this new polyclonal zebrafish Thy-1 antibody, I transfected zebrafish RGCs *in vivo* with a specially designed, translation-blocking morpholino targeted against Thy-1, labeled with a fluorescent lissamine tag (see methods 4.3.). 5 days after morpholino-application to the transected optic nerve, the intracellular red lissamine labeling verified a successful transfection and labeled the RGC layer. Thy-1 MO-mediated knockdown proved specificity of the Thy-1 antibody via microscopic analyses (Fig. 5.1.1.2), the pAb 4716 signal in RGCs was markedly weaker upon Thy-1 MO-treatment (Fig. 5.1.1.2 A). In addition, Western blots of zebrafish retina lysates showed a substantial decrease in intensity of the Thy-1-specific protein bands as well (Fig. 5.1.1.2 B).

Taken together, the specificity of the pAb 4716 was verified via morpholino-mediated knockdown of Thy-1 and optic nerve lesion led to an increase of the Thy-1-specific signal both in Western blot and immunohistochemical analysis (Fig. 5.1.1.1 and 5.1.1.2). The zebrafish retina whole mount immunostainings of Thy-1 with the pAb Thy-1 4716 showed a characteristic, dotted pattern at the cell surface of cell bodies and axons. Critically, the fluorescence signal clearly increased after optic nerve lesion and declined after MO-mediated knockdown. Moreover, the changes in Thy-1 protein levels detected by Western blot of zebrafish retina lysates agree with the result of the immunostainings, and the pAb 4716 recognized its overexpressed, recombinant target. From these data, we concluded that the newly generated polyclonal antibody specific for zebrafish Thy-1 would be a valid tool. Nevertheless, we decided to independently confirm these results and to produce a more specific monoclonal antibody for the subsequent experimental studies.

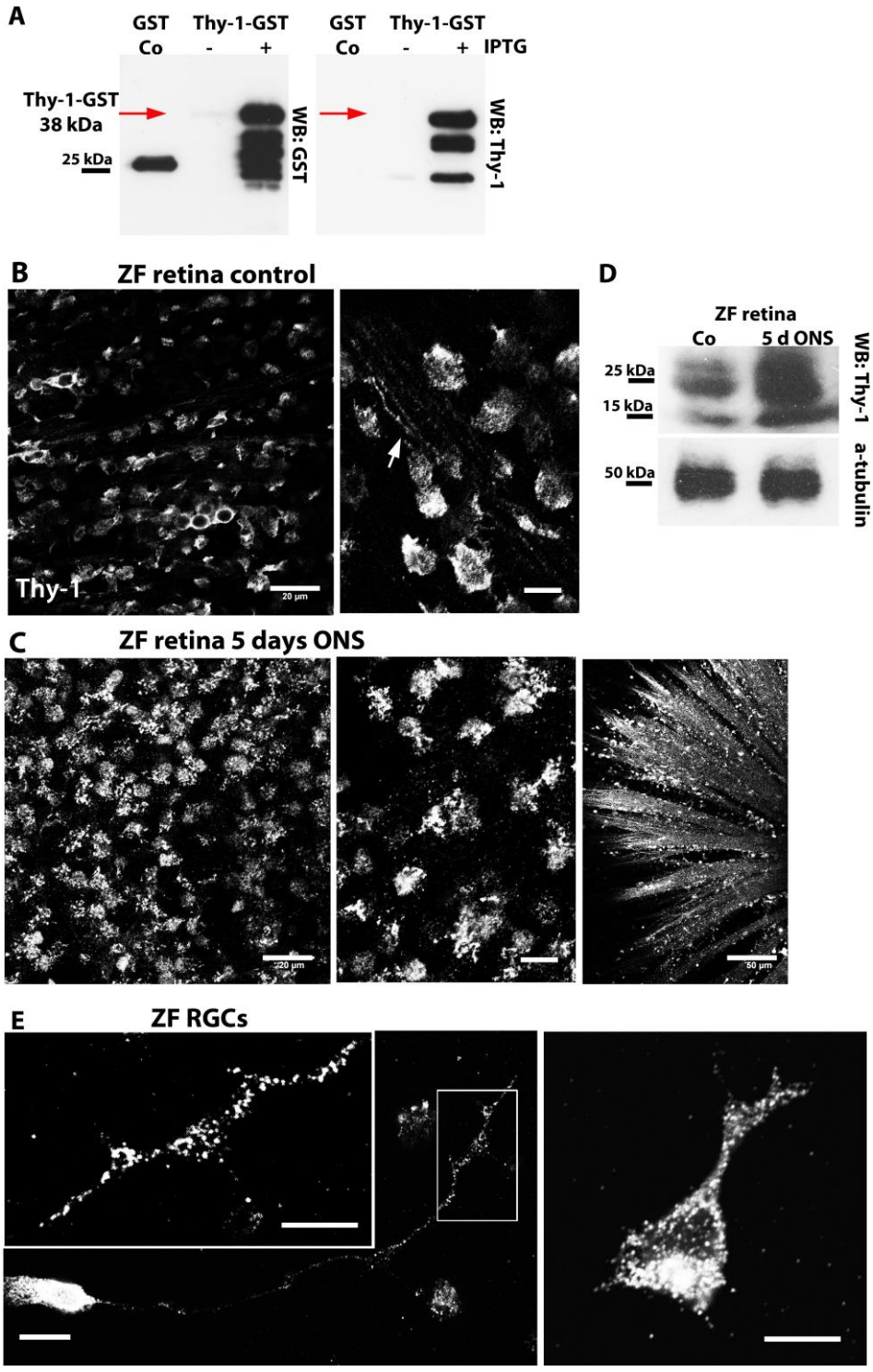

Figure 5.1.1.1 Characterization of the zebrafish Thy-1 pAb 4716. A. WB with recombinant Thy-1-GST fusion protein (~38 kDa), expressed in bacteria after induction with IPTG. **B.** Thy-1 immunohistochemistry in untreated zebrafish retina whole mounts labels cells and axons (arrow). Scale bars left to right: 20, 10 µm. **C.** Cells and axons are intensively stained at 5 days after ONS. Scale bars left to right: 20, 10, 50 µm. **D.** WB of zebrafish retina lysates. The 25 kDa band is increased at 5 days ONS. **E.** Thy-1 in single zebrafish RGCs displays a dotted pattern typical for the GPI-protein immunolabeled with the pAb 4716. Scale bars: 10 µm.

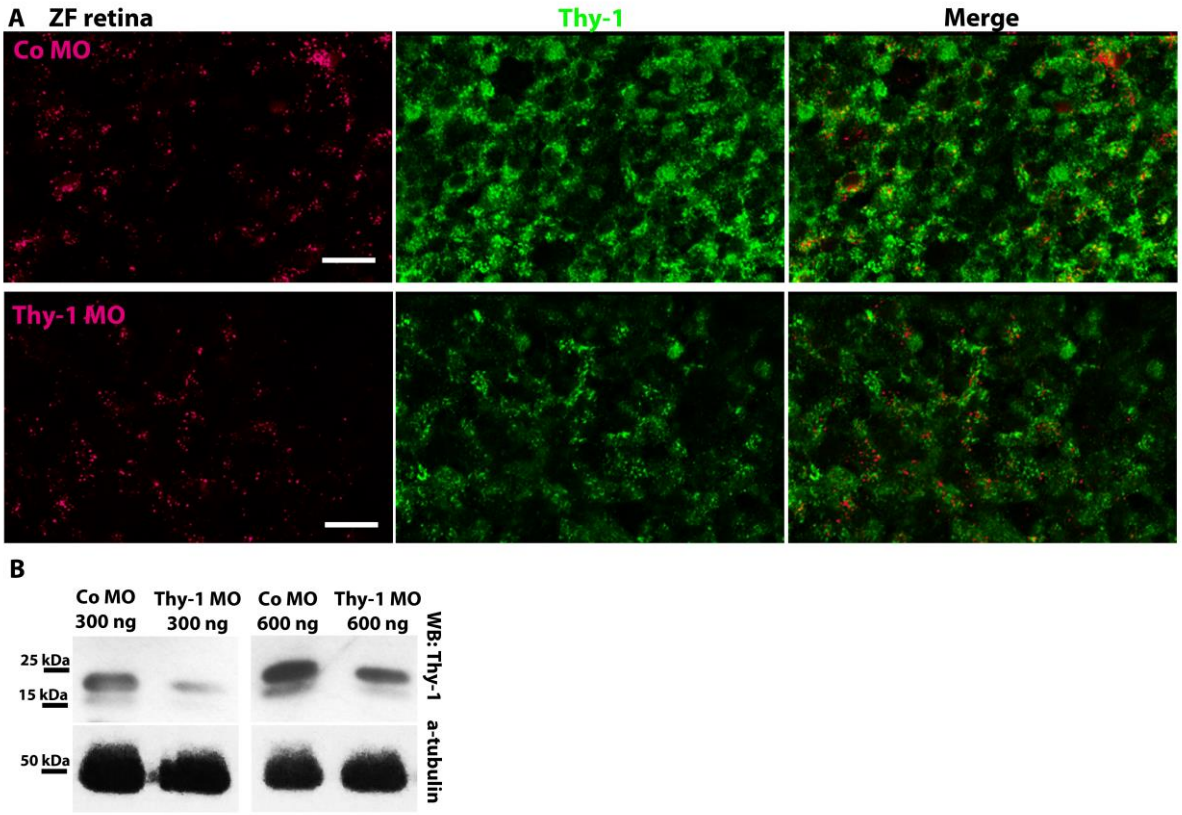

Figure 5.1.1.2 Specific knockdown of Thy-1 detected with the zebrafish pAb 4716. A. Zebrafish retina whole mounts show decreased Thy-1 fluorescence intensity (green) upon Thy-1 MO-mediated protein knockdown (magenta) in confocal microscopy analysis. The lissamine-tag of the MOs verifies transfection and depicts the intracellular localization and the RGC layer. Scale bars: 20 µm. **B.** WB of zebrafish retina lysates. The intensity of the ~25 kDa Thy-1 protein band decreases at a concentration of 300 or 600 ng of Thy-1 MO at 5 days after application to the transected optic nerve.

5.1.2. Generation of a Thy-1-specific zebrafish mAb and analysis of the Thy-1 expression pattern in the retina

For generation of a monoclonal antibody against zebrafish Thy-1, two pre-selected mice were immunized with isolated and purified Thy-1 core protein (~12.6 kDa) tagged to GST (~26 kDa). Spleen cells of both mice were fused to myelomas (= hybridomas). Repeatedly, in a large screening procedure (see chapter 4.17.) clones were tested in Western blots and immunohistochemical analysis to prove the specificity of potential new monoclonal zebrafish Thy-1 antibodies. Finally, the selected mAb 89/9 identified a single polypeptide in Western blots at the predicted ~25 kDa in zebrafish brain and retina lysates (Fig. 5.1.2 A and attachment of supplementary data Fig. 9.1) (Ades et al., 1980). Since Thy-1 comprises three glycosylation sites in mice and two in humans, zebrafish Thy-1 was also expected to be glycosylated (Pont, 1987). Deglycosylation of zebrafish brain lysate by treatment with N-Glycosidase F (method 4.15.7.) resulted in a shift of the 25 kDa band to approximately 17 kDa, confirming glycosylation of the protein recognized by mAb 89/9 (Fig. 5.1.2 B).

Critically, ONS resulted in a significant 1.45-fold upregulation signal in Western blots of retina lysates compared to the untreated control side. Western blots were evaluated densitometrically with the ImageJ software and using alpha-tubulin as a loading control (Fig. 5.1.2 C and G). Accordingly, total Thy-1-specific immunofluorescence signal intensity was enhanced significantly 2.6-fold in retina whole mounts at 5 days after ONS as compared to the untreated control. (Fig. 5.1.2 D, E, F). In the retinae Thy-1 showed a uniform distribution throughout all RGCs, at the membrane and predominantly at cell-contacts of RGCs and their axons. After optic nerve lesion, this pattern changed into a more dense and clustered arrangement of the protein at the cell surface (Fig. 5.1.2 D and E). Of note, the general distribution of Thy-1 in the zebrafish retina and its presence in all RGCs (young ones at the periphery and elder ones in the center) resembled the pattern obtained with the pAb 4716 (Fig. 5.1.1.1.). These results strongly suggest a functional rearrangement of cell surface Thy-1 within specific microdomains. The immunostaining procedure was performed in live retinae where the mAb 89/9 was applied only for 10 min on ice to prevent internalization and to label only antigens that are present at the cell surface. This procedure warrants that the fluorescence signal arises mostly from membrane-bound Thy-1. Nevertheless, the distribution

of Thy-1, especially after optic nerve lesion, might also suggest vesicular localization. This pattern could be explained by transport of upregulated GPI-proteins to the surface via exocytic pathways. Experimental proof for this point is not available (see discussion and Fig. 9.2.1 in the attached supplementary data). The specificity of mAb 89/9 was thus verified in immunohistochemical and Western blot analyses. To validate the lesion-induced increased expression of Thy-1 in the zebrafish retina, an additional, antibody-independent method was applied: relative quantitative real-time PCR. Verifying the mRNA levels of *thy-1* transcripts with real-time PCR after optic nerve lesion confirmed the injury-induced increase of Thy-1 expression (method 4.14.). For relative quantification of Thy-1 expression levels, I compared the amount of mRNA to two different housekeeping genes, already established for this purpose: EF1α (elongation factor 1 alpha) and Rpl13α (ribosomal protein L13 alpha) (Tang et al., 2007). At 5 days after optic nerve lesion, Thy-1 mRNA levels in the zebrafish retina increased 8.7-fold compared to EF1α, and 23-fold compared to Rpl13α (Fig. 5.1.2 H and I). Therefore, analyses of both RNA and protein levels agree that zebrafish Thy-1 is specifically upregulated after ONS.

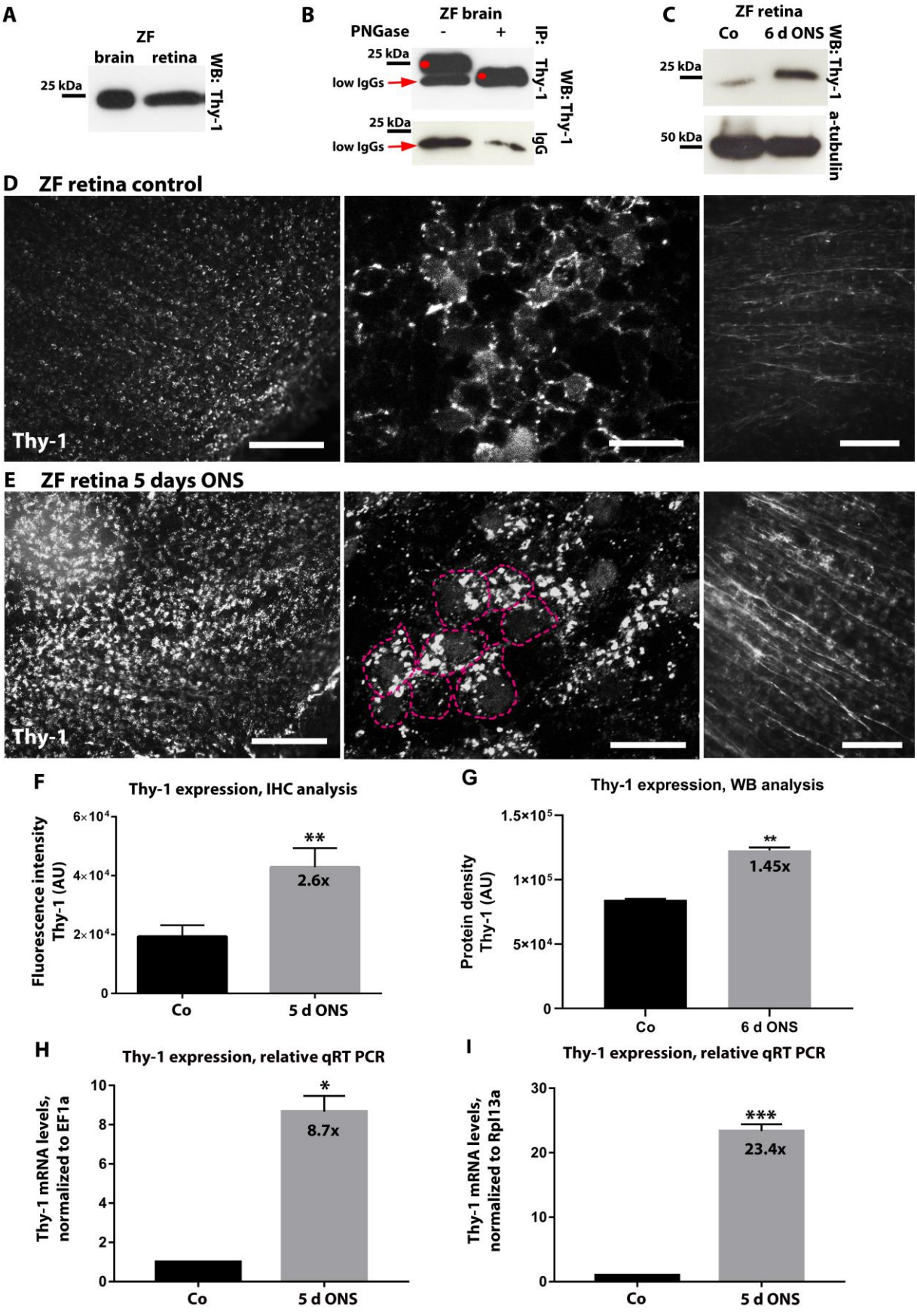
A
ZF
brain
retina
25 kDa
WB: Thy-1
B
ZF brain
PNGase
-
+
25 kDa
low IgGs
IP: Thy-1
WB: Thy-1
25 kDa
low IgGs
IgG
C
ZF retina
Co
6 d ONS
25 kDa
WB: Thy-1
50 kDa
a-tubulin
D ZF retina control
Thy-1
E ZF retina 5 days ONS
Thy-1
F
Thy-1 expression, IHC analysis
Fluorescence intensity Thy-1 (AU)
6×10⁴
4×10⁴
2×10⁴
0
**
2.6x
Co
5 d ONS
G
Thy-1 expression, WB analysis
Protein density Thy-1 (AU)
1.5×10⁵
1×10⁵
5×10⁴
0
**
1.45x
Co
6 d ONS
H
Thy-1 expression, relative qRT PCR
Thy-1 mRNA levels, normalized to EF1a
10
8
6
4
2
0
*
8.7x
Co
5 d ONS
I
Thy-1 expression, relative qRT PCR
Thy-1 mRNA levels, normalized to Rpl13a
30
20
10
0
***
23.4x
Co
5 d ONS

Figure 5.1.2 Verification of the Thy-1 mAb 89/9 and increase of Thy-1 protein levels upon ONS in zebrafish RGCs. A. WB of zebrafish brain and retina lysates shows a single band at ~25 kDa. **B. Immunoprecipitation** with the mAb 89/9 and subsequent deglycosylation of Thy-1 with PNGase F results in a protein band shift in the WB down to approximately the size of lower mouse IgGs (~17 kDa). **C. WB** analysis, specific signal of Thy-1 in zebrafish RGCs increases at 6 days after ONS. **D and E. Staining pattern of Thy-1** labeled with the mAb 89/9 in zebrafish retina whole mounts (unfixed samples). RGCs and axons are labeled ubiquitously in untreated live retinae as expected for a GPI-anchored surface protein such as Thy-1. Fluorescence intensity increases and signals redistribute at 5 days after ONS which are reminiscent of GPI-anchored molecules in membrane microdomains upon activation (Lemansky et al., 1990; Stuermer, 2011). The size of the cell soma increases upon ONS, an effect which is known as cell body response (Cajal & May, 1991) (short live staining, confocal Z-projection). Scale bars left to right: 100, 20, 50 µm**. F. Quantification of Thy-1 fluorescence intensity.** At 5 d after ONS Thy-1 expression is ~2.6-fold higher compared to control retinae (mean values +SEM of 3 different experiments, n = 10 per group, p(**) = 0,0057 in unpaired, two-tailed student`s t-test against the control). **G.** Densitometric quantification of WB protein bands shows a 1.45-fold increase at 6 days post ONS, normalized to the loading control alpha-tubulin. Graph shows mean values +SEM of two experiments, n = ≥ 8 retinae per group, p(**) = 0,0039 in unpaired, two-tailed student`s t-test against untreated retinae. **H and I.** Relative quantitative RT PCR of Thy-1 mRNA levels shows a 9-fold rise at 5 d after ONS, compared to untreated retinae and normalized to EF1alpha, or a 23-fold increase, normalized to Rpl13alpha. Three independent experiments, RNA isolated from at least 5 pooled retinae per group (n = 15). Thy-1 mRNA expression was normalized to the expression of a housekeeping gene as indicated. Levels of control untreated retinae were arbitrarily set to one. Graphs show mean +SEM. One-sample t-test reveals a significant increase of Thy-1 mRNA levels with p(***) = 0,0007 with respect to Rpl13alpha and p(*) = 0,0107 with respect to EF1alpha.

5.1.3. Expression pattern of Thy-1 in cultured single zebrafish RGCs

To specifically address the distribution of Thy-1 in axons that are freshly re-growing, I cultured single RGCs and labeled them with the mAb 89/9. Short incubation (10 min) on ice prevented internalization of the antibody, ensuring that mainly membrane-bound protein was accessible, revealing the arrangement of Thy-1 at the cell surface, where it was expected. High resolution confocal microscopy visualized the membranous localization of Thy-1 (in single Z-slices). Thy-1 was distributed in a dotted pattern exclusively at the cell membrane along the entire axon as shown below in a maximum projection of a confocal Z-stack (Fig. 5.1.3 A). In a complex tissue such as retinal explant (Fig. 5.1.3 B), the Thy-1 protein was enriched at cell-cell-contact sites, as it was described for mammalian Thy-1 (Rege & Hagood, 2006). The membrane-bound localization as well as the dotted, clustered pattern of the mAb 89/9 antigen are characteristic of GPI-linked proteins like Thy-1 and further corroborates the specificity of the anti-Thy-1 monoclonal antibody.

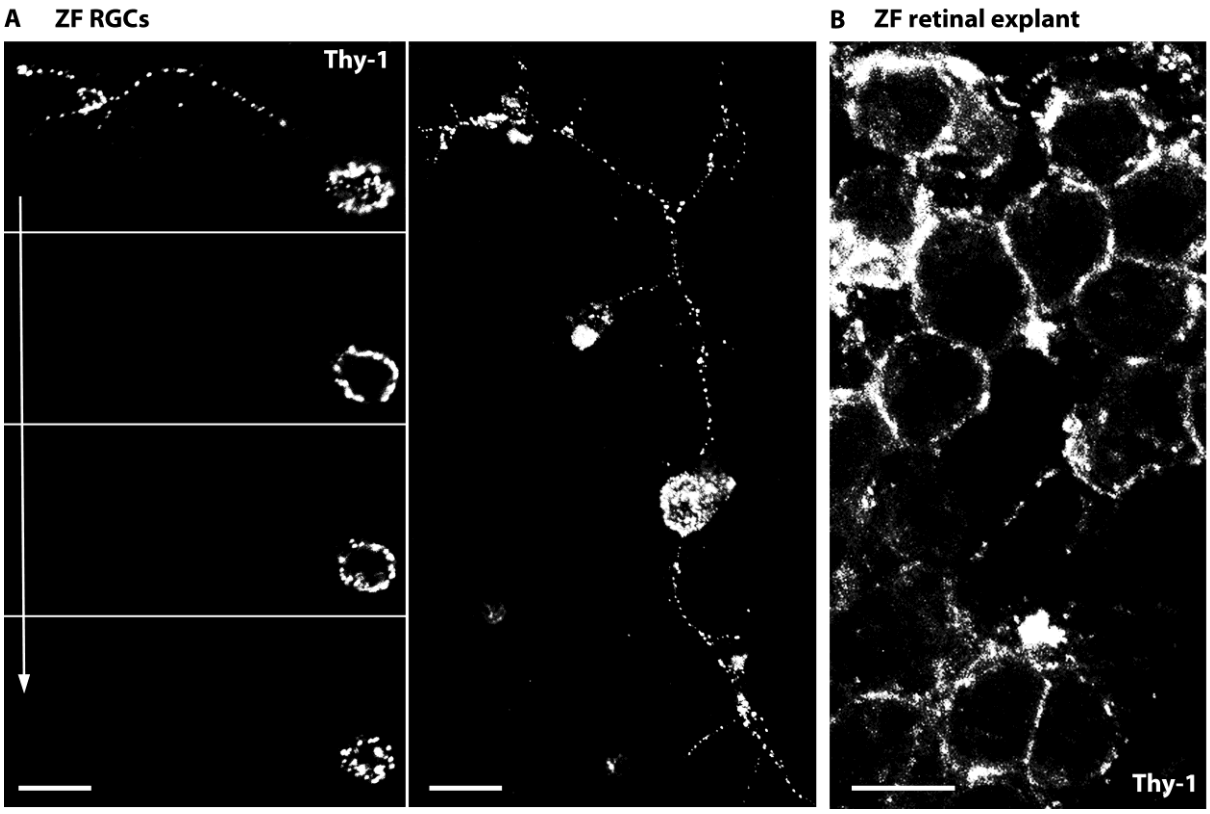

Figure 5.1.3 Thy-1 in cultured zebrafish RGCs. A. Left: series of confocal Z-planes from the bottom of the coverslip to the top of the cell (in the direction of the arrow). Right: Maximum Z-projection of a RGC (short live staining on ice). Thy-1 appears dotted and clustered at the membrane of the cell body and like a string of pearls at the axon. Left images collected at 0.57 µm intervals over a depth of 5.7 µm, right image is a Z-projection collected at 0.57 µm intervals over a depth of 7.97 µm. **B.** Zebrafish retinal explant, PFA-fixed and stained with the mAb Thy-1 89/9 shows a membranous localization of Thy-1, enriched at cell-cell-contacts. Maximum Z-projection of images collected at 0.98 µm intervals over a depth of 7.87 µm. Scale bars in **A** and **B**: 10 µm.

5.1.4. Knockdown of Thy-1 in zebrafish RGCs

Targeted protein knockdown via translation-blocking morpholinos is a valuable tool for confirming the sensitivity and specificity of an antibody. Vice versa, a specific antibody is absolutely required to verify the effectiveness and target specificity of a custom-designed morpholino that is employed to assess whether potential changes in our regeneration assay may be due to Thy-1 loss of function. Using our new antibodies in Western blots and immunostainings, I was able to confirm the reduction in Thy-1 protein levels upon morpholino-mediated knockdown (*in vivo* application of MOs to the optic nerve see 4.3.). As a precondition for these experiments, I had to determine the sufficient concentrations and the time needed for the morpholino to be retrogradely transported from the optic nerve lesion site to the RGCs, which is about 2-3 days. Interestingly, Thy-1 levels were increased upon ONS from the fourth day onwards. Taking these results into account, retinae were

isolated after 5 days and prepared for Western blot or immunohistochemical analysis. Retinae transfected with the Thy-1 morpholino showed considerably less fluorescence in immunostaining than the ones transfected with the control morpholino (Fig. 5.1.4 A). In these assays, the total mean fluorescence intensity of Thy-1 declined by 37% (Fig. 5.1.4 B, application of 140 µM Co or Thy-1 MO to the transected optic nerve). To confirm the specificity of the knockdown, I designed two different morpholino sequences targeting distinct parts of the zebrafish *thy-1* mRNA. Western blots of Thy-1 morpholino-treated retinae confirmed the successful knockdown of Thy-1 for both morpholino sequences and showed reduced protein levels as compared to the control morpholino-treated retinae (Fig. 5.1.4 C). Desitometric quantification of protein levels in Western blots using ImageJ software revealed a 24% reduction with the first Thy-1 MO sequence 1, and -20% for the second Thy-1 MO sequence 2 (Fig. 5.1.4 D).

Since the morpholino-mediated knockdown of Thy-1 in immunostainings and Western blots of zebrafish retinae did not completely abrogate Thy-1 protein levels, an alternative method was chosen to further verify efficacy: the injection of Thy-1 morpholinos directly into one-cell-stage zebrafish embryos. In the zebrafish embryo model system, the knockdown of target proteins is more effective, since translation is blocked from the earliest possible time point of expression.

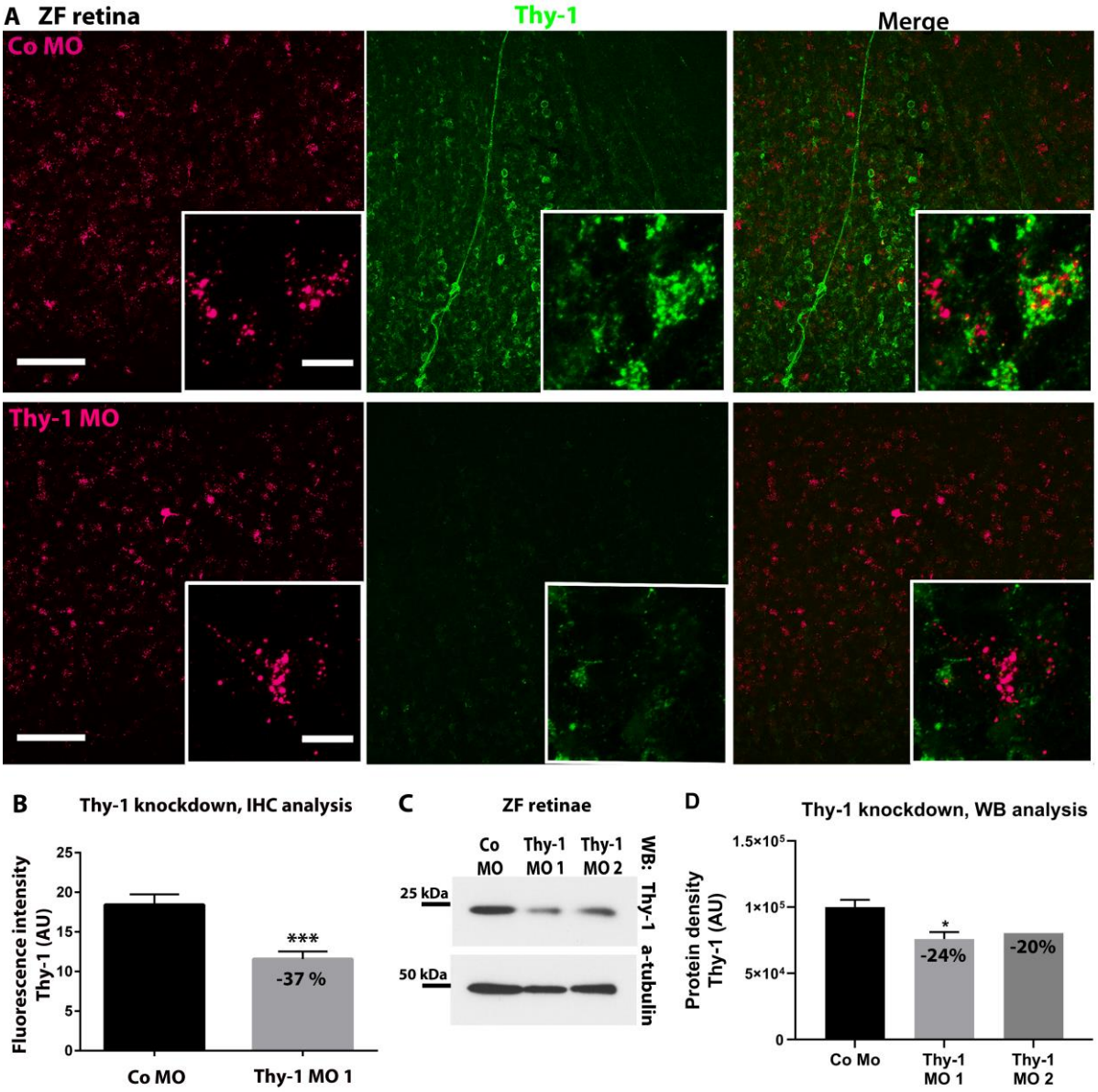

Figure 5.1.4 MO-mediated knockdown of Thy-1 in zebrafish RGCs *in vivo*. A. ZF retina whole mounts, transfected with lissamine-tagged control MO (A) or Thy-1 MO (B) (magenta), live tissue immune-labeled with Thy-1 89/9 (green). Scale bars: 50 µm and 10 µm in the detail. **B. Quantification of Thy-1 fluorescence intensities** shows -37% reduction in Thy-1 MO-treated retinae compared to the control. Graph shows mean +SEM of three different experiments (Co MO n = 7, Thy-1 MO n = 9, p(***) = 0,0007, unpaired, two-tailed student`s t-test against Co MO-treated retinae). **C. WB of retinae** that received control MO or Thy-1 MOs 1 or 2. **D**. **Densitometric quantification of the Thy-1 protein** bands in WBs results in 24% reduced protein levels after Thy-1 MO 1, or -20% after Thy-1 MO 2 knockdown. Graph shows mean +SEM with Thy-1 MO 1 p(*) = 0,047 in unpaired, two-tailed students t-test compared to the Co MO. Experiments done two times for MO 1 and once for MO 2, with about 4 pooled retinae per group each time.

5.1.5. Expression and knockdown of Thy-1 in the zebrafish embryo

An alternative and faster approach to prove the efficacy of the Thy-1-specific morpholinos for blocking Thy-1 expression is to injection them into zebrafish embryos right at their one-cell stage. This technique leads to an even distribution of the reagent in each cell of the entire fish at the start point of its development. It avoids the *in vivo* application of the morpholino, the unpleasant surgery of the adult animals and the subsequent complicated tissue dissection. As expected, the knockdown of Thy-1 was more effective in embryos than in the retinal system. Moreover, in the latter experimental system the number of morpholino-receiving RGCs and the concentration of the oligonucleotide is difficult to monitor and more variable.

Before verifying the Thy-1 embryonic protein knockdown in Western blots, the onset of expression in zebrafish embryos by Western blot and qRT PCR had to be determined. In one day old embryos (1 day post fertilization = 1 dpf) the Thy-1 protein was not present. At 2 dpf it became detectable in Western blot analysis and it was prevalent at 5 dpf (Fig 5.1.5.1 D). Cross-checking of Thy-1 expression levels in zebrafish embryos by an antibody-independent technique -by relative qRT-PCR- showed as well 2.6-fold increase in Thy-1 mRNA levels at 3 dpf and still 1.6-fold at 5 dpf, compared to 1 dpf embryos. All values are normalized to the housekeeping gene Rpl13alpha (Tang et al., 2007) (Fig 5.1.5.1 E). Very similar results were obtained using EF1alpha as a reference gene: Thy-1 expression was 2.4-fold higher at 3 dpf and 1.5-fold higher at 5 dpf (Fig 5.1.5.1 F). Immunolabeling of zebrafish embryo whole mounts with the mAb 89/9 showed weak or no signal in 1 dpf old embryos, neither in the head region (Fig. 5.2.5.1 A.a), nor in the eye or the trunk (Fig. 5.1.5.1 A.b and A.c). At 3 and 5 dpf, there was detectable signal in blood vessels and blood cells in the somites (Fig 5.1.5.1 B.c, C.c). Nevertheless, neurons of the brain or the retina still remained unlabeled. In addition, large star-shaped Thy-1-positive cells were visible at these stages in the dorsal trunk (Fig. 5.1.5.1 B.d).

Thy-1 expression in mammals is developmentally regulated and its levels are very low in developing CNS structures of retina and brain during embryonic and early postnatal stages, rising to high amounts only towards adulthood (Liu et al., 1996; Bolin & Rouse, 1986). Altogether, from what is known in mammals, it could be hypothesized that Thy-1 is rarely expressed in neurons during early embryogenesis of zebrafish, too. This assumption is corroborated by the immunostainings performed in this work.

Injection of Thy-1 morpholinos into zebrafish embryos led to an effective knockdown of Thy-1 protein levels in Western blot analysis (-80%), as measured at 4 dpf by densitometric analysis using alpha-tubulin as a loading control (Fig. 5.1.5.2 C and D). Injected embryos were selected after verifying the presence of the red fluorescent lissamine-tagged morpholinos (Fig. 5.1.5.2 B). Morphological phenotypes due to the loss of Thy-1 during embryonic development were not analyzed in detail, but embryos treated with Thy-1 morpholinos were underdeveloped and malformed in the head region compared to non-injected animals (Fig 5.1.5.2 A and B). Whether these effects were due to Thy-1-specific malfunctions was not assessed further, but would be an aspect for further study.

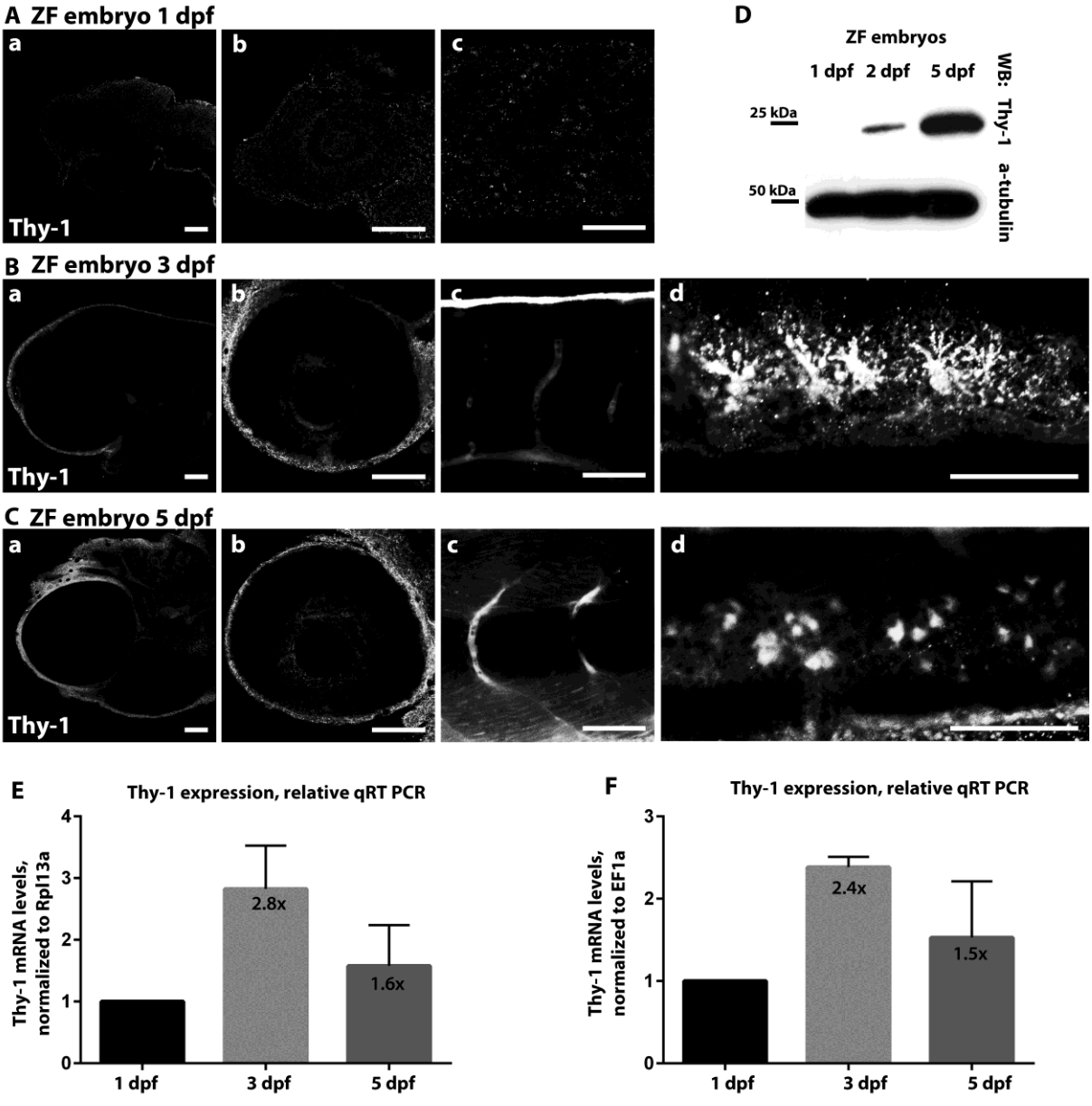

Figure 5.1.5.1 Expression of Thy-1 in early zebrafish embryos. A, B, C. Immunostainings of PFA-fixed zebrafish embryos at 1, 3, 5 dpf with Thy-1 mAb 98/9. At 1 dpf, embryos do not show Thy-1 specific signal in the brain, the eye or the trunk (**A.a, A.b, A.c**). At 3 and 5 dpf, Thy-1 is present in blood vessels, blood cells and skin (**B.c, C.c, C.d**). Scale bars: 50 µm. **D.** A WB with the Thy-1 mAb 89/9 shows increasing protein levels in 2 and 5 days old embryos. **E and F. Relative, quantitative RT PCR of different embryonic stages** shows a 2.8- or 2.4-fold increased expression of Thy-1 mRNA at 3 dpf and 1.6- or 1.5-fold increased levels at 5 dpf, compared to 1 dpf, normalized to the housekeeping genes (hkg) Rpl13alpha or EF1alpha, respectively. Experiments performed 3 times for Rpl13alpha and 2 times for EF1alpha, RNA isolated from n = ~30 embryos per group in each experiment. Ordinary one-way ANOVA between groups 3 dpf and 5 dpf compared to 1 dpf (= hypothetical value "1-times expression") as well as the one-sample t-test shows no significant difference between the individual groups. Bars represent mean +SEM. (This work was done in collaboration with Dr. E. Málaga-Trillo).

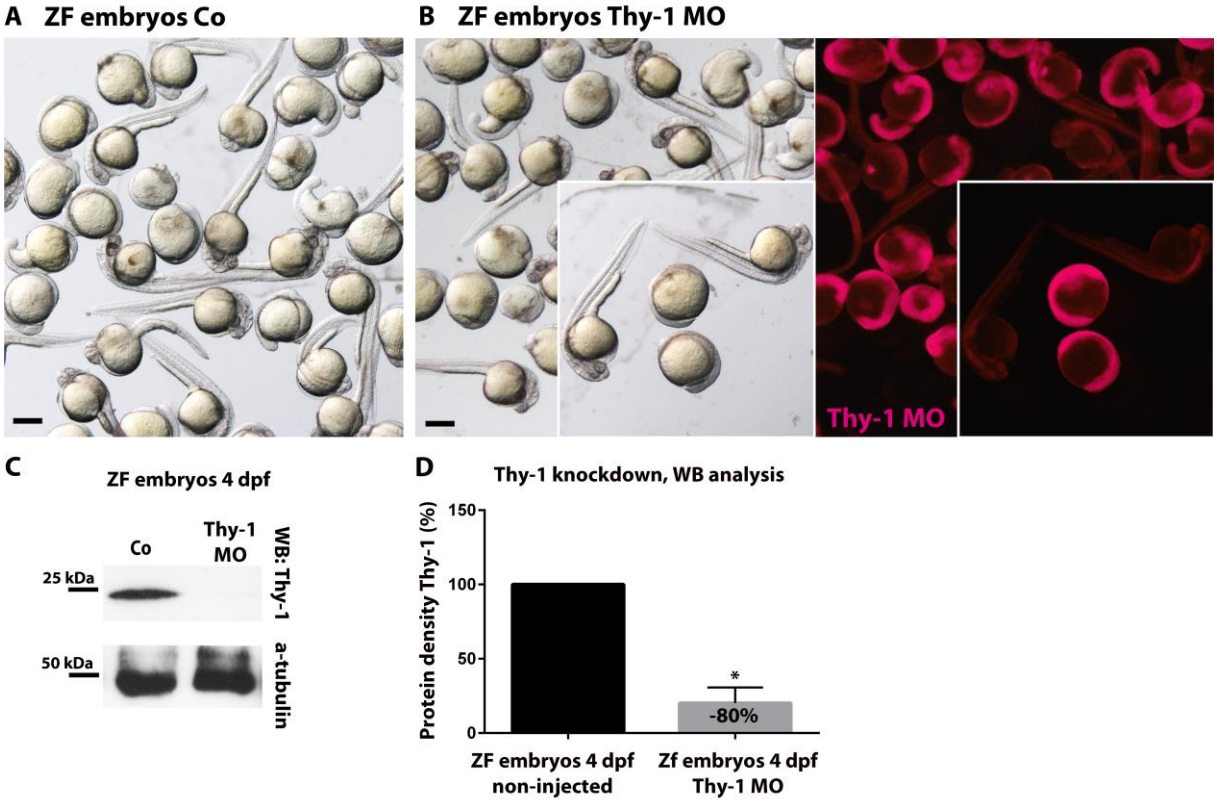

Figure 5.1.5.2 Knockdown of Thy-1 in zebrafish embryos. A and B. Untreated control (A) or Thy-1 MO-injected (B) zebrafish embryos 1 day post fertilization (dpf). **Details in B**: Thy-1 MO-injected embryos, "mild" versus "strong" phenotype, dependent on the amount of Thy-1 MO received (lissamine-labelling in magenta). Scale bars: 100 µm. **C. WB** of control and MO-injected zebrafish embryos (4 dpf) with the new mAb 89/9 against zebrafish Thy-1. The Thy-1-specific 25 kDa band disappears after injection of Thy-1 MO (right lane). **D. Quantification of Thy-1 protein levels** in 3 independent experiments shows a reduction of 80% compared to the control and normalized to alpha-tubulin. Bar shows mean +SEM of three independent experiments (n = ~30 embryos per group), with p(*) = 0,0169 in one-sample t-test compared to the non-injected control as a hypothetical 100%. (This work was done in collaboration with Dr. E. Málaga-Trillo).

5.1.6. The monoclonal zebrafish Thy-1 antibody 89/9 in the goldfish

Although there is no sufficient goldfish genomic data to allow an accurate determination of the sequence homology between gold- and zebrafish *thy-1* genes, the two species are phylogenetically closely related as they belong to the same family of *cyprinidae*. The *thy-1*

mRNA/coding sequence of *Carassius auratus* (goldfish) is not listed in the gene bank and comparative studies between both species are sparse, yet report a degree of gene homology of about 90% (Málaga-Trillo et al., 2002; Velarde et al., 2009; Becker & Becker, 2007).
Similar Thy-1 expression patterns Thy-1 in zebra- and goldfish retinae, as well as a specific protein band in Western blot analyses of both species would help to validate the new monoclonal antibody 89/9 and would provide further confirmation about Thy-1`s general distribution in the fish retina. The existence of cross-reactivity of antibodies between both species has been demonstrated before (e.g. for flotillin antibodies in the Stuermer laboratory, University of Konstanz). In fact, Western blot analysis of goldfish brain and retina lysates using the zebrafish Thy-1 mAb 89/9 detected the expected band at ~25 kDa, similar to the pattern observed in zebrafish lysates (Fig. 5.1.6 C). Immunolabeling of goldfish retinae, untreated or after ONS, with the Thy-1-specific mAb 89/9 displayed a similar pattern as in zebrafish: in the untreated control (Fig 5.1.6 A), all RGCs (young and older) were labeled at the surface, axons were stained moderately, and the protein appeared enriched at cell-cell-contacts (Fig. 5.1.6 A rightmost picture). Goldfish have a slower metabolism as compared to zebrafish, because of the colder water they live in. Therefore, a putative, lesion-induced increase of Thy-1 protein levels was tested at twelve days instead of five days post optic nerve lesion. After ONS, Thy-1 levels increased and the protein became reorganized into a more clustered, less regular pattern at the cell membrane and axons (Fig. 5.1.6 B). Thy-1 immunofluorescence signal intensity increased 2-fold upon ONS, as quantified in ImageJ (Fig. 5.1.6 D).

Altogether, these data led to the conclusion that the newly generated mAb 89/9 specifically recognizes zebrafish -and goldfish- Thy-1.

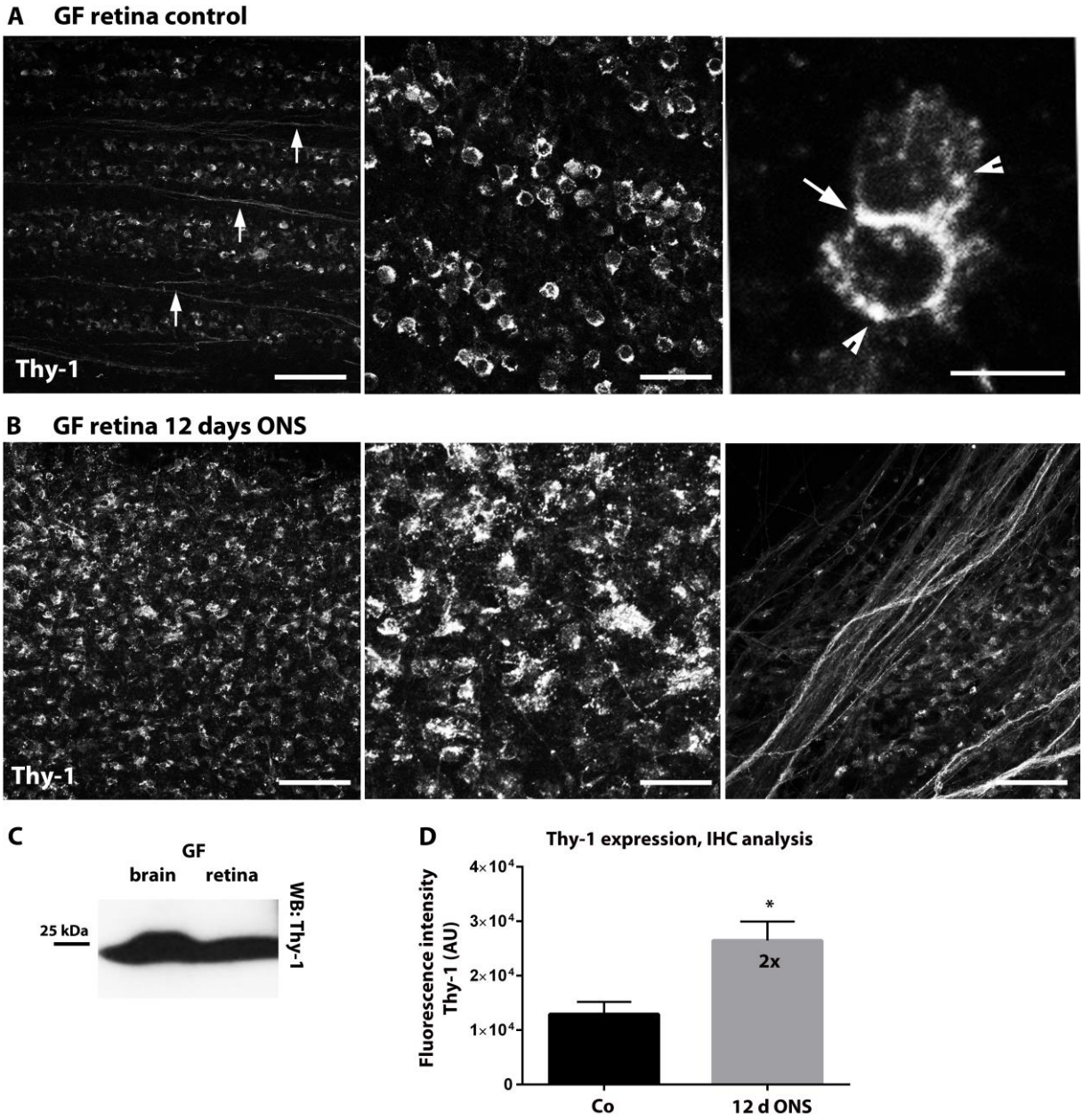

Figure 5.1.6 Characterization of the zebrafish Thy-1 mAb 89/9 in the goldfish. A. Untreated goldfish retina. Live tissue immunostaining with the zebrafish mAb 89/9 Thy-1 shows membranous protein staining of all RGCs in the untreated goldfish retina and weak axonal staining (arrows). The rightmost panel shows Thy-1 in dotted clusters at the membrane (arrowheads), enriched at cell-cell contact sites (arrow). Scale bars left to right: 50, 25, 10 µm. **B. Goldfish retina 12 days after ONS:** Thy-1 is increased and clustered in RGCs and their axons. Scale bars left to right: 50, 25, 50 µm. **C. WB** of goldfish brain and retina lysates with the zebrafish Thy-1 mAb 89/9 detects the single, predicted protein band at ~25 kDa. **D. Thy-1 fluorescence intensity quantification** in goldfish retinae shows significantly increased 2-fold expression 12 days after ONS. Graph shows mean +SEM of 3 experiments, Co n = 3 and 12 d ONS n = 6, p(*) = 0.0381 in an unpaired student`s t-test.

5.2. The neuronal function of Thy-1

Thy-1 is considered to be a mammalian neuronal marker and has been thoroughly investigated in this respect. Still, the role of Thy-1 as promoter or inhibitor of neuronal growth is discussed controversially. Thus, I first focused on the scenario applying to zebrafish retinal ganglion neurons; whether the lesion-induced increase of Thy-1 levels correlates with a supportive role in regeneration of the optic nerve. If this would be the case, would there be a similar role for Thy-1 in regenerating mammalian CNS neurons as well? Possibly, mammals do not re-express important key molecules for regeneration, like Thy-1, or Thy-1 even took over an opposite function during evolution? To address these questions, I studied loss- and gain-of-function effects by morpholino-/siRNA-mediated knockdown of Thy-1, administration of a recombinant Thy-1-GST as a substrate, or Thy-1-EGFP overexpression in fish RGCs and mouse hippocampal neurons.

5.2.1. Thy-1-GST promotes, knockdown of Thy-1 impairs differentiation and growth of zebrafish RGCs *in vitro*

To analyze the effect of extracellular Thy-1 as a neuronal ligand, soluble, recombinant, glutathione S-transferase (GST)-tagged Thy-1 was added into the medium of single zebrafish RGCs in culture and the axonal outgrowth measured. Notably, Thy-1-GST promoted neurite outgrowth in a concentration-dependent manner and significantly increased the average axon length up to +76% compared to the GST control group (Fig 5.2.1.1 A and B).

To investigate the effect of Thy-1 loss-of-function in zebrafish RGCs, I transfected single cultured cells *in vitro* with translation-blocking morpholinos. Consistent with the Thy-1-GST data, knockdown of Thy-1 *in vitro* decreased neurite outgrowth in a dose-dependent manner. Efficiently transfected cells showed the red fluorescent morpholino in their cytoplasm and these cells were chosen for measurements. Neurite length significantly decreased by 28% in average after Thy-1 downregulation in growing RGC cultures (Fig 5.2.1.2 A and B). Among Thy-1 knockdown cells, 2.6 more cells in culture remained undifferentiated/underdeveloped compared to the control group and did not grow any axon (see Fig. 5.2.1.3 A and B).

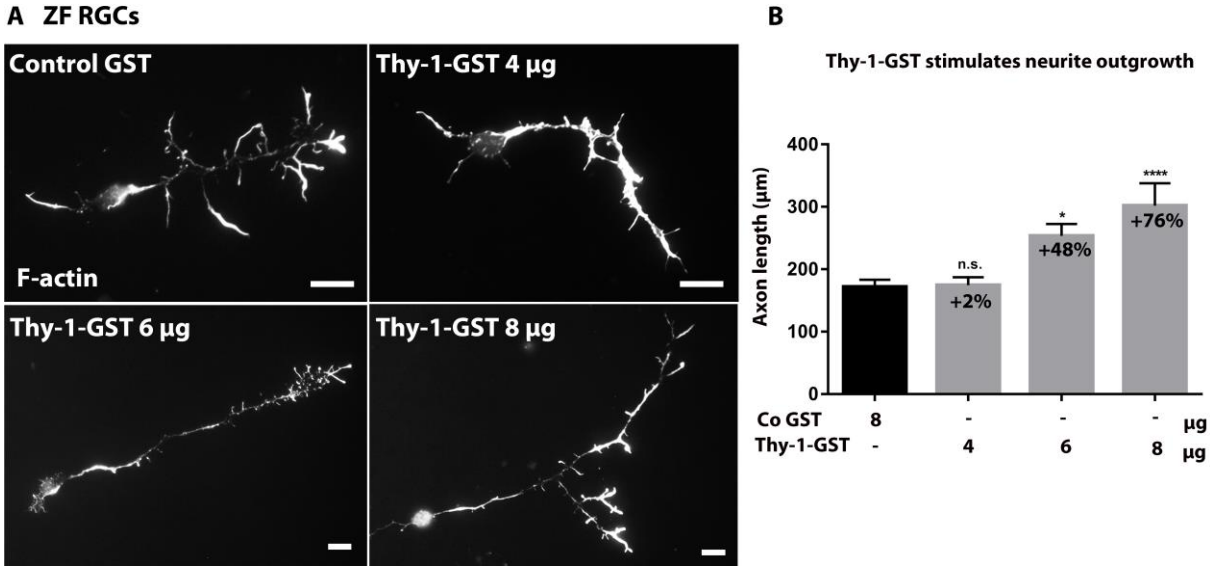

Figure 5.2.1.1 Exogenous Thy-1 stimulates axon growth of zebrafish RGCs *in vitro*. A. Cultured RGCs visualized via F-actin-labeling by phalloidin**.** Recombinant Thy-1-GST as soluble substrate increases axon lengths in a concentration-dependent manner. **B. Quantification of axon lengths.** No significant difference in average axon length for Thy-1-GST at a concentration of 4 µg/ml, but 48% increase for 6 µg/ml and 75% for 8 µg/ml. Experiment done 3 times for groups GST 8 µg/ml and Thy-1-GST 6 µg/ml with n = 636 and 129 cells and 2 times for groups Thy-1-GST 4 µg/ml and 8 µg/ml with n = 503 and 121. Ordinary one-way ANOVA of raw data between groups is significant with p(****) < 0.0001 and F (3, 1384) = 9,369. Bar graph shows mean +SEM with n.s. = not significant, p(*) = 0.0187 and p(****) < 0.0001 in a follow-up Tukey`s multiple comparisons test. Scale bars: 10 µm.

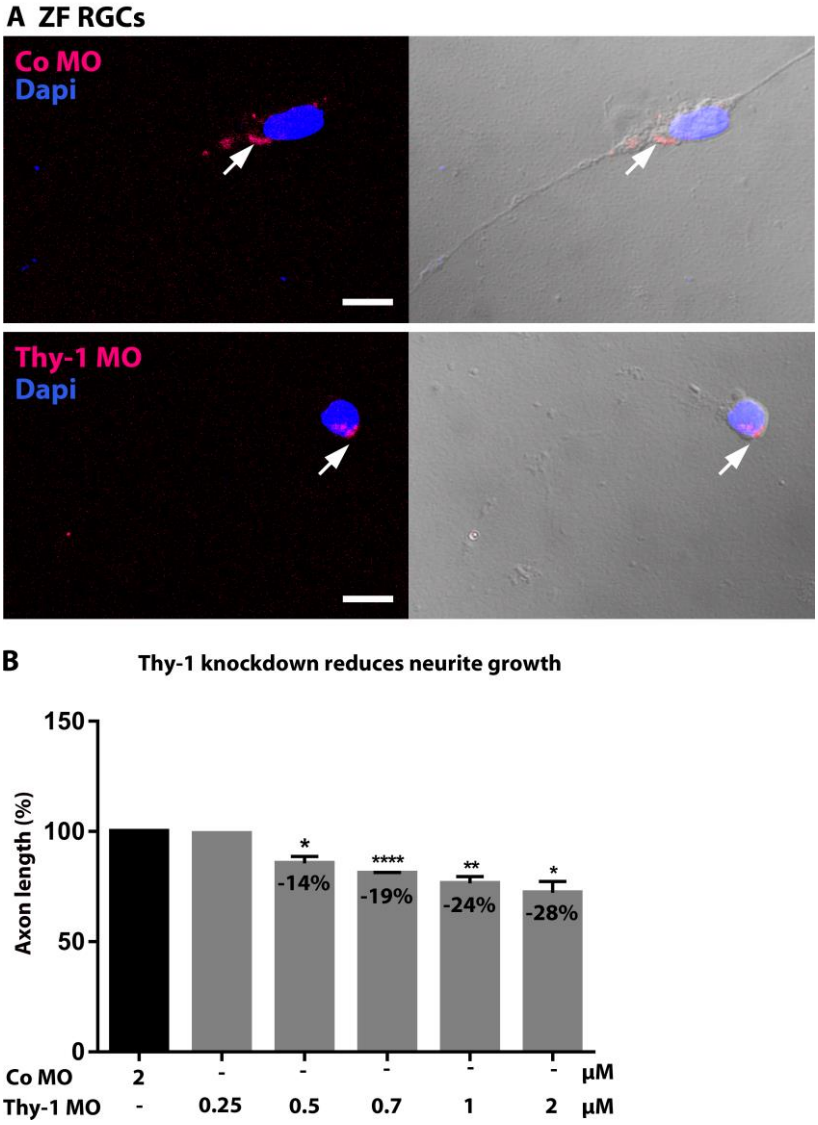

Figure 5.2.1.2 Knockdown of Thy-1 impairs axonal outgrowth of zebrafish RGCs *in vitro*. A. Cultured RGCs, transfected *in vitro* with different concentration of morpholinos (lissamine in magenta, DAPI in blue). **B. Quantification of axon lengths.** Outgrowth decreases in a dose-dependent manner by 14, 19, 24 and 28%, with increasing concentrations of Thy-1 MO compared to Co MO transfected cells. Experiments performed 5 times for the concentrations of Co MO 2 µM, 4 times for Thy-1 MO 0.5 / 0.7 / 1 µM and 3 times for Thy-1 MO 2 µM, with n = 751, 558 / 556 / 580 and 522 cells, respectively. The Thy-1 MO 0.25 µM sample was measured only once and shows no effect on axonal outgrowth, n = 130 cells. Bar graph shows means +SEM. One-way ANOVA between normalized groups is significant, F (5, 14) = 13.7 with p(****) < 0.0001 as well as the post test for a linear trend of data. One-sample t-tests to analyze if the normalized means differ from the hypothetical value "100" (% outgrowth) is significant for Thy-1 Mo conc. 0.5 µM with p(*) = 0,0197, 0.7 µM with p(**) < 0,0001, 0.1 µM with p(**) = 0,0051, 0.2 µM with p(*) = 0,0315. Scale bars: 10 µm.

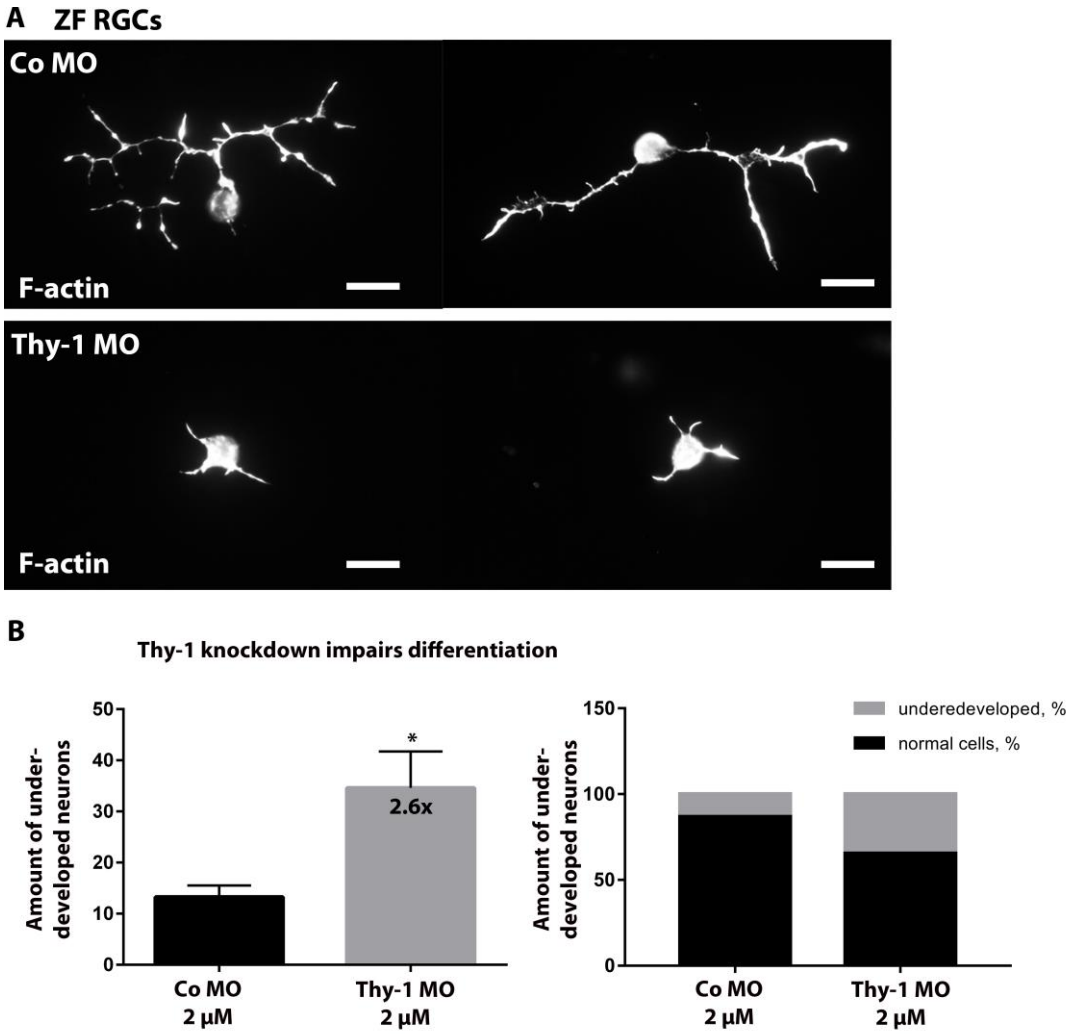

Figure 5.2.1.3 Knockdown of Thy-1 impairs differentiation of zebrafish RGCs. A. Cultured RGCs transfected with either Co or Thy-1 MOs. Cell morphology visualized by F-actin staining with phalloidin. Loss of Thy-1 impairs differentiation of ZF RGCs in culture. **B. Quantification of the amount of undeveloped RGCs.** The amount of undifferentiated RGCs increases 2.6-fold in Thy-1 MO compared to Co MO transfected cells (35% compared to 13%of all cells in culture). 4 different experiments, with Co MO 2 µM n = 396 and Thy-1 MO 2 µM n = 339. Bar graph to the left shows mean +SEM with p(*) = 0,0292 in an unpaired, two-tailed student`s test. Bar graph to the right shows the percentages of underdeveloped and normal cells. Scale bars: 10 µm.

The data obtained from these experiments demonstrated a supportive function of Thy-1 during axon growth in cultured CNS neurons. Therefore, my next aim was to analyze if this finding would also apply to the *in vivo* situation of a regenerating optic nerve.

5.2.2. Knockdown of Thy-1 in zebrafish RGCs *in vivo* impairs neurite outgrowth and optic nerve regeneration

To investigate the role of Thy-1 during regeneration in a physiological context, I applied the morpholino oligo nucleotides directly to the transected zebrafish optic nerve *in vivo* (Veldman et al., 2007). After retrograde axonal transport, the Thy-1 morpholinos were expected to block translation in the soma of RGCs. Subsequently, I examined the retinal tissue`s ability to regrow axons upon Thy-1 depletion. To control for the specificity of the knockdown effects, I used two non-overlapping morpholinos against distinct targets of the Thy-1 mRNA and used them at two different concentrations in these assays. Retinal explants from optic nerves that received a high concentration of Thy-1 morpholino at the time of transection grew about 70% less axons compared to the control morpholino (140 µM of morpholino, 24 h in culture, in case of both Thy-1 morpholino sequences) (Fig. 5.2.2.1 A, B). Reducing the concentration of morpholinos (70 µM) led to a considerably milder effect (-25 to -44%). After two days in culture, outgrowth of the Thy-1 transfected explants recovered to 33 or 35% less axons in average, whereas the control group doubled its amount of axons (Fig. 5.2.2.1 B, rightmost bars). The results of the explant outgrowth assays strongly support a growth-promoting role of Thy-1 during axon regeneration of zebrafish RGCs.

Next, the *in vivo* regeneration potential of transected optic nerves *in vivo* after knockdown of Thy-1 was investigated. For this purpose, I applied the lissamine-tagged Thy-1 morpholinos (red fluorescence) to the dorsal part of the optic nerve only via a partial lesion. After ten days, a second complete section directly behind the first one was introduced and a tracer dye (Alexa-488 dextran, green fluorescence) applied. Due to the retinotopy, the dorsal axons are derived from RGCs in the center of the retina and the ventral axons are projecting from peripheral cells (Scholes, 1979). Thus, the first partial lesion led to transfection of cells in the center of the retina with the red-fluorescent morpholinos while the second complete lesion labeled all RGCs with the green tracer dye. The dense green ring at the retinal margin demonstrates that the second cut was indeed placed behind the first one (Fig 5.2.2.2 A and B). Alexa-488-labeled cells in the retinal center represented regenerated axons that successfully crossed the first injury site and became labeled during the second lesion. In these assays, knockdown of Thy-1 reduced the regeneration capacity of optic nerves *in vivo*, that is the number of Alexa-488-labeled cells in the retinal center, by 65% (Fig. 5.2.2.2 D and E). I used two different techniques to quantify the back-labeled cells: 1) the number of green cells

was determined by visual inspection in 5 randomly chosen squares (200x200 µm/retina). 2) I quantified the total green fluorescence in these 5 randomly chosen squares (200x200 µm/retina) using the image analysis software ImageJ (Fig. 5.2.2.2 C and D). Both techniques yielded similar results and reconfirmed that Thy-1 is an important player of optic nerve regeneration *in vivo*, by supporting axonal outgrowth of zebrafish RGCs.

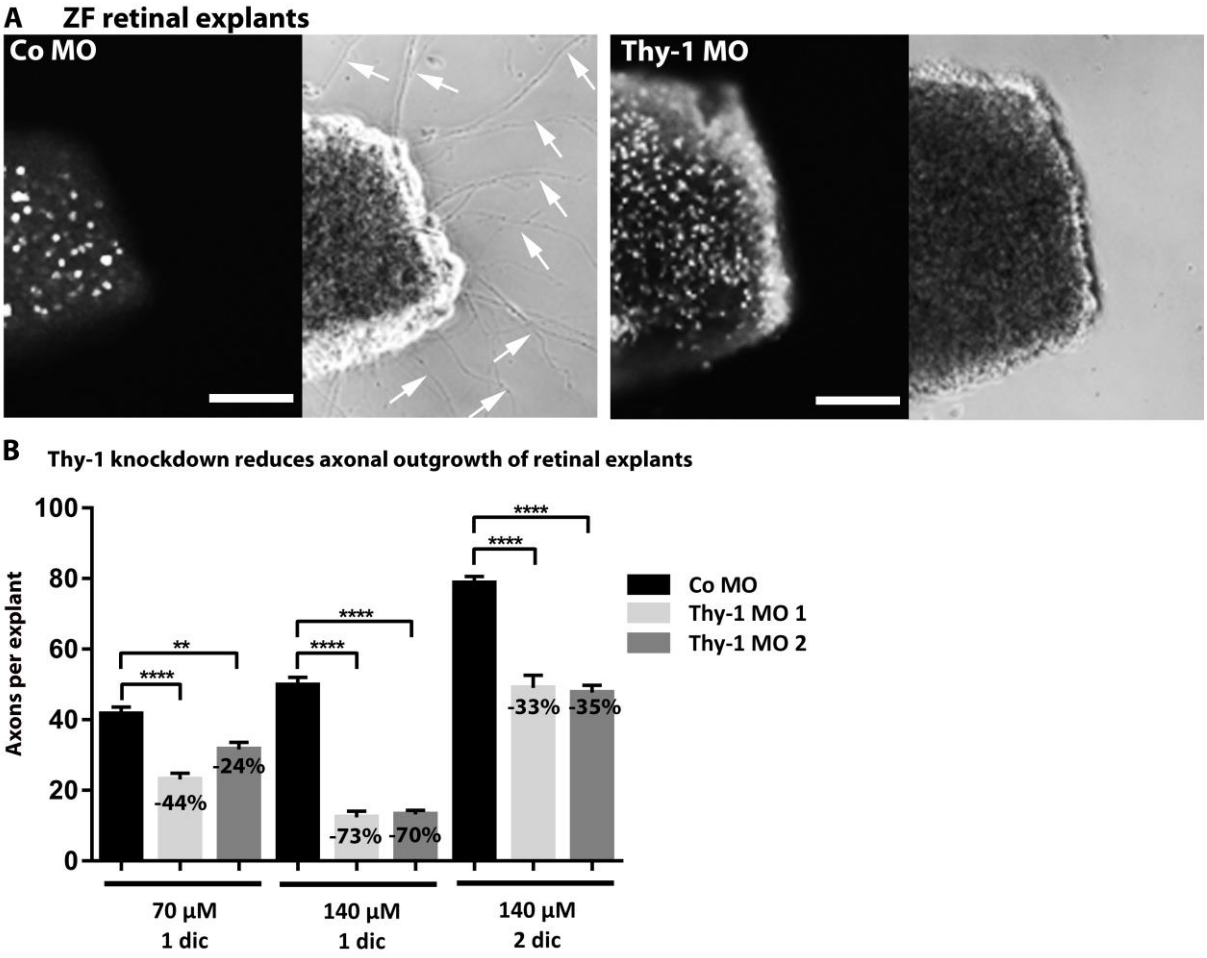

Figure 5.2.2.1 Thy-1 supports axon regeneration *semi-in vivo* in zebrafish retinal explants. A. Retinal explants transfected with Co or Thy-1 MOs. Thy-1 MO-treated retinal explants grow significantly less axons (arrows) in culture than the control. Scale bars: 100 µm **B. Quantification of axonal outgrowth.** 70 µM of MO 1 or MO 2 leads to 44% or 25% less axons after 1 day in culture (dic) as compared to controls, whereas 140 µM leads to -73% or -70% after 1 dic and recovers to -33 or -35% after 2 dic. Experiment done twice independently with two different MO sequences and two different concentrations each time. 70 µM: Co MO n = 167 explants, Thy-1 MO 1 n =103, Thy-1 MO 2 n = 92. 140 µM: Co MO n = 125 explants, Thy-1 MO 1 n = 56, Thy-1 MO 2 n = 99. Bar graph shows means +SEM. Two-way ANOVA of raw data between different morpholino concentrations and sequences was significant with p(****) < 0.0001 and F(2, 915) = 175,5 and F(2, 915) = 184. Follow-up Tukey`s multiple comparisons test between means was significant with p(**) = 0.0082, p(****) < 0.0001. Scale bars: 100 µm.

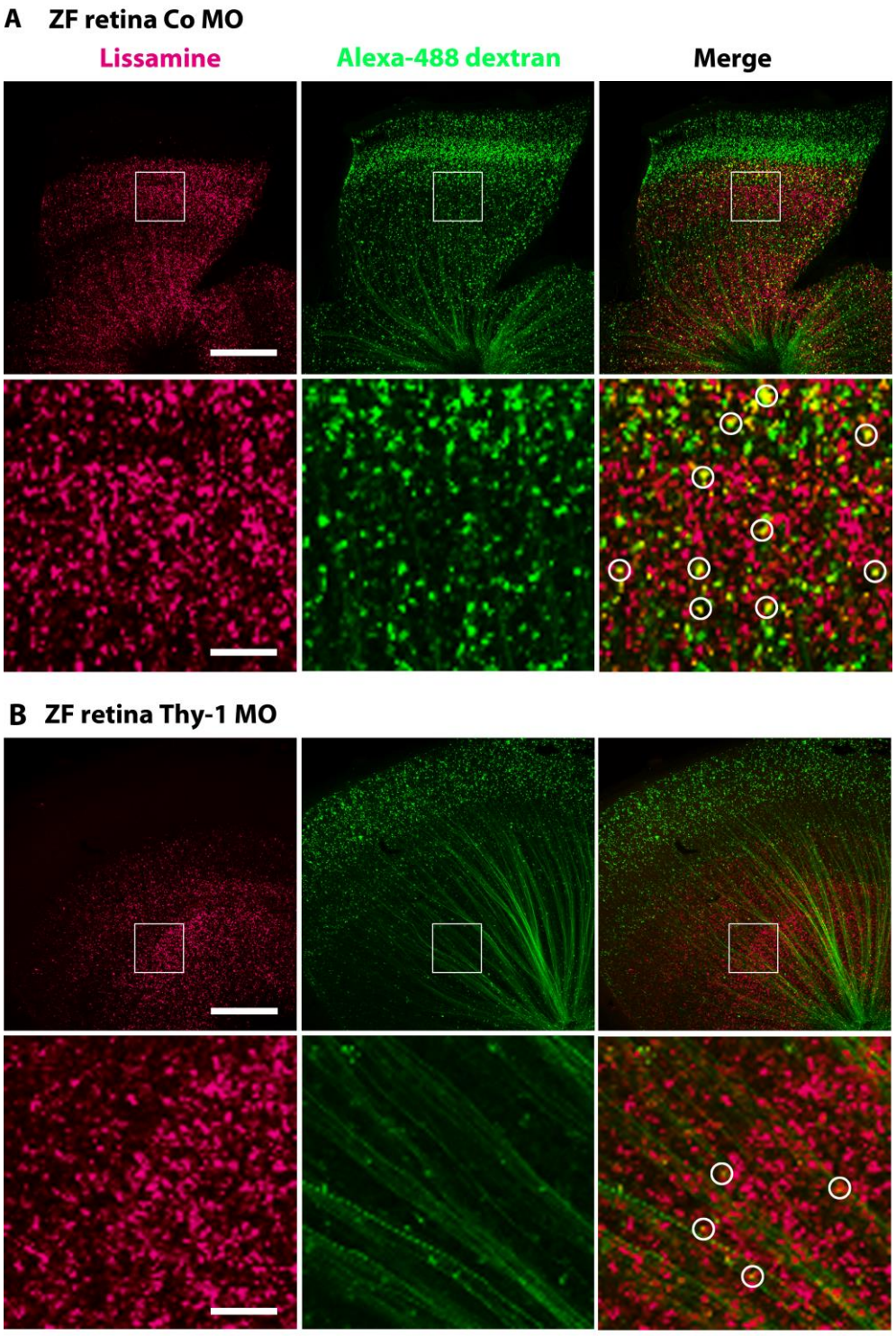
A ZF retina Co MO
Lissamine
Alexa-488 dextran
Merge
B ZF retina Thy-1 MO
C Thy-1 knockdown impairs regeneration
Alexa-488 labeled neurons
50
40
30
20
10
0
****
-65%
Co MO
140 µM
Thy-1 MO
140 µM
D Thy-1 knockdown impairs regeneration
Fluorescence intensity
Alexa-488
20
15
10
5
0
**
-65%
Co MO
140 µM
Thy-1 MO
140 µM

Figure 5.2.2.2 Thy-1 supports zebrafish optic nerve regeneration *in vivo*. A. Retina flat-mounts show RGCs transfected with the Co MO (magenta) and the tracer dye Alexa-488 dextran (green). Green cells within the red Co MO-labeled center represent regenerated axons. **B.** Treatment with Thy-1 MO (magenta) led to fewer regenerated axons, as represented by Alexa-488-dextran-labeled RGCs (green). Scale bars **A** and **B**: upper rows of 300 µm, lower row of zooms 50 µm. **C and D. Quantification of the *in vivo* regeneration assay.** Thy-1 knockdown reduces regeneration significantly by 65%. Number of green cells (**C**) or mean fluorescence (**D**) analyzed in 5 randomly chosen 200x200 µm squares per retina. 5 independent experiments, n = 10 retinae per group. Columns show mean +SEM with p(****) < 0.0001 in an unpaired, two-tailed student`s t-test against the group of Co MO retinae.

5.2.3. Thy-1 overexpression enhances, Thy-1 knockdown impairs neurite outgrowth of mouse hippocampal neurons *in vitro*

Reports about the role of Thy-1 in mammalian neurons are ambiguous. Antibody-mediated growth-blocking but also -promoting effects of Thy-1 have been observed, depending on the on cell type, environment of the neurons (e.g. in astrocyte co-cultures) or the sort of blocking reagent which was used (see introduction section 1.2: Thy-1 in the neuronal context). Therefore, I decided to first clarify the role of Thy-1 in mammalian neurons in order to compare it to the observations made in zebrafish neurons. Since mammalian neurons only grow in culture at the embryonic or neonatal stage but Thy-1 was reported to be physiologically expressed during later developmental stages of the brain, it was necessary to determine if cultured neurons produce Thy-1. In our cultured mouse hippocampal cells (derived from newborn mice) Thy-1 was already present in large quantities after two days in culture, as assessed by immunostaining with the commercial anti-Thy-1 antibody clone 53-2.1 (Fig 5.2.3 A). Interestingly, downregulation of Thy-1 expression via transfection of a mixed pool of four different siRNAs led to a significant reduction by 24% of the neurite length in these cells (Fig. 5.2.3 D, E), whereas overexpression of Thy-1-EGFP resulted in the opposite effect: 37% increase in axon lengths (Fig 5.2.3 B, C). These consistent findings demonstrated a growth-promoting role for endogenous, neuronal Thy-1 in primary mouse hippocampal neurons as well, as shown previously for zebrafish RGCs.

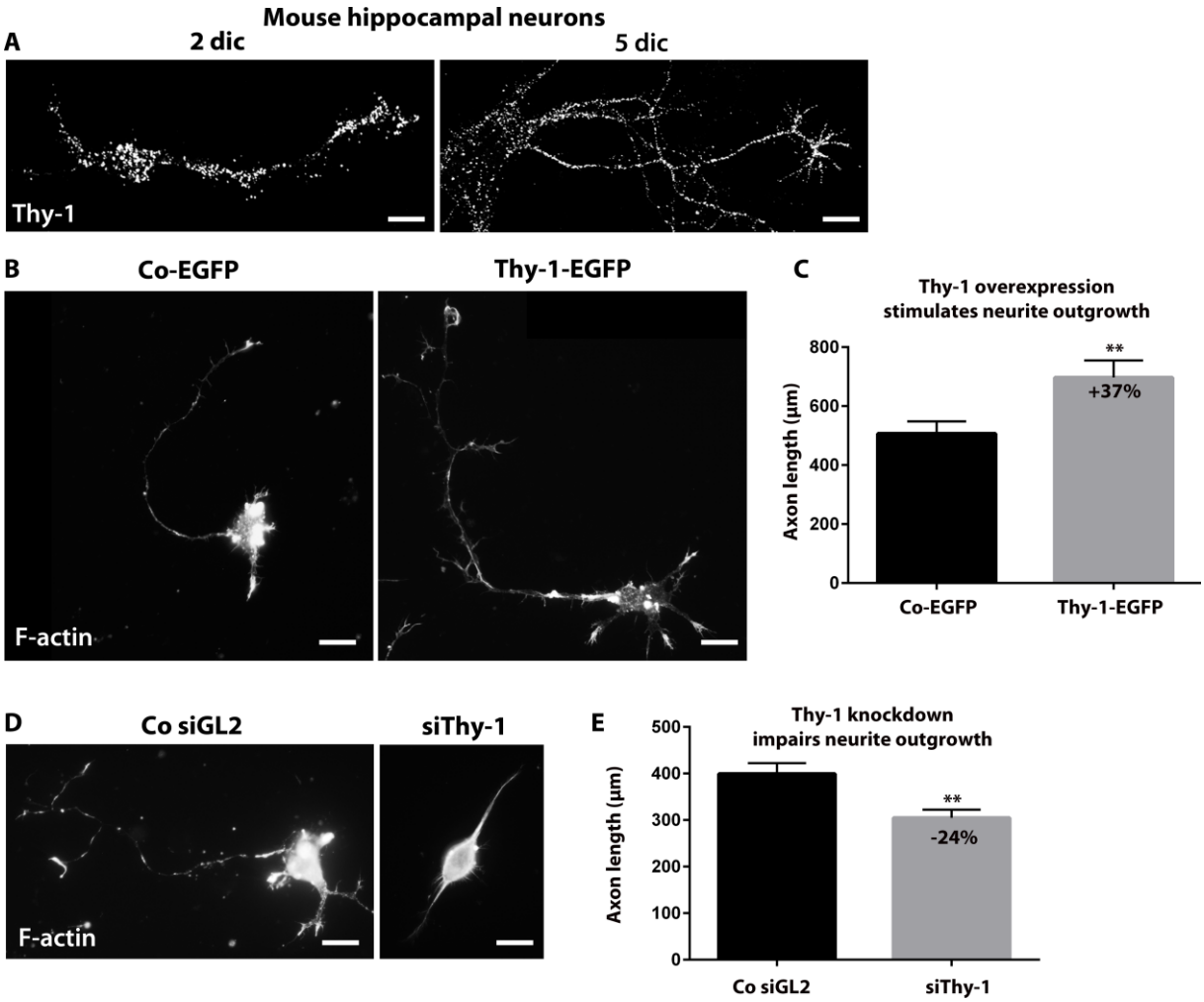

Figure 5.2.3 Thy-1 in primary mouse hippocampal neurons. A. Thy-1 in cultured hippocampal neurons. *In vitro*, Thy-1 is already expressed in high amounts after 2 days in culture (dic). After 5 dic Thy-1 is distributed all over the cell, including axon and growth cone. **B, C. Overexpression of Thy-1-EGFP** leads to 37% longer axons compared to Co-EGFP transfected cells. Experiment done 2 times with Co-EGFP n=101 cells, Thy-1-EGFP n = 110 cells. Columns represent mean +SEM with p(**) = 0.0096 in an unpaired, two-tailed student`s t-test. **D, E. SiRNA-mediated downregulation of Thy-1 expression** leads to 24% shorter axons, compared to control siGL2-transfected hippocampal neurons. Three independent experiments, with Co siGL2 n = 184 and siThy-1 n = 107 cells. Graphs show mean values +SEM with p(**) = 0.0044 in an unpaired, two-tailed student`s t-test. Scale bars: 20 µm. (Data obtained in collaboration with V. Bodrikov)

5.2.4. Thy-1 loss-of-function effect in mouse hippocampal neurons is rescued by Thy-1 overexpression *in vitro*

To further confirm the specificity of the Thy-1 siRNA-mediated knockdown and to exclude off-target effects, a rescue experiment was performed. For this purpose hippocampal neurons were co-transfected simultaneously with Thy-1 siRNAs and Thy-1-EGFP. Control siRNA targeting firefly luciferase GL2 and co-transfection with the empty EGFP vector served as controls. Thy-1 knockdown led to an average reduction of axon lengths by 41%, whereas Thy-1-EGFP overexpression elongated axons by 91% with respect to control in these experiments.

Co-transfection of siThy-1 and Thy-1-EGFP partially rescued the knockdown phenotype resulting in an increase of 36% with respect to the luciferase control (Fig. 5.2.4 A, C).

These additional data confirm the specificity of the Thy-1 siRNA-mediated, growth-impairing effect and support the conclusion, that mammalian Thy-1 -like its fish counterpart- plays a supportive role during axon growth in CNS neurons.

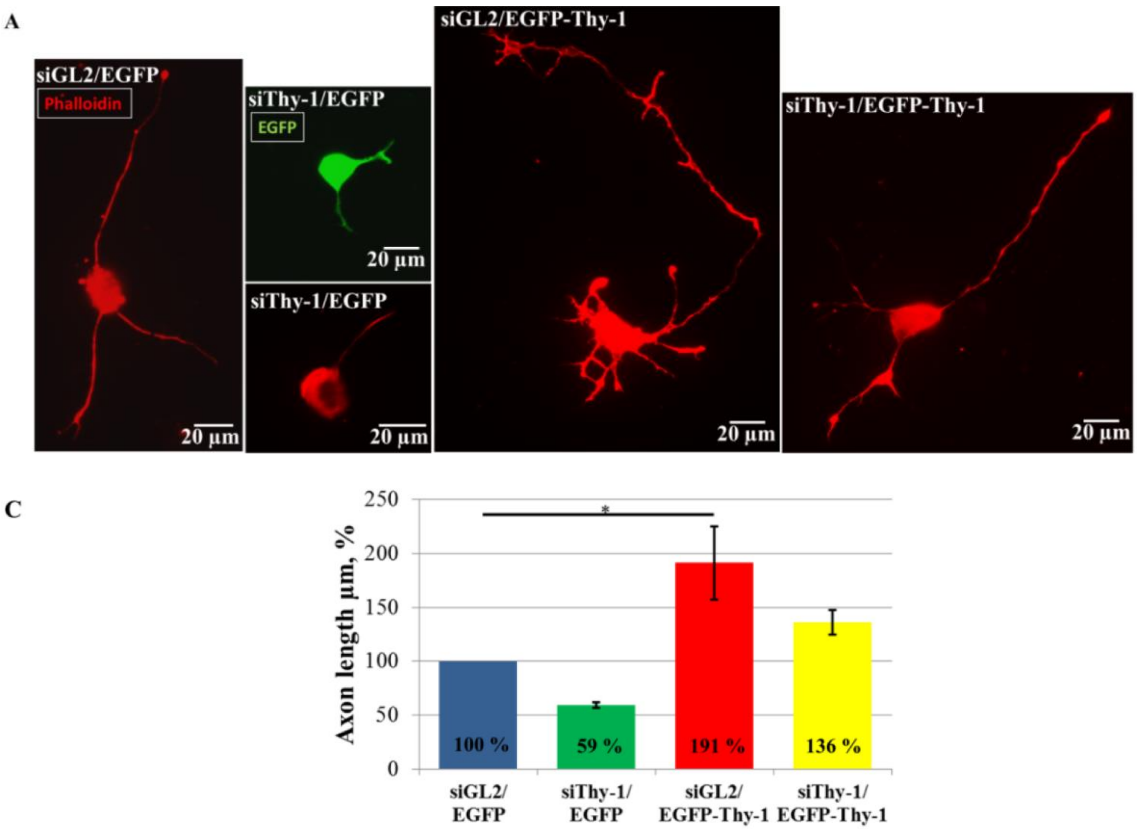

Figure 5.2.4 Functional rescue of the Thy-1 loss of function effect in primary mouse hippocampal axons. A. Neurons transfected with siGL2/EGFP, siThy-1/EGFP, siGL2/Thy-1-EGFP or siThy-1/Thy-1-EGFP visualized by F-actin labeling. **C. Quantification of A**, shown in percentage. SiThy-1/EGFP, siGL2/EGFP-Thy-1; p(*) < 0.05 and siThy-1/EGFP-Thy-1 in an unpaired, two-tailed student`s t-test against siGL2/EGFP. Bars represent mean ±SEM. (Figure taken with permission from the master thesis "Thy-1-induced and flotillin/reggie-mediated signaling", S. Henrich, 2014).

PART I PrP

The prion protein (PrP) is expressed throughout the mammalian CNS, and -beside other functions- promotes neurogenesis and differentiation (Steele et al., 2006). PrP is expressed most abundantly in regions of high plasticity and on elongating axons, which implies a special importance of this protein during axon growth and development (Salès et al., 2002). Particularly in the retina, PrP plays a neuroprotective/anti-apoptotic role (Frigg et al., 2006). Bony fish possess two PrP orthologues, PrP-1 and PrP-2, the former mediating embryonic cell adhesion and morphogenetic movements and the latter supporting neuronal growth and differentiation (Solis et al., 2013; Málaga-Trillo et al., 2011). In zebrafish embryos, PrP-1 is expressed ubiquitously but only at very early stages of embryogenesis, whereas PrP-2 becomes upregulated at a later time in developing neurons (Málaga-Trillo et al., 2009; Cotto et al., 2005).

Just like Thy-1, PrP is a GPI-anchored, growth-associated molecule clustering in lipid microdomains, thus communicating with intracellular signaling molecules and eliciting changes of cytoskeletal dynamics (Stuermer et al., 2001; Stuermer & Plattner, 2005a). Here I addressed the hypothesis that it may play an important role during regeneration of the adult zebrafish optic system.

5.3. Expression pattern of PrP-2 in zebrafish RGCs, characterization of a specific pAb

In order to investigate the distribution of PrP-2 and its functional role in the adult zebrafish optic system, a specific antibody was required. Almost all available PrP antibodies are mouse-specific and unlikely to be suited for studies in zebrafish, given the considerable amino acid divergence between mammalian and fish PrP sequences (Rivera-Milla et al., 2006; Rivera-Milla, Stuermer, & Málaga-Trillo, 2003). Therefore, we set out to generate fish-specific PrP-2 antibodies. To obtain a zebrafish-specific anti-PrP-2 antibody, rabbits were immunized with the recombinant globular domain of zebrafish PrP-2. The best serum was affinity purified and termed “PrP-2 981” (see methods 4.16.). PrP is a GPI-anchored molecule; I expected it to be localized predominantly at the plasma membrane, but not exclusively, since it has a fast turnover and it cycles rapidly between internal membrane compartments and the plasma membrane (Stahl et al., 1987; Griffiths et al., 2007). Fish PrP-2, like the mammalian protein,

contains two C-terminal N-glycosylation sites (Rivera-Milla et al., 2003; Haraguchi et al., 1989). Thus, a band shift in Western blots was anticipated upon deglycosylation.

5.3.1. Characterization of PrP-2 in zebrafish RGCs

Zebrafish PrP-2 has a predicted molecular weight of ~70 kDa (Malaga-Trillo et al., 2009). In contrast to Thy-1, PrP`s turnover is very fast (within few minutes) and its half-life is only a few hours (< 5 h) (Morris et al., 2006; Parizek et al., 2001). In Western blots of zebrafish brain and retina lysates upon strong inhibition of protease/phosphatase, the expected bands at ~70 kDa were detected. The prominent bands between 40 and 50 kDa represented degradation products of PrP-2 (Fig. 5.3.1 A). Western blot analysis of membranous and cytosolic fractions derived from brain lysates by sucrose density gradient centrifugation showed clear enrichment of the protein in the membrane fraction, which was best visible in the presence of ß-ME (Fig. 5.3.1 B). However, under these condition only the band at 40 kDa was visible corresponding to a putative degradation product (Fig. 5.3.1 A). In the presence of ß-mercaptoethanol (ß-ME) to the lysates degradation products increased, but the selected occurrence of PrP-2 in the membrane fraction appeared more evident. For comparison, mammalian PrP appears as three bands in Western blots, corresponding to the di-, mono- or non-glycosylated forms of the protein (Xanthpoulos et al., 2009). N-glycosylation of recombinant zebrafish PrP-1 and PrP-2 had been verified previously using GFP-tagged PrP-1&2; treatment with PNGase F resulted in a discrete band shift in Western blots (Málaga-Trillo et al., 2009). In order to confirm the glycosylation of endogenous PrP-2 under physiological conditions, zebrafish brain lysates was treated with PNGase F, which resulted in a small band shift of the ~70 kDa band to a lower molecular weight in Western blot performed with the polyclonal antibody 981 (Fig. 5.3.1 C).

In order to assess the functional context of PrP-2, its (sub-) cellular distribution of PrP-2 throughout the zebrafish retina is of interest. Therefore, I analyzed zebrafish retina whole mounts and single RGCs immunohistochemically. PrP-2 in zebrafish RGCs was localized at the plasma membrane, as expected, and enriched at the contact sites of adjacent cells (Fig. 5.3.1 D and E). After ONS, PrP-2 protein levels were highly increased, as shown by Western blot and immunohistochemical analyses (Fig. 5.3.1 F and E). PrP-2 appeared in large clusters, diffuse all over the cells, similarly to Thy-1 and reminiscent of GPI-anchored molecules in membrane microdomains upon activation (Fig. 5.1.2 E and Fig. 5.3.1 E) (Lemansky et al., 1990; Stuermer, 2011). Densitometric quantification of Western blot bands or quantification of

immunofluorescence intensities in RGCs revealed a 1.7- or 3-fold increase of PrP-2 levels upon ONS, respectively (Fig. 5.3.1 G and H).

These results indicate that the pAb 891 is a reliable, specific detection tool for zebrafish PrP-2 (for further validation see 5.3.2). Furthermore, these data strongly suggested a supportive function of zebrafish PrP-2 during axon growth, since it became upregulated by RGCs upon optic nerve lesion.

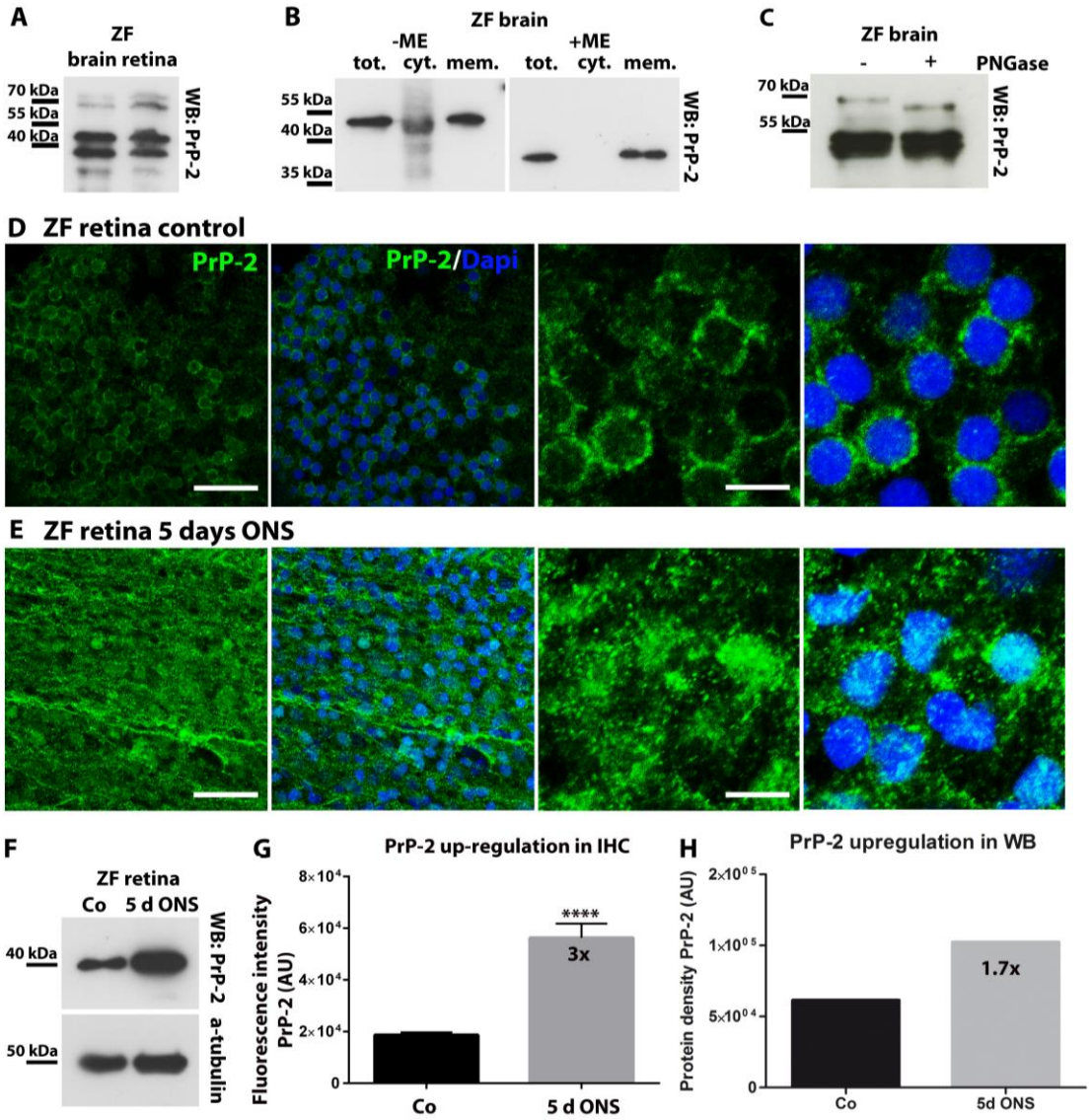

Figure 5.3.1 Verification of the pAb 981 recognizing zebrafish PrP-2 and expression pattern of the protein in the adult retina, untreated and after ONS. A. WB of zebrafish brain lysate with the pAb 981 shows several bands due to PrP-2 degradation. **B. Separation of cytosolic and membranous fractions** shows the expected membranous association of PrP-2, which is most evident in the presence of ß-ME. **C. Deglycosylation** results in a band shift of full length PrP-2 from ~70 kDa to ~60 kDa. **D, E. Zebrafish retina whole mounts**, PFA-fixed, untreated vs. 5 days after ONS. PrP-2 is membrane-bound, signal intensity increases and redistributes/clusters in RGCs and their axons upon ONL, reminiscent of GPI-anchored molecules in membrane microdomains upon activation (Lemansky et al., 1990; Stuermer, 2011). Scale bars: left 100 µm, right 20 µm. **F. Elevated protein levels of PrP-2**, 5 days after ONS in WBs of zebrafish retina lysates. **G. Quantification of immunofluorescence intensity** gives a 3-fold increase of PrP-2 in RCGs at 5 days after ONS compared to the untreated controls (n = 6 retinae per group). Graph shows mean +SEM, p(****) < 0.0001 in an unpaired, two-tailed student`s t-test. **H. Densitometric quantification** of PrP-2-specific bands in WBs at 5 days after ONS gives a 1.7-fold increase compared to untreated retinae. Experiment done once. Lysates obtained from 4 pooled retinae per group.

5.3.2. Knockdown of PrP-2 in zebrafish RGCs

In order to obtain more information about the functional role of PrP-2 in regenerating CNS neurons, an effective and specific knockdown of expression had to be achieved. *In vivo* morpholino application (140 µM) to the transected zebrafish optic nerve and retrograde transport into RGCs was the approach of choice, as described previously in section 5.1.4. Five days after simultaneous lesion and PrP-2 morpholino application, I extracted the retinae and analyzed them immunohistochemically or by immunoblotting using the polyclonal antibody PrP-2 981. PrP-2-specific signal intensity in control morpholino-treated eyes resembled that of untreated eyes (not shown), whereas PrP-2 morpholinos led to an efficient reduction of the immune-fluorescence signal (Fig. 5.3.2 A vs. B). To confirm the specificity of morpholino-mediated effects, two different sequences targeting zebrafish PrP-2 mRNA were used. Quantification of fluorescence intensities showed an average reduction of 44% for the PrP-2 MO sequence 1 and of 47% for PrP-2 MO sequence 2 (Fig. 5.3.1 D). Knockdown of PrP-2 showed a massive reduction PrP-2 protein bands in Western blot analysis compared to control morpholino-treated eyes. Due to the fast turnover and short half-life of the protein, PrP-2 bands cleared efficiently after morpholino-mediated inhibition of protein expression (Fig. 5.3.1 C). Specificity of the two PrP-2 morpholino sequences was also proven in parallel by Prof. Dr. E. Malaga-Trillo and his group in the zebrafish embryo model system (Malaga-Trillo et al., 2009).

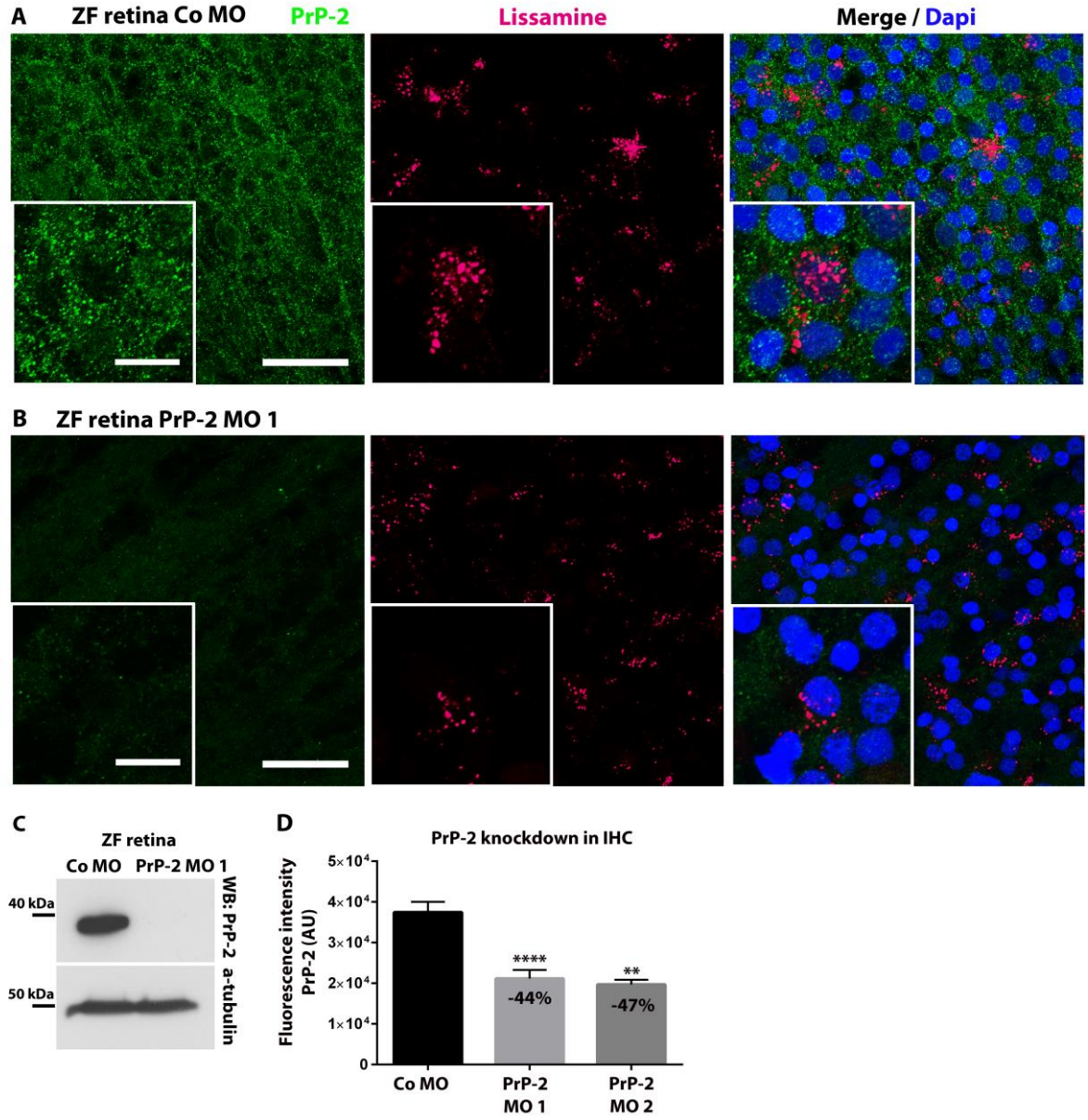

Figure 5.3.2 MO-mediated knockdown of PrP-2 in zebrafish RGCs *in vivo*. A and B. Immunofluorescence labeling of PrP-2 in zebrafish retina whole mounts (PFA fixation) at 5 days after Co MO (**A**) or PrP-2 MO (**B**) application to the transected optic nerve shows reduced signals in the PrP-2 MO-treated retinae. Scale bars: 50 µm, 10 µm in the detail. **C. WB analysis** shows a significant reduction of protein levels in PrP-2 MO- vs. Co MO-treated retina lysates. Experiment shown once for PrP-2 MO 1. Lysates obtained from 4 pooled retinae per group each time and normalized to the loading control alpha-tubulin. Additional confirmation by WB analysis of the efficiency of PrP MO 1s in the ZF retina system can be found in figure 5.4.2. **D. Quantification of immunofluorescence signals** results in a significantly reduced intensity of 44 or 47% for PrP-2 Mo sequence 1 or 2, respectively. Experiment done 3 times for Co MO n = 13 and PrP-2 MO 1 n = 17 and 2 times with PrP-2 MO 2 n = 4. One-way ANOVA between the three treatments reveals significant difference between means with p(****) < 0.0001. Graph shows mean +SEM. Follow-up Tukey`s multiple comparisons test shows p(****) < 0.0001 for Co Mo vs. PrP-2 Mo 1 and p(**) < 0.0032 for Co Mo vs. PrP-2 Mo 1.

With these data I confirmed specificity of the *in vivo* knockdown system and the pAb 981, and continued with functional outgrowth assays in single zebrafish RGCs and retinal explants.

5.4. The neuronal role of PrP-2

Reports in the literature about the neuronal function of PrP in mammals provide ample evidence for a role of PrP in inducing and promoting growth. For instance, in the laboratory of C. Stuermer (University of Konstanz), administration of recombinant mouse PrP-Fc to the medium of primary mouse hippocampal cultures led to a two-fold increase in neurite length (Bodrikov et al., 2011). This effect was connected to clustering of PrP in flotillin microdomains, Fyn and MAP signaling cascade activation and subsequent recruitment of N-Cadherin to the growth cone (Bodrikov et al., 2011). Using recombinant PrP as an extracellular ligand, other researchers have reported positive effects on neuronal outgrowth (Pantera et al., 2009; Chen et al., 2003; Graner et al., 2000). Only one publication showed a growth-blocking function of PrP, where it regulated the proteolysis of Caspr (contactin-associated protein), an inhibitory cue at the neuronal surface (Devanathan et al., 2010). Overexpression of cellular PrP enhanced neurite outgrowth in cultured mammalian neurons and various underlying mechanism have been suggested (Watanabe et al., 2012; Santuccione et al., 2005). Conversely, loss-of PrP impaired neuritogenesis in a neuronal cell line (Loubet et al., 2012). Based on these observations, and on our finding that PrP-2 protein levels increased during optic nerve regeneration in zebrafish, we hypothesized a growth-supportive role of PrP in zebrafish RGCs. Therefore, I analyzed the effect of PrP knockdown on neurite growth in fish and mammalian neurons.

5.4.1. Knockdown of PrP-2 in zebrafish RGCs *in vitro* and *in vivo* impairs neurite outgrowth

In order to analyze PrP-2 loss of function effects in adult primary fish neurons, cultured single RGCs were transfected with translation-blocking antisense morpholinos targeting PrP-2 mRNA. As described above, I employed two different morpholino sequences at two concentrations each. PrP-2 downregulation in single RGCs *in vitro* reduced axon length in a concentration-dependent manner and to a comparable extent for both PrP-morpholino sequences (either applied separately or in combination). The reduction was by 30% as compared to the control morpholino (Fig. 5.4.1 C). Immunolabeling of RGCs with the zebrafish-specific pAb 981 showed PrP-2 clusters localized throughout the entire cell, including axon and growth cone (Fig. 5.4.1 A). Measurement of the longest neurites of transfected cells was performed by means of F-actin visualization (Fig. 5.4.1 B). The fact that both PrP-2 morpholino

sequences (either alone or combined) resulted in a consistent, dose-dependent decrease of neurite lengths strengthens the conclusion of a specific, growth promoting role of PrP-2 during growth of zebrafish RGCs in culture.

In order to confirm this finding and to analyze PrP function in the physiological context, I performed outgrowth assays with zebrafish retinal explants. Knockdown of PrP-2 *in vivo* in fish RGCs drastically impaired axonal outgrowth from retinal tissues. Application of 70 µM PrP-2 morpholino 1 or 2 to the transected optic nerve significantly reduced axonal outgrowth by 52 (or 59) %, compared to the control morpholino-treated retinae. The latter grew an average of ~40 axons per explant after 24 h in culture. Doubling the morpholino concentration (140 µM) resulted in 88% or 92% less axons for PrP-2 morpholino 1 or 2, compared to control explants whose average number of axons (~40) remained unchanged even after receiving a higher dose of control morpholinos (Fig. 5.4.2 A and B). PrP-2 morpholino-transfected explants recovered upon longer incubation times, concomitantly to a restoration of PrP-2 protein levels (see supplementary data 9.9.). These experiments demonstrated that PrP-2 is a key player during axon regeneration of the zebrafish optic nerve.

In order to compare the function of endogenous PrP in fish and mammalian neurons, we searched for consequences of PrP^c knockdown in primary mouse hippocampal neurons on neuronal growth (see Fig. 5.5 C). SiRNA-mediated knockdown of PrP^c in mouse hippocampal neurons *in vitro* resulted in a 40% reduction in axon length, compared to control siGL2 (firefly luciferase) transfected cells (Fig. 5.5). This study further supports the observations made in zebrafish RGCs (Fig. 5.4.1).

Taken together, this data indicates that endogenous PrP represents a growth-promoting molecule in the neuronal system of both species: zebrafish with a high, and mouse with a much lower neuronal regeneration capability.

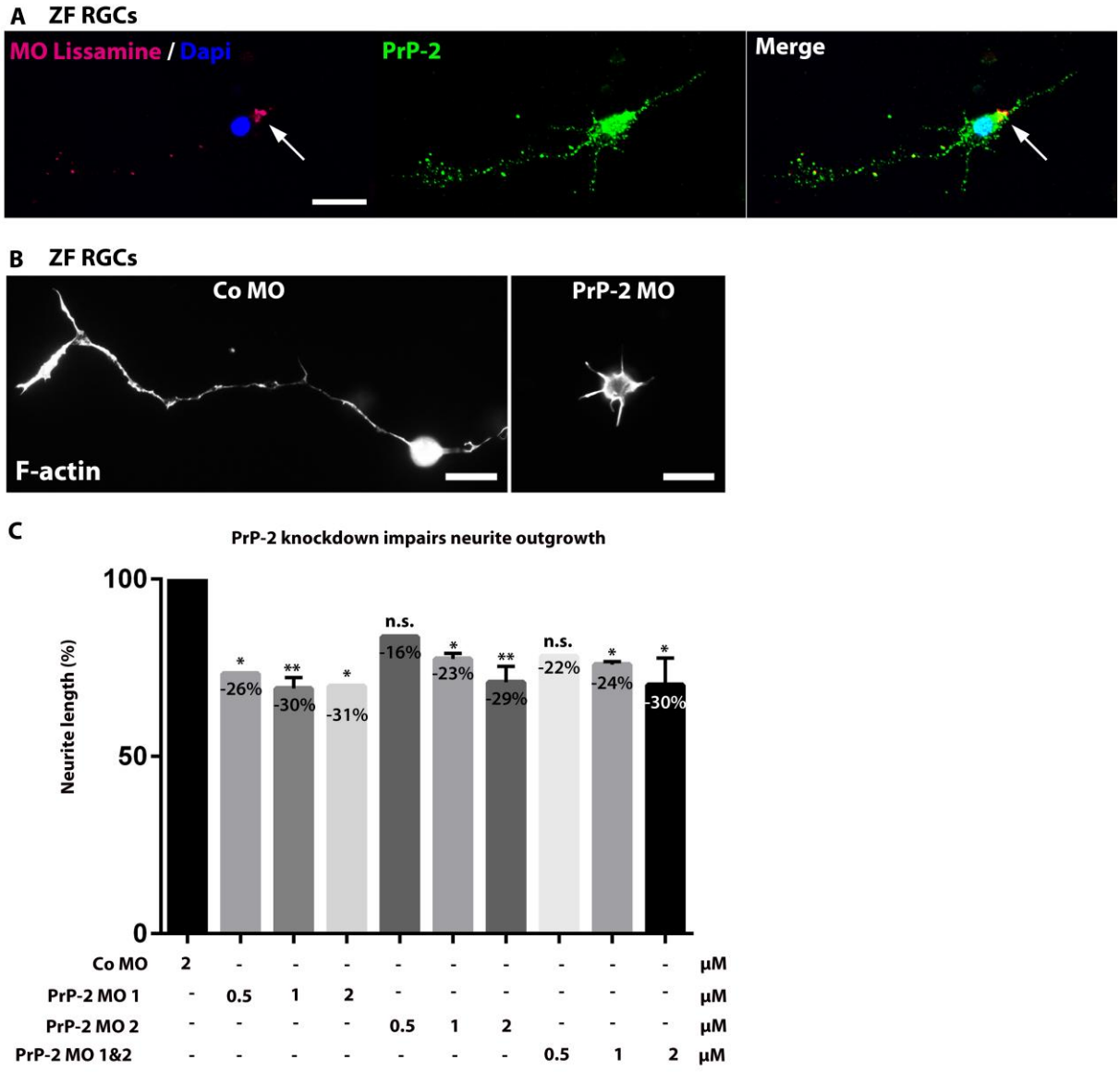

Figure 5.4.1.1 MO-mediated knockdown of PrP-2 impairs axonal outgrowth of zebrafish RGCs *in vitro*. A. Single zebrafish RGCs transfected with Co MO (magenta), stained with DAPI (blue nucleus) and pAb 981 PrP-2 (green). The lissamine-tagged Mo is localized mainly in a perinuclear pattern in the cytoplasm but also along the axon. PrP-2 is present at the cell body and in neurites, showing a clustered, membranous pattern as typical for GPI-molecules. Scale bar: 15 µm. **B. MO-transfected cells** were labeled for F-actin and average lengths of the longest neurites were compared. **C. Quantification of neurite lengths.** Experiment with MO conc. 0.5 µM was done once, with Co MO n = 41, PrP-2 MO 1 n = 104, PrP-2 MO 2 n = 111, PrP-2 MO 1&2 n = 71. Axons were shorter by 26, 16 and 22%, respectively. MO conc. 1 µM: Experiment done 3 times independently for single PrP-2 MO 1 and PrP-2 MO 2 treatment and 2 times for combined PrP-2 MOs 1&2. Co MO n = 316, PrP-2 MO 1 n = 469, PrP-2 MO 2 n = 405, PrP-2 MO 1&2 n = 368. Axons were shorter by 31, 23 and 24%, respectively. MO conc. 2 µM: Experiment done once for PrP-2 MO 1 and twice for PrP-2 MO 2 and PrP-2 MO 1&2. Co MO n = 316, PrP-2 MO 1 n = 297, PrP-2 MO 2 n = 324, PrP-2 Mo 1&2 n = 360. Axon lengths were reduced by 30, 29 and 30%, respectively. Graphs show mean +SEM. Two-way ANOVA between groups was significant with p(**) = 0,0013, F (3, 7) = 17,29. Follow-up Tukey`s multiple comparisons test shows n.s. = not significant, p(*) < 0.05, p(**) < 0.005 of PrP-2 MO groups against the Co MO group.

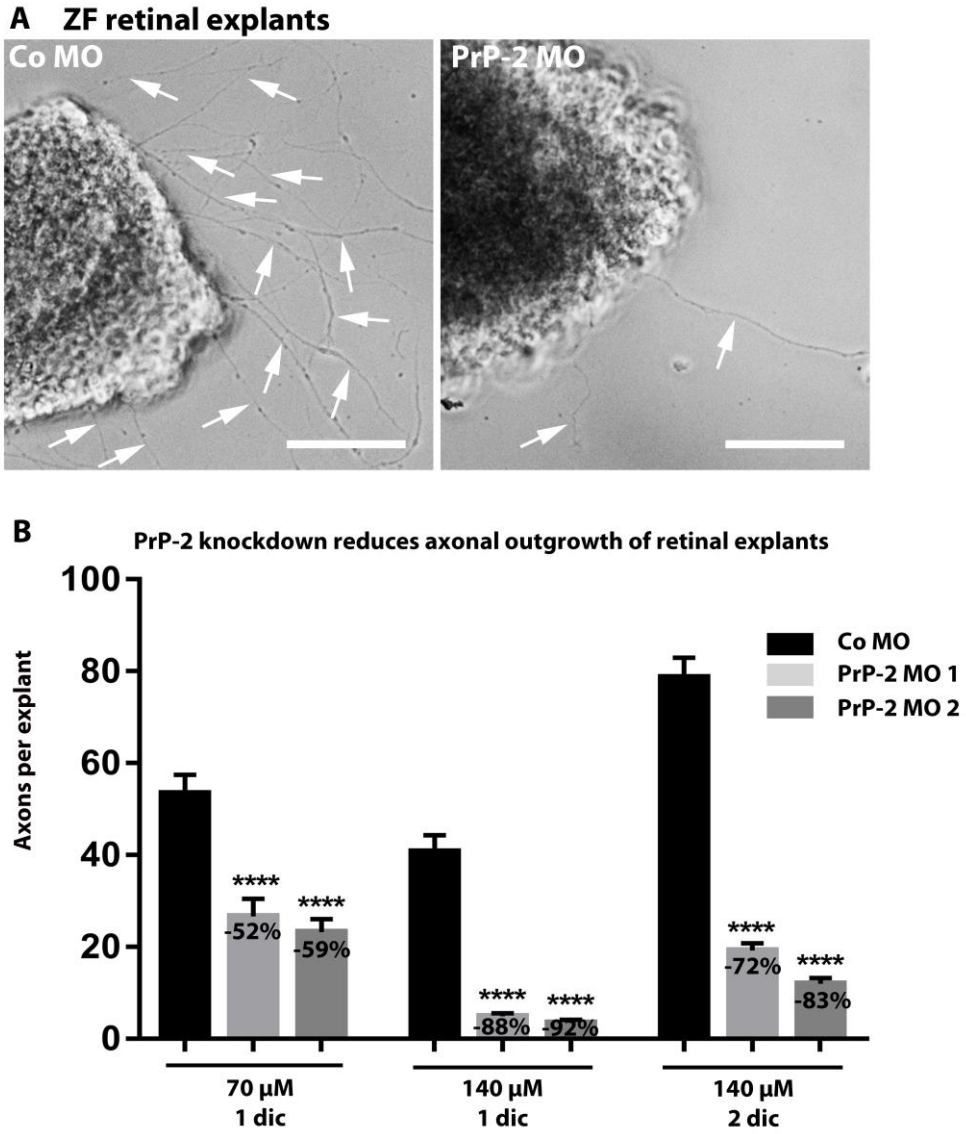

Figure 5.4.1.2 MO-mediated knockdown of PrP-2 impairs axonal outgrowth of zebrafish retinal explants *in vitro*. A. Retina explant tissues transfected with 140 µM Co MO or PrP-2 MO, 1 dic. Control explant tissues grow significantly more axons than PrP-2 MO-treated retinae (arrows). Scale bars: 100 µm. **B. Quantified numbers of axons.** 70 µM of MO 1 or MO 2 leads to -52% or -59% less axons after 1 day in culture (dic), whereas 140 µM leads to -88% or -92% after 1 dic and recovers up to -72 or -83% after 2 dic. Experiment done twice independently with two different MO sequences and two different concentrations each time. 70 µM: Co MO n = 126, PrP-2 MO 1 n = 89, PrP-2 MO 2 n = 95. 140 µM: Co MO n = 64, PrP-2 MO 1 n = 79, PrP-2 Mo2 n = 69 explants. Two-way ANOVA of raw data between different morpholino concentrations and sequences was significant with p(****) < 0.0001 and F (2, 506) = 64,63 and F (2, 506) = 256. Follow-up Sidak`s multiple comparisons test between means of each PrP MO treatment with its control was significant with p(****) < 0.0001. Graph shows mean +SEM. Scale bars: 100 µm.

5.4.2. Knockdown of PrP-2 in zebrafish RGCs impairs Src kinase signaling

GPI-anchored proteins preferentially localize in specialized lipid rafts which function as signaling platforms thereby transducing outside signals inwards (Stuermer et al., 2001; Stuermer et al., 2004; Ochs and Malaga-Trillo, 2014). As a potential signaling partner for fish PrP-2, the Src-family protein kinases (SFKs) were of high interest, because they were shown

to be influenced by Thy-1, PrP and flotillin. Reports about PrP-mediated signaling, connected to enhanced neurite outgrowth, often converge on the activation of SFKs (Pantera et al., 2009; Mouillet-Richard et al., 2000; Santuccione et al., 2005). Therefore, the observed reduced neurite outgrowth upon PrP knockdown could be the consequence of affected SFK levels and/or activation. I examined this scenario by performing Western blots of zebrafish retinae upon PrP-2 knockdown *in vivo* using two different anti-Src antibodies. The first antibody was generated by immunization with the conserved C-terminus of SFKs (termed "totSrc" below) and detected the SFK members Fyn, Yes and Src, with a size of approximately 60 kDa. The second antibody recognized only the active, phosphorylated (Tyr 416) form of these SFKs (called pSrc below). Protein levels of total and activated SFKs strongly decreased upon morpholino-mediated PrP-2 knockdown in zebrafish retina lysates (Fig 5.4.2 A). Quantification of protein levels showed a 45% and 74% reduction, for totSrc and pSrc, respectively (Fig. 5.4.2 B). Given the known role of SFKs in the regulation of the actin cytoskeleton, it is likely that the disturbance of SFKs -in particular pSrc- upon PrP knockdown, affected cytoskeletal structures in zebrafish RGCs, the basis for a properly functioning outgrowth machinery in neurons, and resulted in impaired axonal outgrowth (Ochs & Málaga-Trillo, 2014).

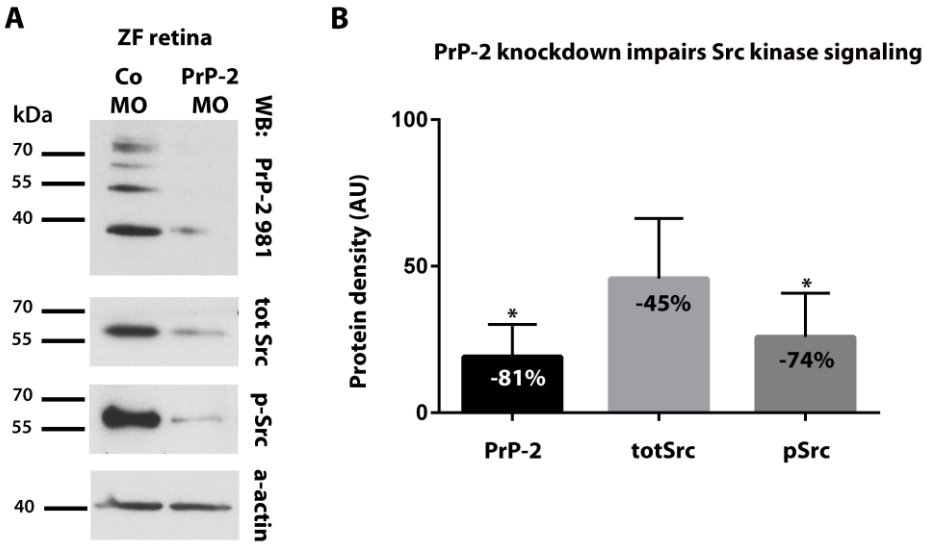

Figure 5.4.2 Knockdown of PrP-2 reduces total/phospho-Src levels in zebrafish retinae. **A. WB analysis** shows a successful knockdown of PrP-2 (81%, upper lane) in all protein bands of PrP-2-specific degradation products. Total (active plus inactive) levels of the SFKs including Fyn, Yes, and Src (totSrc) as well as only the phosphorylated/activated form of Src (pSrc) are reduced by 45% and 74%, respectively. Experiment done 2 times independently, with 3 pooled retinae per group each time. **B. Quantification of protein levels**: PrP-2 MO-treated compared to Co MO-treated retinae, normalized to the loading control alpha-actin. Average values +SEM are shown. One way ANOVA shows significant differences between means with p(****)<0.0001 and follow-up Dunnett`s multiple comparisons test between the control and the other groups results in n.s.=not significant and p(*)<0.5.

5.5. Potential interactions of Thy-1 and PrP in hippocampal neurons

Upon activation, Thy-1 and PrP become redistributed to flotillin-defined microdomains and signal via common pathways (e.g. SFKs and MAPK), thereby exerting changes in cytoskeletal dynamics (Stuermer, 2011a; 2011b; Stuermer et al., 2001). Therefore, we considered the possibility of a functional, potentially compensatory, interaction between Thy-1 and PrP, particularly given that there is no obvious phenotype in knockout animals (in $PrP^{-/-}$ or $Thy\text{-}1^{-/-}$ neurons). If there was a functional connection, we hypothesized that activation/clustering of one or the other protein would increase their co-localization via clustering in lipid raft microdomains. We performed antibody stimulation/clustering assays of PrP and Thy-1 in primary hippocampal neurons and analyzed the degree of co-localization of the two proteins (results in Fig. 5.5). The proteins were visualized by immunohistochemistry and fluorescence signal intensities were measured for each protein. The degree of overlap of two immunolabeled protein clusters was calculated using the software package Scion Image. This technique provides an indication for potentially increasing interactions between two proteins, in close proximity at the cell surface. It allows the identification of a potential functional associations between two molecules. Biochemical assays like co-immunoprecipitation are not feasible due to the very limited number of cells available (Bodrikov et al., 2011, 2008, 2005; Stuermer et al., 2004).

Using this methodology, we found a degree of co-localization between Thy-1 and PrP of already 50% in under unstimulated conditions in wild type primary hippocampal neurons. Some degree of basal co-localization was expected, since both proteins share flotillin-defined microdomains at the cell-surface and antibody stimulation of PrP in T-cells has been observed to trigger its accumulation and increased co-localization with Thy-1 and other signaling molecules in lipid rafts (Stuermer and Plattner, 2005b; Stuermer et al., 2004).

In cultured primary mouse hippocampal neurons, stimulation/activation of either Thy-1 or PrP via antibody clustering did not result in increased spatial connection of both proteins (Fig 5.5 A and B). In order to test whether Thy-1 and PrP share a common signaling pathway connected to neurite outgrowth, I analyzed the effect of siRNA-mediated double knockdown of both proteins. Simultaneous knockdown of Thy-1 and PrP was not additive with respect to axon growth and was not different from single knockdown of either PrP or Thy-1 alone (Fig. 5.5 C). This result suggests that the two proteins use different signaling pathways. Furthermore, in our experimental setup, $PrP^{-/-}$ primary hippocampal neurons showed no increase in total Thy-

1 protein levels compared to wild type cells (Fig 5.5 D). This suggested that these cells compensate for the loss of PrP by other mechanisms than raising the amount of Thy-1 or by altering Thy-1 associated signaling.

Further downstream analysis will be necessary to verify the hypothesis of any potential Thy-1 to flotillin-mediated compensation mechanism in PrP knockout mice.

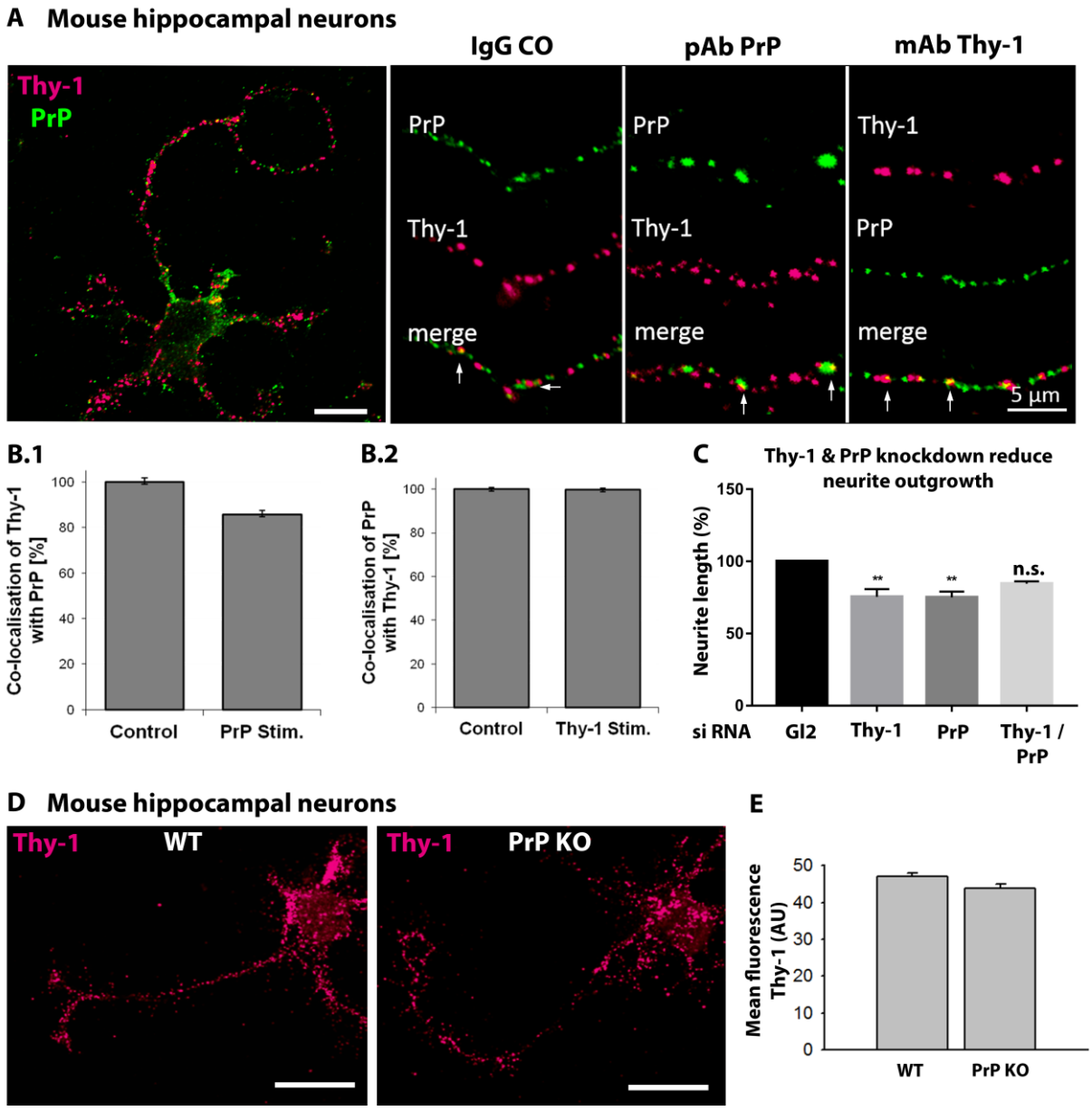

Figure 5.5 Interaction of Thy-1 and PrP in mouse hippocampal neurons. A. Mouse hippocampal neurons, antibody clustering assay. Protein clustering with anti-PrP or anti-Thy-1 antibody shows a similar degree of co-localization (white arrows) between Thy-1 and PrP as in neurites stimulated with an IgG control. Scale bars: 20 µm in the left picture of the whole cell, 5 µm in all details at the right. **B. Quantification of co-localized Thy-1 and PrP clusters** remains unchanged upon PrP or Thy-1 antibody stimulation. Experiment done once. **C. Neurite outgrowth** after siRNA-mediated knockdown of PrP and Thy-1 impairs neurite length to the same extent as siPrP or siThy-1 alone. Experiment done 3 times independently. Co siGl2 n = 184, siPrP = 148, siThy-1 n = 108, siThy-1 & siPrP n = 118. Graph shows mean +SEM with p(**) < 0.05 in a one sample student`s t-test compared to the control. **D. The level of total Thy-1** is of comparable amount in PrP KO and wild type neurons. Immunofluorescence intensities measured in hippocampal cells in culture. Experiment done once, bar graph represents mean +SEM. Scale bars: 30 µm. **E.** 40% increased Thy-1 to flotillin-2 co-localization in PrP KO hippocampal neurons, labeled for Thy-1 (magenta) and flotillin-2 (green) as compared to wild type. One experiment, quantification bars show mean +SEM. Scale bars: 10 µm. (Data and figures obtained in close collaboration with V. Bodrikov and the consolidation course student J. Brandes).

5.6. Studies of Thy-1, PrP and flotillin-2 in the neuronal mouse CAD cell line

Earlier studies in mammalian cells provided evidence that PrP -and likely also Thy-1- are linked to the signaling molecules Src, ERK1/2 and cofilin via flotillin microdomains, which was in case of PrP knockdown the underlying molecular mechanism of impaired neurite outgrowth in mouse hippocampal neurons (see chapters 1.2, 1.3, 6.4, 6.8) (C. Stuermer, 2010; Lang et al., 1998; V. Bodrikov et al., 2011). In order to investigate this signaling pathway via biochemical approaches, a suitable cell line was needed to obtain sufficient sample material. For this reason, I established the culturing of the cell line CAD (cath.-a-differentiated), which expresses all proteins of interest (PrP, Thy-1, flotillin). Prior to functional assays, CAD cells had to be characterized by immunocytochemistry and Western blot analysis. CAD cells are of mouse neuronal origin (cathecholaminergic brain tumor) (Suri et al., 1993; Lazaroff et al., 1998; Herrera-Molina et al., 2012a).

CAD cells cultured in the appropriate medium differentiated, assumed neuron-like morphology and expressed Thy-1 in a clustered, dotted pattern at the plasma membrane, particularly enriched at cell contacts (Fig. 5.6 A). PrP showed a diffuse, grainy staining pattern, uniformly expressed over the entire cell, as well as flotillin-2, which was prominent in the cell soma and also present at neurites (Fig. 5.6 B and C).

All three molecules of interest -Thy-1, PrP, flotillin-, as well as the signaling molecules -Src, ERK 1/2 and cofilin- were characterized by parallel in our laboratory immunocytochemistry and in Western blots.

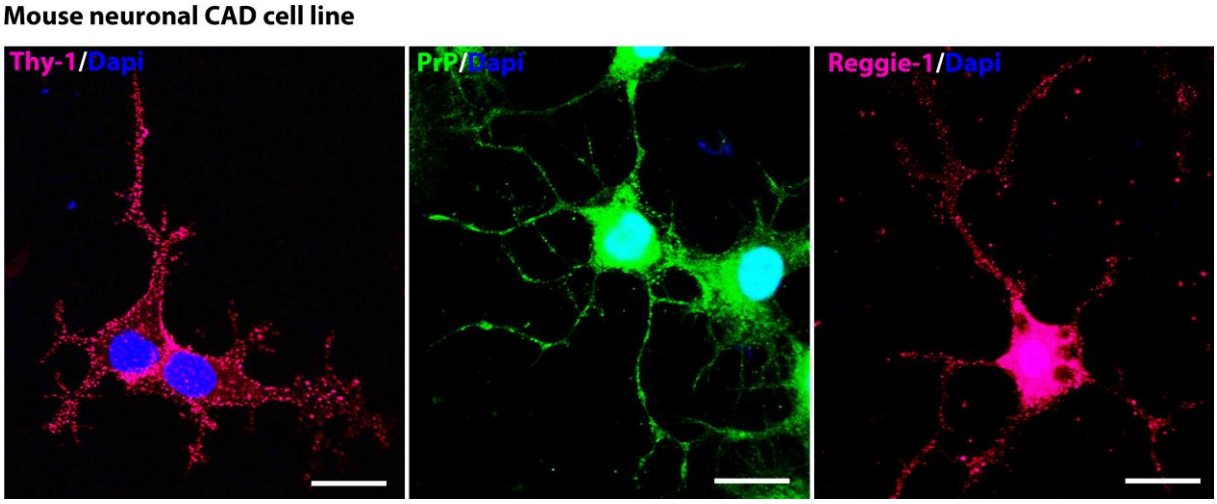

Figure 5.6 Differentiated mouse neuronal CAD cells. A. Immunolabeling for Thy-1 (magenta) shows clustered distribution of the protein, enriched at cell-cell-contact sites. **B.** PrP (green) shows a diffuse, grainy pattern in the cell body and neurites. **C.** Flotillin-2 (reggie-1) is present in the entire neuron, prominent in the soma and dotted in its microdomains along the neurites. Scale bars: 20 µm.

These experiments were carried out as preparatory work and preliminary results for future biochemical experiments, investigating the precise signaling mechanisms underlying the observed malfunctions upon loss of mouse Thy-1 and PrP in axon growth and regeneration.

PART II RTN4b

In the context of my general aim, to study the molecular basis of regeneration in fish and mammals, it was of interest to examine not only the two flotillin-associated proteins Thy-1 and PrP but also another important modulator of regeneration: the mammalian myelin-associated growth inhibitor Nogo-A (*rtn-4/nogo*) and its counterpart RTN4b in fish. While mammalian Nogo-A restricts axon growth after CNS injury, the teleost version of the protein is of high interest because fish do not present hostile conditions for regeneration and fully restore CNS function (Kempf & Schwab, 2013; Becker et al., 1997). Fish myelin seemed to be not as inhibitory to growing CNS axons as rat myelin and it was suggested that the presence of inhibitory RTN4b/Nogo-A could explain the difference between regeneration capacities of fish and mammals (Abdesselem et al., 2009; Bastmeyer et al., 1991). Further research identified two fish homologues of Nogo: RTN4a and RTN4b (Diekmann et al., 2005; Shypitsyna et al., 2011). Mammalian Nogo-A has two major inhibitory regions; the N-terminal Nogo-specific region (NSR, containing the “delta-20” region, or also called “amino-Nogo”) and the

C-terminal reticulon homology domain (RHD, or also called “Nogo-66”). The Nogo-66 region is present in all fish isoforms (RTN4a and RTN4b), with 80% homology to human Nogo-A, whereas the NSR is only present in RTN4b (Diekmann et al., 2005; Shypitsyna et al., 2011).

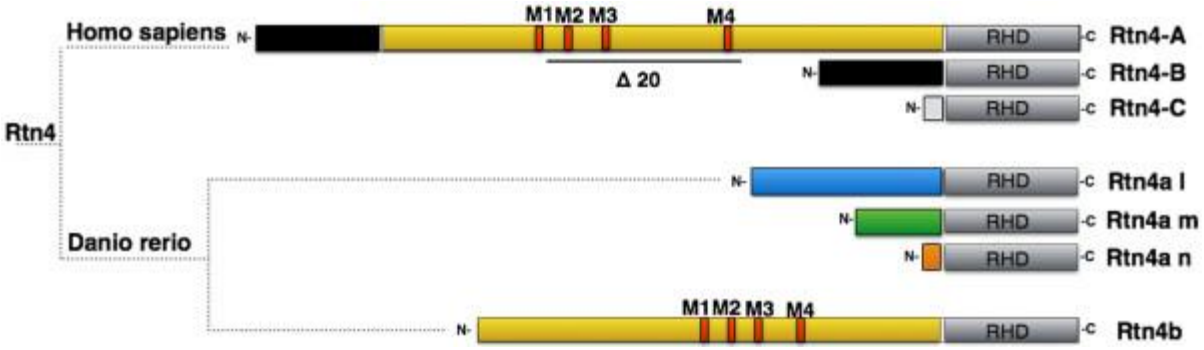

Figure 5.7 Schematic representation of the human *RTN4* gene and its zebrafish paralogues. All three major isoforms encoded in the *RTN4* gene in humans (RTN4A, RTN4B and RTN4C) possess the reticulon homology domain (RHD), which includes the Nogo66 domain. The N-terminal region of RTN4A contains the Nogo-A-specific domain (yellow) and the neurite growth inhibitory delta-20 (Δ20) stretch. The diagnostic M1 to M4 motifs are red. The zebrafish has two *RTN4* paralogues: *rtn4a* and *rtn4b.* Rtn4a is produced in three different isoforms (Rtn4-l (blue), Rtn4-m (green) and Rtn4-n (orange)) with the same C-terminal RHD. Rtn4b also contains the M1 to M4 N-terminal motifs (red) and presents a distinct RHD. (Figure and caption taken from Pinzón-Olejua et al., 2014).

Earlier experiments with recombinant fish Nogo-66/RHD (RTN4a) showed that 20% sequence difference between mammalian and fish RTN4a seemed to make the difference in its inhibitory properties, since it was reported to be permissive for fish and mouse axonal growth (Abdesselem et al., 2009). Mapping of the functional inhibitory regions within the second functional domain of Nogo-A identified the “M1 / M2 / M3 / M4 (M1-4) motifs” within the NSR/delta-20 region, which are highly conserved among all species analyzed and only present in the RTN4b isoform of zebrafish (Shypitsyna et al., 2011).

Regarding the Nogo-A/RTN4b protein I had three aims. Firstly, I wanted to investigate whether the four integrin-binding domains “M1-4” are indeed functional inhibitory motifs of the NSR region by using a mutant peptide encompassing the M1-4 region, in which an aspartic acid (D) is exchanged for alanine (A) in all signature tripeptide sequences (Asp-Leu/Ile-Val/Leu/Ile) of each of the four motifs (Dr. A. Shypitsyna, unpublished).

My second aim was to address the question as to whether the zebrafish homologue of Nogo-A (RTN4b) is inhibitory to neurons by using recombinant rat RTN4 M1-4, the mutated rat RTN4 M1-4 D/A and also the zebrafish RTN4b M1-4 as a substrate for mammalian and fish neurons in functional outgrowth assays.

My third objective was to investigate the expression of RTN4b throughout the zebrafish retina and its intrinsic contribution to regeneration of retinal axons upon knockdown via morpholino oligos.

5.7. Expression of RTN4b in zebrafish RGCs and its role in axon regeneration

In order to characterize expression and function of the zebrafish RTN4b protein, a polyclonal antibody recognizing recombinant fish RTN4b M1-4 was produced in rabbit. The polyclonal serum was tested for reactivity, affinity purified and named K1121 (see method 4.12.3. and 4.16.). The specificity of this new zebrafish RTN4b antibody was confirmed by Western blotting analysis using the recombinant peptide and by RTN4b knockdown in zebrafish embryos and retinae (Pinzón-Olejua et al., 2014; Welte et al., 2015).

Since the "true" zebrafish Nogo-A homolog was discovered just recently (RTN4b instead of RTN4a, as previously thought), its expression and function in fish had not been studied. On the other hand, extensive data about the expression of mammalian Nogo-A is available: it is specific to the CNS and expressed at the cell surface of oligodendroglial cell bodies and their myelin sheaths in nerve fiber tracts (Buss et al., 2005). Also numerous populations of neurons in the brain and spinal cord express Nogo-A to a variable extent at the plasma membrane of cell bodies and neurites (Schwab, 2010). The largest proportion of Nogo-A in a cell (>95%) is restricted to the tubular endoplasmic reticulum (ER), where it is required to shape its curvature and only very small amounts (<10%) are found at the plasma membrane, thereby inhibiting growth (Voeltz et al., 2006). Of particular interest for this thesis was the fact that mammalian Nogo-A is expressed in rat RGCs, and that glial and neuronal Nogo-A were found to play opposite roles in the injured visual system (Pernet et al., 2012; Vajda et al., 2014). Endogenous Nogo-A levels increase in mouse RGCs after optic nerve lesion and its artificial overexpression promotes axonal regeneration (Pernet et al., 2012; Vajda et al., 2014).

5.7.1. Expression of RTN4b in zebrafish RGCs

Immunolabeling of zebrafish RTN4b with the new polyclonal antibody "K1121" showed a diffuse and grainy intracellular expression pattern in all RGCs throughout the zebrafish retina. In untreated retinae, axons were weakly stained and cytoplasmic fluorescence intensities varied from cell to cell but some intersparsed cells were conspicuously bright (Fig. 5.7.1 A, supplementary data 9.12.2). Nogo-A was not restricted to RGCs, apparently glial end-feet were immune-labeled as well (Fig. 9.12.1). Upon optic nerve lesion, intracellular RTN4b

expression increased massively in all RGCs and axons (Fig. 5.7.1 B and C). Quantification of fluorescence intensities revealed an increase of 36%, five days after ONS as compared to controls. After ten days an increase of 33% was still observable (Fig 5.7.1 E). Live staining without fixation and permeabilisation of retinal tissue produced no detectable fluorescence, which implied that RTN4b was localized exclusively intracellularly in fish RGCs. Correspondingly, protein levels in Western blots of retina lysates showed an increase of RTN4b of 54% (at 5 days ONS) (Fig. 5.7.1 D, F). The zebrafish RTN4b amino acid sequence has a predicted molecular mass of 93.6 kDa (ExPASy) and the affinity purified, polyclonal antibody K1121 showed a single protein band at the expected height of ~90 kDa in Western blots (Fig. 5.7.1 D and supplementary data Fig. 9.11).

The increase of RTN4b levels in zebrafish retinae after axonal injury strongly suggest a functional importance of this protein during regeneration in the CNS. To test this hypothesis, the next step was to examine any potential impact on axonal regeneration upon RTN4b knockdown in zebrafish RGCs.

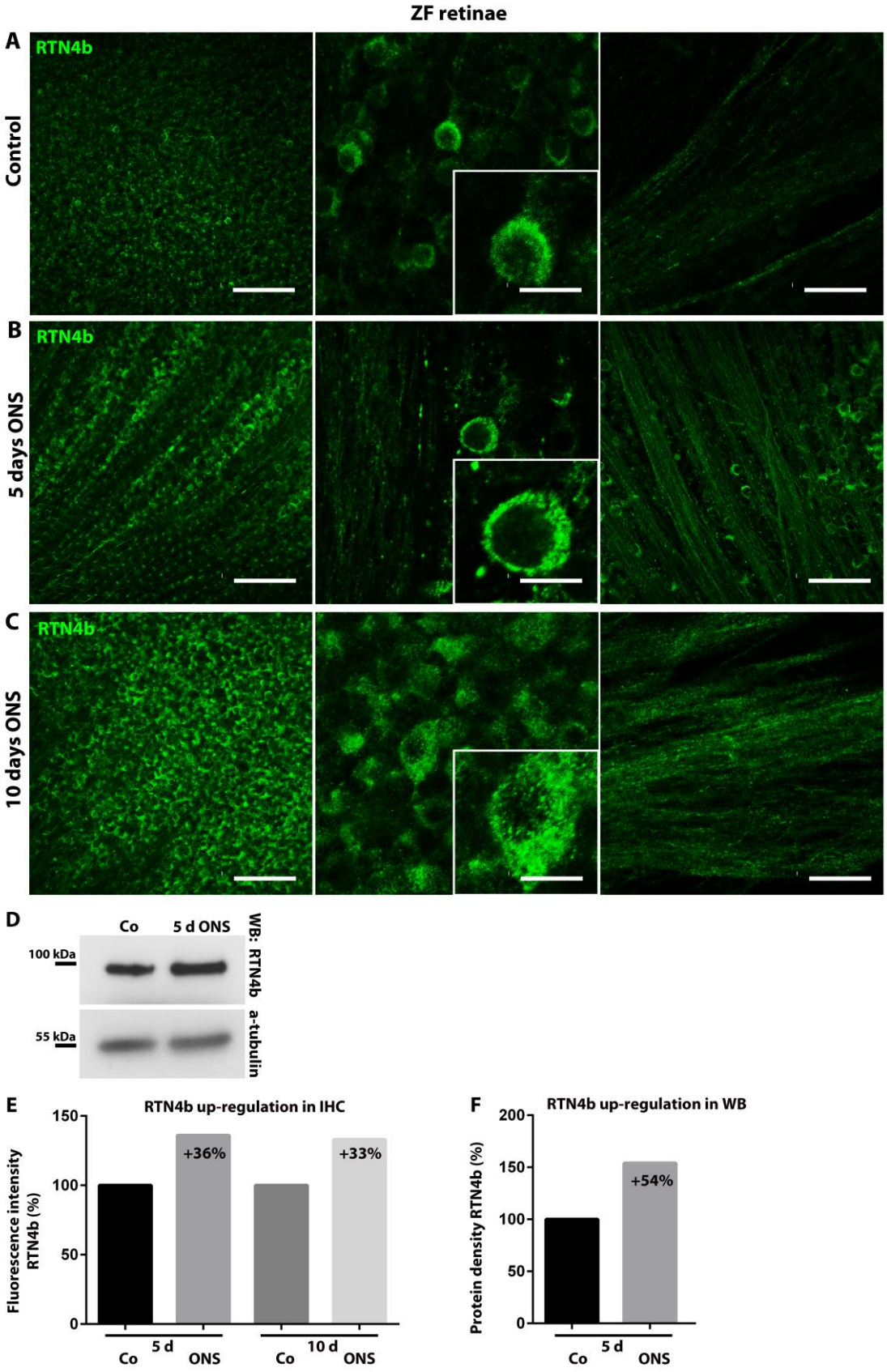
ZF retinae
A
RTN4b
Control
B
RTN4b
5 days ONS
C
RTN4b
10 days ONS
D
Co
5 d ONS
100 kDa
WB: RTN4b
55 kDa
a-tubulin
E
RTN4b up-regulation in IHC
Fluorescence intensity RTN4b (%)
150
100
50
0
+36%
+33%
Co
5 d
ONS
Co
10 d
ONS
F
RTN4b up-regulation in WB
Protein density RTN4b (%)
200
150
100
50
0
+54%
Co
5 d
ONS

Figure 5.7.1 Expression analysis of RTN4b in zebrafish RGCs using the pAb K1121 **A.** RTN4b in fixed and permeabilized, non-transected control retina whole mounts shows diffuse, grainy, intracellular expression throughout all RGCs. Axons are stained weakly. **B and C.** At 5 or 10 days after ONS, RTN4b increases in all retinal ganglion cells and axons. **D.** WB of zebrafish retina lysate shows one specific band at ~90 kDa which increases upon ONS. **E. Quantification of RTN4b fluorescence intensities** at 5 or 10 d after ONS results in a +36 or +33% increase of RTN4b levels, compared to the untreated control. Experiment represented here done once for 5 days ONS and once for 10 days ONS with Co n = 7, 5 d ONS n = 6, Co 10 d n = 6 and 10 d ONS n = 9. Scale bars left to right: 100, 10, 50 µm. **F. Densitometric quantification of RTN4b in WB** results in an increase of RTN4b for +54 at 5 days after ONS. WB done once with ~ 4 retinae per group. Experiments were reproduced and later published in (Welte et al., 2015).

5.7.2. Knockdown of RTN4b in zebrafish RGCs *in vivo* impairs neurite outgrowth

The up-regulation of RTN4b in RGCs induced by optic nerve injury implied an important role of this ER-associated protein during regeneration in the fish CNS. Therefore, I tested if knockdown of RTN4b in RGCs via application of translation-blocking morpholinos to the transected optic nerve had a negative impact on axon regeneration *in vivo*.

Indeed, loss of RTN4b in RGCs substantially reduced the number of re-growing axons from retinal explants in an outgrowth assay (Fig. 5.7.2). As done for other protein knockdowns, to ensure specificity and dose dependence, the tissues were treated with two different concentrations of morpholinos. 70 µM RTN4b morpholino resulted in 67% less axons in average, compared to retinal tissues treated with control morpholinos. Higher concentrations (140 µM) led to a 77% decrease of axon number in zebrafish retinal explants at one day in culture (1 dic) (Fig. 5.7.2 A, B). After two days in culture, the outgrowth recovered to a level corresponding to 47% reduction, as compared to control tissues (two most right columns in Fig. 5.7.2 B). These data were confirmed using a follow-up study using a second morpholino target sequence against zebrafish RTN4b (Welte et al., 2015).

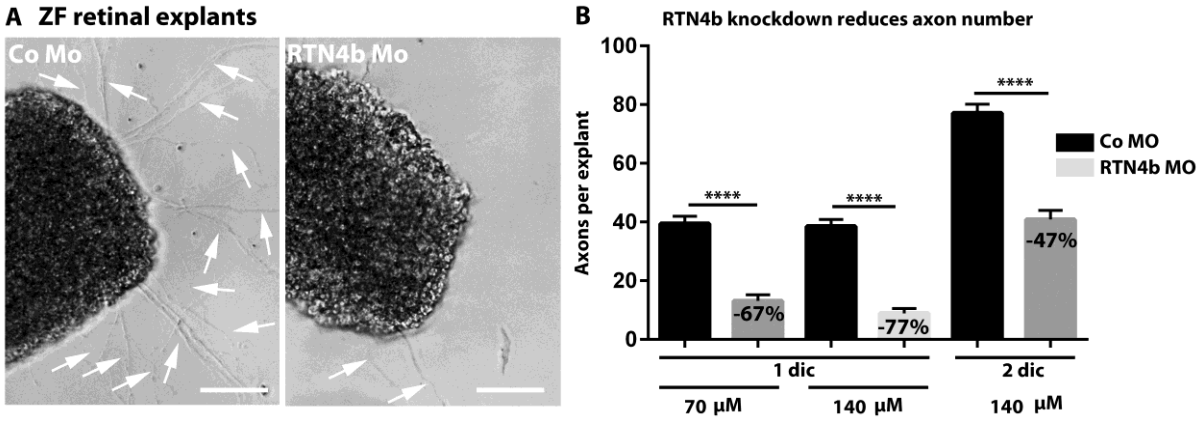

Figure 5.7.2 Knockdown of RTN4b in zebrafish RGCs impairs axon regeneration. A. Zebrafish retinal explants. *In vivo* RTN4b knockdown decreased axonal outgrowth (white arrows). Scale bars: 100 µm. **B. Quantification of axons** emerging from MO-treated retinal explants, 1 day in culture (dic). 70 µM of RTN4b MO significantly reduces outgrowth by 67% compared to the control MO (Co MO n = 41, RTN-4b MO n = 38). 140 µM of RTN4b MO led to a significant decrease of 77% (Co MO n = 39, RTN-4b MO n = 34). After 2 dic Co MO-treated explants had formed about twice as many axons as controls at 1 dic. Tissues treated with RTN4b MO showed a reduction of 47% of this level at 2 dic. Graph shows means +SEM. Two-way ANOVA between groups shows significance with p(****) < 0.0001 and follow-up Tukey`s multiple comparisons between means is significant with p(****) < 0.0001 for RTN4b Mo groups against the control. Results consistently reproduced and published in (Welte et al., 2015).

Thus, endogenous expression of RTN4b was important to regrow new axons from retinal explants. This finding support the notion that in fish, there is a functional difference between intracellular, putatively ER-associated and extracellular, myelin-associated Nogo-A as it was shown for the mammalian Nogo-A counterpart (Vadja et al., 2014). In mammals, the intracellular Nogo-A species is exclusively localized to the tubular ER and exerts its activity in maintaining ER structure and function (Voeltz et al., 2006; Shibata et al., 2010). It may be assumed that an experimentally induced ER-associated dysfunction impinges regeneration, since regeneration processes are dependent on proper *de novo* protein/lipid synthesis. For these reasons, I was interested in relating RTN4b localization to the morphology of the tubular ER in zebrafish RGCs and visualized the latter with the ER marker CLIMP-63.

5.7.3. Localization pattern of CLIMP-63 in zebrafish RGCs

Mammalian RTN4b is localized to the tubular ER (Voeltz et al., 2006; Shibata et al., 2010). To address the question, if the zebrafish counterpart is similarly physically associated to the ER, I analyzed ER structures in the zebrafish retina by visualizing CLIMP-63, a protein well-known to be associated with the tubular ER (Shibata et al., 2010). The microtubule-binding integral cytoskeleton-linking membrane protein (CLIMP-63) contributes to the tubular ER morphology by forming a protein scaffold in the lumen and ensuring its connection to the cytoskeleton

(Klopfenstein et al., 2001). CLIMP-63 is a 63 kDa non-glycosylated type II integral ER membrane protein with an extra-cytoplasmic segment of 474 amino acids and an NH_2-terminal cytoplasmic segment of 106 amino acids, which binds to microtubules (Goyal & Blackstone, 2013; Nikonov et al., 2007; Voeltz et al., 2006). I intended to use it as a specific marker labeling the tubular ER in zebrafish RGCs to find potential similarities with the RTN4b localization pattern. For the immunohistochemical analyses, I employed a polyclonal antibody that recognizes mouse CLIMP-63 but is also known to cross-react with other species, since this protein is highly conserved (kindly provided by Dr. Hesso Farhan, BITg Kreuzlingen, Switzerland).

Immunostainings of RGCs in retina whole mounts showed intracellular ER-labeling as markedly tubular-shaped structures, which was rather different from the pattern observed with the polyclonal RTN4b antibody K1121 (Fig 5.7.3 A vs. Fig. 5.7.1). Zebrafish RGCs are about 15 µm in diameter and the tubular network of the ER is below the limit of resolution of confocal microscopy. It was not possible to perfom co-stainings since both antibodies were raised in rabbits. Nevertheless, the anti-mouse CLIMP-63 antibody yielded a pattern which was quite similar to the expected one also in zebrafish retinae. Western blots of zebrafish brain lysate showed a single band at the predicted size of ~63 kDa (Fig 5.7.3 B).

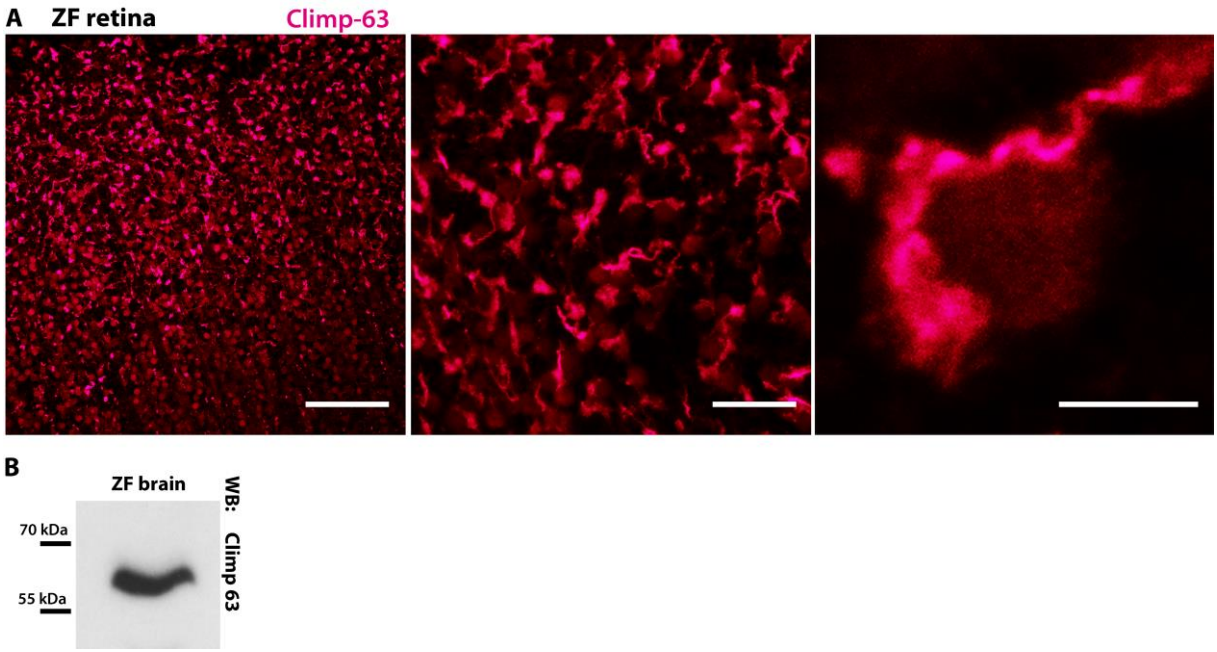

Figure 5.7.3 Expression analysis of the ER-marker protein CLIMP-63 in zebrafish RGCs. A. Confocal images of immunostainings of the fixed and permeabilized zebrafish retinae with anti-CLIMP-63-antibody (magenta) shows a tubular structure. Scale bars from left to right: 100, 50 and 10 µm. **B. WB** of zebrafish brain lysate with the CLIMP-63 pAb shows the single, predicted band at ~63 kDa.

These experiments did not allow to conclusively determine a localization of RTN4b to the ER in zebrafish RGCs. Thus, if the hypothesized impact on regeneration upon its knockdown is due to any disturbed ER-functions.

5.8. Nogo-A (RTN4b) M1-4 peptides as substrates for axonal growth, tested on zebrafish and mammalian neurons

Nogo-A is a predominantly intracellular protein (>95%) (Voeltz et al., 2006). Expression studies on extracellular Nogo-A found it mainly present at the cell surface of oligodendrocytes, at cell bodies and processes, playing a role as a myelin-associated inhibitor of regenerative fiber growth and structural plasticity (Huber et al., 2002). Additionally, Nogo-A was localized at the surface of long projecting neurons, in particular during development, where it might possess axon guiding features (Huber et al., 2002). The extracellular expression of Nogo-A in CNS myelin is considered to be one of the major obstacles to mammalian axonal regeneration, as Nogo-A neutralization via specific antibodies, knock-out or inhibition of the Nogo receptor (NgR) significantly improves recovery after injury (Pernet & Schwab, 2012).

The inhibitory activity of the mammalian Nogo-A/RTN4b protein is attributed to two domains, the C-terminal RHD (reticulon homology domain) and N-terminal NSR (Nogo-specific region). The NSR comprises four conserved ß1-integrin-binding motifs (“M1-4”), which were suggested to block axonal growth and have been identified on the basis of sequence similarity within the homologous zebrafish RTN4b protein (Shypitsyna et al., 2011). In order to investigate the inhibitory potential of the M1-4 motifs of mammalian Nogo-A and its fish homologue on neuronal growth, I compared the effect of the recombinant rat-derived M1-4 polypeptides, their mutated form M1-4 D/A, and the corresponding zebrafish M1-4sequences in cultured fish and mammalian neurons. The myelin-associated rat M1-4 peptide is a strong inhibitor of neuronal growth, but would there be a loss of function after mutation of its four integrin-binding motifs, and would the zebrafish counterpart restrict neuronal outgrowth, although fish myelin was reported to be non-inhibitory? This issue was addressed in the following chapters. The work was done in close collaboration with V. Bodrikov (see 10. Record of contributions).

5.8.1. Rat and zebrafish M1-4 inhibit and mutant rat M1-4 D/A permits outgrowth of zebrafish RGCs *in vitro*

Prior to functional outgrowth assays, the bacterially expressed, recombinant GST-tagged Nogo proteins were analyzed by SDS-PAGE and Coomassie staining or Western blot. The peptides migrated at a higher apparent molecular weight value (~60 kDa) as compared to the predicted molecular mass of ~50 kDa (Fig. 5.8.1.1 A and B) (see methods 4.12.2). Mutation of the amino acids aspartic acid to alanine (acidic to aliphatic) within M1-4 resulted in lower apparent molecular weight (~55 kDa) in the SDS-PAGE (Fig. 5.8.1.1 A).

Zebrafish RGCs that grew on the rat M1-4 protein substrate contained 2.8-times more undifferentiated neurons, which did not develop axons longer than their cell body diameter, compared to control RGCs (see method 4.7.4.). The zebrafish M1-4 substrate showed a similar growth-inhibitory effect (2.3-fold more undeveloped neurons than controls). Notably, neuronal growth on the mutant rat M1-4 D/A substrate was not impaired and appeared equivalent to the control (Fig. 5.8.1.1 D). In addition, the axons of RGCs that developed neurites on the rat M1-4 substrate were 45% shorter compared to those in the control GST group. The mutant M1-4 peptide led to the loss of this inhibitory property and restored axonal outgrowth, being comparable to GST control levels (14% longer than the control, no significant difference) (Fig. 5.8.1.1 C and E). In a second experiment, the zebrafish M1-4 substrate led to 39% shorter axons in cultured RGCs compared to the GST control, being actually more efficient than the rat M1-4 positive control, which inhibited outgrowth by 32% (Fig. 5.8.1.1 C and F).

During an outgrowth assay of zebrafish retinal explants cultured on the different above mentioned substrates, the rat and the zebrafish M1-4 peptides decreased the average number of axons per explant by 86% and 83%, respectively, compared to the GST control protein, whereas explants growing on the mutant rat M1-4 D/A had about as many axons as the control tissues (13% reduction, not significant) (four independent experiments; Fig. 5.8.1.2 A and B) (see method 4.8.2).

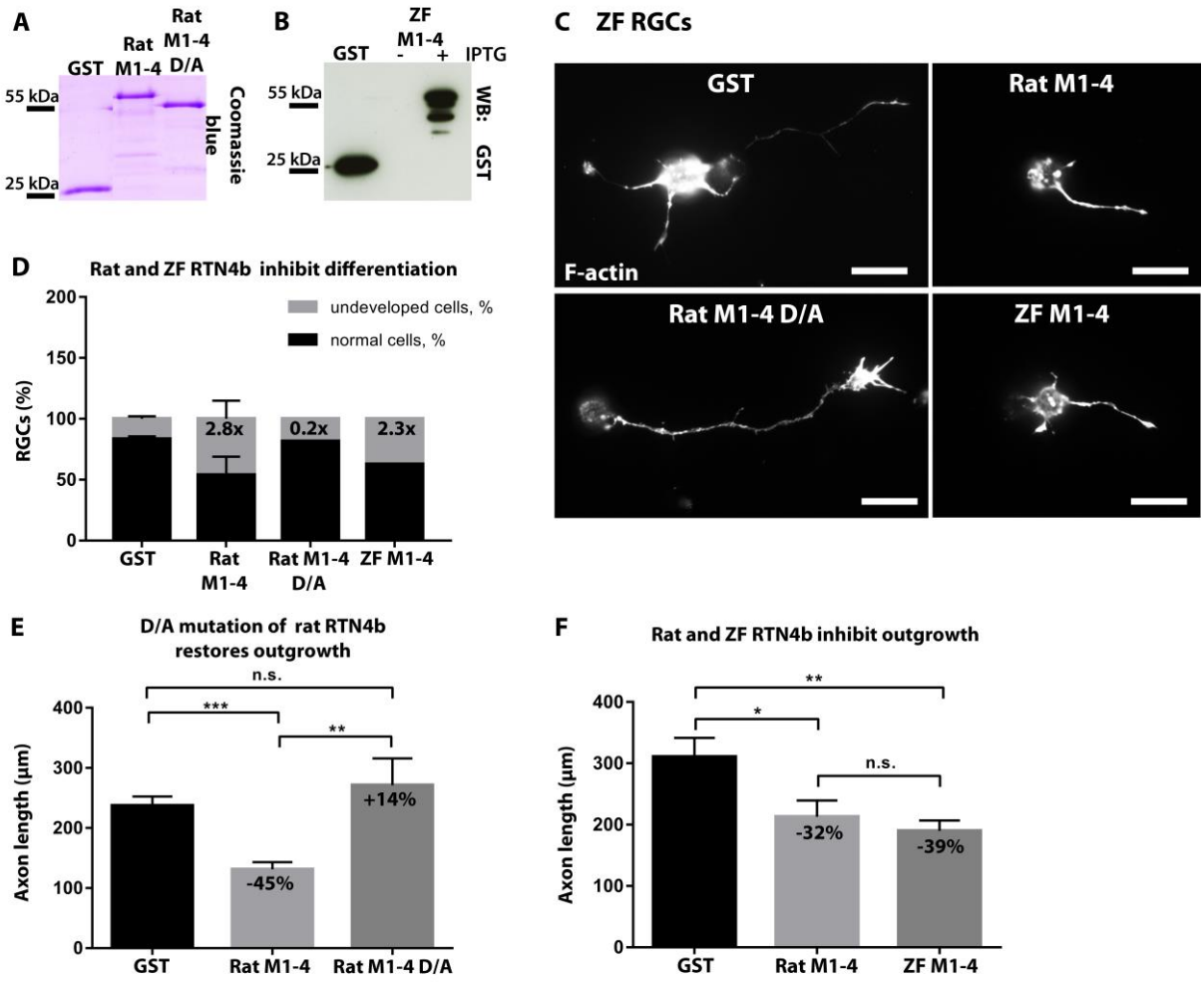

Figure 5.8.1.1 Inhibitory substrate properties of rat M1-4, rat M1-4 D/A and ZF M1-4 tested on zebrafish RGCs. A and B. Characterization of the RTN4b-GST fusion proteins by SDS-PAGE and Coomassie staining and Western blot. The M1-4 peptides run at a molecular mass of ~60 kDa. **C. Zebrafish RGCs** cultured on the rat or ZF M1-4 show impaired outgrowth in contrast to GST and the mutant rat M1-4 D/A substrates. Neurons are visualized by F-actin labeling. Scale bars: 20 µm **D. Quantification of RGCs cultured on RTN4b-substrates.** Rat M1-4 groups contain 278% and ZF M1-4 groups contain 225% more undifferentiated neurons, whereas the mutated rat M1-4 D/A has no effect on differentiation of RGCs compared to the control GST group. Experiment done 3 times for GST n = 302 and rat M1-4 n = 283, and once for rat M1-4 D/A n = 54 or ZF M1-4 n = 134. Graph shows mean +SEM. **E. Quantification of axon lengths.** RGCs grown on rat M1-4 show a 45% decrease in axon length but outgrowth restores to 14% of the GST control when the 4 functional motifs are mutated from D to A. One experiment, GST n = 177, rat M1-4 n = 68, rat M1-4 D/A n = 44. Graph shows mean +SEM. One-way ANOVA is significant with p(***) = 0,0002 and F (3, 507) = 6,591. Follow-up Tukey`s multiple comparison test between means is significant with p(***) = 0,0006, p(*) = 0,463 or n.s. = not significant. **F. Quantification of axon lengths**. RGCs grown on ZF M1-4 show impaired outgrowth as in the case of rat M1-4. The axon length decreases by 39% and 32%, respectively. One experiment, GST n = 73, rat M1-4 n = 65, ZF M1-4 n = 84. Graph shows mean +SEM. One-way ANOVA between groups was significant with p(****) < 0,0001 and F (3, 187) = 17,82. Follow-up Tukey`s multiple comparison test between means shows significance with p(****) < 0,0001 or n.s. = not significant.

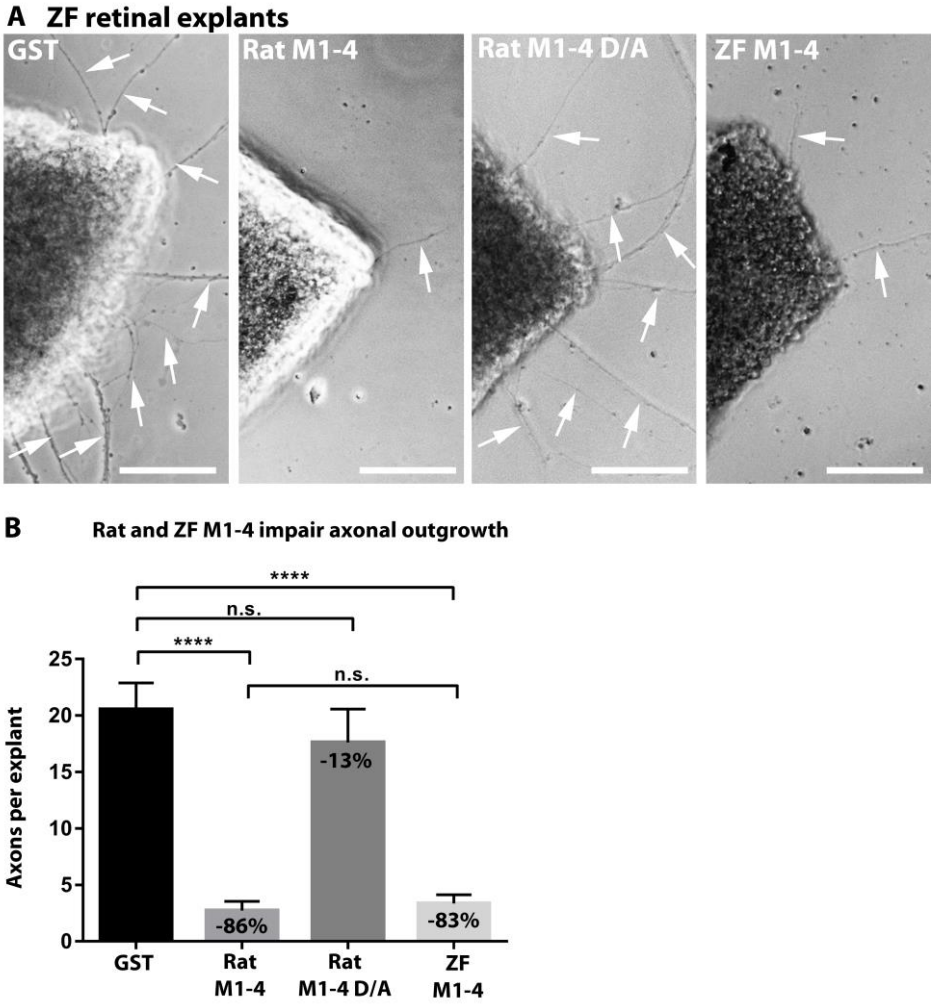

Figure 5.8.1.2 Inhibitory substrate properties of rat M1-4, rat M1-4 D/A and ZF M1-4 tested on zebrafish retinal explants. A. Outgrowth assay. Axonal outgrowth (white arrows) of explants growing on top of different Nogo(RTN4b)-substrates is drastically inhibited in case of the provided rat and ZF M1-4 substrates. D/A mutation of rat M1-4 restores normal outgrowth, compared to control GST. Scale bars: 100 µm. **B. Quantification of the axonal outgrowth**. Zebrafish retinal mini-explants 1 day in culture have in average -86% less axons per explant in the rat and -83% in the ZF M1-4 groups, mutated rat M1-4 D/A shows comparable to the control GST. Experiment done 4 times independently with GST n = 75, rat M1-4 n = 39, ZF M1-4 n = 39 and 3 times with rat M1-4 D/A n = 38. Graph shows mean +SEM. One-way ANOVA between raw data of all groups was significant with p(****) < 0.0001 and F (3, 187) = 17,82. Tukey`s multiple comparisons test is significant with p(****) < 0.0001 or n.s.= not significant.

From these data we may draw the following conclusions. Firstly, the four integrin-binding motifs M1-4 present within the NSR of rat Nogo-A indeed mediate a strong growth-inhibitory effect, because four single amino acid exchanges from the acidic aspartic acid to the aliphatic alanine neutralize its inhibitory properties. Secondly, the zebrafish M1-4 motif, representing the homologous region of Nogo-A in fish has the same inhibitory effect on fish neurite outgrowth as the rat M1-4 peptide. Remarkably, these results strongly question the hypothesis that fish regenerate because these organisms lack an inhibitory Nogo-A homolog.

5.8.2. Effects of M1-4 peptides on the growth ability of rat PC12 cells

To investigate whether the four ß1-integrin-binding motifs M1-4 constitute the functional inhibitory unit of Nogo-A in mammalian neurons and, of special interest, whether the zebrafish Nogo-A homologue is inhibitory to mammalian cells, we used a well-established assay monitoring the ability of cells (in this case the rat neuron-like PC12 cells) to spread when cultured on a substrate of interest (Rubin et al., 1995; Oertle et al., 2003). The PC12 cells were cultured on substrates containing either recombinant GST control or rat M1-4 or rat M1-4 D/A or zebrafish M1-4 peptides at a concentration of 200 nmol. After fixation and immunolabeling of the cytoskeleton visualizing the cell boundary, the spreading behavior of PC12 cells was determined for each group (see method 4.11). Rat PC12 cells seeded on rat M1-4 protein showed 44% less spreading compared to those growing on the GST substrate, whereas the spreading of cells growing on mutant rat M1-4 D/A was comparable to that of control cells (Fig. 5.8.2 A, quantification in B). In a second experiment, the zebrafish M1-4 substrate led to significantly reduced cell spreading (21% less) similar to the rat M1-4 positive control (42% less), both compared to the control GST group (Fig. 5.8.2 A, quantification in C).

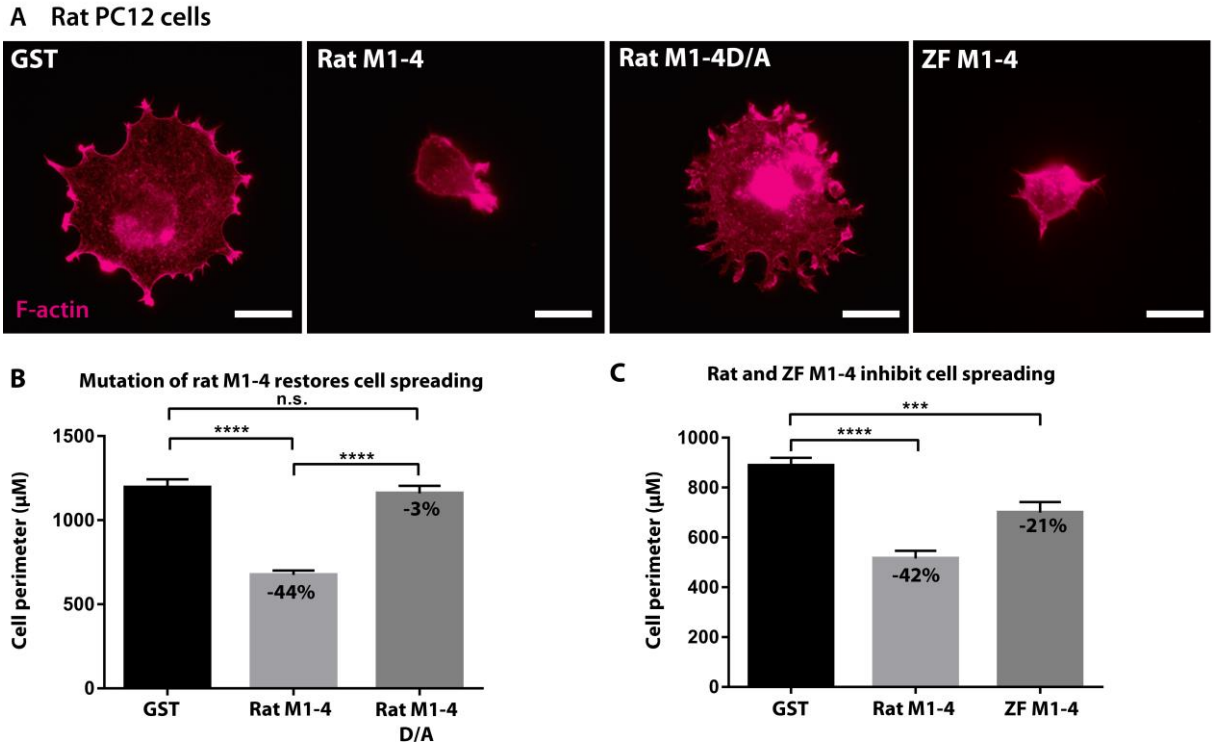

Figure 5.8.2 Growth of rat PC12 cells and primary mouse hippocampal neurons on rat M1-4, rat M1-4 D/A and zebrafish M1-4. A. Spreading assay of rat PC12 neuronal cells (F-actin in magenta) growing on recombinant Nogo-substrates showed impaired cell spreading for rat and the zebrafish M1-4, but not in the case of the mutated rat M1-4 D/A compared to the control. Scale bars: 20 µm. **B. Quantification of cell perimeters.** Rat M1-4 leads to a reduction of 44% compared to the GST control, perimeters in rat M1-4 D/A mutant group are restored to normal levels (3%). Experiment done 2 times with GST n = 334, rat M1-4 n = 372, rat M1-4 D/A n = 313. Graph shows mean +SEM. One-way ANOVA between raw data of all groups is significant with p(****) < 0.0001 and F (2, 1016) = 53,77. Follow-up Tukey`s multiple comparisons test is significant with p(****) < 0.0001 or n.s. = not significant. **C. Quantification of cell perimeters.** Rat M1-4 and ZF M1-4 reduce spreading (42% and 21% less, respectively) compared to the GST control. One experiment with GST n = 114, rat M1-4 n = 94, ZF M1-4 n = 85. Graph shows mean +SEM. One-way ANOVA between raw data of all groups is significant with p(****) < 0.0001 and F (2, 290) = 30,08. Follow-up Tukey`s multiple comparisons test is significant with p(***) = 0.0005 and p(****) < 0.0001.

All *in vitro* outgrowth experiments confirmed the recombinant rat M1-4 peptide being growth-inhibitory for neurons. This result was expected, since M1-4 represents the well-known inhibitory Nogo-specific region within the potent outgrowth inhibitor protein Nogo-A. Moreover, mutation of the four integrin-binding motifs within this Nogo-specific region (NSR) completely abolished inhibition, an interesting result calling for future investigations of the role of integrins in axon regeneration. Surprisingly, we found that the zebrafish Nogo-A homologue restricts growth in fish and mammalian neurons to a comparable extent as its inhibitory rat paralogue (although zebrafish myelin was reported to be growth-permissive) raising new exciting questions in the field of comparative regeneration between fish and mammalian species. These data renew the already complex challenge of how fish and mammals differ in their molecular events leading to Nogo-A-mediated inhibition during growth and regeneration.

6. Discussion

This doctoral thesis investigated the roles of three neurologically important proteins -Thy-1, PrP and RTN4- during axon growth and regeneration. Additionally, it characterized novel zebrafish-specific antibodies against these proteins and their biological function in gain or loss of function experiments *in vitro* and *in vivo*. Firstly, I analyzed the function of Thy-1 and PrP, two neuronal, cell-surface GPI-anchored molecules whose involvement in axonal outgrowth remains a debated issue after decades of intensive research. Secondly, I focused on the Nogo-A protein, a very potent inhibitor of axon growth in mammals whose fish counterpart -RTN4b- had not been examined so far. For my experiments, I used a model organism that readily regenerates axons after CNS injury -the zebrafish- in comparison with an animal with very limited regeneration potential -the mouse-.

PART I Thymocyte antigen 1 (Thy-1) and the Prion Protein (PrP)

6.1. Thy-1 in zebrafish RGCs, its lesion-induced expression and biological relevance

The subcellular localization and the expression pattern of a protein under various conditions (e.g. disease or treatment) provide useful information about the molecular mechanisms in which it may be involved. The distribution and the expression level of a protein in a cell or a tissue is visualized best by immunohistochemistry and subsequent microscopy, given one is in possession of an appropriate antibody which specifically recognizes the target. The proteins of interest in my thesis are the GPI-anchored molecules Thy-1 and PrP investigated in the context of regeneration in the CNS in zebrafish and opposed to mammals. Regeneration takes place to a certain extent also in mammals, e.g. by physiological turnover when cells are renewing, but fish possess the unique ability to regenerate axons of the central nervous system (CNS) after lesion. Therefore, the zebrafish visual system was chosen as main model system to investigate regeneration processes in the CNS, more precisely, the optic nerve and associated RGCs.

When examining the distribution of Thy-1 in the zebrafish retina, I found substantial basal expression throughout all RGCs and axons, as confirmed by Western blot and immunohistochemical analysis (Fig. 5.1.1.1, 5.1.1.2 and 5.1.2). Upon ONS, Thy-1 protein levels

were highly increased in RGCs, which strongly suggested an involvement in regeneration (Fig. 5.1.1.1, 5.1.1.2 and 5.1.2). In untreated RGCs, Thy-1 was largely present at the plasma membrane, as expected for a classical GPI-anchored, cell-surface molecule (Leyton & Hagood, 2014) (Fig. 5.1.2 D). It was particularly enriched at cell-cell-contact sites, emphasizing the role of Thy-1 as a signaling molecule that mediates cell-cell or cell-matrix interactions as well as cellular adhesion and migration (Fig. 5.1.2 D and 5.1.3 B) (Leyton & Hagood, 2014, Liësi et al., 1990). After optic nerve injury, Thy-1 became upregulated and redistributed; it appeared in disordered clusters, not anymore in its typical membranous, cellular rings (Fig. 5.1.1.1 B, C and 5.1.2 D, E). In addition, these clusters became larger, probably redistributed to special microdomains where it can modulate multiple intracellular signaling cascades through interactions with a number of key molecules (e.g. SFKs) (Leyton & Hagood, 2014) (see also detailed discussion about Thy-1-associated signaling partners in 6.4).

Upon ONS, Thy-1 acquired a distribution pattern characteristic of proteins which are linked to vesicles (Fig. 5.1.1.1 C and 5.1.2 E). Despite Thy-1`s well-known role as a plasma membrane-associated signaling molecule, it is also an integral element of secretory synaptic vesicles and plays an important role in the regulated release of neurotransmitters at the synapse (Jeng et al., 1998). Early reports revealed that Thy-1 is present in cell bodies and axons, suggesting that it is synthesized by neurons and transported anterogradely by axoplasmic flow in transport vesicles (Morris et al., 1983). Synaptic activity is known to support regeneration, and axons reestablish synaptic connections as regrowth and functional recovery take place (Houle & Côté, 2013). Whether zebrafish RGCs increase the amount of vesicular and synaptic Thy-1 to promote axon regeneration and formation of synapses after ONS remains to be investigated, by co-immunopecipitation or co-localization assays. Here, specific markers for secretory vesicles, like synaptotagmin or synaptic vesicle protein 2 (SV2), could be utilized.

My quantitative realtime PCR analyses confirmed that the total Thy-1 mRNA levels become increased upon ONS in zebrafish (Fig. 5.1.2 H, I). This result confirms upregulation at the transcriptional level, independently of protein synthesis and antibody-based detection methods. The *thy-1*-specific PCR primers amplified a single cDNA product of the defined size, proving their specificity for only one target. Importantly, the qRT PCR methods helped validating the results obtained with the newly generated antibody: I found increased *thy-1* mRNA transcription in optic nerve-transected retinae as compared to untreated eyes (Fig. 5.1.2 H, I). Unexpectedly, normalization using two different housekeeping genes as reference

resulted in different values for the relative increase of Thy-1 mRNA level, suggesting that expression of one or both of the genes may vary during axon regeneration. EF1α (Elongation factor 1 alpha, α subunit of the EF1 complex) and Rpl13α (Ribosomal protein L13a, part of the 60s subunit) are widely used housekeeping genes in zebrafish transcriptional studies, both in embryonic and adult fish tissues, whereas only EF1α had been used as internal control during zebrafish optic nerve regeneration previously (McCurley & Callard, 2008; Tang et al., 2007; McCurley & Callard, 2010). Normalizing *thy-1* transcript levels using Rpl13α as a reference resulted in a 23-fold increase, whereas EF1α yielded a 9-fold increase (Fig. 5.1.2 H, I). Regardless of this quantitative difference, both results confirmed the observation that fish significantly elevate Thy-1 expression levels upon lesion which supposedly enables them to regenerate axons successfully after ONS.

The ability of cells to up- or downregulate transcriptional sets of genes is central to successful axonal regeneration (Moore & Goldberg, 2011). Changes in protein expression following a certain experimental treatment or during disease are of great biological relevance as the behaviour of a cell arises from complex interactions between their molecular components (Barabási & Oltvai, 2004). Naturally, there is not only one or a few set of genes and proteins that are essential for neuronal regeneration but a complex network of elements that are regulated upon injury. Numerous efforts have been made trying to identify these elements and to categorize them into gene ontology clusters, describing the complex intercellular network of interactions (Müller H., 2008). Nowadays, microarray analysis is used to define special molecular signatures connected to a phenotype, comparing treatments to a control (Müller H., 2008). The goal is to identify gene clusters of factors that are up- or downregulated for example during neuronal regeneration, which can be organized in different functional fields (biological processes) such as cellular protein/lipid metabolism, apoptosis, cytoskeletal reorganization or inflammatory response (Müller H., 2008). Such co-expression modules (genes that co-express under a certain set of experimental conditions) are assumed to be functionally related and to have a common functional role: in essence, the biological functionality of a cell arises from such complex interactions between these molecular components (Minguez & Dopazo, 2011). There is a considerable degree of overlap between members of different ontology clusters. In order to achieve a comprehensive understanding of neuronal survival and regeneration it is necessary to determine the functions of all these factors. Systems biology and high-throughput functional screening will help to link genes to

neuronal outgrowth processes and to elucidate the transcriptional regulatory network underlying successful regeneration (Müller H., 2008). At the next level, it is also important to explore the cellular role of these lesion-induced molecules and their relevance during regeneration, as demonstrated for Thy-1, PrP and RTN4b in this study.

6.2. Thy-1 expression in early zebrafish embryos

In the course of my experiments with zebrafish embryos, when testing the specificity of mAb 89/9, I noticed that Thy-1 can be reliably detected in Western blots only at developmental stages later than 2-3 dpf. This observation was supported by qRT PCR assays, where minimal levels of Thy-1 mRNA were present at 1 dpf but increased 2.8-fold after 3 dpf (Fig.5.1.5.1 E, F). Interestingly, at 5 dpf, Thy-1 transcription levels declined (1.5-fold compared to 1 dpf), whereas Western blots showed a constant increase of protein signal (Fig.5.1.5.1 D). Thus, Thy-1 mRNA and protein levels did not correlate over the entire time of observation. This phenomenon is known from literature and two main explanations are discussed: 1) posttranscriptional mechanisms involved in translating mRNA into protein and 2) protein stability (Greenbaum et al., 2003). It is likely that a stable mRNA, once transcribed, is continuously translated, leading to constantly increasing amounts of protein. The latter may additionally have a long half-live, as is known for Thy-1 and reflected in our morpholino knockdown experiments and biochemical analysis (Lemansky et al., 1990). In order to investigate the temporal and spatial regulation of Thy-1 in zebrafish embryos I used the mAb 89/9. In whole mount immunostainings, no fluorescent signals were detectable at 1 dpf, but at 3 and 5 dpf blood cells/vessels and skin were labeled (Fig. 5.1.5.1 A, B, C). Surprisingly, Thy-1 was not present in the embryonic zebrafish brain or retina up to 5 dpf, despite it is considered as one of the most abundant cell-surface proteins of adult CNS neurons of mammals (Haeryfar & Hoskin, 2004). However, the number of animals analyzed in this experiment was low and possibly a further improved staining method could reveal low protein amounts of Thy-1 in retinal or cerebral structures of zebrafish embryos. The lacking Thy-1-specific signal in the brain or retina of early embryonic stages is in line with its onset of expression in mice and rats, where Thy-1 was reported to be expressed in neurons only later during development. For example, rat RGCs were reported to express Thy-1 only at embryonic day 19 (Schmid et al., 1995). In dorsal root ganglion (DRG) neurons Thy-1 expression increases concomitant with neuronal maturation at postnatal day 2 (Herrera-Molina et al., 2013). Thy-

1 levels in neonatal mouse, rat and human brains were low compared to full-grown individuals (Bolin & Rouse, 1986; Barclay, 1979; Seeger et al. 1982). In adult zebrafish, Thy-1 was substantially expressed in the brain and retina, suggesting that it plays an equally important role in the CNS of fish, as it does in mammals (Fig 5.1.2). The structure and the functional domains of the Thy-1 molecule (GPI-anchorage, IgG-like structure, glycosylation) as well as its distribution in zebrafish tissues seems to be analogous to that of mammals. Based on these results, I analyzed the role of Thy-1 during axon regeneration not solely in fish but also in mammalian neurons of mice.

6.3. Role of Thy-1 in neuronal function

The spontaneous increase of Thy-1 in zebrafish RGCs after ONS suggested an important role during regeneration. To test this hypothesis, I analyzed the growth capacity of RGCs upon morpholino-mediated knockdown of Thy-1. Indeed, knockdown of Thy-1 highly impaired neurite outgrowth of RGCs in single cell and retinal explant cultures (Fig. 5.2.1 & 5.2.2.1). To study the effect of Thy-1 knockdown in its physiological, cellular context, including all extrinsic and intrinsic factors, I performed a regeneration assay *in vivo*. This assay confirmed the hypothesis of a growth-supportive role for Thy-1 since retinae devoid of Thy-1 in ganglion cells poorly regenerated after ONS *in vivo* (-65%, Fig. 5.2.2.2.).

Reports about the role of Thy-1 in mammalian neurons are contradictory. In my thesis I demonstrate that Thy-1 promotes neurite outgrowth in fish and that its levels are increased upon CNS injury. In contrast, mammalian Thy-1 inhibited the growth of neurons cultured on a monolayer of astrocytes, an effect that was dependent on the clustering of Thy-1 by astrocytic αVβ3 integrin, and the ensuing Src kinase inactivation (Herrera-Molina et al., 2012). The authors of this study proposed a bi-directional astrocyte-neuron signaling, negatively impinging on axonal repair *in vivo*, yet in this study only *in vitro* experiments were performed (Herrera-Molina et al., 2012). In a further study, Thy-1 only prevented the growth of neurons that were cultured on an astrocytic substrate, but not on embryonic glia or Schwann cells (Tiveron et al., 1992). These data suggests that Thy-1 inhibits regeneration preferentially in astrocyte-rich regions of the mammalian CNS/brain. In line with this, in fish, the region around the optic nerve injury site remained astrocyte-free, suggesting that regeneration is possible due to the lack of Thy-1-integrin mediated inhibition (Hirsch et al., 1995).

Several studies in isolated neurons stimulated with Thy-1 antibodies resulted either in reduced or enhanced neurite growth, depending on the kind of antibody which was used (Mahanthappa & Patterson, 1992a; Doherty et al., 1993; Chen et al., 2007). Interestingly, valency of the antibody seems to be crucial in determining either an inhibitory or growth-promoting effect: monovalent antibodies blocked growth, whereas divalent ones stimulated it (Kuroiwa et al., 2012).

The growth-stimulating effect of monoclonal antibody-mediated clustering and the observation that soluble recombinant Thy-1 caused a 75% increase in neurite length in cultured zebrafish RGCs (Fig. 5.2.1), suggests that clustering of Thy-1 activates a growth-promoting signaling cascade by default. We used exposure of single zebrafish RGCs in culture to recombinant Thy-1 to mimic an *in vivo* scenario in which Thy-1 molecules clustering at the surface of adjacent axons would homophilically *trans*-interact. The ability of Thy-1 to bind and activate integrins in lipid raft signaling platforms is postulated as additional mechanism underlying the growth-promotive effect of Thy-1 on neurons (see also discussion about Thy-1-associated signaling in 6.4.). Activation of integrins is known to enhance neurite outgrowth and regeneration, and even overcome the inhibitory effect of molecules like CSPGs and Nogo (Ivins et al., 2000; Tan et al., 2011; Tan et al., 2015). It should be noted, though, that reports about Thy-1-integrin interactions are contradictory and scientists in the field are aware that Thy-1 can do both, promote or inhibit integrin activity. It is acknowledged that *"Thy-1 has a kind of yin-yang behavior in controlling integrin engagement and signaling"*, dependent on the exact cellular and molecular context (Sedwick, 2015). To address the question as to whether outgrowth of single zebrafish RGCs induced in culture is due to Thy-1-Thy-1 and/or Thy-1-integrin interaction, one would have to perform biochemical assays and check, for example, if axonal growth is still enhanced after blockage of either Thy-1 or integrins or both at the neuronal surface.

In neonatal brains, Thy-1 was expressed at low levels (Liu et al., 1996; Bolin & Rouse, 1986). We detected substantial Thy-1 expression in neonatal mouse hippocampal neurons after isolation and culturing, consistent with a hypothesized growth-related function of Thy-1 in mammalian neurons (Fig. 5.2.3). In cultured mouse hippocampal neurons, I examined the neuron-intrinsic role of mammalian Thy-1 by testing their growth capabilities upon overexpression or knockdown of the protein. Transfection of neonatal mouse hippocampal neurons with Thy-1-EGFP resulted in a gain-of-function, significantly increasing neurite lengths

(37%). SiRNA-mediated knockdown on the other hand showed a loss-of-function effect reducing outgrowth by 23% (Fig. 5.2.3). From this type of experiment, we cannot define whether enhanced outgrowth was triggered by clustering/multimerization of overexpressed Thy-1-EGFP at the neuronal surface. However, it is known that Thy-1 participates in homophilic interactions, and its multimerization at the cell membrane has been proposed to stabilize preformed neuronal structures and the underlying actin cytoskeleton (Mahanthappa & Patterson, 1992b). If the same situation applies to the zebrafish homolog remains to be analyzed. So far, we can assume that overexpression as well as extracellular stimulation of Thy-1 might lead to clustering and activation of the molecule via homophilic interactions at the membrane, leading to stimulation of intracellular, growth-associated signaling cascades.

6.4. Thy-1-associated signaling partners in neurons

Axonal glycoproteins and cell adhesion molecules belonging to the IgG gene superfamily (IgCAMs) are known to promote outgrowth (Aricescu & Jones, 2007). For instance, IgCAM molecules like L1, TAG-1 or NCAM are supportive guidance molecules expressed at the surface of growning neurons (Gil et al., 1998). Given its structure and neuronal cell-surface expression, it is likely that Thy-1 harbors similar growth-promoting properties. Being localized to specialized lipid membrane microdomains (rafts) via its GPI-anchor, Thy-1 interacts with diverse signaling molecules and with actin cytoskeletal components, allowing it to influence cell dynamics (Leyton & Hagood, 2014). CBP (Csk binding protein) is one example for a transmembrane adaptor protein for Thy-1, which anchors it to signaling platforms and mediates Thy-1-induced SFK activation (Chen et al., 2009). Homophilic Thy-1 interactions are a widely accepted mechanism underlying Thy-1-induced signaling. Moreover, Thy-1`s immunglobulin-like protein structure would support clustering and multimerization as was suggested in a theoretical model, but homophilic interactions remain to be investigated experimentally (Mahanthappa & Patterson, 1992b).

Thy-1 is an important component of protein complexes initiating cell signaling by transmission of environmental cues (Herrera-Molina et al., 2013). Activated Thy-1 and other CAMs have been spatially and temporally linked to flotillin-defined rafts in regenerating rat DRG neurons, suggesting that specified flotillin microdomains serve as signaling platforms (Lang et al., 1998; Stuermer et al., 2001). In this context, flotillins mediated the activation of SFK member Fyn, MAP-Kinases and Rho-GTPases to regulate and control cytoskeletal dynamics during axon

growth (Munderloh et al., 2009; Stuermer, 2011b). Given the mutually exclusive interaction of Thy-1 (extracellular) and flotillin (intracellular) which excludes direct molecular interaction, several explanatory scenarios for signal transduction are currently under debate: signaling has to be mediated either classically via a transmembrane transducer (like CBP), or atypically by protein clustering-induced structural alterations of membrane properties, resulting in direct contact between the two distant proteins enabling interaction and signaling (Kusumi et al., 2004; Morozova et al., 2011; Eisenberg et al., 2006). On the other hand, that lipid rafts are special ordered domains harbouring GPI-anchored proteins is also not yet universally accepted; an Austrian laboratory has recently challenged the existence of higher lipid chain order mediating protein interactions (Sevcsik et al., 2015). They combined protein micropatterning with single-molecule tracking and directly rearranged GPI-anchored raft proteins in the living plasma membrane to measure any effect on the local membrane environment, but this treatment did neither nucleate the formation of an ordered membrane phase nor result in any enrichment of nanoscopic-ordered domains within the micropatterned regions (Sevcsik et al., 2015). They concluded that phase partitioning is no fundamental element of GPI-protein organization inside of the plasma membrane (Sevcsik et al., 2015). In contrast, another study showed that only a dynamic organization of GPI-anchored proteins in rafts was able to transmit stimulation-induced changes: in resting cells, GPI-anchored proteins were mobile and continually formed transient homodimers through ectodomain protein interactions, stabilized by the presence of the GPI-anchoring chain and cholesterol (Suzuki et al., 2012). Upon stimulation, homodimers formed hetero-GPI-anchored protein oligomer rafts through raft-based lipid interactions and triggered intracellular Ca^{2+} responses (Suzuki et al., 2012). Hence, the authors proposed that transiently rearranged GPI-anchored protein homodimers are the basic units for raft organization and function (Suzuki et al., 2012). Another *in vitro* study showed that the ability of mobile GPI-anchored proteins to cluster was essential to transmit activation, as demonstrated by synthetic, fluid, lipid bilayer membranes containing a recombinant GPI-linked extracellular domain of the postsynaptic membrane protein neuroligin-1 (Baksh et al., 2005). The synthetic membranes exhibited biological activity at neuroligin-1 densities of ~1 to 6 proteins/μm^2 whereas polycarbonate beads with neuroligin-1 covalently attached to the surface failed to activate neurons, although binding activity was preserved (Baksh et al., 2005). This observation implied that a lipid membrane environment is likely to be essential for neuroligin-1 activity (Baksh et al., 2005).

As a protein enrichmed in flotillin-defined lipid raft microdomains, working hypothesis of my study was that Thy-1 exerts its function via flotillin-associated signaling molecules (e.g. Erk1/2, Src and Cofilin). This assumption was in line with previous studies (Stuermer & Plattner, 2005b; Stuermer, 2010; Stuermer et al., 2001).

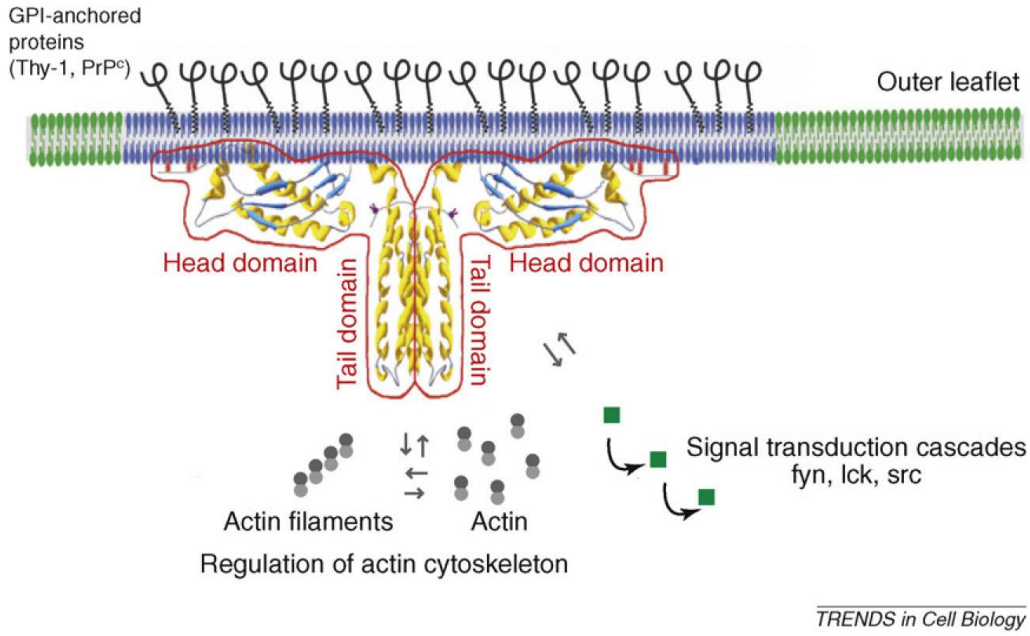

Fig. 6.4.1 Schematic representation of a flotillin cluster in interaction with the plasma membrane. Reggie/flotillin microdomains and co-clustering of the activated GPI-anchored proteins Thy-1 and PrP. Reggie-1/flotillin-2 and reggie-2/flotillin-1 (oversized), are illustrated as two hammer-shaped structures, back-to-back, encircled by a red line, that form homo- and hetero-oligomers at the cytoplasmic face of the plasma membrane and afford scaffolds for microdomains with lipid raft properties (depicted in blue). Acyl residues and hydrophobic amino acids in the N-terminal head domain promote reggie binding to the cytoplasmic face of the plasma membrane. The predicted alpha-helical coiled-coil domains at the C-terminus (tail domain) are involved in oligomerisation. Reggies/flotillins interact with Src tyrosine kinases (Src, Fyn, Lck) as well as with Rho-family GTPases through the CAP-associated signaling complex and affect the dynamics of the actin cytoskeleton. Activated GPI-anchored proteins (pigtailed structures) at the outer leaflet of the plasma membrane are densely packed in the reggie microdomains. The GPI-anchored proteins communicate with signaling molecules most likely through co-clustering with reggie/flotillin. Figure and caption taken from (Stuermer, 2010).

To investigate whether impaired outgrowth of hippocampal neurons after knockdown of Thy-1 is caused by a disturbed Thy-1/flotillin interaction, we performed a cross-rescue experiment. Notably, overexpression of flotillin-2-EGFP in siThy-1 transfected neurons restored neurite outgrowth (Fig. 6.3.2). These data imply that Thy-1 is not essential for axonal growth and that lack of Thy-1 can be compensated for by over-activation of flotillin-associated signaling pathways.

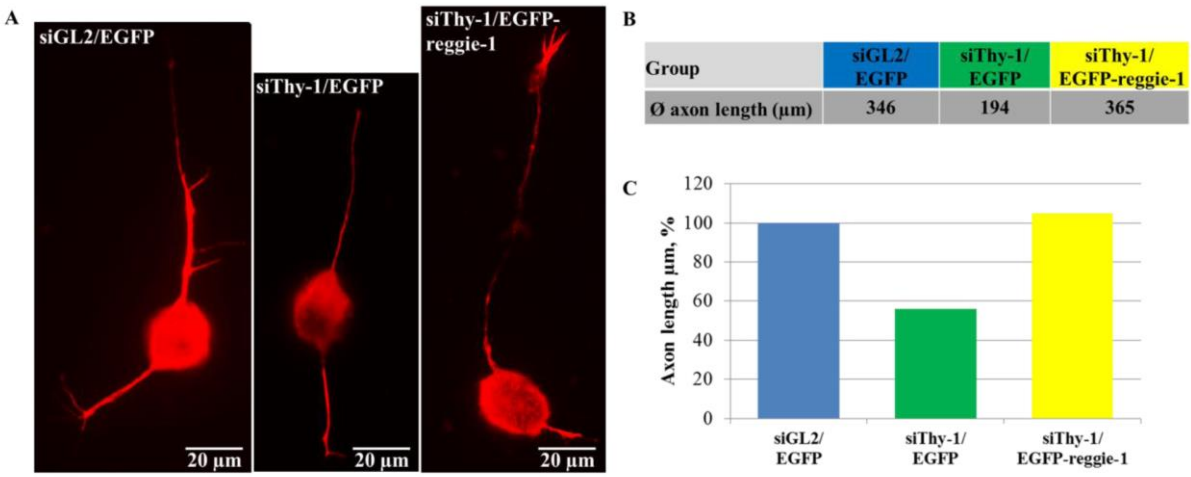

Fig.6.4.2 SiThy-1 and flotillin-2/reggie-1-EGFP cross-rescue in primary mouse hippocampal neurons. **A**. Hippocampal neurons transfected with siGL2/EGFP, siThy-1/EGFP and siThy-1/EGFP-reggie-1, respectively, were visualized by confocal microscopy using AlexaFluor 568 phalloidin (red). Transfection efficiency was verified by EGFP fluorescence (not shown). **B. Average axon lengths in µm** for 1 experiment of each group. The decreased neurite outgrowth after Thy-1 knockdown was rescued by overexpression of reggie-1. **C. Quantification of average axon lengths in %** normalized to the control siGL2/EGFP (n=1 with 36 cells), siThy-1/EGFP (n=1 with 33 cells) and siThy-1/EGFP-reggie-1 (n=1 with 39 cells), respectively. (Figure and caption from "Thy-1 induced and reggie-mediated signaling" by S. Henrich, 2014.)

Our first approach to identify components of Thy-1-associated signaling cascades in neurons was to perform co-localization assays with candidate molecules, like the MAP-Kinase ERK1/2, the SFK Src and the downstream actin-binding protein cofilin. Upon knockdown of Thy-1, we determined signal intensities within flotillin-2 clusters which were increased in case of phospho-Src levels (79%) and decreased for phospho-ERK1/2 (43%) and for phospho-cofilin (48%) (S. Henrich, 2014). The increase in activated Src upon Thy-1 knockdown was unexpected, since knockdown of flotillin-2 reduced activated Src levels and impaired axon growth and regeneration, similar to what was shown for pERK1/2 (Amaddii et al., 2012; Munderloh et al., 2009; Solis et al., 2012). Conversely, overexpression of flotillin activated Src and enhanced neurite outgrowth (Koch et al., 2013). Thus the question arises how knockdown of a growth-supporting molecule like Thy-1 can impair neuronal growth via increased activation of flotillin-associated Src. A plausible explanation could lie in the inactivation (phosphorylation) of cofilin upon knockdown of Thy-1, since Src negatively regulates cofilin via the LIM kinase (LIMK1) (Yang et al., 1998). Additionally, tyrosine phosphorylation of cofilin by Src leads to its degradation through ubiqutin-proteasome pathway (Yoo et al., 2010). In its phosphorylated form, cofilin is inactive and unable to reassemble actin filaments at the minus ends (Sarmiere & Bamburg, 2004). Thus, proper regulation of the LIMK1-cofilin pathway is crucial to maintain axon growth during development and regeneration (Endo et al., 2003).

Increased levels of phosphorylated (active) Src upon Thy-1 knockdown could lead to disturbed levels of cofilin, leading to impaired actin depolymerization and neurite outgrowth. Interestingly, the Ras-Raf-MAPkinase/ERKkinase (MEK) pathway is able to dephosphorylate (activate) cofilin independently from LIMK1 (Nebl et al., 2004). Hence, reduced levels of activated pERK1/2 in flotillin microdomains could also explain changing amounts of phosphorylated (inactive) cofilin upon Thy-1 knockdown in mouse hippocampal neurons.

How does Thy-1 modulate Src activation? Thy-1 antibody clustering induces recruitment of SFKs to the plasma membrane and modifies their activation/phosphorylation status; additionally, SFK members co-immunoprecipitate with Thy-1 in T-cells, fibroblasts and neurons (Chen et al., 2006; Rege & Hagood, 2006). However, it is not clear, whether Thy-1 interacts directly with Src or via a linker molecule. Further research will be required to ascertain the exact signaling mechanisms underlying the influence of Thy-1 on axon growth and regeneration, both in fish and mouse neurons. To gain more mechanistic insights, it would be important to analyze the total levels of inactive and active kinases in Thy-1 knockdown neurons and to determine the amount of flotillin-associated kinases in microdomains. It will also be important to examine whether artificial overexpression of Thy-1 influences flotillin protein levels or vice versa, to exclude that cells activate a rescue mechanism within this pathway. Furthermore, to compare the mechanisms underlying impaired axon regeneration between fish and mammals, it would be necessary to test whether flotillin-associated phospho-Src, phospho-ERK1/2 and phospho-cofilin are affected in zebrafish as well. Otherwise it could be possible that the effects of Thy-1 may be similar, but mechanistically different in both species.

The conclusion of Thy-1 being supportive to axon regeneration, based on its lesion-induced expression in the fish CNS, is reinforced by my gain- and loss-of-function experiments which led to enhanced or impaired neuronal growth, respectively, and are likely due to alterations in signaling cascades responsible for actin cytoskeleton maintenance.

6.5. Specificity and validation of antibodies used in research

As explained in 6.1., the precise subcellular localization of a protein strongly influences its biological function. Nowadays, antibodies represent the most common tool to determine the localization of cellular components and are widely used reagents in life-science laboratories for basic and clinical research (Bordeaux et al., 2010). Antibodies entail major problems for laboratories and scientists, since in many cases their validity is not guaranteed. Generally speaking, three major aspects need to be clarified before an antibody can be considered as validated for research purposes. It has to be demonstrated that they are specific, selective and that they work reproducibly in the particular biological system in which they are employed (Bordeaux et al., 2010). But how to validate and generate evidence that the antibody meets these requirements? Fortunately, a series of systematic tests exist, with which ntibodies can be validated with a reasonable degree of confidence.

Testing the reactivity of the antibody in Western blot analysis is an appropriate first step to check if it recognizes its denatured cognate antigen. If the sequence of the immunogenic (poly-) peptide is known, Western blot analysis using the recombinant protein can be performed. This may show that the antibody has an affinity to its target but does not reveal binding to other proteins. Therefore, the antibody needs to be tested in its physiological environment where it should specifically recognize bind to its intended target amongst a multitude of other surrounding proteins (Saper, 2009). The first indication that the antibody is specific for the selected target would be observing a single band running at the expected molecular weight in Western blot analysis. If the antibody has been raised against a phosphorylated or glycosylated peptide additional proof of specificity can be obtained by enzymatic treatment of the samples using CIAP or PNGase, respectively (Bordeaux et al., 2010).

Especially in immunohistochemical and fluorescence based assays, unspecific background can pose a big problem. Besides optimizing experimental conditions to reduce unspecific “noise” e.g. caused by too high concentrations of primary or secondary antibodies or by contaminated reagents, a preadsorption test can be performed. Mixing the diluted antibody with an excess of the immunogen should completely block binding. If this test is negative it gives clear indication of unspecific binding. For polyclonal antibody sera, which represent a mixture of antibodies against multiple epitopes of the immunogen, this control makes sense. Preadsorption is meaningless in the case of a monoclonal antibody (which is obtained by screening for its binding to the target, and therefore will always recognize it and pass a

preadsorption test, by definition). The same holds true for polyclonal antibodies that have already been affinity purified (for the same reason) (Saper, 2009). If an antibody does not bind to a unique epitope, as is very often the case, cross-reactivity with similar epitopes on other related or unrelated proteins is inevitable and will lead to non-specific background (Voskuil, 2014). In some cases, background can be eliminated by improving experimental conditions, like diluting the antibody or increasing the concentration of blocking reagents thus forming the specific interaction of the antibody to its cognate antigen. Nevertheless, if one takes into account that proteins may share common epitopes, cross-reactivity of the antibody in question with these related proteins if they both are present in the same sample will be inevitable. Such cross-reactivity may render the antibody unusable (Voskuil, 2014). How is it then possible to judge if an antibody is specific and the results obtained can be trusted? In addition to compare results with data from literature, one of the best positive controls is to express the target protein in cells that do not express it endogenously. Another very strong indication that the antibody can identify its target in fixed tissue is to generate two antibodies recognizing different epitopes on the same protein or to compare a monoclonal with a polyclonal antibody. If both show exactly the same pattern, it is most likely that they both recognize the desired target (Saper, 2009).

The best negative control to reveal unspecific antibody binding is to probe it in cells or tissues that are known to be devoid of the protein of interest. If such knockout samples are available, which is often not the case, absence of staining is a strong confirmation of specificity. Still there might be the small chance that the antibody binds unspecifically to a protein which is downregulated in the knockout model as well. Therefore, evidence for the specificity of the knockout has to be provided too, and it must be excluded that the antibody recognizes a truncated, non-functional portion of the protein (Saper, 2009). A better technique is the use of inducible and spatially restricted knockdown of the protein of interest by RNA interference techniques (si/shRNA or morpholino-oligos), with which compensatory up- or downregulation of other proteins can be reduced to a minimum although not fully eliminated (Saper, 2009).

Finally, reproducibility is an important criterion for validation and standardization of an antibody: yielding similar results in independent experiments should be a prerequisite for each researcher working with antibodies. Ultimately, the responsibility to ensure that the antibodies used are validated for specificity and reproducibility lies in the hands of the individual researcher (Bordeaux et al., 2010).

Several journals provide strict guidelines how detailing antibodies used in publications must be validated. The Journal of Neuroscience, for example, gives strict instructions for authors and provides a descriptive database for all antibodies used in its publications since 2006. Authors who want to publish in this journal have to enter their antibodies in the list. In an open letter, the Editor-in-Chief (Clifford B. Saper) gives a brief description of the three basic elements that are necessary in describing an antibody for use in neuroscience: 1) complete information on the antibody, 2) how has the specificity of the antibody been characterized, 3) what controls are necessary for immunostaining (Saper, 2005; Saper & Sawchenko, 2003). Additional, valuable advice to the validation issue of antibodies comes from the laboratory of David Rimm. He published a comprehensive experimental scheme for antibody validation which represents a compromise between rigor and lab economics and results in a level of evidence sufficient for data dissemination (Fig. 6.5.) (Bordeaux et al., 2010).

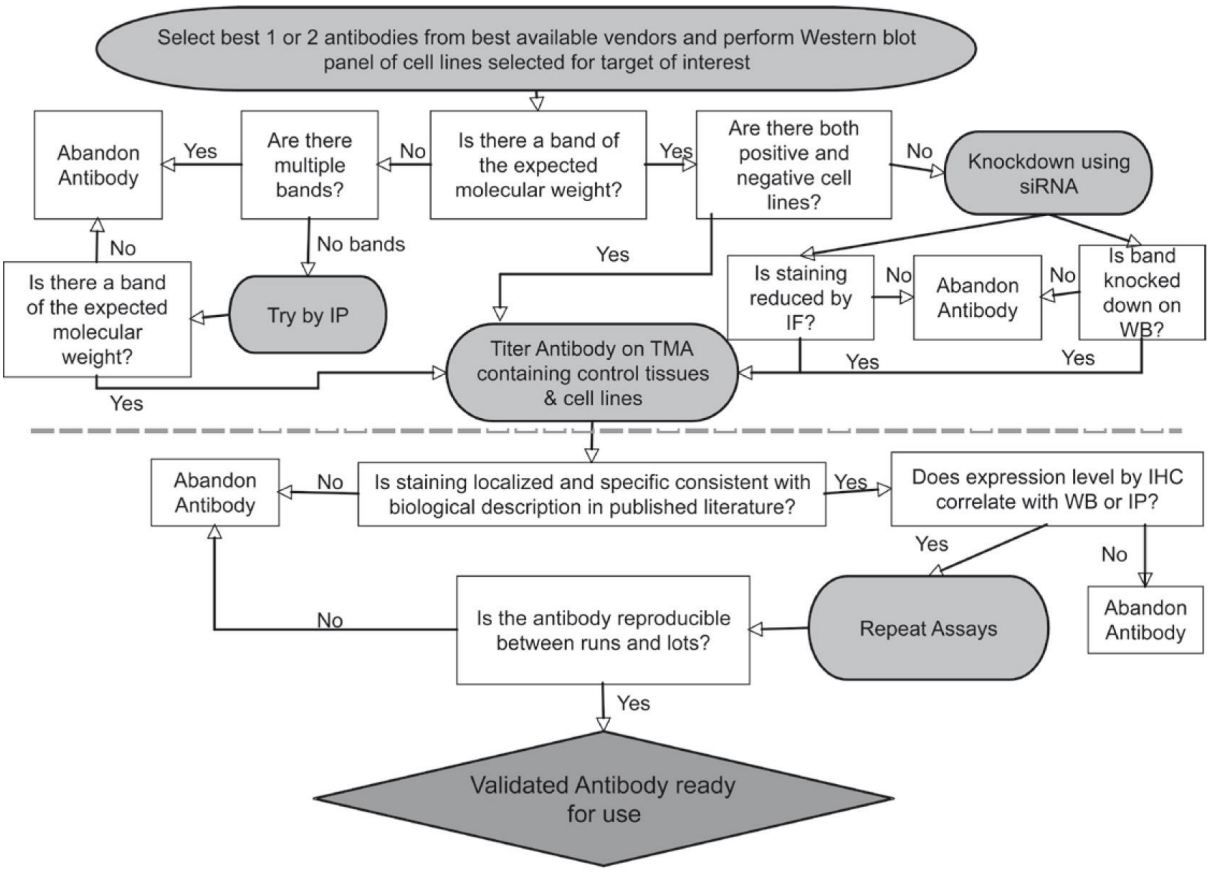

Fig. 6.5. The Rimm Lab Algorithm for antibody validation of immunohistochemistry/-fluorescence. Step 1 of antibody validation is using cell lines in vitro to test antibody specificity. Step 2 (below the dotted line) involves further validation of antibody on tissue microarray (TMA) for expected target localization and reproducibility between assay runs and different antibody lots. Figure and caption from (Bordeaux et al., 2010).

Nowadays, there are clear guidelines to provide specificity of antibodies, although, they are not always uniform and overlapping due to the complexity and the rapid development of this scientific discipline. The Thy-1 antibody generated in this thesis was validated taking into account these recommendations and guidelines and putting them into practice with the highest possible accuracy as described in the following:

6.5.1. Validation of the polyclonal and monoclonal Abs specific for zebrafish Thy-1 used in this research

Two purchased polyclonal rabbit sera (4716 & 4717), generated against short zebrafish Thy-1 peptides were the first attempt to obtain a specific detection tool for zebrafish Thy-1. After affinity-purification, the selected polyclonal antibody 4716 labeled all (old and young) RGCs in untreated control retinae. Upon ONS the fluorescence signal strongly increased, showing larger Thy-1 protein clusters at the cell membrane (Fig. 5.1.1.1 B and C). In order to verify that this antibody specifically recognizes its target, I generated an expression vector and expressed recombinant Thy-1-GST-fusion protein in bacteria. Western blot analysis yielded a positive result showing a band of the predicted molecular mass of ~38 kDa, which was visible only after IPTG-induced expression (Fig. 5.1.1.1 A). In zebrafish retina lysates, the polyclonal antibody 4716 detected a ~25 kDa band in Western blots, which was -like the signal in the immunohistochemistry- also increased after ONS (Fig. 5.1.1.1 D). Upon specific morpholino-mediated knockdown of Thy-1 in RGCs *in vivo*, the protein bands in the Western blot as well as the fluorescence intensity in immunostainings decreased, suggesting that the antibody detected the correct antigen and the designed morpholino specifically downregulated its target (Fig 5.1.1.2). However, since the antibody produced some undesired background in Western blot and immunohistochemical analyses, I undertook new attempts to obtain -better- monoclonal antibodies.

In order to obtain a more specific monoclonal antibody specific for zebrafish Thy-1, I cloned the cDNA encoding the full-length Thy-1 core protein, expressed it and purified it from bacteria, used to immunize two mice (method 4.12.2.). Firstly, I tested the pre-immunization blood of these mice for non-reactivity which was positive so that they could be used for immunization. Both immunizations resulted in immune-reactive sera. B-cells of both mice were fused to hybridoma cells. As a pre-screening, I tested the positive hybridoma supernatants in Western blots. Those which recognized the ~38 kDa protein band corresponding to recombinant Thy-1-GST and the predicted ~25 kDa protein bands in

zebrafish brain lysates were further tested by immunohistochemistry of retinae, with or without ONS. The hybridoma clone showing the clearest signals was number 89/9. Several lines of evidence strongly suggested that the "mAb 89/9" specifically recognizes the functional Thy-1 protein at the surface of retinal cells in zebrafish:

Firstly, the mAb Thy-1 89/9 recognized recombinant Thy-1 in the Western blot only in samples obtained from bacteria tested with IPTG for inducing expression of the protein. Further, mAb 89/9 detected a single band at ~25 kDa in zebrafish brain and retina lysates (Fig. 5.1.2 A and Fig. 10.1). Upon ONS, the mAb 89/9 detected elevated expression levels of Thy-1 in Western blots and immunostainings. Induction of Thy-1 expression by ONS was verified by an independent method -quantitative realtime PCR (Fig. 5.1.2). The circular, membranous labeling of Thy-1 in all RGCs became stronger, more disordered and clustered (Fig. 5.1.2 D, E). Furthermore, the monoclonal mouse mAb 89/9 and the polyclonal rabbit pAb 4716 targeting zebrafish Thy-1 yielded similar results with respect to behaviour of expression and pattern of localization in immunohistochemical and Western blot analysis. Reproducing the results obtained with one antibody using a second one, generated in a different species is one of the strongest arguments for validation (Bordeaux et al., 2010).

Secondly, enzymatic deglycosylation of an immunoprecipitate obtained with mAb 89/9 from zebrafish brain lysate using PNGase F resulted in a protein band shift in Western blots from ~25 to ~18 kDa, proving that the antibody recognizes a glycosylated protein like Thy-1 (Fig. 5.1.2 B). These data thus demonstrate that zebrafish Thy-1 is glycosylated like its mammalian counterpart, which is of functional relevance, since glycosylation is a crucial determinant of the biophysiological role of a protein (Cumming, 1992).

A third evidence for specificity of the mAb 89/9 was the reduced protein level in Western blots of retinal and embryonic lysates, as well as a reduced immunofluorescence signal upon morpholino-mediated knockdown of Thy-1 expression in zebrafish. These results highlight the specificity of both, the antibody and the morpholinos (Fig. 5.1.4 and 5.1.5.2).

Thy-1 is a very stable protein with a long half-life, which could explain the more efficient knockdown in embryos as compared to adult retinae (Lemansky et al., 1990) (Fig. 5.1.4 D and E versus Fig. 5.1.5.2 C and D). The embryos received the translation-blocking morpholinos at the one- to four-cell stage thereby suppressing expression right from the beginning of development, whereas in the retinae existing protein first has to be degraded before the effect of knockdown becomes detectable.

A fourth confirmation that the mAb 89/9 recognizes a retinal cell surface protein like Thy-1 came from immunostainings of live tissues. Here, samples were exposed to mAb 89/9 only for a short-time on ice. This procedure prevents internalization of the antibody and no intracellular proteins become labeled. For these stainings, I used whole retina flat-mounts as well as single RGCs, where the mAb 89/9 steadily labeled cell surface Thy-1 in a dotted pattern, enriched at cell-cell-contacts (Fig. 5.1.2 and 5.1.3). The antibody mAb 89/9 was specifically generated against zebrafish Thy-1, but produced consistent results also in a very close relative -the goldfish-, which is also a strong indication for antibody specificity (Fig. 5.1.6).

Taken together, these data build a strong case for the antibody presented in this thesis.

During regeneration studies in the goldfish retina and optic nerve, Schulte et al. described a monoclonal antibody raised against a goldfish membrane homogenate of transected optic nerves. This antibody M802, exclusively stained those few retinal axons which arise from new ganglion cells forming at the retinal margin during the whole life span of the fish (Schulte et al., 1997) (Fig. 6.5.1 a, b). After optic nerve injury, M802 labeled all RGCs and retinal axons throughout their path into the tectum (Schulte et al., 1997) (Fig. 6.5.1 a, b). This antibody was generated to enable the identification of lesion-induced proteins in the fish CNS which would also be very likely be actively involved in successful regeneration processes. The antibody M802 was obtained by immunization of mice with complete membrane fractions from regenerating goldfish optic nerves (Schulte et al., 1997). Initially, the M802 antibody was reported to detect goldfish flotillin, because it labeled a prominent band with an apparent MW of ~48 kDa in Western blots of goldfish brain and retina lysates (Schulte et al., 1997). This band was isolated by PAGE, and the protein fraction was subjected to Edman sequencing. This work led to the identification of goldfish flotillin (Schulte et al., 1997). Moreover, the monoclonal antibody M802 was reported to recognize recombinant flotillin proteins in Western blots and revealed the same immunostaining pattern as a polyclonal flotillin antiserum which was generated at the same time. In situ hybridization experiments localizing flotillin mRNA expression yielded a very similar pattern, confirming the Western blot and IHC data (Schulte et al., 1997) (Fig. 6.5.1). Six years later, a second weak band at MW ~25 kDa was detected in Western blots of goldfish retina lysate using M802 (Deininger et al., 2003). After immunoprecipitation of goldfish retina lysate using M802 and subsequent extraction of the respective protein by preparative SDS-PAGE, the material was Edman-sequenced. The sequences of five short fragments were aligned with protein databases and showed 68%

homology to the zebrafish Thy-1 amino acid sequence (Deininger et al., 2003) (Fig. 6.5.2 A). The result was interpreted in term of a cross-reactivity of the M802 antibody which would recognize both goldfish flotillins and Thy-1, because of a shared epitope (Lang et al., 1998). Since goldfish and zebrafish are phylogenetically very closely related, a similar expression pattern of Thy-1 in both species would be expected. However, data presented in this thesis suggest that the distribution of Thy-1 in zebra- and goldfish retinae is different from that as described for the antibody M802. Therefore, my data suggest that M802 may label another protein that like many other factors becomes upregulated upon optic nerve injury in fish but not Thy-1. Possible reasons for this conflicting data are discussed further in the following paragraph.

When I started my experiments, M802 was assumed to reveal the characteristic expression pattern for Thy-1 in the fish retina. Nevertheless, all of the zebrafish-specific antibodies available in the laboratory consistently showed a different pattern. This was surprising because zebra- and goldfish are evolutionarily closely related with high overall sequence homology (Málaga-Trillo et al., 2002). One possible explanation for this discrepancy could be that the expression patterns of Thy-1 in gold- and zebrafish are indeed different. However, this case seems rather unlikely, since the zebrafish-specific mAb 89/9 also detects goldfish Thy-1 in Western blot and immunohistochemistry analyses, revealing a staining pattern similar to the one in zebrafish retinae, but differing from M802 (Fig. 5.1.6, 6.5.1). In contrast, the goldfish-specific M802 antibody does not cross-react with zebrafish samples. These results raise the possibility that the M802 antibody recognizes goldfish Thy-1 only partially or under conditions that are difficult to reproduce. Of note, M802 binds most strongly to a ~48 kDa protein in Western blots (Schulte et al., 1997) (Fig. 6.5.2 B). Essentially, flotillins as well as Thy-1 might have been identified both using M802 due to co-immunoprecipitation of these proteins with the actual antigen. However, since the antibody M802 was generated using a complex protein fraction as immunogen, it is understandable that the results obtained by Schulte et al. and Deininger et al. were difficult to interpret back then. At the time when M802 was characterized, it was no common method -and technically still difficult- to validate the specificity of an antibody by using knockdown/overexpression strategies. Nowadays these approaches are state-of-the-art and I used them in my experiments to validate mAb 89/9. Immunohistochemical experiments with the monoclonal antibody M802, which I performed during my thesis yielded an immunostaining pattern in goldfish retinae which was consistent

with data shown in Schulte et al. In Western blots of goldfish lysates, a prominent band always appeared at ~48 kDa and I did not succeed in detecting a weaker band at ~25 kDa, regardless whether I used reducing or non-reducing conditions (Fig. 6.5.2 B). To check any putative cross-reactivity of M802 with flotillins, I did Western blots with recombinant proteins (kindly provided by Dr. G. Solis). M802 did not bind to recombinant flotillins in these experiments (data not shown, but available upon request). In light of these data, I conclude that M802 likely recognizes neither Thy-1 nor flotillins in goldfish but a different ~48 kDa protein affected by optic nerve regeneration in zebrafish. It is well established that optic nerve regeneration specifically affects the expression of a large number of genes belonging to several functional groups including cell adhesion, apoptosis, cell cycle energy metabolism, ion channel activity and calcium signaling (McCurley & Callard, 2010).

An alternative scenario could be that two divergent Thy-1 gene duplicates evolved independently in gold- and zebrafish as a result of the well-known teleost genome duplication (Glasauer & Neuhauss, 2014). However, the zebrafish genome has been entirely sequenced and only one Thy-1 gene was identified so far. If there are two copies of Thy-1 in goldfish, one of them may be orthologous to the zebrafish single copy and therefore recognized by the 89/9 antibody, whereas the second one may have diverged to the point of having acquired a novel expression pattern in the goldfish retina being solely recognized by the mAb M802. Differences in gene copy numbers between gold- and zebrafish have in fact been reported. For instance, unlike mammals which have two closely related flotillin 1 and 2 proteins, goldfish possess four duplicated flotillins: flotillin 1a, 1b, 2a and 2b, but zebrafish only three: flotillin 1a, 1b, and 2a (Málaga-Trillo et al., 2002). Interestingly, the embryonic expression patterns of zebrafish flotillins have evolved to become nearly non-overlapping (Von Philipsborn et al., 2005). Based on that present data, and regardless of the two scenarios discussed above, the assumption that Thy-1 has an idiosyncratic expression pattern in the fish retina that corresponds to the picture previously obtained with the antibody M802 would have to be revised.

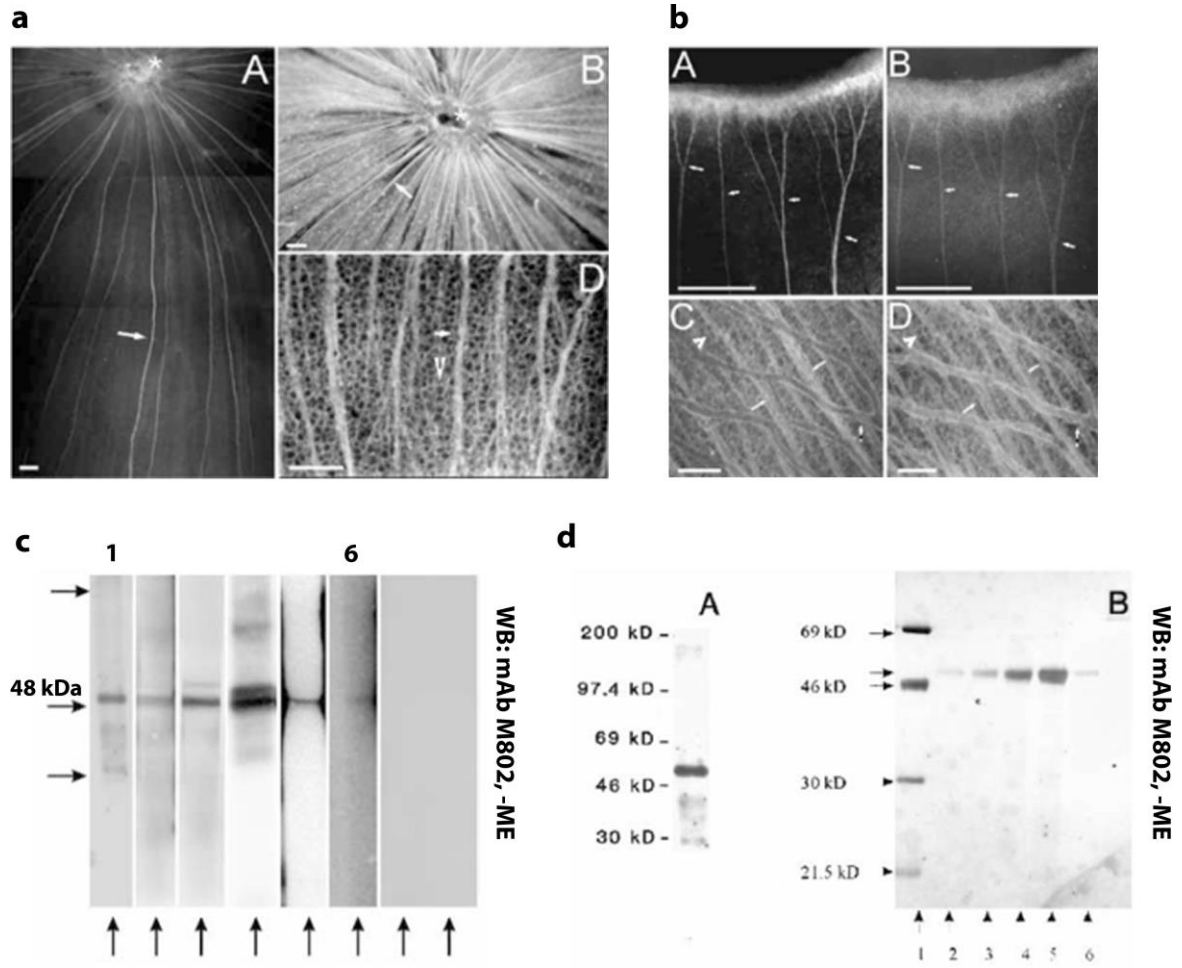

Fig. 6.5.1 The monoclonal antibody M802 in goldfish retina flat-mounts and WB analysis. a) (A) In normal retinae, M802 selectively binds to axon fascicles of emerging RGCs (small arrows; asterisk: optic disc). Scale bar in A: 200 µm. (B) (D) After ONS, all RGCs (arrowhead) and axons (arrows) are labeled (asterisk: optic disk). Scale bars in B: 200 µm; in D: 50 µm. **b)** Double-immunostaining with M802 and the polyclonal flotillin-2 antiserum (flot-2). (A, B) Whole mount of a normal retina (unfixed). 504 antiserum against flot-1 (B) and M802 (A) recognize the same new RGCs at the retinal margin and axons (arrows). Scale bars: 100 µm. (C, D) Whole mount of a retina 14 days after ONS with the retinal blood vessel layer on top. Fixed with methanol prior to exposure to M802 (C) and antiserum 504 against flot-2 (D). The same structures are labeled in C, D: all RGCs (arrowheads) and axons (long arrows) and blood vessels (short arrow). Scale bars: 50 µm. **c)** WBs with flot-1 and flot-2 antisera. Detergent extracted proteins of adult goldfish brain (50 mg protein) in lanes 1, 2, 3, 7, 8; rec. flot-2, lane 4; rec. flot-1, lanes 5, 6 (100 ng each), after 10% SDS-PAGE, non-reducing condition (-ME). Exposed to flot-2 antiserum 504 (lanes 2, 4), to flot-1 antiserum 513 (lanes 3, 5) and to M802 (lanes 1, 6) as reference. Secondary antibodies (goat anti mouse) in lane 7 and goat anti rabbit in lane 8 serve as controls. Flot-2 and flot-1 antisera (lanes 2, 3) recognize the same major 48 kDa band as M802 (lane 1). Flot-2 antiserum recognizes rec. flot-2 protein; two bands at 48 kDa (lane 4), and flot-1 antiserum binds to rec. flot-1 (lane 5). M802 weakly recognizes rec. flot-1 (lane 6). **d)** WB with M802 and elution profile of 48 kDa flotillin after immune affinity purification. (A) WBs with mAb M802 and detergent extracted proteins of adult goldfish brain, non-reducing conditions (-ME). M802 recognizes a major protein band of 48 kDa and some lower relative molecular mass (probably degradation) products. (B) Elution profile of the M802 immune affinity column. Lane 1, molecular weight markers; lanes 2-6, elution profile showing a protein at 48 kDa, silver staining, non-reducing conditions. Figures and caption modified from (Schulte et al., 1997).

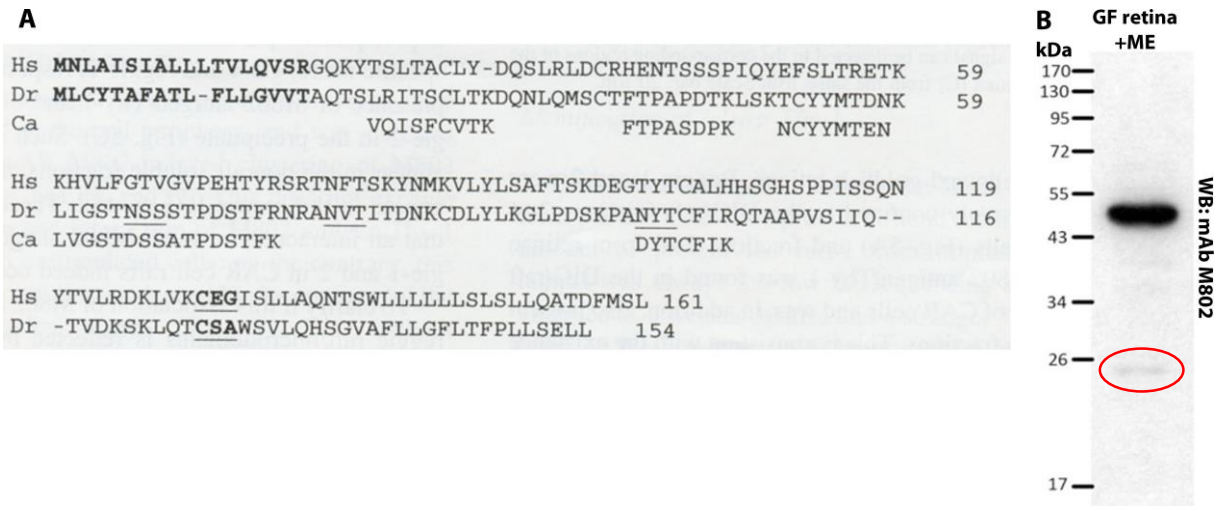

Fig. 6.5.2 A. M802 antigen; Edman sequencing after immune affinity purification, in-gel-deglycosylation, tryptic in-gel-digestion, isolation of a ~30 kDa protein band and subsequent PBLAST database search. Alignment of the Thy-1 precursor protein sequences from human (Hs) and zebrafish (Dr) and the peptides obtained from goldfish (Ca) M802 antigen/Thy-1. Boldface, signal peptide; underscored, putative N-linked glycosylation sites; boldface and underscored, GPI modification site. Hs, Homo sapiens; Dr, danio rerio; Ca, Carassius auratus. Figure and caption from (Deininger et al., 2003).
B. WB with goldfish retina lysate, reducing conditions (+ME), with the mAb M802 shows a very prominent band at ~ 48 kDa like in Schulte et al., 1997 (Schulte et al., 1997). One very weak band can be recognized at ~25 kDa, which was isolated and sequenced in Deininger et al., 2003.

6.6. PrP-2 in zebrafish RGCs, its lesion-induced expression and validation of the pAb 981

The expression pattern of the GPI-anchored protein PrP-2 in the zebrafish retina with the polyclonal antibody “981” revealed a ubiquitous, membranous localization of PrP-2 throughout all RGCs, particularly enriched at cell contacts. This pattern was expected, since PrP-2 was reported to mediate cell-adhesion via homophilic *trans*-interactions between globular domains on opposing cells (Fig. 5.3.1 D) (Solis et al., 2013; Malaga-Trillo et al., 2009). My immunohistochemical data show increased levels of PrP-2 in zebrafish RGCs after ONS, along with its accumulation at the plasma membrane (Fig. 5.3.1 E). While in my studies, I exclusively focused on the ganglion cell layer of zebrafish retinae, in neurons of rodent and human retinae PrP is expressed abundantly. There it is found within somas of the inner nuclear and ganglion cell layer, and enriched in synaptic terminals of the outer and inner plexiform layer, where it plays a neuroprotective role (Chiarini et al., 2002; Head et al., 2003; Williams et al., 2011; Gong et al., 2007).

Western blots of zebrafish retina lysates confirmed the lesion-stimulated expression of PrP-2, and separation of membrane and cytosolic fractions verified its mainly membrane-associated

localization (Fig. 5.3.1 F, B). While the predicted molecular mass of zebrafish PrP-2 is ~70 kDa, its rapid degradation led to several protein bands in Western blots, with a predominant band at ~40 kDa (Fig. 5.3.1 A). Enzymatic deglycosylation with PNGase F led to a band shift of the full length protein, confirming that the antibody recognized a glycosylated protein as it was expected for endogenous zebrafish PrP-2 (Fig. 5.3.1 C) (Rivera-Milla et al., 2006). Only the band of full length PrP-2 -but not its degradation products- shifted down upon PNGase F treatment and therefore one could speculate that degradation of the protein may begin C-terminally, where the predicted glycosylation sites are localized (Rivera-Milla et al., 2006). Another strong proof for validation of the polyclonal antibody 981 raised against zebrafish PrP-2 was the successful reduction of all bands in Western blots and immunofluorescence signal intensity in retina whole mount preparations upon transfection of RGCs with specific morpholinos (Fig. 5.3.2 C and Fig. 5.4.2 A). Prof. Dr. E. Malaga-Trillo and his group provided additional confirmation by testing the pAb 891 in Western blots and immunostainings using overexpressed, recombinant PrP-2 or protein knockdown using morpholinos in zebrafish embryos (personal communication). Altogether, these data provide strong evidence for the reliability and specificity of the described tools -the antibody and the morpholino- for further functional analyses of zebrafish PrP-2.

6.7. Role of PrP in neuronal function and its biological relevance

The lesion-induced expression of PrP-2 in axotomized RGCs implied a supportive role during regeneration (Fig. 5.3.1). In order to assess the role of PrP in neuronal growth, I performed functional outgrowth assays with primary zebrafish single RGCs. Upon PrP-2 morpholino-mediated knockdown *in vitro*, transfected cells had reduced neurite lengths by up to 30% in a concentration-dependent manner (Fig. 5.4.1 A, B, C). *In vivo* transfection of RGCs by application of PrP-2 morpholinos to the transected optic nerves of anesthetized zebrafish led to 90% less emerging axons from retinal explants in culture (Fig. 5.4.1 D, E). Given the consistent effect using different morpholino sequences and concentrations, it is reasonable to conclude that PrP-2 plays a supportive role in growth and regeneration in the zebrafish CNS. Furthermore, knockdown of PrP with siRNA in primary mouse hippocampal neurons *in vitro* induced a comparable impact and reduced axon growth by 24% (Fig. 5.5 C). Hence, all of these loss-of-function data suggested that fish and mammalian PrPs support axon regeneration and growth. In other studies investigating PrP`s role in regeneration of mammalian neurons, PrP

was absent from injured sciatic nerves of rats in degenerating axons but significantly increased in axons where regeneration took place, decreasing again at the time of functional recovery (Moya et al., 2005). These authors analyzed the expression of PrP in developing and adult mammalian brains where it was predominantly located in elongating and growing axons (Salès et al., 2002). In adult brain structures, low levels of PrP were observed, except for regions with high remaining plasticity like the olfactory bulb and the hippocampus (Salès et al., 2002). These results indicated a positive role of PrP during development and growth of axons *in vivo*, likely acting as an adhesion molecule interacting with the extracellular environment (Salès et al., 2002). Following up on this idea, the same authors uncovered a positive function of PrP in neural precursor proliferation during developmental and adult mammalian neurogenesis (Steele et al., 2006). However, an opposite role of PrP has also been reported, when it stabilized and potentiated the inhibitory effect of the neurite outgrowth inhibitor Caspr (contactin-associated protein) at neuronal surfaces (Devanathan et al., 2010).

Impaired axonal outgrowth upon transient loss of PrP in single zebrafish ganglion cells and mouse hippocampal neurons confirmed the established notion of a growth-supportive role of PrP in the mammalian CNS, and unveiled its importance also in zebrafish. This organism regrows axons during its whole lifetime but apparently needs PrP to regenerate effectively, as demonstrated in this study.

These findings raise the following question: why do PrP knockout mice survive, show an apparently normal development and do not exhibit impaired axon growth? The most common explanation, as for other knockout animals with no apparent phenotype (e.g. Thy-1$^{-/-}$), are genetic compensation mechanisms and technical limitations. During the generation of knockout animals, only stem cells which compensate the loss and survive become selected. Genetic compensatory mechanisms remain poorly understood but a few potential ones have been proposed in the case of the PrP knockout mouse. For example, a rescue mechanism via integrins was suggested (Hajj et al., 2007). To circumvent these unwanted genetic compensation effects, conditional PrP knockout mice were generated (Mallucci et al., 2002). Interestingly, the acute, post-natal knockout of PrP in 9 weeks old mice resulted in healthy adult animals without signs of neurodegeneration or other histopathological changes for up to 15 months post-knockout (Mallucci et al., 2002). However, in the neurophysiological evaluation, these animals showed a significant reduction of after hyperpolarization potentials (AHPs) in hippocampal CA1 cells, implying a direct role for PrP in neuronal excitability (Mallucci

et al., 2002). Due to the absence of a severe neurodegenerative phenotype in these mice, the authors ruled out loss of PrP function as a pathogenic mechanism in prion disease (Mallucci et al., 2002). Most notably, they showed that prion-infected mice fully recovered from prion disease after conditional knockout of PrP (Mallucci et al., 2002). This work pioneered more recent attempts that targeted PrP expression via RNA interference, in order to identify new therapeutic strategies against prion and other neurodegenerative diseases (Mallucci et al., 2007; Verity & Mallucci, 2011; White & Mallucci, 2009). Long-term risks and unintended consequences of such treatments have to be awaited for. Given PrP`s implication in synaptic (dys-) function and importance in mediating neuroinflammation it seems unlikely that these treatment will remain without side-effects (Senatore et al., 2013; Gupta & Pulliam, 2014). Furthermore, recent studies indicated that PrP has multiple functions and is involved in cognition, learning, anxiety, locomotion, depression, offensive aggression and nest building behavior (Schmitz et al., 2014). While young knockout animals (3 months of age) showed only marginal abnormalities, most of the deficits became apparent as the animals aged, which emphasized PrP`s role in neurodegeneration or neuroprotection (Schmitz et al., 2014).

Taken together, my results as well as the existing literature suggest a growth-supportive role of PrP during regeneration of fish and mouse CNS neurons. Additionally, it has been previously shown by the group of Prof. Dr. E. Malaga-Trillo that PrP is important for the developing fish CNS, since PrP-2 morphant embryos displayed severely malformed CNS structures (head and eyes) as well as misguided and truncated axonal projections of spinal cord motoneurons (unpublished results, (Ochs & Málaga-Trillo, 2014; Málaga-Trillo & Sempou, 2009)). In conclusion, PrP appears to be a supportive regulator of proper axonal growth in regenerating CNS neurons and also during embryonic development of zebrafish and most probably also of mammals. This a complex scenario may have been somewhat overlooked in mammalian PrP research so far.

6.8. PrP-associated signaling partners in neurons

In search of cellular signaling mechanisms underlying the negative effects of PrP knockdown on axon growth and regeneration, I performed biochemical experiments which yielded preliminary information. Analysis of zebrafish retina lysates after morpholino-mediated knockdown of PrP revealed an association between reduced axonal outgrowth and altered Src

kinase signaling: total levels of SFKs (including Src, Fyn and Yes), as well as levels of the activated form of Src were reduced (Fig. 5.4.2).

Consistent with these findings, the involvement of SFKs in PrP-associated signaling was connected to neurite outgrowth in PC12 cells, where PrP activation induced neurite outgrowth and differentiation by a Fyn-dependent activation of the Ras-Raf pathway (Pantera et al., 2009). Fyn activation after antibody-mediated cross-linking of PrP in a neuronal cell line was the first evidence for PrP being a signaling molecule of relevance for neurites (Mouillet-Richard et al., 2000). In another study, *cis*- and *trans*-interactions between PrP and NCAM (neuronal cell adhesion molecule) promoted the recruitment of NCAM to lipid rafts and the activation of Fyn kinase, thereby enhancing neurite outgrowth (Santuccione et al., 2005). Moreover, a strikingly important role for PrP was recently discovered by Um and colleagues, who identified PrP as a postsynaptic receptor for Amyloid-beta (Aβ) oligomers (Um et al., 2012). The altered surface expression of the NMDA-receptor and the loss of dendritic spines in this model reflected the pathology of Alzheimer`s disease and were dependent on Fyn kinase activity (Um et al., 2012). By using different PrP knockout mouse models, Schmitz et al. recently proposed that PrP plays an important role in the regulation of the cytoskeleton and associated (signaling) proteins, a process highly relevant for regeneration (Schmitz et al., 2014).

Similarly, the neuronal PrP-1/-2 loss of function phenotypes in zebrafish embryos observed by Malaga-Trillo and colleagues were attributable to altered SFK signaling and the regulation of zebrafish embryonic cell adhesion by PrP required SFK activation (Malaga-Trillo et al., 2009; Sempou et al., 2016). Recent in-depth analysis led to the hypothesis that PrP-signaling via SFKs is central to diverse knockout and mutant PrP phenotypes observed in mice (Ochs & Málaga-Trillo, 2014).

Not only the SFK member p59 (Fyn) controls neuronal outgrowth and survival downstream of PrP; other important signaling molecules like MAPK, PI3K and PKA functionally interact with PrP as well (Chen et al., 2003). Interestingly, PrP is not only a receptor for NCAM, as mentioned above, but also for Laminin (LN), a molecule which plays a major role in neuronal differentiation, migration and survival (Timpl et al., 1979; Durbeej, 2010). In studies by Martins, Bretani and colleagues the PrP-LN receptor-ligand interaction was decisive for neuritogenesis in PC-12 cells and primary rat hippocampal neurons (Graner et al., 2000; Lima et al., 2007).

The mechanism by which PrP, like other GPI-linked outer-membrane molecules, would elicit intracellular signaling is undefined thus far. Evidence for a putative direct protein interaction in a larger complex, for example, came from epithelial cells, where co-immunoprecipitation experiments discovered a PrP-Src association in raft domains (Morel et al., 2004). If the influence of PrP on Src observed in my preliminary experiments using zebrafish RGCs was due to a direct interaction between both proteins in a complex could be clarified in further biochemical analyses, like co-immunoprecipitation and pull-down assays.

The data of my thesis revealed a new, important role of PrP during axon regeneration in the visual system of zebrafish and in mammalian hippocampal neurons, acting as a growth supportive molecule. This goes in line with previous studies about the function of PrP in neurons. Taken together, these data suggest a common, conserved physiological role of PrP in mammalian and teleost organisms. Most likely by acting as an extracellular receptor, PrP modulates cell adhesion, neurite outgrowth and synaptic plasticity in mammals and fish -at least- via SFK signal activation and alteration of subsequent endocytic processes (Ochs & Málaga-Trillo, 2014).

6.9. Functional similarities and differences between Thy-1 and PrP

In my studies, I found increased levels of Thy-1 and PrP after CNS injury in a successful regenerating model organism -the zebrafish-, which demonstrated their common important role during this process. Consistently, knockdown of Thy-1 and PrP diminished axon growth (Fig. 5.2.1, 5.2.2.1, 5.2.2.2, 5.2.3, 5.4.1, 5.5). These findings were supported by experiments in mouse hippocampal neurons, from which we might conclude that the neuronal function of both proteins is conserved between these distantly related species. Furthermore, my data showed that both GPI-linked molecules are highly expressed at the neuronal surface of RGCs in the zebrafish retina, contributing to successful axon growth and regeneration. Based on the currently available information, we could summarize that Thy-1 and PrP act as membranous receptors, influence actin cytoskeleton dynamics by transmitting signals to intracellular cascades and regulating the growth potential of neurons.

Beside this fundamental similarity, important differences between the two proteins are evident. Neuronal Thy-1 and PrP were localized to distinct membrane microdomains which differed in lipid composition and therefore activated distinct sets of signaling molecules (Brügger et al., 2004).

In terms of protein stability at the plasma membrane and turnover, PrP has a half-life of only a few hours and is rapidly and constitutively endocytosed at the neuronal surface (Parizek et al., 2001; Shyng et al., 1993). The opposite is true for Thy-1, which undergoes slow internalization, with a half-life of >100 h (Sunyach et al., 2003; Lemansky et al., 1990).

Interestingly, even though both proteins modulate SFK activity during axon regeneration, they seem to do so in opposite directions. Consistent with a previous report where Thy-1 inhibited SFK activity in T-cells, we observed increased pSrc levels after siRNA-mediated knockdown of Thy-1 in mouse hippocampal neurons (Hueber et al., 1997, S. Henrich, 2014). In case of PrP, the opposite -decreased pSrc levels- was reported, a result in line with the general consensus, obtained from a variety of *in vitro* and *in vivo* models, that PrP stimulates SFK activation (Ochs & Málaga-Trillo, 2014). Although knockdown of Thy-1 or PrP in neurons had the same phenotypic effect of impaired axon growth, the subsequent signaling events induced by both proteins seemed to be of opposite sign and revealed different SFK signaling mechanisms. In our experiments we were not able to detect any functional link between Thy-1 and PrP, since cross-linking/activation of one of the molecules did not result in a redistribution of the other and a double knockdown in hippocampal neurons had no additive impact on outgrowth (Fig. 5.5 A, B). The opposite effect on SFK signaling cascades triggered by Thy-1 or PrP, demonstrated that proper cell function and neurite outgrowth is not based on one particular mechanism but rather dependent on the equilibrium of all molecules that are involved in multiple processes.

This study showed that the GPI-anchored molecules Thy-1 and PrP play significant supportive roles during axon regeneration and growth in neurons of fish and mammals. The data presented demonstrate that successful regeneration upon CNS damage to a large extent depends on the molecular basis and the intrinsic ability of neurons to directly upregulate growth-supportive molecules.

PART II Reticulon-4 (RTN4b)

The myelin-associated neurite outgrowth inhibitor Reticulon-4/Nogo-A restricts axonal growth, regeneration, migration and sprouting of cells in the mammalian CNS and was examined extensively in this context because it bears a great potential for the treatment of auto-immune mediated demyelinating diseases and spinal cord injury regeneration (Karnezis et al., 2004). In contrast to mammals, fish and lower vertebrates are able to regenerate their CNS axons and restore neuronal function. Therefore, in this study, I investigated the recently identified zebrafish counterpart RTN4b (Shypitsyna et al., 2011). I was interested in its expression and cell-intrinsic function in zebrafish RGCs as well as in potentially new unknown effects in the context of neuronal outgrowth.

6.10. RTN4b/Nogo-A in zebrafish RGCs, its lesion-induced expression and endogenous neuronal function

In order to investigate RTN4b expression and function during optic nerve regeneration in zebrafish RGCs, we generated a new polyclonal antibody (see methods 4.16 and Welte et al., 2015). In zebrafish RGCs, RTN4b was localized intracellularly in a grainy pattern, consistent with its known function as a structural component of the endoplasmic reticulum (Fig. 5.7.1) (Jozsef et al., 2014). There was no RTN4b evident at the cell surface; short immunostaining of unfixed cells on ice showed no fluorescence signal. As a reference, in rat retinae Nogo-A is present on RGCs but also on Müller glia cells in their RGC-connected end-feet (Pernet et al., 2012). After axotomy, rodent Nogo-A was not increased in Müller glia cells, but in RGCs (Pernet et al., 2012). In zebrafish retinae, the expression of Nogo-A was not restricted to RGCs, glial end-feet seemed to be immune-labeled as well (Fig. 9.12.3). Like in the study of Pernet et al., RTN4b became upregulated upon ONS in zebrafish retinae as well, as demonstrated by immunostainings and Western blots (Fig. 5.7.1 and Welte et al., 2014). The overall fluorescence signal in cell bodies and axons increased at 5 or 10 days post lesion (Fig. 5.7.1 A-C). This result implied a growth-supportive role of RTN4b during regeneration. Therefore I investigated if optic nerve regeneration would be impaired due to RTN4b knockdown in RGCs. Axonal outgrowth from morpholino-treated retinal mini explants was reduced by 70% upon loss of RTN4b (Fig. 5.7.2). Vice versa, in rat RGCs, virally-induced overexpression of Nogo-A improved axon regeneration *in vitro* and *in vivo* (Pernet et al., 2012).

Like the other members of the reticulon family, RTN4/Nogo-A is mainly associated with the endoplasmic reticulum (ER) (Yang & Strittmatter, 2007). How does this localization influence cellular events that are mainly governed by molecular interactions at the plasma membrane? A plausible explanation would be that knockdown of intrinsic RTN4b leads to ER dysfunction, thereby disrupting the correct processing and trafficking of proteins required for axon growth and regeneration. Interestingly, it was reported that there are functional equivalents of ER and Golgi compartments in rat and Xenopus axons (of DRG and RGC neurons), secreting locally synthesized proteins and maintaining neurite growth, in particular during regeneration (in isolated axons as well) (Merianda et al., 2009). In the study of Merianda et al. it was highlighted that especially growing and regenerating axons contain more of these ER and Golgi components (Merianda et al., 2009). RTN4b fluorescence signals were detectable in the long projecting axons overhead of the retina, which were increased upon ONS (Fig. 5.7.1). Probably, in zebrafish, RTN4b is associated to these axonal ER-equivalent structures as well and promotes growth in neurites of RGCs by maintaining proper ER function and local protein synthesis in axons.

Still, the hypothesis that downregulation of RTN4b in zebrafish RGCs leads to disturbed ER function must be verified yet. However, fish RTN4b is likely to play a similar important role in ER maintenance as it was shown for mammals. I visualized the ER of zebrafish RGCs by using a polyclonal antibody specific for the membrane protein Climp63, an ER-marker that links the organelle to the cytoskeleton (Pépin et al., 2012). Since this antibody was a rabbit polyclonal like the RTN4b/Nogo antibody double immunostaining to determine co-localization of RTN4b and Clipm63 was not possible (Fig. 5.7.3). Both antibodies revealed different expression patterns in the zebrafish retina; Climp63 marked discrete tubular structures, whereas RTN4b was diffuse and grainy (Fig 5.7.7 and 5.7.3). Further comprehensive studies will show if the ER undergoes a change in its functional tubular structure upon loss of RTN4b, being responsible for the decreased potential of zebrafish RGCs to regenerate after knockdown.

6.11. Substrate properties of fish and mammalian RTN4b/Nogo-A, identification of its four inhibitory motifs

The Nogo-A protein is one of the most potent growth inhibitors in the mammalian CNS, involved in many neurodegenerative diseases (Schmandke & Schwab, 2014). This inhibitory function requires Nogo-A expression at the surface of glial cells that surround the neurons and

form the glial scar after CNS injury, thereby building a physiological and chemical barrier for axons to re-grow (Yiu & He, 2006). Since fish in contrast to mammals are able to regenerate after CNS injury, the hypothesis was put forward in the laboratory, that this difference may be explained by a lack of inhibitory molecules. In earlier *in vitro* studies, growth of fish retinal explants on fish myelin was substantial and caused only minimal growth cone collapse (Bastmeyer et al., 1993) (Wanner et al., 1995). Therefore, it was assumed that fish completely lack Nogo-like growth inhibitors. The fact that mammalian myelin/Nogo-A inhibited the growth of fish axons demonstrated that fish growth cones are able to recognize mammalian myelin-associated inhibitors and possess relevant, functional Nogo receptors (Wanner et al., 1995). In contrast, it other studies demonstrated that fish myelin indeed contains inhibitors similar to those of rat, inasmuch as fish and rat neuronal growth was inhibited when grown on fish optic nerves (Sivron et al., 1994). Interestingly, the inhibitory effect was observed only with untreated optic nerves. If they were injured 1-2 weeks prior to explantation they lost their inhibitory properties, suggesting a similar mechanism to rat sciatic nerves which also regenerate better after a conditioning lesion (Sivron et al., 1994; Saunders, 2005). Importantly, the studies which supported the absence of inhibitory molecules consistently used goldfish optic nerves that had been lesioned 2-3 weeks before usage (Wanner et al., 1995; Lang et al., 1995; Saunders, 2005). The loss of myelin-associated inhibitory properties after optic nerve injury was attributed to cytotoxicity of invading macrophages and removal of oligodendrocytes was suggested as a factor for successful regeneration in fish optic nerves (Cohen et al., 1990; Lang et al. , 1996; Saunders, 2005). However, these studies did not receive much consideration in the field since the hypothesis of fish lacking Nogo-like inhibitors became established over the years.

Until now, it was unclear if fish possess a Nogo-A-like inhibitor, but if not, why would they retain a Nogo receptor? The recent discovery of RTN4b, the fish counterpart for Nogo-A, answered this question but raised more critical ones: if fish possess Nogo-A and its corresponding receptor, why do they regenerate axons in contrast to mammals? Did the fish protein lose its inhibitory property or is it actually actively removed/inactivated during successful regeneration in fish (as proposed above)? To help address this issue, I analyzed the molecular inhibitory substrate properties of recombinant zebrafish RTN4b, outside of its natural environment and physiological, cellular context.

During the comparative sequence analysis of fish and mammalian Nogo-A, four putative integrin binding motifs within the inhibitory NSR/delta-20 region were identified and named "M1-4" (Shypitsyna et al., 2011) (more detailed description in 1.4 and 5.8). As expected, recombinant rat M1-4 blocked growth. The fact that amino acid mutation (D to A) inside the putative inhibitory motifs indeed completely abrogated the inhibitory properties of the NSR was, however a novel finding (Fig. 5.8.1.1, 5.8.1.2, 5.8.2). These data confirmed that the identified four conserved motifs are the functional elements required for Nogo-A-mediated inhibition and strengthened the notion that Nogo-A blocks axon regeneration via an integrin-associated signaling mechanism (Shypitsyna et al., 2011; Hu & Strittmatter, 2008; Huo et al., 2015). Strikingly, the corresponding fish RTN4b M1-4 recombinant peptide inhibited growth to the same extent as its mammalian homologue, when provided as a substrate *in vitro* (Figures 5.8.1.1, 5.8.1.2, 5.8.2). Thus, in single zebrafish RGCs or retinal explants, in rat PC12 cells and in primary mouse hippocampal neurons, the mammalian and zebrafish peptide comprising the four putative inhibitory NSR domains M1-4 led to reduced neurite length, less number of axons and diminished cell spreading, in contrast to the control and the mutated mammalian M1-4 D/A constructs. This finding is certainly unexpected and raises many controversial questions, since fish do regenerate successfully and it has been assumed then for decades that fish myelin does not inhibit axon growth *in vitro* (Bastmeyer et al., 1993; Wanner et al., 1995). In this regard, it is important to note that the results regarding fish RTN4b were obtained only *in vitro*, so far. Beside the fact that *in vitro* experiments never fully reflect physiological *in vivo* situations, one possible, and verifiable explanation for this observation could be that RTN4b (or its receptor) is not expressed at sufficient levels in fish myelin to block regeneration. Localization and expression of RTN4b during regeneration can now be addressed by immunohistochemical studies using the appropriate antibody K1121 specific for zebrafish RTN4b, which was described and characterized in this thesis and published in Welte et al., 2015 (5.7 and 6.10). In any case, it is known that the inhibitory properties of mammalian Nogo-A are dose-dependent, as was demonstrated in various assays like cell spreading, migration, sprouting and growth cone collapse (Wälchli et al., 2013; Oertle et al., 2003).

Nogo-A at the surface of neurons and glial cells represents a repulsive guidance molecule during axonal development and regeneration, whereas intracellular (ER-associated) Nogo-A is important for neuronal cell survival and outgrowth (Giger et al., 2010). These notions are supported by the data presented in this thesis, as well as by the impressive study from Vajda

et al. Here, cell-type specific, conditional Nogo-A gene ablation in mouse oligodendrocytes or RGCs led to either enhanced or reduced regeneration of the optic nerve, respectively (Vajda et al., 2015). In this respect, it should be ensured that reduced regeneration does not arise from increased cell-death of RGCs, particularly because Nogo-A was recently shown to promote neuronal cell survival by controlling the Rac1/RhoA balance (Kilic et al., 2010). Furthermore, the fact that Nogo-A regulates correct fasciculation and branching of growing neurons, might compromise the proper functionality of regenerated axons in absence of Nogo-A (Petrinovic et al., 2010). Nevertheless, antibody-mediated blockage of surface-expressed Nogo-A restored functional recovery, as demonstrated comprehensively in various studies and currently under clinical investigation by M. Schwab and his colleagues (Pernet & Schwab, 2012).

The underlying mechanisms of inhibited axonal regeneration caused by myelin-associated molecules (Nogo-A, MAG, OMgp) or invading reactive astrocytes (expressing inhibitory CSPGs) all converge at the level of RhoA/ROCK signaling and its downstream effectors, which regulate cytoskeletal reorganization during growth cone collapse and neurite outgrowth inhibition (Fujita & Yamashita, 2014). One important downstream signaling effector of ROCK is the actin depolymerizing factor ADF/cofilin, which becomes phosphorylated (inactivated) upon ROCK activation, leading to actin filament stabilization and arrested growth. Other downstream factors have also been identified, leading, for example, to inhibition of tubulin polymerization (Fujita & Yamashita, 2014; Hsieh et al., 2006). Since all of these inhibitory molecules merge at the RhoA pathway, not only Nogo-A neutralization but also blockage of RhoA/ROCK-mediated signaling was proposed as a therapeutic target to address degenerative CNS diseases (Kilic et al., 2010; Tan et al., 2011; Alabed et al., 2006). In this context, the opposite approach, i.e. the stabilization and strengthening of the microtubule and actin polymerization machinery by activation of RhoA, was investigated as well and represents a potential strategy enabling neurons to regenerate (Hellal et al., 2011; Baas & Ahmad, 2013).

In my doctoral thesis, I considered the challenging complexity of Nogo-A/RTN4`s opposing roles in the CNS. The data suggests that fish -just as mammalian- Nogo-A plays two discrete, cell context-dependent but conserved roles during axon regeneration: as an intrinsic, ER-associated supporter of neuronal growth but also as an extrinsic, inhibitory substrate.

7. Conclusions and outlook

PART I Thy-1 and PrP

In this doctoral thesis, two new key players of CNS axon growth and regeneration were characterized. The GPI-linked surface molecules Thy-1 and PrP, were found to be spontaneously upregulated in the zebrafish retina upon optic nerve lesion. Their loss-of function led to impaired growth and regeneration. It would be very interesting to study if the supportive function of these molecules is evolutionarily conserved and applies also for the mammalian counterparts *in vivo*. Whether the ability of fish to increase these growth-promoting molecules upon CNS injury is the key to their high regeneration potential is an exciting question that could be addressed with *in vivo* regeneration studies in mice, where overexpression could lead to enhanced recovery. Our data indicate that both PrP and Thy-1 most likely act via the activation SFKs and the modulation of cytoskeletal dynamics. Of note, the implication of both molecules in cellular events like cell-cell adhesion and endocytosis may also provide potential explanation for the reduced axon growth observed upon knockdown in fish and mammalian neurons. For instance, studies on cell-cell adhesion mechanisms have shown that clustering of cell-adhesion molecules, *trans*-interacting at opposing sites of cells, leadings to reorganization of the underlying cytoskeleton and are controlled by Rho GTPases. On the other hand, SFKs are known to regulate cell-adhesion complexes by controlling their phosphorylation and endocytosis (Nelson, 2008). To further investigate these signaling events and the associated cell morphological changes *in vivo*, the zebrafish embryo would be an ideal experimental model. Genetic and phenotypic analysis as well as quantitative biochemical assays can be conveniently assessed without the need for animal experiments in adult fish. As demonstrated here, the necessary tools to pursue these issues (like specific antibodies and translation-blocking oligos) are now available.

PART II RTN4b

Regarding RTN4b, the zebrafish homologue of the myelin-associated inhibitor Nogo-A, this thesis provides evidence that the protein serves two distinct roles in neurons, depending on its subcellular localization and context. On one hand we showed that neuron-intrinsic RTN4b becomes upregulated after optic nerve lesion, and that its morpholino-mediated knockdown leads to diminished axon growth. The precise mechanisms mediating this effect remain to be

characterized, although they most likely involve ER-associated events. Our data suggest that zebrafish upregulate cellular RTN4b certainly to maintain proper regeneration after CNS injury. On the other hand, the striking observation that zebrafish RTN4b inhibits neurite outgrowth in fish and mammalian neurons rises many new questions. Future research should explore where, how, and in which amounts RTN4b and its receptor(s) are expressed in the zebrafish optic system in order to explain why fish myelin was previously shown to be non-inhibitory to regenerating axons. Following the present finding, namely that the four conserved integrin-binding motifs (M1-4) within the rat Nogo-A specific region (NSR) are responsible for outgrowth inhibition in primary neurons and reduced spreading in PC12 cells, the next step would be to perform the same experiments using the zebrafish RTN4b M1-4 motifs. Furthermore, it would be interesting to determine whether the molecular events and downstream signaling molecules involved are the same in fish and mammals. Unfortunately, not many zebrafish-specific antibodies are available. Yet, the zebrafish holds a unique position in regeneration studies because it is able to recover injuries of the CNS to a high extent and it also provides the molecular tools (genome database, transgenic/knockout animals, morpholinos, etc.) that are necessary to perform functional assays. In future, the increasing set of research tools and the expanding community of zebrafish researchers will help to identify new mechanistic prerequisites of regeneration which may guide novel therapeutic strategies (Poss et al., 2003; Becker & Becker, 2008; Gemberling et al., 2013).

Overall, this study contributes to the ongoing efforts in the field of neuroscience to identify intra- and extracellular components contributing to successful axon growth and regeneration across vertebrates. It will be a great challenge for the future to manipulate the neuron-intrinsic abilities of injured CNS components in such a way that regeneration and functional recovery *in vivo* can be ensured. Someday, we might be able to use a balanced combination of strategies by enhancing intrinsic growth support and eliminating extrinsic inhibition.

8. References

Abdesselem, H., Shypitsyna, A., Solis, G. P., Bodrikov, V., & Stuermer, C. a O. (2009). No Nogo66- and NgR-mediated inhibition of regenerating axons in the zebrafish optic nerve. *The Journal of Neuroscience : The Official Journal of the Society for Neuroscience*, *29*(49), 15489–15498. doi:10.1523/JNEUROSCI.3561-09.2009

Abeysinghe, H. R., Cao, Q., Xu, J., Pollock, S., Veyberman, Y., Guckert, N. L., … Wang, N. (2003). THY1 expression is associated with tumor suppression of human ovarian cancer. *Cancer Genetics and Cytogenetics*, *143*, 125–132. doi:10.1016/S0165-4608(02)00855-5

Ades, E. W., Zwerner, R. K., Acton, R. T., & Balch, C. M. (1980). Isolation and partial characterization of the human homologue of Thy-1. *The Journal of Experimental Medicine*, *151*, 400–406.

Alabed, Y. Z., Grados-Munro, E., Ferraro, G. B., Hsieh, S. H. K., & Fournier, A. E. (2006). Neuronal responses to myelin are mediated by rho kinase. *Journal of Neurochemistry*, *96*, 1616–1625. doi:10.1111/j.1471-4159.2006.03670.x

Amaddii, M., Meister, M., Banning, A., Tomasovic, A., Mooz, J., Rajalingam, K., & Tikkanen, R. (2012). Flotillin-1/Reggie-2 protein plays dual role in activation of receptor-tyrosine kinase/mitogen-activated protein kinase signaling. *Journal of Biological Chemistry*, *287*, 7265–7278. doi:10.1074/jbc.M111.287599

Amores, A., Force, A., Yan, Y. L., Joly, L., Amemiya, C., Fritz, A., … Postlethwait, J. H. (1998). Zebrafish hox clusters and vertebrate genome evolution. *Science (New York, N.Y.)*, *282*, 1711–1714. doi:10.1126/science.282.5394.1711

Aricescu, A. R., & Jones, E. Y. (2007). Immunoglobulin superfamily cell adhesion molecules: zippers and signals. *Current Opinion in Cell Biology*. doi:10.1016/j.ceb.2007.09.010

Atwal, J. K., Pinkston-Gosse, J., Syken, J., Stawicki, S., Wu, Y., Shatz, C., & Tessier-Lavigne, M. (2008). PirB is a functional receptor for myelin inhibitors of axonal regeneration. *Science (New York, N.Y.)*, *322*, 967–970. doi:10.1126/science.1161151

Avalos, A. M., Valdivia, A. D., Muñoz, N., Herrera-Molina, R., Tapia, J. C., Lavandero, S., … Leyton, L. (2009). Neuronal Thy-1 induces astrocyte adhesion by engaging syndecan-4 in a cooperative interaction with alphavbeta3 integrin that activates PKCalpha and RhoA. *Journal of Cell Science*, *122*(Pt 19), 3462–3471. doi:10.1242/jcs.034827

Baas, P. W., & Ahmad, F. J. (2013). Beyond taxol: Microtubule-based treatment of disease and injury of the nervous system. *Brain*. doi:10.1093/brain/awt153

Baksh, M. M., Dean, C., Pautot, S., DeMaria, S., Isacoff, E., & Groves, J. T. (2005). Neuronal activation by GPI-linked neuroligin-1 displayed in synthetic lipid bilayer membranes. *Langmuir*, *21*(23), 10693–10698. doi:10.1021/la051243d

Ballerini, C., Gourdain, P., Bachy, V., Blanchard, N., Levavasseur, E., Grégoire, S., … Carnaud, C. (2006). Functional implication of cellular prion protein in antigen-driven interactions between T cells and dendritic cells. *Journal of Immunology (Baltimore, Md. : 1950)*, *176*, 7254–7262. doi:10.4049/jimmunol.176.12.7254

Banning, A., Tomasovic, A., & Tikkanen, R. (2011). Functional Aspects of Membrane Association of Reggie/Flotillin Proteins. *Current Protein and Peptide Science*. doi:10.2174/138920311798841708

Barabási, A.-L., & Oltvai, Z. N. (2004). Network biology: understanding the cell's functional organization. *Nature Reviews. Genetics*, *5*(2), 101–113. doi:10.1038/nrg1272

Barlow, J. Z., Kelley, K. A., Bozdagi, O., & Huntley, G. W. (2002). Testing the role of the cell-surface molecule Thy-1 in regeneration and plasticity of connectivity in the CNS. *Neuroscience*, *111*, 837–852. doi:10.1016/S0306-4522(02)00023-4

Barnstable, C. J., & Drager, U. C. (1984). Thy-1 antigen: A ganglion cell specific marker in rodent retina. *Neuroscience*, *11*, 847–855. doi:10.1016/0306-4522(84)90195-7

Bashaw, G. J., & Klein, R. (2010). Signaling from axon guidance receptors. *Cold Spring Harbor Perspectives in Biology*, *2*(5), a001941.

Bastmeyer, M., Bähr, M., & Stuermer, C. a. (1993). Fish optic nerve oligodendrocytes support axonal regeneration of fish and mammalian retinal ganglion cells. *Glia*, *8*(1), 1–11.

Bastmeyer, M., Beckmann, M., Schwab, M. E., & Stuermer, C. A. (1991). Growth of regenerating goldfish axons is inhibited by rat oligodendrocytes and CNS myelin but not but not by goldfish optic nerve tract oligodendrocytelike cells and fish CNS myelin. *The Journal of Neuroscience : The Official Journal of the Society for Neuroscience*, *11*, 626–640.

Bastmeyer, M., Schwab, E., & Stuermerl, A. (1991). Growth of Regenerating Goldfish Axons Is Inhibited by Rat Oligodendrocytes and CNS Myelin but Not by Goldfish Optic Nerve Tract Oligodendrocytelike Cells and Fish CNS Myelin, (March).

Baumann, C. A., Ribon, V., Kanzaki, M., Thurmond, D. C., Mora, S., Shigematsu, S., … Saltiel, A. R. (2000). CAP defines a second signalling pathway required for insulin-stimulated glucose transport. *Nature*, *407*, 202–207. doi:10.1038/35025089

Becker, C. G., & Becker, T. (2007). Zebrafish as a Model System for Successful Spinal Cord Regeneration. In *Model Organisms in Spinal Cord Regeneration* (pp. 289–319). doi:10.1002/9783527610365.ch10

Becker, C. G., & Becker, T. (2008). Adult zebrafish as a model for successful central nervous system regeneration. *Restorative Neurology and Neuroscience*, *26*, 71–80.

Becker, C. G., Lieberoth, B. C., Morellini, F., Feldner, J., Becker, T., & Schachner, M. (2004). L1.1 is involved in spinal cord regeneration in adult zebrafish. *The Journal of*

Neuroscience : The Official Journal of the Society for Neuroscience, *24*, 7837–7842. doi:10.1523/JNEUROSCI.2420-04.2004

Becker, T., Wullimann, M. F., Becker, C. G., Bernhardt, R. R., & Schachner, M. (1997). Axonal regrowth after spinal cord transection in adult zebrafish. *Journal of Comparative Neurology*, *377*, 577–595. doi:10.1002/(SICI)1096-9861(19970127)377:4<577::AID-CNE8>3.0.CO;2-#

Beech, J. N., Morris, R. J., & Raisman, G. (1983). Density of Thy-1 on axonal membrane of different rat nerves. *Journal of Neurochemistry*, *41*, 411–417.

Behrens, A., Genoud, N., Naumann, H., Rülicke, T., Janett, F., Heppner, F. L., … Aguzzi, A. (2002). Absence of the prion protein homologue Doppel causes male sterility. *EMBO Journal*, *21*, 3652–3658. doi:10.1093/emboj/cdf386

Bodrikov, V., Leshchyns'ka, I., Sytnyk, V., Overvoorde, J., den Hertog, J., & Schachner, M. (2005). RPTPalpha is essential for NCAM-mediated p59fyn activation and neurite elongation. *The Journal of Cell Biology*, *168*, 127–139. doi:10.1083/jcb.200405073

Bodrikov, V., Leshchyns'ka, I., Sytnyk, V., Overvoorde, J., Den Hertog, J., & Schachner, M. (2005). RPTPα is essential for NCAM-mediated p59 fyn activation and neurite elongation. *Journal of Cell Biology*, *168*, 127–139. doi:10.1083/jcb.200405073

Bodrikov, V., Solis, G. P., & Stuermer, C. A. O. (2011). Prion Protein Promotes Growth Cone Development through Reggie/Flotillin-Dependent N-Cadherin Trafficking. *Journal of Neuroscience*. doi:10.1523/JNEUROSCI.4729-11.2011

Bodrikov, V., Sytnyk, V., Leshchyns'ka, I., den Hertog, J., & Schachner, M. (2008). NCAM induces CaMKIIalpha-mediated RPTPalpha phosphorylation to enhance its catalytic activity and neurite outgrowth. *The Journal of Cell Biology*, *182*, 1185–1200. doi:10.1083/jcb.200803045

Bolin, L. M., & Rouse, R. V. (1986). Localization of Thy-1 expression during postnatal development of the mouse cerebellar cortex. *Journal of Neurocytology*, *15*, 29–36.

Bolton, D. C., McKinley, M. P., & Prusiner, S. B. (1982). Identification of a protein that purifies with the scrapie prion. *Science (New York, N.Y.)*, *218*, 1309–1311. doi:10.1126/science.6815801

Bordeaux, J., Welsh, A. W., Agarwal, S., Killiam, E., Baquero, M. T., Hanna, J. a., … Rimm, D. L. (2010). Antibody validation. *BioTechniques*, *48*(3), 197–209. doi:10.2144/000113382

Bros-Facer, V., Krull, D., Taylor, A., Dick, J. R. T., Bates, S. A., Cleveland, M. S., … Greensmith, L. (2014). Treatment with an antibody directed against nogo-a delays disease progression in the SOD1G93A mouse model of Amyotrophic lateral sclerosis. *Human Molecular Genetics*, *23*, 4187–4200. doi:10.1093/hmg/ddu136

Brügger, B., Graham, C., Leibrecht, I., Mombelli, E., Jen, A., Wieland, F., & Morris, R. (2004). The Membrane Domains Occupied by Glycosylphosphatidylinositol-anchored Prion

Protein and Thy-1 Differ in Lipid Composition. *Journal of Biological Chemistry*, *279*, 7530–7536. doi:10.1074/jbc.M310207200

Büeler, H., Aguzzi, A., Sailer, A., Greiner, R. A., Autenried, P., Aguet, M., & Weissmann, C. (1993). Mice devoid of PrP are resistant to scrapie. *Cell*, *73*, 1339–1347. doi:10.1016/0092-8674(93)90360-3

Büeler, H., Fischer, M., Lang, Y., Bluethmann, H., Lipp, H. P., DeArmond, S. J., … Weissmann, C. (1992). Normal development and behaviour of mice lacking the neuronal cell-surface PrP protein. *Nature*, *356*, 577–582. doi:10.1038/356577a0

Buss, A., Sellhaus, B., Wolmsley, A., Noth, J., Schwab, M. E., & Brook, G. A. (2005). Expression pattern of NOGO-A protein in the human nervous system. *Acta Neuropathologica*, *110*, 113–119. doi:10.1007/s00401-004-0942-z

Bustin, S. A. (2002). Quantification of mRNA using real-time reverse transcription PCR (RT-PCR): trends and problems. *Journal of Molecular Endocrinology*, *29*, 23–39. doi:10.1677/jme.0.0290023

Bustin, S. A., Benes, V., Nolan, T., & Pfaffl, M. W. (2005). Quantitative real-time RT-PCR--a perspective. *Journal of Molecular Endocrinology*, *34*, 597–601. doi:10.1677/jme.1.01755

Cajal, S. R. y. (1928). Degeneration and regeneration of the nervous system. *New York: Oxford University Press, American Branch*, *2*, 396–769.

Caroni, P., & Schwab, M. E. (1988). Two membrane protein fractions from rat central myelin with inhibitory properties for neurite growth and fibroblast spreading. *The Journal of Cell Biology*, *106*, 1281–1288.

Caughey, B. (1993). Scrapie associated PrP accumulation and its prevention: insights from cell culture. *British Medical Bulletin*, *49*, 860–872.

Cheatwood, J. L., Emerick, A. J., Schwab, M. E., & Kartje, G. L. (2008). Nogo-A expression after focal ischemic stroke in the adult rat. *Stroke*, *39*, 2091–2098. doi:10.1161/STROKEAHA.107.507426

Chen, C. H., Chen, Y. J., Jeng, C. J., Yang, S. H., Tung, P. Y., & Wang, S. M. (2007). Role of PKA in the anti-Thy-1 antibody-induced neurite outgrowth of dorsal root ganglionic neurons. *Journal of Cellular Biochemistry*, *101*, 566–575. doi:10.1002/jcb.21217

Chen, S., Mangé, A., Dong, L., Lehmann, S., & Schachner, M. (2003). Prion protein as trans-interacting partner for neurons is involved in neurite outgrowth and neuronal survival. *Molecular and Cellular Neuroscience*, *22*, 227–233. doi:10.1016/S1044-7431(02)00014-3

Chen, Y., Thelin, W. R., Yang, B., Milgram, S. L., & Jacobson, K. (2006). Transient anchorage of cross-linked glycosylphosphatidylinositol-anchored proteins depends on cholesterol, Src family kinases, caveolin, and phosphoinositides. *Journal of Cell Biology*, *175*, 169–178. doi:10.1083/jcb.200512116

Chen, Y., Veracini, L., Benistant, C., & Jacobson, K. (2009). The transmembrane protein CBP plays a role in transiently anchoring small clusters of Thy-1, a GPI-anchored protein, to the cytoskeleton. *Journal of Cell Science*, *122*, 3966–3972. doi:10.1242/jcs.049346

Chesebro, B., Trifilo, M., Race, R., Meade-White, K., Teng, C., LaCasse, R., … Oldstone, M. (2005). Anchorless prion protein results in infectious amyloid disease without clinical scrapie. *Science (New York, N.Y.)*, *308*, 1435–1439. doi:10.1126/science.1110837

Chiarini, L. B., Freitas, A. R. O., Zanata, S. M., Brentani, R. R., Martins, V. R., & Linden, R. (2002). Cellular prion protein transduces neuroprotective signals. *EMBO Journal*, *21*(13), 3317–3326. doi:10.1093/emboj/cdf324

Cohen, A., Sivron, T., Duvdevani, R., & Schwartz, M. (1990). Oligodendrocyte cytotoxic factor associated with fish optic nerve regeneration: implications for mammalian CNS regeneration. *Brain Research*, *537*(1-2), 24–32. doi:10.1016/0006-8993(90)90335-9

Coitinho, A. S., Freitas, A. R. O., Lopes, M. H., Hajj, G. N. M., Roesler, R., Walz, R., … Brentani, R. R. (2006). The interaction between prion protein and laminin modulates memory consolidation. *European Journal of Neuroscience*, *24*, 3255–3264. doi:10.1111/j.1460-9568.2006.05156.x

Coitinho, A. S., Lopes, M. H., Hajj, G. N. M., Rossato, J. I., Freitas, A. R., Castro, C. C., … Martins, V. R. (2007). Short-term memory formation and long-term memory consolidation are enhanced by cellular prion association to stress-inducible protein 1. *Neurobiology of Disease*, *26*, 282–290. doi:10.1016/j.nbd.2007.01.005

Cotto, E., André, M., Forgue, J., Fleury, H. J., & Babin, P. J. (2005). Molecular characterization, phylogenetic relationships, and developmental expression patterns of prion genes in zebrafish (Danio rerio). *The FEBS Journal*, *272*, 500–513. doi:10.1111/j.1742-4658.2004.04492.x

Criado, J. R., Sánchez-Alavez, M., Conti, B., Giacchino, J. L., Wills, D. N., Henriksen, S. J., … Oldstone, M. B. A. (2005). Mice devoid of prion protein have cognitive deficits that are rescued by reconstitution of PrP in neurons. *Neurobiology of Disease*, *19*, 255–265. doi:10.1016/j.nbd.2005.01.001

Cumming, D. A. (1992). Physiological relevance of protein glycosylation. *Developments in Biological Standardization*, *76*, 83–94.

David, S., & Aguayo, A. J. (1981). Axonal elongation into peripheral nervous system “bridges” after central nervous system injury in adult rats. *Science (New York, N.Y.)*, *214*, 931–933. doi:10.1126/science.6171034

Deininger, S. O., Rajendran, L., Lottspeich, F., Przybylski, M., Illges, H., Stuermer, C. A. O., & Reuter, A. (2003). Identification of teleost Thy-1 and association with the microdomain/lipid raft reggie proteins in regenerating CNS axons. *Molecular and Cellular Neuroscience*, *22*, 544–554. doi:10.1016/S1044-7431(03)00028-9

Devanathan, V., Jakovcevski, I., Santuccione, A., Li, S., Lee, H. J., Peles, E., … Schachner, M. (2010). Cellular form of prion protein inhibits Reelin-mediated shedding of Caspr from the neuronal cell surface to potentiate Caspr-mediated inhibition of neurite outgrowth. *The Journal of Neuroscience : The Official Journal of the Society for Neuroscience*, *30*, 9292–9305. doi:10.1523/JNEUROSCI.5657-09.2010

Diekmann, H., Klinger, M., Oertle, T., Heinz, D., Pogoda, H. M., Schwab, M. E., & Stuermer, C. A. O. (2005). Analysis of the reticulon gene family demonstrates the absence of the neurite growth inhibitor Nogo-A in fish. *Molecular Biology and Evolution*, *22*, 1635–1648. doi:10.1093/molbev/msi158

Dimou, L., Schnell, L., Montani, L., Duncan, C., Simonen, M., Schneider, R., … Schwab, M. E. (2006). Nogo-A-deficient mice reveal strain-dependent differences in axonal regeneration. *The Journal of Neuroscience : The Official Journal of the Society for Neuroscience*, *26*, 5591–5603. doi:10.1523/JNEUROSCI.1103-06.2006

Dodd, D. A., Niederoest, B., Bloechlinger, S., Dupuis, L., Loeffler, J. P., & Schwab, M. E. (2005). Nogo-A, -B, and -C are found on the cell surface and interact together in many different cell types. *Journal of Biological Chemistry*, *280*, 12494–12502. doi:10.1074/jbc.M411827200

Doherty, P., Singh, A., Rimon, G., Bolsover, S. R., & Walsh, F. S. (1993). Thy-1 antibody-triggered neurite outgrowth requires an influx of calcium into neurons via N- and L-type calcium channels. *Journal of Cell Biology*, *122*, 181–189. doi:10.1083/jcb.122.1.181

Donne, D. G., Viles, J. H., Groth, D., Mehlhorn, I., James, T. L., Cohen, F. E., … Dyson, H. J. (1997). Structure of the recombinant full-length hamster prion protein PrP(29-231): the N terminus is highly flexible. *Proceedings of the National Academy of Sciences of the United States of America*, *94*, 13452–13457. doi:10.1073/pnas.94.25.13452

Durbeej, M. (2010). Laminins. *Cell and Tissue Research*. doi:10.1007/s00441-009-0838-2

Eisenberg, S., Shvartsman, D. E., Ehrlich, M., & Henis, Y. I. (2006). Clustering of raft-associated proteins in the external membrane leaflet modulates internal leaflet H-ras diffusion and signaling. *Molecular and Cellular Biology*, *26*, 7190–7200. doi:10.1128/MCB.01059-06

Endo, M., Ohashi, K., Sasaki, Y., Goshima, Y., Niwa, R., Uemura, T., & Mizuno, K. (2003). Control of growth cone motility and morphology by LIM kinase and Slingshot via phosphorylation and dephosphorylation of cofilin. *The Journal of Neuroscience : The Official Journal of the Society for Neuroscience*, *23*, 2527–2537. doi:23/7/2527 [pii]

Ertmer, A., Gilch, S., Yun, S. W., Flechsig, E., Klebl, B., Stein-Gerlach, M., … Schätzl, H. M. (2004). The tyrosine kinase inhibitor STI571 induces cellular clearance of PrP Sc in prion-infected cells. *Journal of Biological Chemistry*, *279*, 41918–41927. doi:10.1074/jbc.M405652200

Ford, M. J., Burton, L. J., Morris, R. J., & Hall, S. M. (2002). Selective expression of prion protein in peripheral tissues of the adult mouse. *Neuroscience*, *113*, 177–192. doi:10.1016/S0306-4522(02)00155-0

Fournier, A. E., GrandPre, T., & Strittmatter, S. M. (2001). Identification of a receptor mediating Nogo-66 inhibition of axonal regeneration. *Nature*, *409*, 341–346. doi:10.1038/35053072

Fournier, A. E., Takizawa, B. T., & Strittmatter, S. M. (2003). Rho kinase inhibition enhances axonal regeneration in the injured CNS. *The Journal of Neuroscience : The Official Journal of the Society for Neuroscience*, *23*, 1416–1423. doi:23/4/1416 [pii]

Freund, P., Schmidlin, E., Wannier, T., Bloch, J., Mir, A., Schwab, M. E., & Rouiller, E. M. (2006). Nogo-A-specific antibody treatment enhances sprouting and functional recovery after cervical lesion in adult primates. *Nature Medicine*, *12*, 790–792. doi:10.1038/nm1436

Freund, P., Schmidlin, E., Wannier, T., Bloch, J., Mir, A., Schwab, M. E., & Rouiller, E. M. (2009). Anti-Nogo-A antibody treatment promotes recovery of manual dexterity after unilateral cervical lesion in adult primates - Re-examination and extension of behavioral data. *European Journal of Neuroscience*, *29*, 983–996. doi:10.1111/j.1460-9568.2009.06642.x

Frigg, R., Wenzel, A., Samardzija, M., Oesch, B., Wariwoda, H., Navarini, A. A., … Grimm, C. (2006). The prion protein is neuroprotective against retinal degeneration in vivo. *Experimental Eye Research*, *83*, 1350–1358. doi:10.1016/j.exer.2006.07.010

Fuhrmann, M., Bittner, T., Mitteregger, G., Haider, N., Moosmang, S., Kretzschmar, H., & Herms, J. (2006). Loss of the cellular prion protein affects the Ca2+ homeostasis in hippocampal CA1 neurons. *Journal of Neurochemistry*, *98*, 1876–1885. doi:10.1111/j.1471-4159.2006.04011.x

Fujita, N., Kato, Y., Naito, M., & Tsuruo, T. (1996). A novel anti-Thy-1 (CD90) monoclonal antibody induces apoptosis in mouse malignant T-lymphoma cells in spite of inducing bcl-2 expression. *International Journal of Cancer*, *66*, 544–550. doi:10.1002/(SICI)1097-0215(19960516)66:4<544::AID-IJC20>3.0.CO;2-6

Gemberling, M., Bailey, T. J., Hyde, D. R., & Poss, K. D. (2013). The zebrafish as a model for complex tissue regeneration. *Trends in Genetics : TIG*, *29*, 611–20. doi:10.1016/j.tig.2013.07.003

Giger, R. J., Hollis, E. R., & Tuszynski, M. H. (2010). Guidance molecules in axon regeneration. *Cold Spring Harbor Perspectives in Biology*, *2*(7), a001867.

Giguére, V., Isobe, K., & Grosveld, F. (1985). Structure of the murine Thy-1 gene. *The EMBO Journal*, *4*, 2017–2024.

Gil, O. D., Zanazzi, G., Struyk, A. F., & Salzer, J. L. (1998). Neurotrimin mediates bifunctional effects on neurite outgrowth via homophilic and heterophilic interactions. *The Journal of Neuroscience : The Official Journal of the Society for Neuroscience*, *18*, 9312–9325.

Glasauer, S. M. K., & Neuhauss, S. C. F. (2014). Whole-genome duplication in teleost fishes and its evolutionary consequences. *Molecular Genetics and Genomics*. doi:10.1007/s00438-014-0889-2

Goldshmit, Y., Sztal, T. E., Jusuf, P. R., Hall, T. E., Nguyen-Chi, M., & Currie, P. D. (2012). Fgf-Dependent Glial Cell Bridges Facilitate Spinal Cord Regeneration in Zebrafish. *Journal of Neuroscience*. doi:10.1523/JNEUROSCI.0758-12.2012

Gong, J., Jellali, A., Forster, V., Mutterer, J., Dubus, E., Altrock, W. D., … Picaud, S. (2007). The toxicity of the PrP106-126 prion peptide on cultured photoreceptors correlates with the prion protein distribution in the mammalian and human retina. *The American Journal of Pathology*, *170*(4), 1314–24. doi:10.2353/ajpath.2007.060340

Gordon-Weeks, P. R., & Fournier, A. E. (2014). Neuronal cytoskeleton in synaptic plasticity and regeneration. *Journal of Neurochemistry*, *129*(2), 206–12. doi:10.1111/jnc.12502

Goyal, U., & Blackstone, C. (2013). Untangling the web: Mechanisms underlying ER network formation. *Biochimica et Biophysica Acta - Molecular Cell Research*, *1833*, 2492–2498. doi:10.1016/j.bbamcr.2013.04.009

GrandPré, T., Nakamura, F., Vartanian, T., & Strittmatter, S. M. (2000). Identification of the Nogo inhibitor of axon regeneration as a Reticulon protein. *Nature*, *403*, 439–444. doi:10.1038/35000226

Graner, E., Mercadante, A. F., Zanata, S. M., Forlenza, O. V., Cabral, A. L. B., Veiga, S. S., … Brentani, R. R. (2000). Cellular prion protein binds laminin and mediates neuritogenesis. *Molecular Brain Research*, *76*, 85–92. doi:10.1016/S0169-328X(99)00334-4

Greenbaum, D., Colangelo, C., Williams, K., & Gerstein, M. (2003). Comparing protein abundance and mRNA expression levels on a genomic scale. *Genome Biology*, *4*, 117. doi:10.1186/gb-2003-4-9-117

Griffiths, R. E., Heesom, K. J., & Anstee, D. J. (2007). Normal prion protein trafficking in cultured human erythroblasts. *Blood*, *110*, 4518–4525. doi:10.1182/blood-2007-04-085183

Gupta, A., & Pulliam, L. (2014). Exosomes as mediators of neuroinflammation. *Journal of Neuroinflammation*, *11*, 68. doi:10.1186/1742-2094-11-68

Haeberlé, A. M., Ribaut-Barassin, C., Bombarde, G., Mariani, J., Hunsmann, G., Grassi, J., & Bailly, Y. (2000). Synaptic prion protein immuno-reactivity in the rodent cerebellum. *Microscopy Research and Technique*, *50*, 66–75. doi:10.1002/1097-0029(20000701)50:1<66::AID-JEMT10>3.0.CO;2-3

Haeryfar, S. M. M., & Hoskin, D. W. (2004). Thy-1: more than a mouse pan-T cell marker. *Journal of Immunology (Baltimore, Md. : 1950)*, *173*(6), 3581–3588.

Hagood, J. S., Prabhakaran, P., Kumbla, P., Salazar, L., MacEwen, M. W., Barker, T. H., … Selman, M. (2005). Loss of fibroblast Thy-1 expression correlates with lung fibrogenesis. *The American Journal of Pathology*, *167*, 365–379. doi:10.1016/S0002-9440(10)62982-3

Hajj, G. N. M., Lopes, M. H., Mercadante, A. F., Veiga, S. S., da Silveira, R. B., Santos, T. G., … Martins, V. R. (2007). Cellular prion protein interaction with vitronectin supports axonal growth and is compensated by integrins. *Journal of Cell Science*, *120*, 1915–1926. doi:10.1242/jcs.03459

Haraguchi, T., Fisher, S., Olofsson, S., Endo, T., Groth, D., Tarentino, A., … Burlingame, A. (1989). Asparagine-linked glycosylation of the scrapie and cellular prion proteins. *Archives of Biochemistry and Biophysics*, *274*, 1–13. doi:10.1016/0003-9861(89)90409-8

Harris, D. A. (2003). Trafficking, turnover and membrane topology of PrP. *British Medical Bulletin*. doi:10.1093/bmb/66.1.71

Harris, D. A., Huber, M. T., van Dijken, P., Shyng, S. L., Chait, B. T., & Wang, R. (1993). Processing of a cellular prion protein: identification of N- and C-terminal cleavage sites. *Biochemistry*, *32*, 1009–1016.

Harrison, P. M., Khachane, A., & Kumar, M. (2010). Genomic assessment of the evolution of the prion protein gene family in vertebrates. *Genomics*, *95*, 268–277. doi:10.1016/j.ygeno.2010.02.008

Head, B. P., Patel, H. H., & Insel, P. a. (2014). Interaction of membrane/lipid rafts with the cytoskeleton: Impact on signaling and function: Membrane/lipid rafts, mediators of cytoskeletal arrangement and cell signaling. *Biochimica et Biophysica Acta - Biomembranes*, *1838*(2), 532–545. doi:10.1016/j.bbamem.2013.07.018

Head, M. W., Northcott, V., Rennison, K., Ritchie, D., McCardle, L., Bunn, T. J. R., … Bonshek, R. E. (2003). Prion protein accumulation in eyes of patients with sporadic and variant Creutzfeldt-Jakob disease. *Investigative Ophthalmology & Visual Science*, *44*(1), 342–346. doi:10.1167/iovs.01-1273

Hellal, F., Hurtado, A., Ruschel, J., Flynn, K. C., Laskowski, C. J., Umlauf, M., … Bradke, F. (2011). Microtubule stabilization reduces scarring and causes axon regeneration after spinal cord injury. *Science (New York, N.Y.)*, *331*, 928–931. doi:10.1126/science.1201148

Hermosilla, T., Muñoz, D., Herrera-molina, R., Valdivia, A., Nham, S., Schneider, P., … Leyton, L. (2009). Direct Thy-1/alphaVbeta3 integrin interaction mediates neuron to astrocyte communication, *1783*(6), 1111–1120. doi:10.1016/j.bbamcr.2008.01.034.DIRECT

Herms, J., Tings, T., Gall, S., Madlung, A., Giese, A., Siebert, H., … Kretzschmar, H. (1999). Evidence of presynaptic location and function of the prion protein. *The Journal of Neuroscience : The Official Journal of the Society for Neuroscience*, *19*, 8866–8875.

Herrera-Molina, R., Frischknecht, R., Maldonado, H., Seidenbecher, C. I., Gundelfinger, E. D., Hetz, C., … Leyton, L. (2012a). Astrocytic ?? v?? 3 integrin inhibits neurite outgrowth and promotes retraction of neuronal processes by clustering thy-1. *PLoS ONE*, *7*(3), e34295. doi:10.1371/journal.pone.0034295

Herrera-Molina, R., Frischknecht, R., Maldonado, H., Seidenbecher, C. I., Gundelfinger, E. D., Hetz, C., … Leyton, L. (2012b). Astrocytic α vβ 3 integrin inhibits neurite outgrowth and promotes retraction of neuronal processes by clustering thy-1. *PLoS ONE*, *7*. doi:10.1371/journal.pone.0034295

Herrera-Molina, R., Valdivia, A., Kong, M., Alvarez, A., Cárdenas, A., Quest, A. F. G., & Leyton, L. (2013). *Thy-1-interacting molecules and cellular signaling in cis and trans. International review of cell and molecular biology* (Vol. 305, pp. 163–216). doi:10.1016/B978-0-12-407695-2.00004-4

Hirsch, S., Cahill, M. A., & Stuermer, C. A. O. (1995). Fibroblasts at the transection site of the injured goldfish optic nerve and their potential role during retinal axonal regeneration. *Journal of Comparative Neurology*, *360*, 599–611. doi:10.1002/cne.903600405

Horiuchi, M., Yamazaki, N., Ikeda, T., Ishiguro, N., & Shinagawa, M. (1995). A cellular form of prion protein (PrP(C)) exists in many non-neuronal tissues of sheep. *Journal of General Virology*, *76*, 2583–2587. doi:10.1099/0022-1317-76-10-2583

Houle, J. D., & Côté, M. P. (2013). Axon regeneration and exercise-dependent plasticity after spinal cord injury. *Annals of the New York Academy of Sciences*, *1279*(1), 154–163. doi:10.1111/nyas.12052

Hsieh, S. H.-K., Ferraro, G. B., & Fournier, A. E. (2006). Myelin-associated inhibitors regulate cofilin phosphorylation and neuronal inhibition through LIM kinase and Slingshot phosphatase. *The Journal of Neuroscience : The Official Journal of the Society for Neuroscience*, *26*, 1006–1015. doi:10.1523/JNEUROSCI.2806-05.2006

Hu, F., & Strittmatter, S. M. (2008). The N-terminal domain of Nogo-A inhibits cell adhesion and axonal outgrowth by an integrin-specific mechanism. *The Journal of Neuroscience : The Official Journal of the Society for Neuroscience*, *28*, 1262–1269. doi:10.1523/JNEUROSCI.1068-07.2008

Huber, A. B., Weinmann, O., Brösamle, C., Oertle, T., & Schwab, M. E. (2002). Patterns of Nogo mRNA and protein expression in the developing and adult rat and after CNS lesions. *The Journal of Neuroscience : The Official Journal of the Society for Neuroscience*, *22*, 3553–67. doi:20026323

Hueber, A. O., Bernard, A. M., Battari, C. L., Marguet, D., Massol, P., Foa, C., … He, H. T. (1997). Thymocytes in Thy-1-/- mice show augmented TCR signaling and impaired differentiation. *Current Biology : CB*, *7*, 705–708. doi:10.1016/S0960-9822(06)00300-9

Hui, S. P., Dutta, A., & Ghosh, S. (2010). Cellular response after crush injury in adult zebrafish spinal cord. *Developmental Dynamics : An Official Publication of the American Association of Anatomists*, *239*, 2962–2979. doi:10.1002/dvdy.22438

Hunt, D., Coffin, R. S., Prinjha, R. K., Campbell, G., & Anderson, P. N. (2003). Nogo-A expression in the intact and injured nervous system. *Molecular and Cellular Neuroscience*, *24*, 1083–1102. doi:10.1016/j.mcn.2003.09.002

Imran, M., & Mahmood, S. (2011). An overview of human prion diseases. *Virology Journal*, *8*(1), 559. doi:10.1186/1743-422X-8-559

Ivins, J. K., Yurchenco, P. D., & Lander, A. D. (2000). Regulation of neurite outgrowth by integrin activation. *The Journal of Neuroscience : The Official Journal of the Society for Neuroscience*, *20*(17), 6551–60. doi:20/17/6551 [pii]

Jeng, C. J., McCarroll, S. A., Martin, T. F. J., Floor, E., Adams, J., Krantz, D., … Schweitzer, E. S. (1998). Thy-1 is a component common to multiple populations of synaptic vesicles. *Journal of Cell Biology*, *140*, 685–698. doi:10.1083/jcb.140.3.685

Jozsef, L., Tashiro, K., Kuo, A., Park, E., Skoura, A., Albinsson, S., … Sessa, W. C. (2014). Reticulon 4 is necessary for endoplasmic reticulum tubulation, STIM1-Orai1 coupling, and store-operated calcium entry. *Journal of Biological Chemistry*, *289*(13), 9380–9395. doi:10.1074/jbc.M114.548602

Joset, A., Dodd, D. A., Halegoua, S., & Schwab, M. E. (2010). Pincher-generated Nogo-A endosomes mediate growth cone collapse and retrograde signaling. *Journal of Cell Biology*, *188*, 271–285. doi:10.1083/jcb.200906089

Kanaani, J., Prusiner, S. B., Diacovo, J., Baekkeskov, S., & Legname, G. (2005). Recombinant prion protein induces rapid polarization and development of synapses in embryonic rat hippocampal neurons in vitro. *Journal of Neurochemistry*, *95*, 1373–1386. doi:10.1111/j.1471-4159.2005.03469.x

Kardos, J., Kovács, I., Hajós, F., Kálmán, M., & Simonyi, M. (1989). Nerve endings from rat brain tissue release copper upon depolarization. A possible role in regulating neuronal excitability. *Neuroscience Letters*, *103*, 139–144. doi:10.1016/0304-3940(89)90565-X

Karnezis, T., Mandemakers, W., McQualter, J. L., Zheng, B., Ho, P. P., Jordan, K. A., … Bernard, C. C. A. (2004). The neurite outgrowth inhibitor Nogo A is involved in autoimmune-mediated demyelination. *Nature Neuroscience*, *7*, 736–744. doi:10.1038/nn1261

Kempf, A., Montani, L., Petrinovic, M. M., Schroeter, A., Weinmann, O., Patrignani, A., & Schwab, M. E. (2013). Upregulation of axon guidance molecules in the adult central nervous system of Nogo-A knockout mice restricts neuronal growth and regeneration. *European Journal of Neuroscience*, *38*, 3567–3579. doi:10.1111/ejn.12357

Kempf, A., & Schwab, M. E. (2013). Nogo-A represses anatomical and synaptic plasticity in the central nervous system. *Physiology (Bethesda, Md.)*, *28*(3), 151–63. doi:10.1152/physiol.00052.2012

Kempf, A., Tews, B., Arzt, M. E., Weinmann, O., Obermair, F. J., Pernet, V., … Schwab, M. E. (2014). The Sphingolipid Receptor S1PR2 Is a Receptor for Nogo-A Repressing Synaptic Plasticity. *PLoS Biology*, *12*. doi:10.1371/journal.pbio.1001763

Kemshead, J., Ritter, M., Cotmore, S., & Greaves, M. (1982). Human Thy-1: expression on the cell surface of neuronal and glial cells. *Brain Res*, *236*, 451–61.

Kilic, E., ElAli, A., Kilic, U., Guo, Z., Ugur, M., Uslu, U., … Hermann, D. M. (2010). Role of Nogo-A in neuronal survival in the reperfused ischemic brain. *Journal of Cerebral Blood Flow and Metabolism : Official Journal of the International Society of Cerebral Blood Flow and Metabolism*, *30*, 969–984. doi:10.1038/jcbfm.2009.268

Kim, J. E., Li, S., GrandPré, T., Qiu, D., & Strittmatter, S. M. (2003). Axon regeneration in young adult mice lacking Nogo-A/B. *Neuron*, *38*, 187–199. doi:10.1016/S0896-6273(03)00147-8

Kimura, A., Baumann, C. A., Chiang, S. H., & Saltiel, A. R. (2001). The sorbin homology domain: a motif for the targeting of proteins to lipid rafts. *Proceedings of the National Academy of Sciences of the United States of America*, *98*, 9098–9103. doi:10.1073/pnas.151252898

Klopfenstein, D. R., Klumperman, J., Lustig, A., Kammerer, R. A., Oorschot, V., & Hauri, H. P. (2001). Subdomain-specific localization of CLIMP-63 (p63) in the endoplasmic reticulum is mediated by its luminal ??-helical segment. *Journal of Cell Biology*, *153*, 1287–1299. doi:10.1083/jcb.153.6.1287

Koch, J. C., Solis, G. P., Bodrikov, V., Michel, U., Haralampieva, D., Shypitsyna, A., … Stuermer, C. A. O. (2013). Upregulation of reggie-1/flotillin-2 promotes axon regeneration in the rat optic nerve in vivo and neurite growth in vitro. *Neurobiology of Disease*, *51*, 168–176. doi:10.1016/j.nbd.2012.11.007

Kuroiwa, K., Torikai, Y., Osawa, M., Nakashima, T., Nakashima, M., Endo, H., & Arai, T. (2012). Epitope Determination of Anti Rat Thy-1 Monoclonal Antibody That Regulates Neurite Outgrowth. *Hybridoma*. doi:10.1089/hyb.2012.0002

Kurowska, Z., Brundin, P., Schwab, M. E., & Li, J. Y. (2014). Intracellular Nogo-A facilitates initiation of neurite formation in mouse midbrain neurons in vitro. *Neuroscience*, *256*, 456–466. doi:10.1016/j.neuroscience.2013.10.029

Kusumi, A., Koyama-Honda, I., & Suzuki, K. (2004). Molecular dynamics and interactions for creation of stimulation-induced stabilized rafts from small unstable steady-state rafts. *Traffic*. doi:10.1111/j.1600-0854.2004.0178.x

Laemmli, U. K. (1970). Cleavage of structural proteins during the assembly of the head of bacteriophage T4. *Nature*, *227*, 680–685. doi:10.1038/227680a0

Lan, C.-C., Tang, R., Un San Leong, I., & Love, D. R. (2009). Quantitative real-time RT-PCR (qRT-PCR) of zebrafish transcripts: optimization of RNA extraction, quality control

considerations, and data analysis. *Cold Spring Harbor Protocols*, *2009*, pdb.prot5314. doi:10.1101/pdb.prot5314

Lang, D. M., Hille, M. G., Schwab, M. E., & Stuermer, C. A. (1996). Modulation of the inhibitory substrate properties of oligodendrocytes by platelet-derived growth factor. *The Journal of Neuroscience : The Official Journal of the Society for Neuroscience*, *16*(18), 5741–8.

Lang, D. M., Lommel, S., Jung, M., Ankerhold, R., Petrausch, B., Laessing, U., … Stuermer, C. A. O. (1998). Identification of reggie-1 and reggie-2 as plasmamembrane-associated proteins which cocluster with activated GPI-anchored cell adhesion molecules in non-caveolar micropatches in neurons. *Journal of Neurobiology*, *37*, 502–523. doi:10.1002/(SICI)1097-4695(199812)37:4<502::AID-NEU2>3.0.CO;2-S

Lang, D. M., Rubin, B. P., Schwab, M. E., & Stuermer, C. a. (1995). CNS myelin and oligodendrocytes of the Xenopus spinal cord--but not optic nerve--are nonpermissive for axon growth. *The Journal of Neuroscience : The Official Journal of the Society for Neuroscience*, *15*(1 Pt 1), 99–109.

Langhorst, M. F., Solis, G. P., Hannbeck, S., Plattner, H., & Stuermer, C. A. O. (2007). Linking membrane microdomains to the cytoskeleton: Regulation of the lateral mobility of reggie-1/flotillin-2 by interaction with actin. *FEBS Letters*, *581*, 4697–4703. doi:10.1016/j.febslet.2007.08.074

Lazaroff, M., Qi, Y., & Chikaraishi, D. M. (1998). Differentiation of a catecholaminergic CNS cell line modifies tyrosine hydroxylase transcriptional regulation. *Journal of Neurochemistry*, *71*, 51–59.

Lee, M. J., Shin, J. O., & Jung, H. S. (2013). Thy-1 knockdown retards wound repair in mouse skin. *Journal of Dermatological Science*, *69*, 95–104. doi:10.1016/j.jdermsci.2012.11.009

Lee, W. S., Jain, M. K., Arkonac, B. M., Zhang, D., Shaw, S. Y., Kashiki, S., … Haber, E. (1998). Thy-1, a novel marker for angiogenesis upregulated by inflammatory cytokines. *Circulation Research*, *82*, 845–851. doi:10.1161/01.RES.82.8.845

Leifer, D., Lipton, S. A., Barnstable, C. J., & Masland, R. H. (1984). Monoclonal antibody to Thy-1 enhances regeneration of processes by rat retinal ganglion cells in culture. *Science (New York, N.Y.)*, *224*, 303–306. doi:10.1126/science.6143400

Lemansky, P., Fatemi, S. H., Gorican, B., Meyale, S., Rossero, R., & Tartakoff, A. M. (1990). Dynamics and longevity of the glycolipid-anchored membrane protein, Thy-1. *Journal of Cell Biology*, *110*, 1525–1531. doi:10.1083/jcb.110.5.1525

Leshchyns'ka, I., Sytnyk, V., Morrow, J. S., & Schachner, M. (2003). Neural cell adhesion molecule (NCAM) association with PKCbeta2 via betaI spectrin is implicated in NCAM-mediated neurite outgrowth. *The Journal of Cell Biology*, *161*(3), 625–39. doi:10.1083/jcb.200303020

Leyton, L., & Hagood, J. S. (2014). Thy-1 modulates neurological cell-cell and cell-matrix interactions through multiple molecular interactions. *Advances in Neurobiology*, *8*, 3–20.

Li, H., Leung, T. C., Hoffman, S., Balsamo, J., & Lilien, J. (2000). Coordinate regulation of cadherin and integrin function by the chondroitin sulfate proteoglycan neurocan. *Journal of Cell Biology*, *149*, 1275–1288. doi:10.1083/jcb.149.6.1275

Li, S., & Strittmatter, S. M. (2003). Delayed systemic Nogo-66 receptor antagonist promotes recovery from spinal cord injury. *The Journal of Neuroscience : The Official Journal of the Society for Neuroscience*, *23*, 4219–4227. doi:23/10/4219 [pii]

Liebscher, T., Schnell, L., Schnell, D., Scholl, J., Schneider, R., Gullo, M., … Schwab, M. E. (2005). Nogo-A antibody improves regeneration and locomotion of spinal cord-injured rats. *Annals of Neurology*, *58*, 706–719. doi:10.1002/ana.20627

Liësi, P. P., Salonen, E. M. E. M., Dahl, D. D., Vaheri, A. A., & Richards, S. J. S. J. (1990). Thy-1 is a neuronal and glial surface antigen which interacts with matrix proteins and plasminogen activator. *Experimental Brain Research*, *79*(3), 642–650.

Lima, F. R. S., Arantes, C. P., Muras, A. G., Nomizo, R., Brentani, R. R., & Martins, V. R. (2007). Cellular prion protein expression in astrocytes modulates neuronal survival and differentiation. *Journal of Neurochemistry*, *103*, 2164–2176. doi:10.1111/j.1471-4159.2007.04904.x

Linden, R., Martins, V. R., Prado, M. A. M., Cammarota, M., Izquierdo, I., & Brentani, R. R. (2008). Physiology of the prion protein. *Physiological Reviews*, *88*, 673–728. doi:10.1152/physrev.00007.2007

Link, V., Shevchenko, A., & Heisenberg, C.-P. (2006). Proteomics of early zebrafish embryos. *BMC Developmental Biology*, *6*, 1. doi:10.1186/1471-213X-6-1

Lipton, S. A., Leifer, D., & Barnstable, C. J. (1992). Selectivity of Thy-1 monoclonal antibodies in enhancing neurite outgrowth. *Neuroscience Letters*, *137*, 75–77. doi:10.1016/0304-3940(92)90302-N

Liu, C. J. L., Chaturvedi, N., Barnstable, C. J., & Dreyer, E. B. (1996). Retinal Thy-1 expression during development. *Investigative Ophthalmology and Visual Science*, *37*, 1469–1473.

Liu, K., Tedeschi, A., Park, K. K., & He, Z. (2011). Neuronal intrinsic mechanisms of axon regeneration. *Annual Review of Neuroscience*, *34*, 131–152. doi:10.1146/annurev-neuro-061010-113723

López-Muñoz, F., Boya, J., & Alamo, C. (2006). Neuron theory, the cornerstone of neuroscience, on the centenary of the Nobel Prize award to Santiago Ramón y Cajal. *Brain Research Bulletin*, *70*, 391–405. doi:10.1016/j.brainresbull.2006.07.010

Loubet, D., Dakowski, C., Pietri, M., Pradines, E., Bernard, S., Callebert, J., … Schneider, B. (2012). Neuritogenesis: the prion protein controls 1 integrin signaling activity. *The FASEB Journal*, *26*(2), 678–690. doi:10.1096/fj.11-185579

Lugaresi, E., Tobler, I., Gambetti, P., & Montagna, P. (1998). The pathophysiology of fatal familial insomnia. *Brain Pathology (Zurich, Switzerland)*, *8*, 521–526.

Lung, H. L., Bangarusamy, D. K., Xie, D., Cheung, A. K. L., Cheng, Y., Kumaran, M. K., … Lung, M. L. (2005). THY1 is a candidate tumour suppressor gene with decreased expression in metastatic nasopharyngeal carcinoma. *Oncogene*, *24*, 6525–6532. doi:10.1038/sj.onc.1208812

Mahanthappa, N. K., & Patterson, P. H. (1992a). Thy-1 involvement in neurite outgrowth: perturbation by antibodies, phospholipase C, and mutation. *Developmental Biology*, *150*(1), 47–59.

Mahanthappa, N. K., & Patterson, P. H. (1992b). Thy-1 multimerization is correlated with neurite outgrowth. *Developmental Biology*, *150*, 60–71. doi:10.1016/0012-1606(92)90007-4

Málaga-Trillo, E., Laessing, U., Lang, D. M., Meyer, A., & Stuermer, C. A. O. (2002). Evolution of duplicated reggie genes in zebrafish and goldfish. *Journal of Molecular Evolution*, *54*, 235–245. doi:10.1007/s00239-001-0005-1

Málaga-Trillo, E., Salta, E., Figueras, A., Panagiotidis, C., & Sklaviadis, T. (2011). Fish models in prion biology: Underwater issues. *Biochimica et Biophysica Acta - Molecular Basis of Disease*. doi:10.1016/j.bbadis.2010.09.013

Málaga-Trillo, E., & Sempou, E. (2009). PrPs: Proteins with a purpose: Lessons from the zebrafish. *Prion*, *3*, 129–133. doi:10.4161/pri.3.3.9651

Malaga-Trillo, E., Solis, G. P., Schrock, Y., Geiss, C., Luncz, L., Thomanetz, V., & Stuermer, C. a. (2009). Regulation of embryonic cell adhesion by the prion protein. *PLoS Biol*, *7*(3), e55. doi:10.1371/Citation

Mallucci, G. R., Ratté, S., Asante, E. A., Linehan, J., Gowland, I., Jefferys, J. G. R., & Collinge, J. (2002). Post-natal knockout of prion protein alters hippocampal CA1 properties, but does not result in neurodegeneration. *EMBO Journal*, *21*, 202–210. doi:10.1093/emboj/21.3.202

Mallucci, G. R., White, M. D., Farmer, M., Dickinson, A., Khatun, H., Powell, A. D., … Collinge, J. (2007). Targeting Cellular Prion Protein Reverses Early Cognitive Deficits and Neurophysiological Dysfunction in Prion-Infected Mice. *Neuron*, *53*, 325–335. doi:10.1016/j.neuron.2007.01.005

Manson, J., West, J. D., Thomson, V., McBride, P., Kaufman, M. H., & Hope, J. (1992). The prion protein gene: a role in mouse embryogenesis? *Development (Cambridge, England)*, *115*, 117–122.

Martínez del Hoyo, G., López-Bravo, M., Metharom, P., Ardavín, C., & Aucouturier, P. (2006). Prion protein expression by mouse dendritic cells is restricted to the nonplasmacytoid subsets and correlates with the maturation state. *Journal of Immunology (Baltimore, Md. : 1950)*, *177*, 6137–6142.

Mathis, C., Schröter, A., Thallmair, M., & Schwab, M. E. (2010). Nogo-A regulates neural precursor migration in the embryonic mouse cortex. *Cerebral Cortex*, *20*, 2380–2390. doi:10.1093/cercor/bhp307

Mayeux-Portas, V., File, S. E., Stewart, C. L., & Morris, R. J. (2000). Mice lacking the cell adhesion molecule Thy-1 fail to use socially transmitted cues to direct their choice of food. *Current Biology : CB*, *10*, 68–75. doi:10.1016/S0960-9822(99)00278-X

McCurley, A. T., & Callard, G. V. (2008). Characterization of housekeeping genes in zebrafish: male-female differences and effects of tissue type, developmental stage and chemical treatment. *BMC Molecular Biology*, *9*, 102. doi:10.1186/1471-2199-9-102

McCurley, A. T., & Callard, G. V. (2010). Time Course Analysis of Gene Expression Patterns in Zebrafish Eye During Optic Nerve Regeneration. *Journal of Experimental Neuroscience*, *2010*, 17–33.

McGuinness, C. M., & Grafstein, B. (1985). Nucleolar changes in goldfish retinal ganglion cells in response to an optic nerve lesion are not perturbed by a second lesion. *Experimental Neurology*, *89*(2), 461–464. doi:10.1016/0014-4886(85)90105-0

McGuinness, C. M., & Grafstein, B. (1985). Nucleolar changes in goldfish retinal ganglion cells in response to an optic nerve lesion are not perturbed by a second lesion. *Experimental Neurology*, *89*(2), 461–464. doi:10.1016/0014-4886(85)90105-0

Meininger, V., Pradat, P. F., Corse, A., Al-Sarraj, S., Brooks, B. R., Caress, J. B., … Wurthner, J. (2014). Safety, pharmacokinetic, and functional effects of the Nogo-A monoclonal antibody in amyotrophic lateral sclerosis: A randomized, first-in-human clinical trial. *PLoS ONE*, *9*. doi:10.1371/journal.pone.0097803

Merianda, T. T., Lin, A. C., Lam, J. S. Y., Vuppalanchi, D., Willis, D. E., Karin, N., … Twiss, J. L. (2009). A functional equivalent of endoplasmic reticulum and Golgi in axons for secretion of locally synthesized proteins. *Molecular and Cellular Neuroscience*, *40*, 128–142. doi:10.1016/j.mcn.2008.09.008

Minguez, P., & Dopazo, J. (2011). Assessing the biological significance of gene expression signatures and co-expression modules by studying their network properties. *PLoS ONE*, *6*(3), e17474. doi:10.1371/journal.pone.0017474

Milhavet, O., McMahon, H. E., Rachidi, W., Nishida, N., Katamine, S., Mangé, A., … Lehmann, S. (2000). Prion infection impairs the cellular response to oxidative stress. *Proceedings of the National Academy of Sciences of the United States of America*, *97*, 13937–13942. doi:10.1073/pnas.250289197

Moore, D. L., & Goldberg, J. L. (2011). Multiple transcription factor families regulate axon growth and regeneration. *Developmental Neurobiology*, *71*, 1186–1211. doi:10.1002/dneu.20934

Montani, L., Gerrits, B., Gehrig, P., Kempf, A., Dimou, L., Wollscheid, B., & Schwab, M. E. (2009). Neuronal Nogo-A modulates growth cone motility via Rho-GTP/LIMK1/cofilin in the unlesioned adult nervous system. *Journal of Biological Chemistry*, *284*, 10793–10807. doi:10.1074/jbc.M808297200

Moore, D. L., & Goldberg, J. L. (2011). Multiple transcription factor families regulate axon growth and regeneration. *Developmental Neurobiology*, *71*, 1186–1211. doi:10.1002/dneu.20934

Morel, E., Fouquet, S., Chateau, D., Yvernault, L., Frobert, Y., Pinçon-Raymond, M., … Rousset, M. (2004). The Cellular Prion Protein PrPc Is Expressed in Human Enterocytes in Cell-Cell Junctional Domains. *Journal of Biological Chemistry*, *279*, 1499–1505. doi:10.1074/jbc.M308578200

Morozova, D., Guigas, G., & Weiss, M. (2011). Dynamic structure formation of peripheral membrane proteins. *PLoS Computational Biology*, *7*(6), e1002067. doi:10.1371/journal.pcbi.1002067

Morris, R. J., Barber, P. C., Beech, J., & Raisman, G. (1983). The distribution of Thy-1 antigen in the P.N.S. of the adult rat. *Journal of Neurocytology*, *12*(6), 1017–39.

Morris, R. J., Parkyn, C. J., & Jen, A. (2006). Traffic of prion protein between different compartments on the neuronal surface, and the propagation of prion disease. *FEBS Letters*. doi:10.1016/j.febslet.2006.07.053

Moser, M., Colello, R. J., Pott, U., & Oesch, B. (1995). Developmental expression of the prion protein gene in glial cells. *Neuron*. doi:10.1016/0896-6273(95)90307-0

Mosley, K., Collar, J., & Cattell, V. (2000). Mesangial cell necrosis in Thy 1 glomerulonephritis--an ultrastructural study. *Virchows Archiv : An International Journal of Pathology*, *436*, 567–573.

Mouillet-Richard, S., Ermonval, M., Chebassier, C., Laplanche, J. L., Lehmann, S., Launay, J. M., & Kellermann, O. (2000). Signal transduction through prion protein. *Science (New York, N.Y.)*, *289*, 1925–1928. doi:10.1126/science.289.5486.1925

Moya, K. L., Hassig, R., Breen, K. C., Volland, H., & Di Giamberardino, L. (2005). Axonal transport of the cellular prion protein is increased during axon regeneration. *Journal of Neurochemistry*, *92*, 1044–1053.

Moya, K. L., Salès, N., Hässig, R., Créminon, C., Grassi, J., & Di Giamberardino, L. (2000). Immunolocalization of the cellular prion protein in normal brain. *Microscopy Research and Technique*, *50*, 58–65. doi:10.1002/1097-0029(20000701)50:1<58::AID-JEMT9>3.0.CO;2-5

Müller, H. W. (2008). Neural Degeneration and Repair, Gene Expression Profiling, Proteomics and System Biology. Wiley VCH Verlag GmbH & Co. KGaA.

Munderloh, C., Solis, G. P., Bodrikov, V., Jaeger, F. a, Wiechers, M., Málaga-Trillo, E., & Stuermer, C. a O. (2009). Reggies/flotillins regulate retinal axon regeneration in the zebrafish optic nerve and differentiation of hippocampal and N2a neurons. *The Journal of Neuroscience : The Official Journal of the Society for Neuroscience*, *29*(20), 6607–15. doi:10.1523/JNEUROSCI.0870-09.2009

Naslavsky, N., Stein, R., Yanai, A., Friedlander, G., & Taraboulos, A. (1997). Characterization of detergent-insoluble complexes containing the cellular prion protein and its scrapie isoform. *Journal of Biological Chemistry*, *272*, 6324–6331. doi:10.1074/jbc.272.10.6324

Nebl, G., Fischer, S., Penzel, R., & Samstag, Y. (2004). Dephosphorylation of cofilin is regulated through Ras and requires the combined activities of the Ras-effectors MEK and PI3K. *Cellular Signalling*, *16*, 235–243. doi:10.1016/S0898-6568(03)00133-5

Nelson, W. J. (2008). Regulation of cell-cell adhesion by the cadherin-catenin complex. *Biochemical Society Transactions*, *36*, 149–155. doi:10.1042/BST0360149

Niethammer, P., Delling, M., Sytnyk, V., Dityatev, A., Fukami, K., & Schachner, M. (2002). Cosignaling of NCAM via lipid rafts and the FGF receptor is required for neuritogenesis. *The Journal of Cell Biology*, *157*, 521–532. doi:10.1083/jcb.200109059

Nikonov, A. V, Hauri, H.-P., Lauring, B., & Kreibich, G. (2007). Climp-63-mediated binding of microtubules to the ER affects the lateral mobility of translocon complexes. *Journal of Cell Science*, *120*, 2248–2258. doi:10.1242/jcs.008979

Nishida, N. (1997). Prion protein is necessary for latent learning and long-term memory retention. *Cellular and Molecular Neurobiology*, *17*, 537–545. doi:10.1023/A:1026315006619

Nosten-Bertrand, M., Errington, M. L., Murphy, K. P., Tokugawa, Y., Barboni, E., Kozlova, E., … Morris, R. J. (1996). Normal spatial learning despite regional inhibition of LTP in mice lacking Thy-1. *Nature*, *379*, 826–829. doi:10.1038/379826a0

Nygaard, H. B., van Dyck, C. H., & Strittmatter, S. M. (2014). Fyn kinase inhibition as a novel therapy for Alzheimer's disease. *Alzheimer's Research & Therapy*, *6*, 8. doi:10.1186/alzrt238

Ochs, K., & Málaga-Trillo, E. (2014). Common themes in PrP signaling: the Src remains the same. *Frontiers in Cell and Developmental Biology*, *2*(October), 63. doi:10.3389/fcell.2014.00063

Oertle, T., Huber, C., Van der Putten, H., & Schwab, M. E. (2003). Genomic structure and functional characterisation of the promoters of human and mouse nogo/rtn4. *Journal of Molecular Biology*, *325*, 299–323. doi:10.1016/S0022-2836(02)01179-8

Oertle, T., & Schwab, M. E. (2003). Nogo and its paRTNers. *Trends in Cell Biology*. doi:10.1016/S0962-8924(03)00035-7

Oertle, T., van der Haar, M. E., Bandtlow, C. E., Robeva, A., Burfeind, P., Buss, A., … Schwab, M. E. (2003). Nogo-A inhibits neurite outgrowth and cell spreading with three discrete regions. *The Journal of Neuroscience : The Official Journal of the Society for Neuroscience*, *23*, 5393–5406. doi:23/13/5393 [pii]

Paisley, D., Banks, S., Selfridge, J., McLennan, N. F., Ritchie, A.-M., McEwan, C., … Melton, D. W. (2004). Male infertility and DNA damage in Doppel knockout and prion protein/Doppel double-knockout mice. *The American Journal of Pathology*, *164*, 2279–2288. doi:10.1016/S0002-9440(10)63784-4

Paltrinieri, S., Spagnolo, V., Giordano, A., Gelmetti, D., & Comazzi, S. (2006). Bovine prion (PrP) and Doppel (Dpl) proteins expression after in vitro leukocyte activation or Dpl/PrP blocking. *Journal of Cellular Physiology*, *208*, 446–450. doi:10.1002/jcp.20682

Pan, K. M., Baldwin, M., Nguyen, J., Gasset, M., Serban, A., Groth, D., … Cohen, F. E. (1993). Conversion of alpha-helices into beta-sheets features in the formation of the scrapie prion proteins. *Proceedings of the National Academy of Sciences of the United States of America*, *90*, 10962–10966. doi:VL - 90

Pantera, B., Bini, C., Cirri, P., Paoli, P., Camici, G., Manao, G., & Caselli, A. (2009). PrPc activation induces neurite outgrowth and differentiation in PC12 cells: Role for caveolin-1 in the signal transduction pathway. *Journal of Neurochemistry*, *110*, 194–207. doi:10.1111/j.1471-4159.2009.06123.x

Parizek, P., Roeckl, C., Weber, J., Flechsig, E., Aguzzi, A., & Raeber, A. J. (2001). Similar Turnover and Shedding of the Cellular Prion Protein in Primary Lymphoid and Neuronal Cells. *Journal of Biological Chemistry*, *276*, 44627–44632. doi:10.1074/jbc.M107458200

Peng, X., Kim, J., Zhou, Z., Fink, D. J., & Mata, M. (2011). Neuronal Nogo-A regulates glutamate receptor subunit expression in hippocampal neurons. *Journal of Neurochemistry*, *119*, 1183–1193. doi:10.1111/j.1471-4159.2011.07520.x

Pépin, G., Perron, M. P., & Provost, P. (2012). Regulation of human Dicer by the resident ER membrane protein CLIMP-63. *Nucleic Acids Research*, *40*, 11603–11617. doi:10.1093/nar/gks903

Pernet, V., Joly, S., Christ, F., Dimou, L., & Schwab, M. E. (2008). Nogo-A and myelin-associated glycoprotein differently regulate oligodendrocyte maturation and myelin formation. *The Journal of Neuroscience : The Official Journal of the Society for Neuroscience*, *28*, 7435–7444. doi:10.1523/JNEUROSCI.0727-08.2008

Pernet, V., Joly, S., Dalkara, D., Schwarz, O., Christ, F., Schaffer, D., … Schwab, M. E. (2012). Neuronal Nogo-A upregulation does not contribute to ER stress-associated apoptosis but participates in the regenerative response in the axotomized adult retina. *Cell Death and Differentiation*, *19*(7), 1096–1108. doi:10.1038/cdd.2011.191

Pernet, V., & Schwab, M. E. (2012). The role of Nogo-A in axonal plasticity, regrowth and repair. *Cell and Tissue Research*, *349*(1), 97–104. doi:10.1007/s00441-012-1432-6

Petrinovic, M. M., Duncan, C. S., Bourikas, D., Weinman, O., Montani, L., Schroeter, A., … Schwab, M. E. (2010). Neuronal Nogo-A regulates neurite fasciculation, branching and extension in the developing nervous system. *Development (Cambridge, England)*, *137*, 2539–2550. doi:10.1242/dev.048371

Petrinovic, M. M., Hourez, R., Aloy, E. M., Dewarrat, G., Gall, D., Weinmann, O., … Schwab, M. E. (2013). Neuronal Nogo-A negatively regulates dendritic morphology and synaptic transmission in the cerebellum. *Proceedings of the National Academy of Sciences of the United States of America*, *110*, 1083–8. doi:10.1073/pnas.1214255110

Pfaffl, M. W., Horgan, G. W., & Dempfle, L. (2002). Relative expression software tool (REST) for group-wise comparison and statistical analysis of relative expression results in real-time PCR. *Nucleic Acids Research*, *30*, e36. doi:10.1093/nar/30.9.e36

Pinzón-Olejua, A., Welte, C., Abdesselem, H., Málaga-Trillo, E., & Stuermer, C. A. (2014). Essential roles of zebrafish rtn4/Nogo paralogues in embryonic development. *Neural Development*, *9*, 8. doi:10.1186/1749-8104-9-8

Pont, S. (1987). Thy-1: a lymphoid cell subset marker capable of delivering an activation signal to mouse T lymphocytes. *Biochimie*, *69*, 315–320. doi:10.1016/0300-9084(87)90022-8

Poss, K. D., Keating, M. T., & Nechiporuk, A. (2003). Tales of regeneration in zebrafish. *Developmental Dynamics*. doi:10.1002/dvdy.10220

Postlethwait, J. H., Yan, Y. L., Gates, M. A., Horne, S., Amores, A., Brownlie, A., … Talbot, W. S. (1998). Vertebrate genome evolution and the zebrafish gene map. *Nature Genetics*, *18*, 345–349. doi:10.1038/ng0498-345

Premzl, M., Gready, J. E., Jermiin, L. S., Simonic, T., & Marshall Graves, J. A. (2004). Evolution of vertebrate genes related to prion and Shadoo proteins--clues from comparative genomic analysis. *Molecular Biology and Evolution*, *21*, 2210–2231. doi:10.1093/molbev/msh245

Premzl, M., Sangiorgio, L., Strumbo, B., Marshall Graves, J. A., Simonic, T., & Gready, J. E. (2003). Shadoo, a new protein highly conserved from fish to mammals and with similarity to prion protein. *Gene*, *314*, 89–102. doi:10.1016/S0378-1119(03)00707-8

Prusiner, S. B. (1982). Novel proteinaceous infectious particles cause scrapie. *Science (New York, N.Y.)*, *216*, 136–144. doi:10.1126/science.6801762

Prusiner, S. B., Stahl, N., & DeArmond, S. J. (1988). Novel mechanisms of degeneration of the central nervous system--prion structure and biology. *Ciba Foundation Symposium*, *135*, 239–260.

Rege, T. A., & Hagood, J. S. (2006a). Thy-1 as a regulator of cell-cell and cell-matrix interactions in axon regeneration, apoptosis, adhesion, migration, cancer, and fibrosis. *The FASEB Journal : Official Publication of the Federation of American Societies for Experimental Biology*, *20*, 1045–1054. doi:10.1096/fj.05-5460rev

Rege, T. A., & Hagood, J. S. (2006b). Thy-1, a versatile modulator of signaling affecting cellular adhesion, proliferation, survival, and cytokine/growth factor responses. *Biochimica et Biophysica Acta - Molecular Cell Research*. doi:10.1016/j.bbamcr.2006.08.008

Reich, J. B., Burmeister, D. W., Schmidt, J. T., & Grafstein, B. (1990). Effect of conditioning lesions on regeneration of goldfish optic axons: Time course of the cell body reaction to axotomy. *Brain Research*, *515*(1-2), 256–260. doi:10.1016/0006-8993(90)90604-A

Reif, A. E., & Allen, J. M. (1964). The AKR thymic antigen and its distribution in leukemias and nervous tissues. *The Journal of Experimental Medicine*, *120*, 413–433. doi:10.1084/jem.120.3.413

Reuter, A., Málaga-Trillo, E., Binkle, U., Rivera-Milla, E., Beltre, R., Zhou, Y., … Stuermer, C. a O. (2004). Evolutionary analysis and expression of teleost Thy-1. *Zebrafish*, *1*(3), 191–201.

Rivera-Milla, E., Oidtmann, B., Panagiotidis, C. H., Baier, M., Sklaviadis, T., Hoffmann, R., … Málaga-Trillo, E. (2006). Disparate evolution of prion protein domains and the distinct origin of Doppel- and prion-related loci revealed by fish-to-mammal comparisons. *The FASEB Journal : Official Publication of the Federation of American Societies for Experimental Biology*, *20*(2), 317–319.

Rivera-Milla, E., Stuermer, C. A. O., & Málaga-Trillo, E. (2003). An evolutionary basis for scrapie disease: Identification of a fish prion mRNA. *Trends in Genetics*. doi:10.1016/S0168-9525(02)00032-X

Roesch, K., Jadhav, A. P., Trimarchi, J. M., Stadler, M. B., Roska, B., Sun, B. B., & Cepko, C. L. (2008). The transcriptome of retinal Müller glial cells. *Journal of Comparative Neurology*, *509*(2), 225–238. doi:10.1002/cne.21730

Rossi, D., Cozzio, A., Flechsig, E., Klein, M. A., Rülicke, T., Aguzzi, A., & Weissmann, C. (2001). Onset of ataxia and Purkinje cell loss in PrP null mice inversely correlated with Dpl level in brain. *EMBO Journal*, *20*, 694–702. doi:10.1093/emboj/20.4.694

Rossi, F., Jankovski, A., & Sotelo, C. (1995). Differential regenerative response of Purkinje cell and inferior olivary axons confronted with embryonic grafts: Environmental cues versus intrinsic neuronal determinants. *Journal of Comparative Neurology*, *359*, 663–677. doi:10.1002/cne.903590412

Rubin, B. P., Spillmann, A. A., Bandtlow, C. E., Hillenbrand, R., Keller, F., & Schwab, M. E. (1995). Inhibition of PC12 cell attachment and neurite outgrowth by detergent solubilized CNS myelin proteins. *European Journal of Neuroscience*, *7*, 2524–2529. doi:10.1111/j.1460-9568.1995.tb01052.x

Russelakis-Carneiro, M., Saborio, G. P., Anderes, L., & Soto, C. (2002). Changes in the glycosylation pattern of prion protein in murine scrapie. Implications for the mechanism of neurodegeneration in prion diseases. *Journal of Biological Chemistry*, *277*, 36872–36877. doi:10.1074/jbc.M202229200

Saalbach, A., Wetzig, T., Haustein, U. F., & Anderegg, U. (1999). Detection of human soluble Thy-1 in serum by ELISA. Fibroblasts and activated endothelial cells are a possible source of soluble Thy-1 in serum. *Cell and Tissue Research*, *298*, 307–315. doi:10.1007/s004419900079

Salès, N., Hässig, R., Rodolfo, K., Di Giamberardino, L., Traiffort, E., Ruat, M., … Moya, K. L. (2002). Developmental expression of the cellular prion protein in elongating axons. *The European Journal of Neuroscience*, *15*, 1163–1177.

Sambrook, J., & Russell, D. (2001). *Molecular Cloning: A Laboratory Manual*. *Cold Spring Harbor Laboratory Press, Cold Spring Harbor, NY* (p. 999).

Santuccione, A., Sytnyk, V., Leshchyns'ka, I., & Schachner, M. (2005). Prion protein recruits its neuronal receptor NCAM to lipid rafts to activate p59fyn and to enhance neurite outgrowth. *Journal of Cell Biology*, *169*, 341–354. doi:10.1083/jcb.200409127

Saper, C. B., & Sawchenko, P. E. (2003). Magic peptides, magic antibodies: Guidelines for appropriate controls for immunohistochemistry. *Journal of Comparative Neurology*, *465*(2), 161–163. doi:10.1002/cne.10858

Saper, C. B., & Sawchenko, P. E. (2005). An open letter to our readers on the use of antibodies. *Journal of Comparative Neurology*, 493(4):477-8

Saper, C. B. (2009). A guide to the perplexed on the specificity of antibodies. *The Journal of Histochemistry and Cytochemistry : Official Journal of the Histochemistry Society*, *57*(1), 1–5. doi:10.1369/jhc.2008.952770

Sarmiere, P. D., & Bamburg, J. R. (2004). Regulation of the Neuronal Actin Cytoskeleton by ADF/Cofilin. *Journal of Neurobiology*. doi:10.1002/neu.10267

Saunder, N. R., Dziegielewska, K.M. (2005). Degeneration and Regeneration in the Nervous system. *harwood academic publishers.*

Schäfer, H., Bartels, T., Hahn, G., Otto, A., & Burger, R. (1999). T-cell-activating monoclonal antibodies, reacting with both leukocytes and erythrocytes, recognize the guinea pig Thy-1 differentiation antigen: characterization and cloning of guinea pig CD90. *Cellular Immunology*, *197*, 116–128. doi:10.1006/cimm.1999.1564

Schmandke, A., Schmandke, A., & Schwab, M. E. (2014). Nogo-A: Multiple Roles in CNS Development, Maintenance, and Disease. *The Neuroscientist : A Review Journal Bringing Neurobiology, Neurology and Psychiatry*, *20*, 372–386. doi:10.1177/1073858413516800

Schmid, S., Guenther, E., & Kohler, K. (1995). Changes in Thy-1 antigen immunoreactivity in the rat retina during pre- and postnatal development. *Neuroscience Letters*, *199*, 91–94. doi:10.1016/0304-3940(95)12020-5

Schmitz, M., Zafar, S., Silva, C. J., & Zerr, I. (2014). Behavioral abnormalities in prion protein knockout mice and the potential relevance of PrP(C) for the cytoskeleton. *Prion*. doi:10.4161/19336896.2014.983746

Scholes, J. H. (1979). Nerve fibre topography in the retinal projection to the tectum. *Nature*, *278*, 620–624. doi:10.1038/278620a0

Schrock, Y., Solis, G. P., & Stuermer, C. A. O. (2009). Regulation of focal adhesion formation and filopodia extension by the cellular prion protein (PrPC). *FEBS Letters*, *583*, 389–393. doi:10.1016/j.febslet.2008.12.038

Schulte, T., Paschke, K. A., Laessing, U., Lottspeich, F., & Stuermer, C. A. O. (1997). Reggie-1 and reggie-2 , two cell surface proteins expressed by retinal ganglion cells during axon regeneration, *587*, 577–587.

Schwab, M. E. (2004). Nogo and axon regeneration. *Current Opinion in Neurobiology*. doi:10.1016/j.conb.2004.01.004

Schwab, M. E. (2010). Functions of Nogo proteins and their receptors in the nervous system. *Nature Reviews. Neuroscience*, *11*, 799–811. doi:10.1038/nrn2936

Sedwick C., (2015). Thy-1: Shade and sun for integrin signaling. *The Journal of Cell Biology,* 211:3. doi:10.1083/jcb.2111if.

Seki, M., Nawa, H., Morioka, T., Fukuchi, T., Oite, T., Abe, H., & Takei, N. (2002). Establishment of a novel enzyme-linked immunosorbant assay for Thy-1; quantitative assessment of neuronal degeneration. *Neuroscience Letters*, *329*, 185–188. doi:10.1016/S0304-3940(02)00654-7

Seki, T., Spurr, N., Obata, F., Goyert, S., Goodfellow, P., & Silver, J. (1985). The human Thy-1 gene: structure and chromosomal location. *Proceedings of the National Academy of Sciences of the United States of America*, *82*, 6657–6661. doi:10.1073/pnas.82.19.6657

Sempou, E., Biasini, E., Pinzon-Olejua, A., Harris D., Malaga-Trillo, E. (2016). Activation of zebrafish Src family kinases by the prion protein is an amyloid-β-sensitive signal that prevents the endocytosis and degradation of E-cadherin/β-catenin complexes in vivo. *Molecular Neurodegeneration, 11(1):*18. doi: 10.1186/s13024-016-0076-5.

Senatore, A., Restelli, E., & Chiesa, R. (2013). Synaptic dysfunction in prion diseases: A trafficking problem? *International Journal of Cell Biology*, *2013*.

Sevcsik, E., Brameshuber, M., Fölser, M., Weghuber, J., Honigmann, A., & Schütz, G. J. (2015). GPI-anchored proteins do not reside in ordered domains in the live cell plasma membrane. *Nature Communications*, *6*, 6969. doi:10.1038/ncomms7969

Shibata, Y., Shemesh, T., Prinz, W. A., Palazzo, A. F., Kozlov, M. M., & Rapoport, T. A. (2010). Mechanisms determining the morphology of the peripheral ER. *Cell*, *143*, 774–788. doi:10.1016/j.cell.2010.11.007

Shyng, S. L., Huber, M. T., & Harris, D. A. (1993). A prion protein cycles between the cell surface and an endocytic compartment in cultured neuroblastoma cells. *Journal of Biological Chemistry*, *268*, 15922–15928.

Shypitsyna, A., M??laga-Trillo, E., Reuter, A., & Stuermer, C. a O. (2011). Origin of Nogo-A by domain shuffling in an early jawed vertebrate. *Molecular Biology and Evolution*, *28*(4), 1363–1370. doi:10.1093/molbev/msq313

Shypitsyna, A., Málaga-Trillo, E., Reuter, A., & Stuermer, C. a O. (2011). Origin of Nogo-A by domain shuffling in an early jawed vertebrate. *Molecular Biology and Evolution*, *28*(4), 1363–70. doi:10.1093/molbev/msq313

Simon, P. D., McConnell, J., Zurakowski, D., Vorwerk, C. K., Naskar, R., Grosskreutz, C. L., & Dreyer, E. B. (1999). Thy-1 is critical for normal retinal development. *Developmental Brain Research*, *117*(2), 219–223.

Simonen, M., Pedersen, V., Weinmann, O., Schnell, L., Buss, A., Ledermann, B., … Schwab, M. E. (2003). Systemic deletion of the myelin-associated outgrowth inhibitor Nogo-A improves regenerative and plastic responses after spinal cord injury. *Neuron*, *38*, 201–211. doi:10.1016/S0896-6273(03)00226-5

Simons, K., & Ikonen, E. (1997). Functional rafts in cell membranes. *Nature*, *387*, 569–572. doi:10.1038/42408

Simons, K., & Toomre, D. (2000). Lipid rafts and signal transduction. *Nature Reviews. Molecular Cell Biology*, *1*, 31–39. doi:10.1038/35036052

Sivron, T., Schwab, M. E., & Schwartz, M. (1994). Presence of growth inhibitors in fish optic nerve myelin: postinjury changes. *J Comp Neurol*, *343*(2), 237–246. doi:10.1002/cne.903430205

Solis, G. P., Hoegg, M., Munderloh, C., Schrock, Y., Malaga-Trillo, E., Rivera-Milla, E., & Stuermer, C. a O. (2007). Reggie/flotillin proteins are organized into stable tetramers in membrane microdomains. *The Biochemical Journal*, *403*(2), 313–322. doi:10.1042/BJ20061686

Solis, G. P., Radon, Y., Sempou, E., Jechow, K., Stuermer, C. a O., & Málaga-Trillo, E. (2013). Conserved roles of the prion protein domains on subcellular localization and cell-cell adhesion. *PloS One*, *8*(7), e70327. doi:10.1371/journal.pone.0070327

Solis, G. P., Schrock, Y., Hulsbusch, N., Wiechers, M., Plattner, H., & Stuermer, C. A. O. (2012). Reggies/flotillins regulate E-cadherin-mediated cell contact formation by affecting EGFR trafficking. *Molecular Biology of the Cell*. doi:10.1091/mbc.E11-12-1006

Stahl, N., Borchelt, D. R., Hsiao, K., & Prusiner, S. B. (1987). Scrapie prion protein contains a phosphatidylinositol glycolipid. *Cell*, *51*, 229–240. doi:10.1016/0092-8674(87)90150-4

Steele, A. D., Emsley, J. G., Ozdinler, P. H., Lindquist, S., & Macklis, J. D. (2006). Prion protein (PrPc) positively regulates neural precursor proliferation during developmental and adult mammalian neurogenesis. *Proceedings of the National Academy of Sciences of the United States of America*, *103*, 3416–3421. doi:10.1073/pnas.0511290103

Steele, A. D., Lindquist, S., & Aguzzi, A. (2007). The prion protein knockout mouse: a phenotype under challenge. *Prion*, *1*, 83–93. doi:10.4161/pri.1.2.4346

Stuermer, C. a, Lang, D. M., Kirsch, F., Wiechers, M., Deininger, S. O., & Plattner, H. (2001). Glycosylphosphatidyl inositol-anchored proteins and fyn kinase assemble in noncaveolar plasma membrane microdomains defined by reggie-1 and -2. *Molecular Biology of the Cell*, *12*(10), 3031–3045.

Stuermer, C. a O. (2011a). Microdomain-forming proteins and the role of the reggies/flotillins during axon regeneration in zebrafish. *Biochimica et Biophysica Acta - Molecular Basis of Disease*, *1812*(3), 415–422. doi:10.1016/j.bbadis.2010.12.004

Stuermer, C. a O. (2011b). Reggie/flotillin and the targeted delivery of cargo. *Journal of Neurochemistry*, *116*(5), 708–713. doi:10.1111/j.1471-4159.2010.07007.x

Stuermer, C. a O. (2012). How reggies regulate regeneration and axon growth. *Cell and Tissue Research*, *349*(1), 71–77. doi:10.1007/s00441-012-1343-6

Stuermer, C. a O., Langhorst, M. F., Wiechers, M. F., Legler, D. F., Von Hanwehr, S. H., Guse, A. H., & Plattner, H. (2004). PrPc capping in T cells promotes its association with the lipid raft proteins reggie-1 and reggie-2 and leads to signal transduction. *The FASEB Journal : Official Publication of the Federation of American Societies for Experimental Biology*, *18*(14), 1731–1733.

Stuermer, C. A. O. (2010). The reggie/flotillin connection to growth. *Trends in Cell Biology*, *20*, 6–13. doi:10.1016/j.tcb.2009.10.003

Stuermer, C. A. O., & Plattner, H. (2005a). The lipid raft microdomain proteins reggie-1 and reggie-2 (flotillins) are scaffolds for protein interaction and signalling. *Biochem. Soc. Symp.*, *72*, 109–118.

Stuermer, C. A. O., & Plattner, H. (2005b). The “lipid raft” microdomain proteins reggie-1 and reggie-2 (flotillins) are scaffolds for protein interaction and signalling. *Biochemical Society Symposium*, 109–118.

Stys, P. K., You, H., & Zamponi, G. W. (2012). Copper-dependent regulation of NMDA receptors by cellular prion protein: implications for neurodegenerative disorders. *The Journal of Physiology*, *590*, 1357–68. doi:10.1113/jphysiol.2011.225276

Sunyach, C., Jen, A., Deng, J., Fitzgerald, K. T., Frobert, Y., Grassi, J., … Morris, R. (2003). The mechanism of internalization of glycosylphosphatidylinositol-anchored prion protein. *EMBO Journal*, *22*(14), 3591–3601.

Suri, C., Fung, B. P., Tischler, A. S., & Chikaraishi, D. M. (1993). Catecholaminergic cell lines from the brain and adrenal glands of tyrosine hydroxylase-SV40 T antigen transgenic mice. *The Journal of Neuroscience : The Official Journal of the Society for Neuroscience*, *13*, 1280–1291.

Suzuki, T., Kurokawa, T., Hashimoto, H., & Sugiyama, M. (2002). cDNA sequence and tissue expression of Fugu rubripes prion protein-like: A candidate for the teleost orthologue of tetrapod PrPs. *Biochemical and Biophysical Research Communications*, *294*, 912–917. doi:10.1016/S0006-291X(02)00546-6

Suzuki, K. G. N., Kasai, R. S., Hirosawa, K. M., Nemoto, Y. L., Ishibashi, M., Miwa, Y., … Kusumi, A. (2012). Transient GPI-anchored protein homodimers are units for raft organization and function. *Nature Chemical Biology*, *8*(9), 774–83. doi:10.1038/nchembio.1028

Tan, C. L., Kwok, J. C. F., Patani, R., Ffrench-Constant, C., Chandran, S., & Fawcett, J. W. (2011). Integrin activation promotes axon growth on inhibitory chondroitin sulfate proteoglycans by enhancing integrin signaling. *The Journal of Neuroscience : The Official Journal of the Society for Neuroscience*, *31*(17), 6289–6295. doi:10.1523/JNEUROSCI.0008-11.2011

Tan, C. L., Kwok, J. C. F., Heller, J. P. D., Zhao, R., Eva, R., & Fawcett, J. W. (2015). Full length talin stimulates integrin activation and axon regeneration. *Molecular and Cellular Neurosciences*, *68*, 1–8. doi:10.1016/j.mcn.2015.03.011

Tan, H.-B., Zhong, Y.-S., Cheng, Y., & Shen, X. (2011). Rho/ROCK pathway and neural regeneration: a potential therapeutic target for central nervous system and optic nerve damage. *International Journal of Ophthalmology*, *4*, 652–7. doi:10.3980/j.issn.2222-3959.2011.06.16

Tang, R., Dodd, A., Lai, D., McNabb, W. C., & Love, D. R. (2007). Validation of zebrafish (Danio rerio) reference genes for quantitative real-time RT-PCR normalization. *Acta Biochimica et Biophysica Sinica*, *39*, 384–390. doi:10.1111/j.1745-7270.2007.00283.x

Timpl, R., Rohde, H., Robey, P. G., Rennard, S. I., Foidart, J. M., & Martin, G. R. (1979). Laminin--a glycoprotein from basement membranes. *The Journal of Biological Chemistry*, *254*(19), 9933–9937.

Tiveron, M. C., Barboni, E., Pliego Rivero, F. B., Gormley, A. M., Seeley, P. J., Grosveld, F., & Morris, R. (1992). Selective inhibition of neurite outgrowth on mature astrocytes by Thy-1 glycoprotein. *Nature*, *355*, 745–748. doi:10.1038/355745a0

Tobler, I., Gaus, S. E., Deboer, T., Achermann, P., Fischer, M., Rülicke, T., … Manson, J. C. (1996). Altered circadian activity rhythms and sleep in mice devoid of prion protein. *Nature*, *380*, 639–642. doi:10.1038/380639a0

Towbin, H., Staehelin, T., & Gordon, J. (1979). Electrophoretic transfer of proteins from polyacrylamide gels to nitrocellulose sheets: procedure and some applications. *Proceedings of the National Academy of Sciences of the United States of America*, *76*, 4350–4354. doi:10.1073/pnas.76.9.4350

Tuzi, N. L., Cancellotti, E., Baybutt, H., Blackford, L., Bradford, B., Plinston, C., … Manson, J. C. (2008). Host PrP glycosylation: A major factor determining the outcome of prion infection. *PLoS Biology*, *6*, 872–882. doi:10.1371/journal.pbio.0060100

Udvadia, A. J., Köster, R. W., & Skene, J. H. (2001). GAP-43 promoter elements in transgenic zebrafish reveal a difference in signals for axon growth during CNS development and regeneration. *Development (Cambridge, England)*, *128*, 1175–1182.

Um, J. W., Nygaard, H. B., Heiss, J. K., Kostylev, M. A., Stagi, M., Vortmeyer, A., … Strittmatter, S. M. (2012). Alzheimer amyloid-β oligomer bound to postsynaptic prion protein activates Fyn to impair neurons. *Nature Neuroscience*. doi:10.1038/nn.3178

Vajn, K., Plunkett, J. A., Tapanes-Castillo, A., & Oudega, M. (2013). Axonal regeneration after spinal cord injury in zebrafish and mammals: Differences, similarities, translation. *Neuroscience Bulletin*. doi:10.1007/s12264-013-1361-8

Vassallo, N., & Herms, J. W. (2003). Cellular prion protein function in copper homeostasis and redox signalling at the synapse. *Journal of Neurochemistry*. doi:10.1046/j.1471-4159.2003.01882.x

Velarde, E., Haque, R., Iuvone, P. M., Azpeleta, C., Alonso-Gómez, A. L., & Delgado, M. J. (2009). Circadian clock genes of goldfish, Carassius auratus: cDNA cloning and rhythmic expression of period and cryptochrome transcripts in retina, liver, and gut. *Journal of Biological Rhythms*, *24*, 104–113. doi:10.1177/0748730408329901

Veldman, M. B., Bemben, M. a, Thompson, R. C., & Goldman, D. (2007). Gene expression analysis of zebrafish retinal ganglion nerve regeneration identifies KLF6a and KLF7a regulators of axon regeneration cells during optic as important. *Developmental Biology*, *312*(2), 596–612. doi:10.1016/j.ydbio.2007.09.019

Verity, N. C., & Mallucci, G. R. (2011). Rescuing neurons in prion disease. *The Biochemical Journal*, *433*, 19–29. doi:10.1042/BJ20101323

Vielmetter, J., & Stuermer, C. A. (1989). Goldfish retinal axons respond to position-specific properties of tectal cell membranes in vitro. *Neuron*, *2*, 1331–1339. doi:10.1016/0896-6273(89)90071-8

Vitriol, E. a, & Zheng, J. Q. (2012). Growth cone travel in space and time: the cellular ensemble of cytoskeleton, adhesion, and membrane. *Neuron*, *73*(6), 1068–81. doi:10.1016/j.neuron.2012.03.005

Voeltz, G. K., Prinz, W. A., Shibata, Y., Rist, J. M., & Rapoport, T. A. (2006). A class of membrane proteins shaping the tubular endoplasmic reticulum. *Cell*, *124*, 573–586. doi:10.1016/j.cell.2005.11.047

Von Philipsborn, A. C., Ferrer-Vaquer, A., Rivera-Milla, E., Stuermer, C. A. O., & Málaga-Trillo, E. (2005). Restricted expression of reggie genes and proteins during early zebrafish development. *Journal of Comparative Neurology*, *482*, 257–272. doi:10.1002/cne.20423

Voskuil, J. (2014). Commercial antibodies and their validation. *F1000Research*, *232*, 1–13. doi:10.12688/f1000research.4966.1

Wälchli, T., Pernet, V., Weinmann, O., Shiu, J.-Y., Guzik-Kornacka, A., Decrey, G., … Schwab, M. E. (2013). Nogo-A is a negative regulator of CNS angiogenesis. *Proceedings of the National Academy of Sciences of the United States of America*, *110*, E1943–52. doi:10.1073/pnas.1216203110

Waller, B. A. (1850). Experiments on the Section of the Glossopharyngeal and Hypoglossal Nerves of the Frog, and Observations of the Alterations Produced Thereby in the Structure of Their Primitive Fibres. *Philosophical Transactions of the Royal Society of London.*, *140*, 423–429.

Walz, R., Amaral, O. B., Rockenbach, I. C., Roesler, R., Izquierdo, I., Cavalheiro, E. A., … Brentani, R. R. (1999). Increased sensitivity to seizures in mice lacking cellular prion protein. *Epilepsia*, *40*, 1679–1682.

Wang, X., Wiesinger, J., Beard, J., Felt, B., Menzies, S., Earley, C., … Connor, J. (2004). Thy1 expression in the brain is affected by iron and is decreased in Restless Legs Syndrome. *Journal of the Neurological Sciences*, *220*, 59–66. doi:10.1016/j.jns.2004.02.004

Wanner, M., Lang, D. M., Bandtlow, C. E., Schwab, M. E., Bastmeyer, M., & Stuermer, C. A. (1995). Reevaluation of the growth-permissive substrate properties of goldfish optic nerve myelin and myelin proteins. *The Journal of Neuroscience : The Official Journal of the Society for Neuroscience*, *15*, 7500–7508.

Watanabe, T., Yasutaka, Y., Nishioku, T., Nakashima, A., Futagami, K., Yamauchi, A., & Kataoka, Y. (2012). Atorvastatin stimulates neuroblastoma cells to induce neurite outgrowth by increasing cellular prion protein expression. *Neuroscience Letters*, *531*, 114–119. doi:10.1016/j.neulet.2012.10.032

Watts, J. C., & Westaway, D. (2007). The prion protein family: Diversity, rivalry, and dysfunction. *Biochimica et Biophysica Acta - Molecular Basis of Disease*. doi:10.1016/j.bbadis.2007.05.001

Westerfield M (1995) The zebrafish book: a guide for the laboratory use of zebrafish (Danio rerio). Eugene, OR: M. Westerfield.

Westergard, L., Christensen, H. M., & Harris, D. A. (2007). The cellular prion protein (PrP(C)): its physiological function and role in disease. *Biochimica et Biophysica Acta*, *1772*, 629–644. doi:10.1016/j.bbadis.2007.02.011

White, M. D., & Mallucci, G. R. (2009). RNAi for the treatment of prion disease: a window for intervention in neurodegeneration? *CNS & Neurological Disorders Drug Targets*, *8*, 342–352. doi:10.2174/187152709789541934

Whittington, M. A., Sidle, K. C., Gowland, I., Meads, J., Hill, A. F., Palmer, M. S., … Collinge, J. (1995). Rescue of neurophysiological phenotype seen in PrP null mice by transgene encoding human prion protein. *Nature Genetics*, *9*, 197–201. doi:10.1038/ng0295-197

Williams, a F., & Gagnon, J. (1982). Neuronal cell Thy-1 glycoprotein: homology with immunoglobulin. *Science (New York, N.Y.)*, *216*(4547), 696–703.

Williams, S. K., Fairless, R., Weise, J., Kalinke, U., Schulz-Schaeffer, W., & Diem, R. (2011). Neuroprotective effects of the cellular prion protein in autoimmune optic neuritis. *The American Journal of Pathology*, *178*(6), 2823–31. doi:10.1016/j.ajpath.2011.02.046

Wills, Z., Mandel-Brehm, C., Mardinly, A., McCord, A., Giger, R., & Greenberg, M. (2012). The nogo receptor family restricts synapse number in the developing hippocampus. *Neuron*, *73*, 466–481. doi:10.1016/j.neuron.2011.11.029

Wong, B. S., Liu, T., Li, R., Pan, T., Petersen, R. B., Smith, M. A., … Sy, M. S. (2001). Increased levels of oxidative stress markers detected in the brains of mice devoid of prion protein. *Journal of Neurochemistry*, *76*, 565–572. doi:10.1046/j.1471-4159.2001.00028.x

Xanthpoulos, K., Polymenidou, M., Bellworthy, S. J., Benestad, S. L., & Sklaviadis, T. (2009). Species and strain glycosylation patterns of PrPSc. *PLoS ONE*, *4*. doi:10.1371/journal.pone.0005633

Yang, N., Higuchi, O., Ohashi, K., Nagata, K., Wada, A., Kangawa, K., … Mizuno, K. (1998). Cofilin phosphorylation by LIM-kinase 1 and its role in Rac-mediated actin reorganization. *Nature*, *393*, 809–812. doi:10.1038/31735

Yang, S. H., Chen, Y. J., Tung, P. Y., Lai, W. L., Chen, Y., Jeng, C. J., & Wang, S. M. (2008). Anti-Thy-1 antibody-induced neurite outgrowth in cultured dorsal root ganglionic neurons is mediated by the c-Src-MEK signaling pathway. *Journal of Cellular Biochemistry*, *103*(1), 67–77. doi:10.1002/jcb.21387

Yang, Y. S., & Strittmatter, S. M. (2007). The reticulons: a family of proteins with diverse functions. *Genome Biology*, *8*(12), 234. doi:10.1186/gb-2007-8-12-234

Yiu, G., & He, Z. (2006). Glial inhibition of CNS axon regeneration. *Nature Reviews. Neuroscience*, *7*, 617–627. doi:10.1038/nrn1956

Yoo, Y., Ho, H. J., Wang, C., & Guan, J.-L. (2010). Tyrosine phosphorylation of cofilin at Y68 by v-Src leads to its degradation through ubiquitin-proteasome pathway. *Oncogene*, *29*(2), 263–72. doi:10.1038/onc.2009.319

Zagrebelsky, M., Schweigreiter, R., Bandtlow, C. E., Schwab, M. E., & Korte, M. (2010). Nogo-A stabilizes the architecture of hippocampal neurons. *The Journal of Neuroscience : The Official Journal of the Society for Neuroscience*, *30*, 13220–13234. doi:10.1523/JNEUROSCI.1044-10.2010

Zemmar, A., Weinmann, O., Kellner, Y., Yu, X., Vicente, R., Gullo, M., … Schwab, M. E. (2014). Neutralization of nogo-a enhances synaptic plasticity in the rodent motor cortex and

improves motor learning in vivo. *The Journal of Neuroscience : The Official Journal of the Society for Neuroscience*, *34*, 8685–98. doi:10.1523/JNEUROSCI.3817-13.2014

Zhang, C. C., Steele, A. D., Lindquist, S., & Lodish, H. F. (2006). Prion protein is expressed on long-term repopulating hematopoietic stem cells and is important for their self-renewal. *Proceedings of the National Academy of Sciences of the United States of America*, *103*, 2184–2189. doi:10.1073/pnas.0510577103

Zheng, B., Ho, C., Li, S., Keirstead, H., Steward, O., & Tessier-Lavigne, M. (2003). Lack of enhanced spinal regeneration in Nogo-deficient mice. *Neuron*, *38*, 213–224. doi:10.1016/S0896-6273(03)00225-3

Zomosa-Signoret, V., Arnaud, J.-D., Fontes, P., Alvarez-Martinez, M.-T., & Liautard, J.-P. (2008). Physiological role of the cellular prion protein. *Veterinary Research*, *39*, 9. doi:10.1051/vetres:2007048

9. Supplementary data and statistics

This chapter shows more detailed information about the indicated chapters and the statistical evaluation underlying the graphs and figures shown in the results section.

PART I Thy-1 and PrP

9.1. Chapter 5.1.2: Verification of the specificity of the mAb 89/9 raised against zebrafish Thy-1

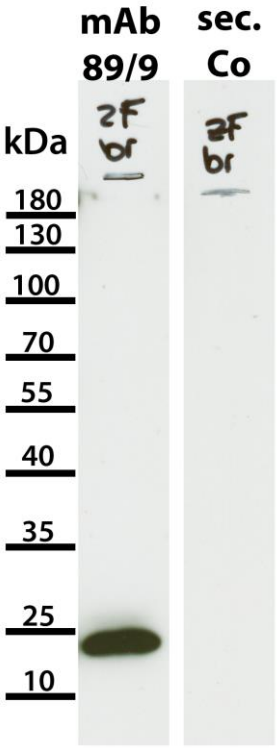

Figure 9.1 Characterization of the zebrafish (ZF) Thy-1-specific mAb 89/9 via WB. ZF brain lysate was separated by PAGE and proteins transferred to a nitrocellulose membrane. The blot was probed either with mAb 89/9 (left lane) or with HRP-labeled secondary antibody (right lane). MAb 89/9 labels a single protein band in zebrafish brain lysate (ZF br) running at ~ 25 kDa app. MW.

9.2. Chapter 5.1.2: Analysis of Thy-1 expression upon ONL in zebrafish RGCs

(Re-) arrangement of Thy-1 and its optic nerve lesion-induced up-regulation

Figure 9.2.1 below shows the confocal scan of the zebrafish RGC layer. The single planes of the confocal Z-stack are displayed. They illustrate the reorganization and accumulation of Thy-1 upon ONL from a ring-shaped, membranous pattern into big, diffuse clusters, probably in specialized signaling rafts at the cell surface and maybe also in cytoplasmic signaling vesicles. After ONL, zebrafish RGCs survived and stayed intact during the preparation, as demonstrated by the Dapi staining of the nuclei. Cell bodies were enlarged, which is a known phenomenon due to optic nerve injury and is referred to the “cell body reaction” (McGuinness & Grafstein, 1985; Reich et al., 1990; Welte et al. 2015).

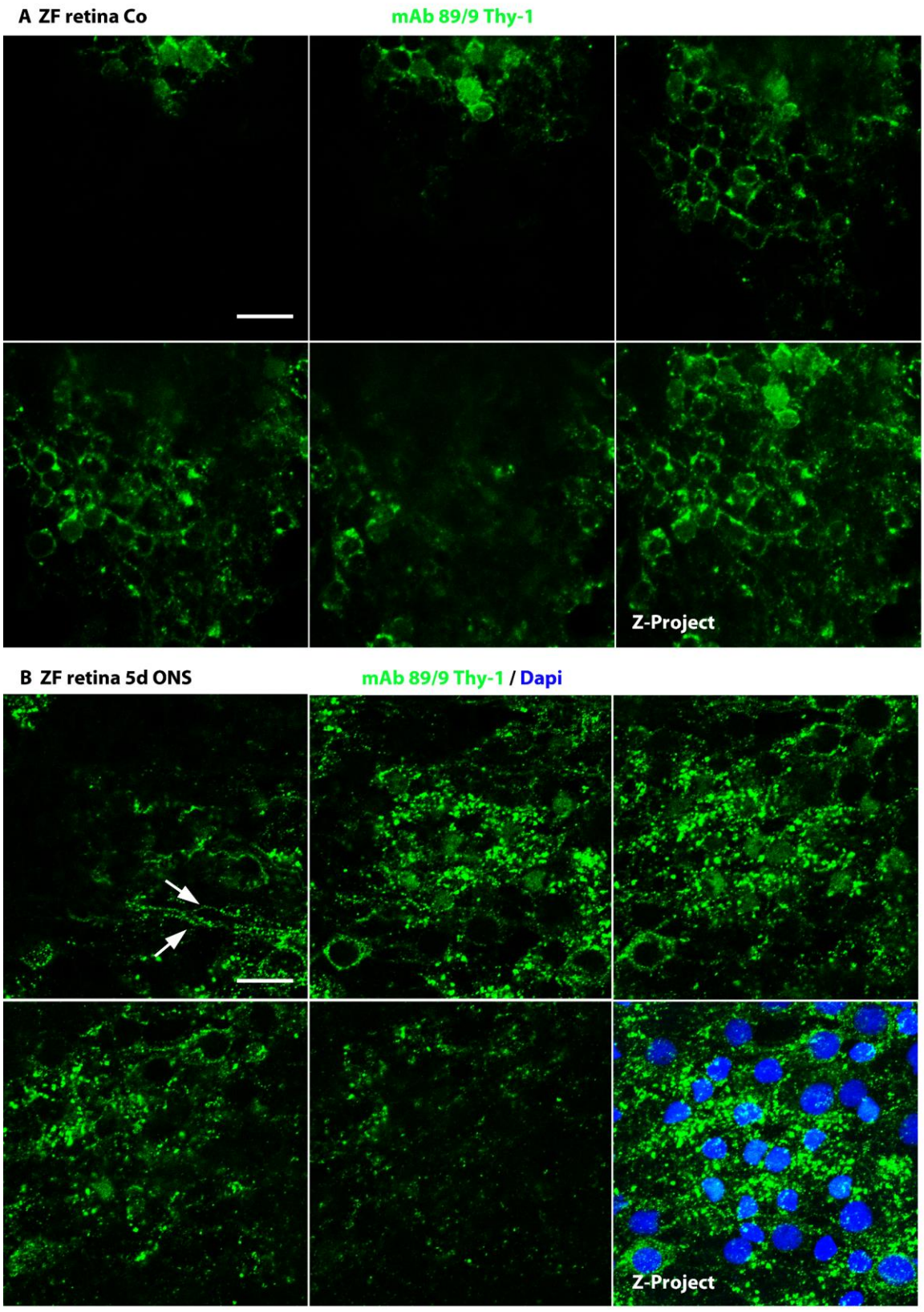

Figure 9.2.1 Characterization of the mAb Thy-1 89/9 pattern in zebrafish retinae. A. Control retina. Short live staining of unfixed tissue shows a membranous pattern of Thy-1 in zebrafish RGCs throughout all confocal stacks. **B.** After ONS, besides the quantitative increase, the protein seems to be reorganized all over the cell body and in much bigger clusters. Axons show Thy-1, looking like a pearl of strings (arrows in the first picture). Cell bodies of RGCs are enlarged. Thy-1 in green, Dapi in blue. Scale bars: 25 µm. Images collected at 0.93 µm intervals in a depth of 10.19 µm for **A** and 5.56 µm for **B**.

Figure 5.1.2 F IHC: Thy-1 protein fluorescence intensity quantification

Zebrafish retinae	Control, fluorescence intensity (AU)	5d ONS, fluorescence intensity (AU)
Exp. 1	13.977	59.157
	10.041	64.856
	13.531	43.505
Exp. 2	7.024	13.185
	7.874	25.385
	8.405	11.959
Exp. 3	36.686	46.396
	33.406	43.932
	27.778	49.331
	34.356	71.109
Mean ± SEM	**19.308 ± 3869**	**42.882 ± 6450**
%	**100**	**271**
N retinae	**10**	**10**

Unpaired, two-tailed t-test

Column B	5 d ONS
vs.	vs,
Column A	Control
Unpaired t test	
P value	0,0057
P value summary	**
Significantly different (P < 0.05)?	Yes
One- or two-tailed P value?	Two-tailed
t, df	t=3,134 df=18
How big is the difference?	
Mean ± SEM of column A	19308 ± 3869, n=10
Mean ± SEM of column B	42882 ± 6450, n=10
Difference between means	23574 ± 7521
95% confidence interval	7772 to 39375
R squared (eta squared)	0,3531
F test to compare variances	
F, DFn, Dfd	2,779, 9, 9
P value	0,1438
P value summary	ns
Significantly different (P < 0.05)?	No

Figure 5.1.2 G: Thy-1 protein density quantification in WBs with the mAb 89/9

Zebrafish retinae	Control, protein density (AU), normalized to α-tubulin	6 d ONS, protein density (AU), normalized to α-tubulin
Exp. 1	83.726	120.520
Exp. 2	85.217	125.112
Mean ± SEM	**84.472 ± 745,5**	**122.816 ± 2296**
%	**100**	**145**

Unpaired, two-tailed t-test

Column B	6 d ONS
vs.	vs,
Column A	Co
Unpaired t test	
P value	0,0039
P value summary	**
Significantly different (P < 0.05)?	Yes
One- or two-tailed P value?	Two-tailed
t, df	t=15,88 df=2
How big is the difference?	
Mean ± SEM of column A	84472 ± 745,5, n=2
Mean ± SEM of column B	122816 ± 2296, n=2
Difference between means (B-A) ± SEM	38345 ± 2414
95% confidence interval	27958 to 48731
R squared (eta squared)	0,9921

Exp. 1

Exp. 2

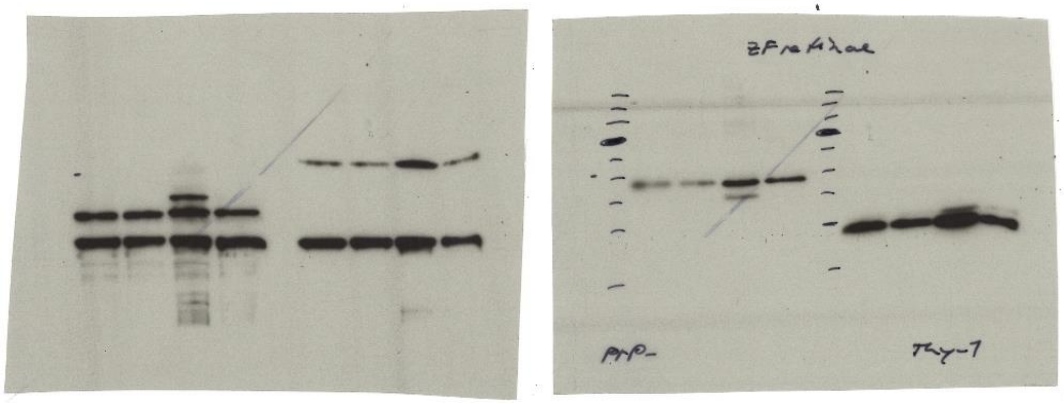

Figure 5.1.2 H & I: Relative, quantitative RT PCR: quantification of Thy-1 mRNA levels 5 days after optic nerve lesion (ONL)

Zebrafish retinae		$\bar{x}$ CT Rpl 13α	$\bar{x}$ CT Thy-1	delta CT (CT Thy-1 - CT Rpl13)	deltadelta CT (delta CT Exp. - delta CT Co)	%	regulation=ratio 2^-deltadeltaCT
Exp. 1	Co	18,03	24,27	6,24		**100**	1x
	ONL	17,51	19,27	1,76	-4,48	**2231**	22.3x
Exp. 2	Co	17,11	24,21	7,1		**100**	1x
	ONL	16,72	19,27	2,55	-4,55	**2342**	23.4x
Exp. 3	Co	17,06	23,94	6,88		**100**	1x
	ONL	16,22	18,49	2,27	-4,61	**2442**	24.4x
Zebrafish retinae		**$\bar{x}$ CT EF1α**	**$\bar{x}$ CT Thy-1**	**delta CT (CT Thy-1 - CT EF1α)**	**deltadelta CT (delta CT Exp. - delta CT Co)**	**%**	**regulation=ratio 2^-deltadeltaCT**
Exp. 1	Co	19,92	24,27	4,35		**100**	1x
	ONL	17,93	19,27	1,34	-3,01	**805**	8.05x
Exp. 2	Co	19,11	24,21	5		**100**	1x
	ONL	17,21	19,27	2,06	-2,94	**767**	7.7x
Exp. 3	Co	19,67	23,94	4,27		**100**	1x
	ONL	17,58	18,49	0,91	-3,36	**1026**	10.26x

One-sample t-test, analyzing if the mean of Thy-1 expression after optic nerve lesion differs from the hypothetical value "1-times expression" of the untreated control, normalized to the housekeeping gene RPL13alpha.

Number of values	3	3
Minimum	1	22,3
25% Percentile	1	22,3
Median	1	23,4
75% Percentile	1	24,4
Maximum	1	24,4
Mean	1	23,37
Std. Deviation	0	1,05
Std. Error of Mean	0	0,6064
Lower 95% CI of mean	1	20,76
Upper 95% CI of mean	1	25,98
Sum	3	70,1
One sample t test	Sample difference has zero SD	
Theoretical mean		1
Actual mean		23,37
Discrepancy		22,37
95% CI of discrepancy		19,76 to 24,98
t, df		t=36,88 df=2
P value (two tailed)		0,0007
Significant (alpha=0.05)?		Yes

One-sample t-test, analyzing if the mean of Thy-1 expression after optic nerve lesion differs from the hypothetical value "1-times expression" of the untreated control, normalized to the housekeeping gene EF1alpha.

Number of values	3	3
Minimum	1	7,7
25% Percentile	1	7,7
Median	1	8,05
75% Percentile	1	10,26
Maximum	1	10,26
Mean	1	8,67
Std. Deviation	0	1,388
Std. Error of Mean	0	0,8014
Lower 95% CI of mean	1	5,222
Upper 95% CI of mean	1	12,12
Sum	3	26,01
One sample t test	Sample difference has zero SD	
Theoretical mean		1
Actual mean		8,67
Discrepancy		7,67
95% CI of discrepancy		4,222 to 11,12
t, df		t=9,571 df=2
P value (two tailed)		0,0107
Significant (alpha=0.05)?		Yes

9.3. Chapter 5.1.4: MO-mediated knockdown of Thy-1, quantification of protein levels in zebrafish RGCs and embryos

Figure 5.1.4 B: Thy-1 protein fluorescence intensity quantification in zebrafish retinae

Zebrafish retinae	Control MO 140 µM Fluorescence intensity (AU)	Thy-1 MO 1 140 µM Fluorescence intensity (AU)
Exp. 1	17,59	12,14
	19,24	10,32
	16,14	18,09
Exp. 2	19,71	11,18
	23,71	8,98
	--	11,18
Exp. 3	12,54	10,92
	20,02	13,53
	--	9,17
Mean ± SEM	**18,42 ± 1,321**	**11,58 ± 0,9443**
%	**100**	**62,9**

Unpaired, two-tailed t-test

Column B	Thy-1 Mo 5d
vs.	vs,
Column A	Control Mo 5 d
Unpaired t test	
P value	0,0007
P value summary	***
Significantly different (P < 0.05)?	Yes
One- or two-tailed P value?	Two-tailed
t, df	t=4,333 df=14
How big is the difference?	
Mean ± SEM of column A	18,42 ± 1,321, n=7
Mean ± SEM of column B	11,58 ± 0,9443, n=9
Difference between means	-6,845 ± 1,58
95% confidence interval	-10,23 to -3,457
R squared (eta squared)	0,5729
F test to compare variances	
F, DFn, Dfd	1,523, 6, 8
P value	0,5674
P value summary	ns
Significantly different (P < 0.05)?	No

Figure 5.1.4 D: Thy-1 protein density quantification in WBs of zebrafish retinae

Zebrafish retinae	Control MO 140 µM, protein density (AU), normalized to α-tub	Thy-1 MO 1 140 µM, protein density (AU), normalized to α-tub	Thy-1 MO 2 140 µM, protein density (AU), normalized to α-tub
Exp. 1	103.960	72.249	--
Exp. 2	96.046	79.628	80.399
Mean ± SEM	**100.003 ± 3.957**	**75.939 ± 3.690**	**80.399 ± --**
%	**100**	**76**	**80,4**

Unpaired, two-tailed t-test: Thy-1 morpholino sequence 1 vs. control morpholino

Column B	Thy-1
vs.	vs,
Column A	Co MO
Unpaired t test	
P value	0,0470
P value summary	*
Significantly different (P < 0.05)?	Yes
One- or two-tailed P value?	Two-tailed
t, df	t=4,448 df=2
How big is the difference?	
Mean ± SEM of column A	100003 ± 3957, n=2
Mean ± SEM of column B	75939 ± 3690, n=2
Difference between means ± SEM	-24065 ± 5410
95% confidence interval	-47343 to -786,3
R squared (eta squared)	0,9082

Exp. 1

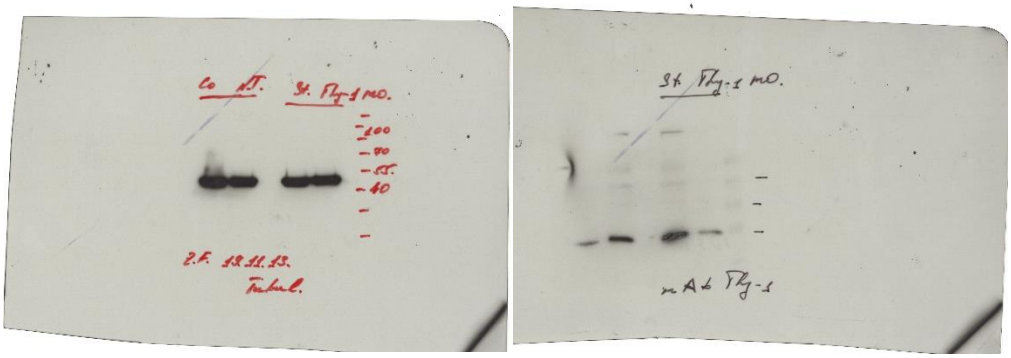

Exp. 2

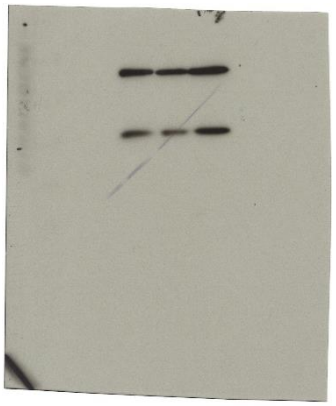

Figure 5.1.5.1 Expression and knockdown of Thy-1 in the zebrafish embryo

Figure 5.1.5.1 E & F: Relative, quantitative RT PCR: Thy-1 mRNA levels in zebrafish embryos at 1, 3 and 5 days post fertilization (dpf)

Embryonic stage / exp. group	$\bar{x}$ CT Rpl 13α	$\bar{x}$ CT Thy-1	delta CT (CT Thy-1 - CT Rpl13)	deltadelta CT (delta CT Exp. - delta CT Co)	%	regulation=ratio 2^-deltadeltaCT
1 dpf/A	17,16	22,55	5,39		100%	**1x**
3 dpf/A	16,56	21,13	4,57	-0,82	176%	**1.76x**
5 dpf/A	16,93	22,54	5,61	0,22	86%	**0.86x**
1 dpf/B	16,03	23,7	7,67		100%	**1x**
3 dpf/B	17,05	22,67	5,62	-2,05	414%	**4.14x**
5 dpf/B	16,43	22,56	6,13	-1,54	290%	**2.9x**
1 dpf/C	16,45	23,29	6,84		100%	**1x**
3 dpf/C	15,05	20,52	5,47	-1,37	258%	**2.58x**
5 dpf/C	15,07	21,95	6,88	0,04	97%	**0.97x**

Embryonic stage / exp. group	$\bar{x}$ CT EF1α	$\bar{x}$ CT Thy-1	delta CT (CT Thy-1 - CT EF1α)	deltadelta CT (delta CT Exp. - delta CT Co)	%	regulation=ratio 2^-deltadeltaCT
1 dpf/B	19,11	23,7	4,59		100%	**1x**
3 dpf/B	19,26	22,67	3,41	-1,18	226%	**2.26x**
5 dpf/B	19,12	22,56	3,44	-1,15	221%	**2.21x**
1 dpf/C	19,19	23,29	4,1		100%	**1x**
3 dpf/C	17,75	20,52	2,77	-1,33	251%	**2.51x**
5 dpf/C	17,62	21,95	4,33	0,23	85%	**0.85x**

One-way ANOVA between developmental stages shows no significant difference in the case of Rpl13alpha:

Data sets analyzed	A : 1 dpf	B : 3 dpf	C : 5 dpf		
ANOVA summary					
F	2,825				
P value	0,1366				
P value summary	ns				
Significant diff. among means (P < 0.05)?	No				
R square	0,485				
Brown-Forsythe test					
F (DFn, DFd)	0,9289 (2, 6)				
P value	0,4452				
P value summary	ns				
Are SDs significantly different (P < 0.05)?	No				
Bartlett's test					
Bartlett's statistic (corrected)					
P value					
P value summary					
Are SDs significantly different (P < 0.05)?					
ANOVA table	SS	DF	MS	F (DFn, DFd)	P value
Treatment (between columns)	5,232	2	2,616	F (2, 6) = 2,825	P=0,1366
Residual (within columns)	5,556	6	0,9261		
Total	10,79	8			
Data summary					
Number of treatments (columns)	3				
Number of values (total)	9				

Ordinary one-way ANOVA between developmental stages shows no significant difference in the case of EF1alpha:

Data sets analyzed	A : 1 dpf	B : 3 dpf	C : 5 dpf		
ANOVA summary					
F	3,065				
P value	0,1884				
P value summary	ns				
Significant diff. among means (P < 0.05)?	No				
R square	0,6714				
Brown-Forsythe test					
F (DFn, DFd)	1,417e+031 (2, 3)				
P value	<0,0001				
P value summary	****				
Are SDs significantly different (P < 0.05)?	Yes				
Bartlett's test					
Bartlett's statistic (corrected)					
P value					
P value summary					
Are SDs significantly different (P < 0.05)?					
ANOVA table	SS	DF	MS	F (DFn, DFd)	P value
Treatment (between columns)	1,953	2	0,9767	F (2, 3) = 3,065	P=0,1884
Residual (within columns)	0,9561	3	0,3187		
Total	2,909	5			
Data summary					
Number of treatments (columns)	3				
Number of values (total)	6				

Figure 5.1.5.2 D: Thy-1 WB protein density quantification of Thy-1 MO-injected embryos

Zebrafish embryos (4dpf)	Control non-injected, protein density (AU), normalized to α-tub	Thy-1 MO 1 5 ng, protein density (AU), normalized to α-tub
Exp. 1 (n= ~30)	100	36,02335
Exp. 2 (n= ~30)	100	24,17064
Exp. 3 (n= ~30)	100	0,3161807
Mean ± SEM	**100 ± 0**	**20,17 ± 10,5**

One-sample t-test, analyzing if the mean of Thy-1 protein density in WB analysis after Thy-1 Mo injection differs from the hypothetical value “100% density” of the non-injected control, normalized to the housekeeping gene alpha-tubulin.

Number of values	3	3
Minimum	100	0,3162
25% Percentile	100	0,3162
Median	100	24,17
75% Percentile	100	36,02
Maximum	100	36,02
Mean	100	20,17
Std. Deviation	0	18,19
Std. Error of Mean	0	10,5
Lower 95% CI of mean	100	-25,01
Upper 95% CI of mean	100	65,35
Sum	300	60,51
One sample t test	Sample difference has zero SD	
Theoretical mean		100
Actual mean		20,17
Discrepancy		-79,83
95% CI of discrepancy		-125 to -34,65
t, df		t=7,603 df=2
P value (two tailed)		0,0169
Significant (alpha=0.05)?		Yes

9.4. Chapter 5.1.6: Characterization of the zebrafish Thy-1 mAb 89/9 in the goldfish

Figure 5.1.6 D: Thy-1 fluorescence intensity quantification in goldfish RGCs

Goldfish retinae	Control, fluorescence intensity (AU)	12d ONS, fluorescence intensity (AU)
Exp. 1	11.636	24.080, 40.965
Exp. 2	9.777	21.997, 17.738
Exp. 3	17.313	21.885, 32.042
Mean ± SEM	**12.909 ± 2.267**	**26451 ± 3.484**
%	**100**	**204,9**

Unpaired, two-tailed t-test

Column B	12d ONS
vs.	vs,
Column A	untreated
Unpaired t test	
P value	0,0381
P value summary	*
Significantly different (P < 0.05)?	Yes
One- or two-tailed P value?	Two-tailed
t, df	t=2,55 df=7
How big is the difference?	
Mean ± SEM of column A	12909 ± 2267, n=3
Mean ± SEM of column B	26451 ± 3484, n=6
Difference between means	13543 ± 5311
95% confidence interval	982,9 to 26102
R squared (eta squared)	0,4815
F test to compare variances	
F, DFn, Dfd	4,725, 5, 2
P value	0,3677
P value summary	ns
Significantly different (P < 0.05)?	No

9.5. Chapter 5.2: The neuronal role of Thy-1

Figure 5.2.1.1 B: Thy-1-GST promotes growth of zebrafish RGCs *in vitro*

Cultured primary RGCs	GST 8µg, $\overline{x}$ axon lengths, µm	Thy-1 4µg, $\overline{x}$ axon lengths, µm	Thy-1 6µg, $\overline{x}$ axon lengths, µm	Thy-1 8µg, $\overline{x}$ axon lengths, µm
Exp. 1	167,8	169,6	209,9	348,1
Exp. 2	140,0	248,6	245,8	246,2
Exp. 3	261,1		279,5	
Mean ± SEM	**171,9 ± 11,37**	**174,7 ± 12,45**	**253,5 ± 19,04**	**301,8 ± 35,92**
%	**100**	**101,6**	**147,5**	**175,6**
N neurons	**635**	**503**	**129**	**121**

One-way ANOVA between columns:

Data sets analyzed	A : GST 8 µg	B : Thy-1-GST 4 µg	C : Thy-1-GST 6 µg	D : Thy-1-GST 8 µg
ANOVA summary				
F	9,369			
P value	<0,0001			
P value summary	****			
Significant diff. among means (P < 0.05)?	Yes			
R square	0,0199			
Brown-Forsythe test				
F (DFn, DFd)	5,123 (3, 1384)			

P value	0,0016
P value summary	**
Are SDs significantly different (P < 0.05)?	Yes
Bartlett's test	
Bartlett's statistic (corrected)	48,33
P value	<0,0001
P value summary	****
Are SDs significantly different (P < 0.05)?	Yes

ANOVA table	SS	DF	MS	F (DFn, DFd)	P value
Treatment (between columns)	2354168	3	784723	F (3, 1384) = 9,369	P<0,0001
Residual (within columns)	115921165	1384	83758		
Total	118275333	1387			

Data summary	
Number of treatments (columns)	4
Number of values (total)	1388

Follow-up multiple comparison between means:

Number of families	1
Number of comparisons per family	6
Alpha	0,05

Tukey's multiple comparisons test	Mean Diff.	95,00% CI of diff.	Significant?	Summary	Adjusted P Value	
GST 8 µg vs. Thy-1-GST 4 µg	-2,77	-47,2 to 41,66	No	ns	0,9985	A-B
GST 8 µg vs. Thy-1-GST 6 µg	-81,61	-153,5 to -9,717	Yes	*	0,0187	A-C
GST 8 µg vs. Thy-1-GST 8 µg	-129,9	-203,7 to -56,05	Yes	****	<0,0001	A-D
Thy-1-GST 4 µg vs. Thy-1-GST 6 µg	-78,84	-152,3 to -5,372	Yes	*	0,0298	B-C
Thy-1-GST 4 µg vs. Thy-1-GST 8 µg	-127,1	-202,5 to -51,75	Yes	****	<0,0001	B-D
Thy-1-GST 6 µg vs. Thy-1-GST 8 µg	-48,28	-142,5 to 45,93	No	ns	0,5514	C-D

Test details	Mean 1	Mean 2	Mean Diff.	SE of diff.	n1	n2	q	DF
GST 8 µg vs. Thy-1-GST 4 µg	171,9	174,7	-2,77	17,27	635	503	0,2268	1384
GST 8 µg vs. Thy-1-GST 6 µg	171,9	253,5	-81,61	27,95	635	129	4,129	1384
GST 8 µg vs. Thy-1-GST 8 µg	171,9	301,8	-129,9	28,71	635	121	6,399	1384
Thy-1-GST 4 µg vs. Thy-1-GST 6 µg	174,7	253,5	-78,84	28,56	503	129	3,904	1384
Thy-1-GST 4 µg vs. Thy-1-GST 8 µg	174,7	301,8	-127,1	29,3	503	121	6,135	1384
Thy-1-GST 6 µg vs. Thy-1-GST 8 µg	253,5	301,8	-48,28	36,63	129	121	1,864	1384

Post test for linear trend	
Slope	39,42
P value	<0,0001
P value summary	****
Is linear trend significant (P < 0.05)?	Yes

ANOVA table	SS	DF	MS	R square (alerting)	R square (effect size)	F (DFn, DFd)	P value
Treatment (between columns)	2354168	3	784723				
Linear	2233162	1	2233162	0,9486	0,01888	F (1, 1384) = 26,66	P<0,0001
Nonlinear	121007	2	60503	0,0514	0,001023	F (2, 1384) = 0,7224	P=0,4858
Residual (within columns)	115921165	1384	83758				
Total	118275333	1387					

Correlation: Pearson r

GST 8 µg	Thy-1-GST 4 µg	Thy-1-GST 6 µg		Thy-1-GST 8 µg
GST 8 µg		-0,0514298028439693	-0,0618398386283175	-0,0729217097444666
Thy-1-GST 4 µg	-0,0514298028439693		-0,0564351754906771	-0,0338427523930808
Thy-1-GST 6 µg	-0,0618398386283175	-0,0564351754906771		-0,0520106311480992
Thy-1-GST 8 µg	-0,0729217097444666	-0,0338427523930808	-0,0520106311480992	

P-values

GST 8 µg	Thy-1-GST 4 µg	Thy-1-GST 6 µg		Thy-1-GST 8 µg
GST 8 µg		0,250064891204037	0,48630616917145	0,426688186121893
Thy-1-GST 4 µg	0,250064891204037		0,525266663433383	0,712491720617633
Thy-1-GST 6 µg	0,48630616917145	0,525266663433383		0,571011771026332
Thy-1-GST 8 µg	0,426688186121893	0,712491720617633	0,571011771026332	

Sample size

GST 8 µg	Thy-1-GST 4 µg	Thy-1-GST 6 µg	Thy-1-GST 8 µg	
GST 8 µg		502	129	121
Thy-1-GST 4 µg	502		129	121
Thy-1-GST 6 µg	129	129		121
Thy-1-GST 8 µg	121	121	121	

Figure 5.2.1.2 B: Knockdown of Thy-1 *in vitro* impairs neurite outgrowth of zebrafish RGCs

Cultured primary RGCs	Morpholino (µM)	$\bar{x}$ axon length (µm)	%	N neurons	
Exp. 1	Co MO (2)	508,2	100	46	
	Thy-1 (0,7)	410,7	80,80	60	
Exp. 2	Co MO (2)	202	100	41	
	Thy-1 (0,25)	200	99	130	
	Thy-1 (0,5)	184,3	91,20	168	
	Thy-1 (0,7)	164,2	81,30	119	
	Thy-1 (1)	152,1	75,30	35	
Exp. 3	Co MO (2)	240,1	100	177	
	Thy-1 (0,5)	203,6	84,80	168	
	Thy-1 (0,7)	191,9	79,90	195	
	Thy-1 (1)	172,8	72	138	
	Thy-1 (2)	149,6	62,30	59	
Exp. 4	Co MO (2)	253,4	100	196	
	Thy-1 (0,5)	226,2	89,30	132	
	Thy-1 (1)	184	72,60	124	
	Thy-1 (2)	200	78,90	135	
Exp. 5	Co MO (2)	353,7	100	291	
	Thy-1 (0,5)	272,2	77	90	
	Thy-1 (0,7)	290,2	82	181	
	Thy-1 (1)	303	85,70	283	
	Thy-1 (2)	266,2	75,40	327	
	0,25 µM	**0,5 µM**	**0,7 µM**	**1 µM**	**2 µM**
Mean ± SEM (normalized)	**99**	**85,58 ± 3,158**	**81 ± 0,4416**	**76,4 ± 3,182**	**72,2 ± 5,05**
N neurons	**130**	**558**	**555**	**480**	**521**
N experiments	**1**	**4**	**4**	**4**	**3**

Ordinary one-way ANOVA between columns:

Table Analyzed	Data 1				
Data sets analyzed	A : Co Mo 2 µM	B : Thy-1 Mo 0,25 µM	C : Thy-1 Mo 0,5 µM	D : Thy-1 Mo 0,7 µM	E : Thy-1 Mo 1 µM
ANOVA summary					
F	13,7				
P value	<0,0001				
P value summary	****				
Significant diff. among means (P < 0.05)?	Yes				
R square	0,8303				
ANOVA table	SS	DF	MS	F (DFn, DFd)	P value
Treatment (between columns)	1941	5	388,2	F (5, 14) = 13,7	P<0,0001
Residual (within columns)	396,6	14	28,33		
Total	2337	19			
Data summary					
Number of treatments (columns)	6				
Number of values (total)	20				

Post test for linear trend	
Slope	-5,748
P value	<0,0001
P value summary	****
Is linear trend significant (P < 0.05)?	Yes

ANOVA table	SS	DF	MS	R square (alerting)	R square (effect size)	F (DFn, DFd)	P value
Treatment (between columns)	1941	5	388,2				
Linear	1697	1	1697	0,8742	0,7259	F (1, 14) = 59,89	P<0,0001
Nonlinear	244,2	4	61,05	0,1258	0,1045	F (4, 14) = 2,155	P=0,1276
Residual (within columns)	396,6	14	28,33				
Total	2337	19					

One-sample t-test to analyze if the means differ from the hypothetical value “100” (normalized to the control):

	Co Mo 2 µM	Thy-1 Mo 0.25 µM	Thy-1 Mo 0.5 µM	Thy-1 Mo 0.7 µM	Thy-1 Mo 1 µM	Thy-1 Mo 2 µM
Number of values	4	1	4	4	4	3
Minimum	100	99	77	79,9	72	62,3
25% Percentile	100	99	78,95	80,13	72,15	62,3
Median	100	99	87,05	81,05	73,95	75,4
75% Percentile	100	99	90,73	81,83	83,1	78,9
Maximum	100	99	91,2	82	85,7	78,9
Mean	100	99	85,58	81	76,4	72,2
Std. Deviation	0	0	6,315	0,8832	6,364	8,75
Std. Error of Mean	0	0	3,158	0,4416	3,182	5,052
Lower 95% CI of mean	100		75,53	79,59	66,27	50,46
Upper 95% CI of mean	100		95,62	82,41	86,53	93,94
Sum	400	99	342,3	324	305,6	216,6
One sample t test	Sample difference has zero SD	Too few points				
Theoretical mean			100	100	100	100
Actual mean			85,58	81	76,4	72,2
Discrepancy			-14,43	-19	-23,6	-27,8
95% CI of discrepancy			-24,47 to -4,376	-20,41 to -17,59	-33,73 to -13,47	-49,54 to -6,063
t, df			t=4,568 df=3	t=43,03 df=3	t=7,417 df=3	t=5,503 df=2
P value (two tailed)			0,0197	<0,0001	0,0051	0,0315
Significant (alpha=0.05)?			Yes	Yes	Yes	Yes

Correlation: Pearson r

	Co Mo 2 µM	Thy-1 Mo 0.25 µM	Thy-1 Mo 0.5 µM	Thy-1 Mo 0.7 µM	Thy-1 Mo 1 µM	Thy-1 Mo 2 µM
Co Mo 2 µM						
Thy-1 Mo 0.25 µM						
Thy-1 Mo 0.5 µM				-0,405200479734533	-0,801856563603523	-0,851144313111891
Thy-1 Mo 0.7 µM			-0,405200479734533		0,864098963310909	-0,884331662291007
Thy-1 Mo 1 µM			-0,801856563603523	0,864098963310909		-0,999554689855083
Thy-1 Mo 2 µM			-0,851144313111891	-0,884331662291007	-0,999554689855083	

P-values

	Co Mo 2 µM	Thy-1 Mo 0.25 µM	Thy-1 Mo 0.5 µM	Thy-1 Mo 0.7 µM	Thy-1 Mo 1 µM	Thy-1 Mo 2 µM
Co Mo 2 µM						
Thy-1 Mo 0.25 µM						
Thy-1 Mo 0.5 µM				0,594799520265468	0,198143436396469	0,351818331592247
Thy-1 Mo 0.7 µM			0,594799520265468		0,135901036689088	0,309229029774859
Thy-1 Mo 1 µM			0,198143436396469	0,135901036689088		0,0189995157944067
Thy-1 Mo 2 µM			0,351818331592247	0,309229029774859	0,0189995157944067	

Sample size

Co Mo 2 µM	Thy-1 Mo 0.25 µM	Thy-1 Mo 0.5 µM	Thy-1 Mo 0.7 µM	Thy-1 Mo 1 µM	Thy-1 Mo 2 µM	
Co Mo 2 µM						
Thy-1 Mo 0.25 µM						
Thy-1 Mo 0.5 µM				4	4	3
Thy-1 Mo 0.7 µM			4		4	3
Thy-1 Mo 1 µM			4	4		3
Thy-1 Mo 2 µM			3	3	3	

Figure 5.2.1.3 B: Knockdown of Thy-1 *in vitro* impairs differentiation of zebrafish RGCs

Cultured primary RGCs	Morpholino (2 µM)	N total neurons	N undifferentiated neurons	undifferentiated neurons, %
Exp. 1	Co MO	35	4	**11,4**
	Thy-1 MO 1	102	21	**20,6**
Exp. 2	Co MO	123	11	**8,9**
	Thy-1 MO 1	22	12	**54,5**
Exp. 3	Co MO	151	20	**13,2**
	Thy-1 MO 1	113	32	**32,9**
Exp. 4	Co MO	87	17	**19,5**
	Thy-1 MO 1	102	31	**30,4**
undifferentiated neurons	**Control MO (2 µM)**		**Thy-1 MO 1 (2 µM)**	
Mean (%)	**13,25**		**34,6**	

Unpaired, two-tailed t-test

Column B	Thy-1 Mo 2 µM
vs.	vs,
Column A	Co Mo 2 µM
Unpaired t test	
P value	0,0292
P value summary	*
Significantly different (P < 0.05)?	Yes
One- or two-tailed P value?	Two-tailed
t, df	t=2,849 df=6
How big is the difference?	
Mean ± SEM of column A	13,25 ± 2,262, n=4
Mean ± SEM of column B	34,6 ± 7,145, n=4
Difference between means	21,35 ± 7,494
95% confidence interval	3,012 to 39,69
R squared (eta squared)	0,575
F test to compare variances	
F, DFn, Dfd	9,975, 3, 3
P value	0,0908
P value summary	ns
Significantly different (P < 0.05)?	No

Figure 5.2.2.1 B: Knockdown of Thy-1 *in vivo* impairs axonal outgrowth of zebrafish retinal explants *in vitro*

Cultured retinal explants	**Co MO, 70 µM, 1 dic, $\bar{x}$ axons / explant**	**Co MO, 70 µM, 2 dic, $\bar{x}$ axons / explant**	**Thy-1 MO 1, 70 µM, 1 dic, $\bar{x}$ axons / explant**	**Thy-1 MO 1, 70 µM, 2 dic, $\bar{x}$ axons / explant**	**Thy-1 MO 2, 70 µM, 1 dic, $\bar{x}$ axons / explant**	**Thy-1 MO 2, 70 µM, 2 dic, $\bar{x}$ axons / explant**
Exp. 1	30,2	60,6	14,9	44,9	30,4	--
Exp. 2	58	--	32,2	--	33,1	--
Exp. 3	39,5	65,5	--	--		--
Exp. 4	39,6	--	--	--		--
Mean ± SEM	**41,7 ± 1,9**	**63,1**	**23,1 ± 1,7**	**44,9**	**31,6 ± 1,96**	**--**
%	**100**	**100**	**56,5**	**71,2**	**76**	**--**
N explants	**167**		**103**		**92**	
Cultured retinal explants	**Co MO, 140 µM, 1 dic, $\bar{x}$ axons / explant**	**Co MO, 140 µM, 2 dic, $\bar{x}$ axons / explant**	**Thy-1 MO 1, 140 µM, 1 dic, $\bar{x}$ axons / explant**	**Thy-1 MO 1, 140 µM, 2 dic, $\bar{x}$ axons / explant**	**Thy-1 MO 2, 140 µM, 1 dic, $\bar{x}$ axons / explant**	**Thy-1 MO 2, 140 µM, 2 dic, $\bar{x}$ axons / explant**
Exp. 1	53,2	81,3	7,7	54,2	10,1	47,8
Exp. 2	23,7	51,5	16,4	44,3	16	47,6
Exp. 3	61,3	85,2	--	--	--	--
Exp. 4	37,9	77,1	--	--	--	--
Mean ± SEM	**49,8 ± 2,23**	**78,7 ± 1,9**	**12,4 ± 1,78**	**49,1 ± 3,5**	**13,2 ± 1,23**	**47,7 ± 2,09**
%	**100**	**100**	**27,5**	**66,8**	**29,8**	**64,6**
N explants	**125**		**56**		**99**	

Two-way ANOVA between groups 70 and 140 µM of control and Thy-1 morpholino sequences 1 and 2

Table Analyzed	raw grouped				
Two-way ANOVA	Ordinary				
Alpha	0,05				
Source of Variation	% of total variation	P value	P value summary	Significant?	
Interaction	3,174	<0,0001	****	Yes	
Row Factor	20,02	<0,0001	****	Yes	
Column Factor	21	<0,0001	****	Yes	
ANOVA table	SS	DF	MS	F (DFn, DFd)	P value
Interaction	24739	4	6185	F (4, 915) = 13,91	P<0,0001
Row Factor	156011	2	78005	F (2, 915) = 175,5	P<0,0001
Column Factor	163653	2	81826	F (2, 915) = 184	P<0,0001
Residual	406798	915	444,6		
Number of missing values	579				

Follow-up multiple comparisons between means of rows and columns

Compare cell means regardless of rows and columns					
Number of families	1				
Number of comparisons per family	36				
Alpha	0,05				
Tukey's multiple comparisons test	Mean Diff,	95,00% CI of diff,	Significant?	Summary	Adjusted P Value
70 µM 1 dic:Co MO vs. 70 µM 1 dic:Thy-1 Mo 1	18,53	10,32 to 26,75	Yes	****	<0,0001
70 µM 1 dic:Co MO vs. 70 µM 1 dic:Thy-1 MO 2	10,02	1,505 to 18,53	Yes	**	0,0082
70 µM 1 dic:Co MO vs. 140 µM 1 dic:Co MO	-8,149	-15,9 to -0,3956	Yes	*	0,0308
70 µM 1 dic:Co MO vs. 140 µM 1 dic:Thy-1 Mo 1	29,28	19,16 to 39,41	Yes	****	<0,0001
70 µM 1 dic:Co MO vs. 140 µM 1 dic:Thy-1 MO 2	28,49	20,17 to 36,8	Yes	****	<0,0001
70 µM 1 dic:Co MO vs. 140 µM 2 dic:Co MO	-37,03	-44,62 to -29,44	Yes	****	<0,0001
70 µM 1 dic:Co MO vs. 140 µM 2 dic:Thy-1 Mo 1	-7,397	-17,66 to 2,866	No	ns	0,3799
70 µM 1 dic:Co MO vs. 140 µM 2 dic:Thy-1 MO 2	-6,029	-14,51 to 2,453	No	ns	0,3998
70 µM 1 dic:Thy-1 Mo 1 vs. 70 µM 1 dic:Thy-1 MO 2	-8,515	-17,92 to 0,8894	No	ns	0,1123
70 µM 1 dic:Thy-1 Mo 1 vs. 140 µM 1 dic:Co MO	-26,68	-35,41 to -17,96	Yes	****	<0,0001
70 µM 1 dic:Thy-1 Mo 1 vs. 140 µM 1 dic:Thy-1 Mo 1	10,75	-0,1335 to 21,64	No	ns	0,0559
70 µM 1 dic:Thy-1 Mo 1 vs. 140 µM 1 dic:Thy-1 MO 2	9,954	0,7273 to 19,18	Yes	*	0,0234
70 µM 1 dic:Thy-1 Mo 1 vs. 140 µM 2 dic:Co MO	-55,56	-64,14 to -46,99	Yes	****	<0,0001
70 µM 1 dic:Thy-1 Mo 1 vs. 140 µM 2 dic:Thy-1 Mo 1	-25,93	-36,94 to -14,91	Yes	****	<0,0001
70 µM 1 dic:Thy-1 Mo 1 vs. 140 µM 2 dic:Thy-1 MO 2	-24,56	-33,94 to -15,18	Yes	****	<0,0001
70 µM 1 dic:Thy-1 MO 2 vs. 140 µM 1 dic:Co MO	-18,17	-27,17 to -9,161	Yes	****	<0,0001
70 µM 1 dic:Thy-1 MO 2 vs. 140 µM 1 dic:Thy-1 Mo 1	19,27	8,155 to 30,38	Yes	****	<0,0001
70 µM 1 dic:Thy-1 MO 2 vs. 140 µM 1 dic:Thy-1 MO 2	18,47	8,976 to 27,96	Yes	****	<0,0001
70 µM 1 dic:Thy-1 MO 2 vs. 140 µM 2 dic:Co MO	-47,05	-55,91 to -38,18	Yes	****	<0,0001
70 µM 1 dic:Thy-1 MO 2 vs. 140 µM 2 dic:Thy-1 Mo 1	-17,41	-28,65 to -6,176	Yes	****	<0,0001
70 µM 1 dic:Thy-1 MO 2 vs. 140 µM 2 dic:Thy-1 MO 2	-16,05	-25,69 to -6,407	Yes	****	<0,0001
140 µM 1 dic:Co MO vs. 140 µM 1 dic:Thy-1 Mo 1	37,43	26,89 to 47,97	Yes	****	<0,0001
140 µM 1 dic:Co MO vs. 140 µM 1 dic:Thy-1 MO 2	36,64	27,82 to 45,46	Yes	****	<0,0001
140 µM 1 dic:Co MO vs. 140 µM 2 dic:Co MO	-28,88	-37,02 to -20,74	Yes	****	<0,0001
140 µM 1 dic:Co MO vs. 140 µM 2 dic:Thy-1 Mo 1	0,7524	-9,923 to 11,43	No	ns	>0,9999
140 µM 1 dic:Co MO vs. 140 µM 2 dic:Thy-1 MO 2	2,12	-6,858 to 11,1	No	ns	0,9983
140 µM 1 dic:Thy-1 Mo 1 vs. 140 µM 1 dic:Thy-1 MO 2	-0,7967	-11,76 to 10,17	No	ns	>0,9999
140 µM 1 dic:Thy-1 Mo 1 vs. 140 µM 2 dic:Co MO	-66,31	-76,73 to -55,89	Yes	****	<0,0001
140 µM 1 dic:Thy-1 Mo 1 vs. 140 µM 2 dic:Thy-1 Mo 1	-36,68	-49,18 to -24,18	Yes	****	<0,0001
140 µM 1 dic:Thy-1 Mo 1 vs. 140 µM 2 dic:Thy-1 MO 2	-35,31	-46,4 to -24,22	Yes	****	<0,0001
140 µM 1 dic:Thy-1 MO 2 vs. 140 µM 2 dic:Co MO	-65,52	-74,19 to -56,84	Yes	****	<0,0001
140 µM 1 dic:Thy-1 MO 2 vs. 140 µM 2 dic:Thy-1 Mo 1	-35,88	-46,97 to -24,79	Yes	****	<0,0001
140 µM 1 dic:Thy-1 MO 2 vs. 140 µM 2 dic:Thy-1 MO 2	-34,52	-43,98 to -25,05	Yes	****	<0,0001
140 µM 2 dic:Co MO vs. 140 µM 2 dic:Thy-1 Mo 1	29,63	19,08 to 40,19	Yes	****	<0,0001
140 µM 2 dic:Co MO vs. 140 µM 2 dic:Thy-1 MO 2	31	22,17 to 39,84	Yes	****	<0,0001
140 µM 2 dic:Thy-1 Mo 1 vs. 140 µM 2 dic:Thy-1 MO 2	1,367	-9,849 to 12,58	No	ns	>0,9999

Figure 5.2.2.2 C&D: Knockdown of Thy-1 impairs zebrafish optic nerve regeneration *in vivo*

Zebrafish retinae	$\bar{x}$ Alexa-488-labeled RGCs in 200.000 µm² / retina
1 Co MO, 140 µM	33
2 Co MO, 140 µM	34,2
3 Co MO, 140 µM	29,2
4 Co MO, 140 µM	25,4
5 Co MO, 140 µM	41,6
6 Co MO, 140 µM	42,8
7 Co MO, 140 µM	32,3
8 Co MO, 140 µM	36
9 Co MO, 140 µM	41,8
10 Co MO, 140 µM	64,6
Sum	**380,9**
Mean ± SEM	**38,09 ± 3,448**
%	**100**
N retinae	**10**

Zebrafish retinae	$\bar{x}$ Alexa-488-labeled RGCs in 200.000 µm² / retina
1 Thy-1 MO, 140 µM	8,1
2 Thy-1 MO, 140 µM	16
3 Thy-1 MO, 140 µM	13,75
4 Thy-1 MO, 140 µM	12,8
5 Thy-1 MO, 140 µM	12,8
6 Thy-1 MO, 140 µM	12,3
7 Thy-1 MO, 140 µM	19,4
8 Thy-1 MO, 140 µM	10,4
9 Thy-1 MO, 140 µM	15,6
10 Thy-1 MO, 140 µM	11,5
Sum	**132,65**
Mean ± SEM	**13,27 ± 1,001**
%	**35**
N retinae	**10**

Unpaired, two-tailed t-test

Column B	Thy-1 Mo 140 µM
vs.	vs,
Column A	Co Mo 140 µM
Unpaired t test	
P value	<0,0001
P value summary	****
Significantly different (P < 0.05)?	Yes
One- or two-tailed P value?	Two-tailed
t, df	t=6,914 df=18
How big is the difference?	
Mean ± SEM of column A	38,09 ± 3,448, n=10
Mean ± SEM of column B	13,27 ± 1,001, n=10
Difference between means	-24,83 ± 3,59
95% confidence interval	-32,37 to -17,28
R squared (eta squared)	0,7265
F test to compare variances	
F, DFn, Dfd	11,87, 9, 9
P value	0,0011
P value summary	**
Significantly different (P < 0.05)?	Yes

Welch`s test (unequal variances t-test)

Column B	Thy-1 Mo 140 µM
vs.	vs,
Column A	Co Mo 140 µM
Unpaired t test with Welch's correction	
P value	<0,0001
P value summary	****
Significantly different (P < 0.05)?	Yes
One- or two-tailed P value?	Two-tailed
Welch-corrected t, df	t=6,914 df=10,51
How big is the difference?	
Mean ± SEM of column A	38,09 ± 3,448, n=10
Mean ± SEM of column B	13,27 ± 1,001, n=10
Difference between means	-24,83 ± 3,59
95% confidence interval	-32,77 to -16,88
R squared (eta squared)	0,8198
F test to compare variances	
F, DFn, Dfd	11,87, 9, 9
P value	0,0011
P value summary	**
Significantly different (P < 0.05)?	Yes

Zebrafish retinae	**$\bar{x}$ fluorescence intensity Alexa-488 (AU) in 200.000 µm² / retina**
1 Co MO, 140 µM	11,2
2 Co MO, 140 µM	4,7
3 Co MO, 140 µM	10,9
4 Co MO, 140 µM	6,8
5 Co MO, 140 µM	28,4
6 Co MO, 140 µM	16,4
7 Co MO, 140 µM	16
8 Co MO, 140 µM	18,9
9 Co MO, 140 µM	13,1
10 Co MO, 140 µM	27
Sum	**153,4**
Mean ± SEM	**15,34 ± 2,469**
%	**100**

Zebrafish retinae	**$\bar{x}$ fluorescence intensity Alexa-488 (AU) in 200.000 µm² / retina**
1 Thy-1 MO, 140 µM	7,5
2 Thy-1 MO, 140 µM	3,2
3 Thy-1 MO, 140 µM	4,1
4 Thy-1 MO, 140 µM	3,2
5 Thy-1 MO, 140 µM	9,3
6 Thy-1 MO, 140 µM	4,9
7 Thy-1 MO, 140 µM	6,9
8 Thy-1 MO, 140 µM	4
9 Thy-1 MO, 140 µM	5,4
10 Thy-1 MO, 140 µM	5,8
Sum	**54,3**
Mean ± SEM	**5,43 ± 0,6289**
%	**35,4**

Unpaired, two-tailed t-test

Column B	Thy-1 Mo 140 µM
vs.	vs,
Column A	Co Mo 140 µM
Unpaired t test	
P value	0,0011
P value summary	**
Significantly different (P < 0.05)?	Yes
One- or two-tailed P value?	Two-tailed
t, df	t=3,889 df=18
How big is the difference?	
Mean ± SEM of column A	15,34 ± 2,469, n=10
Mean ± SEM of column B	5,43 ± 0,6289, n=10
Difference between means	-9,91 ± 2,548
95% confidence interval	-15,26 to -4,557
R squared (eta squared)	0,4566
F test to compare variances	
F, DFn, Dfd	15,41, 9, 9
P value	0,0004
P value summary	***
Significantly different (P < 0.05)?	Yes

Welch`s test (unequal variances t-test)

Column B	Thy-1 Mo 140 µM
vs.	vs,
Column A	Co Mo 140 µM
Unpaired t test with Welch's correction	
P value	0,0029
P value summary	**
Significantly different (P < 0.05)?	Yes
One- or two-tailed P value?	Two-tailed
Welch-corrected t, df	t=3,889 df=10,16
How big is the difference?	
Mean ± SEM of column A	15,34 ± 2,469, n=10
Mean ± SEM of column B	5,43 ± 0,6289, n=10
Difference between means	-9,91 ± 2,548
95% confidence interval	-15,58 to -4,245
R squared (eta squared)	0,5981
F test to compare variances	
F, DFn, Dfd	15,41, 9, 9
P value	0,0004
P value summary	***
Significantly different (P < 0.05)?	Yes

Figure 5.2.3 C: Overexpression of Thy-1-EGFP enhances axonal outgrowth of mouse hippocampal neurons *in vitro*

Primary hippocampal neurons	**Control-EGFP $\bar{x}$ axon length (µm)**	**Thy-1-EGFP $\bar{x}$ axon length (µm)**
Exp. 1	673,1	903,6
Exp. 2	437	619
Mean ± SEM	**507 ± 41,58**	**696,7 ± 58,07**
%	**100**	**137,5**
N neurons	**101**	**110**

Unpaired, two-tailed t-test

Column B	Thy-1 EGFP
vs.	vs,
Column A	EGFP
Unpaired t test	
P value	0,0096
P value summary	**
Significantly different (P < 0.05)?	Yes
One- or two-tailed P value?	Two-tailed
t, df	t=2,615 df=209
How big is the difference?	
Mean ± SEM of column A	507 ± 41,58, n=101
Mean ± SEM of column B	696,7 ± 58,07, n=110
Difference between means	189,7 ± 72,53
95% confidence interval	46,7 to 332,7
R squared (eta squared)	0,03169
F test to compare variances	
F, DFn, Dfd	2,124, 109, 100
P value	0,0002
P value summary	***
Significantly different (P < 0.05)?	Yes

Welch`s test (unequal variances t-test)

Column B	Thy-1 EGFP
vs.	vs,
Column A	EGFP
Unpaired t test with Welch's correction	
P value	0,0086
P value summary	**
Significantly different (P < 0.05)?	Yes
One- or two-tailed P value?	Two-tailed
Welch-corrected t, df	t=2,656 df=193,9
How big is the difference?	
Mean ± SEM of column A	507 ± 41,58, n=101
Mean ± SEM of column B	696,7 ± 58,07, n=110
Difference between means	189,7 ± 71,42
95% confidence interval	48,82 to 330,5
R squared (eta squared)	0,0351
F test to compare variances	
F, DFn, Dfd	2,124, 109, 100
P value	0,0002
P value summary	***
Significantly different (P < 0.05)?	Yes

Figure 5.2.3 E: SiRNA-mediated knockdown of Thy-1 impairs axonal outgrowth of mouse hippocampal neurons *in vitro*

Primary hippocampal neurons	siCo $\bar{x}$ axon length (µm)	siThy-1 $\bar{x}$ axon length (µm)
Exp. 1	250,5	206,3
Exp. 2	569,6	374,6
Exp. 3	309,7	260,9
Mean ± SEM	**399,3 ± 22,95**	**304,8 ± 17,56**
%	**100**	**76,3**
N neurons	**184**	**107**

Unpaired, two-tailed t-test

Column B	siThy-1
vs.	vs,
Column A	siCo
Unpaired t test	
P value	0,0044
P value summary	**
Significantly different (P < 0.05)?	Yes
One- or two-tailed P value?	Two-tailed
t, df	t=2,87 df=289
How big is the difference?	
Mean ± SEM of column A	399,3 ± 22,95, n=184
Mean ± SEM of column B	304,8 ± 17,56, n=107
Difference between means	-94,56 ± 32,95
95% confidence interval	-159,4 to -29,71
R squared (eta squared)	0,02771
F test to compare variances	
F, DFn, Dfd	2,937, 183, 106
P value	<0,0001
P value summary	****
Significantly different (P < 0.05)?	Yes

Welch`s test (unequal variances t-test)

Column B	siThy-1
vs.	vs,
Column A	siCo
Unpaired t test with Welch's correction	
P value	0,0012
P value summary	**
Significantly different (P < 0.05)?	Yes
One- or two-tailed P value?	Two-tailed
Welch-corrected t, df	t=3,273 df=289
How big is the difference?	
Mean ± SEM of column A	399,3 ± 22,95, n=184
Mean ± SEM of column B	304,8 ± 17,56, n=107
Difference between means	-94,56 ± 28,9
95% confidence interval	-151,4 to -37,69
R squared (eta squared)	0,03574
F test to compare variances	
F, DFn, Dfd	2,937, 183, 106
P value	<0,0001
P value summary	****
Significantly different (P < 0.05)?	Yes

9.6. Chapter 5.3.1: Specificity of the zebrafish PrP-2 pAb 981

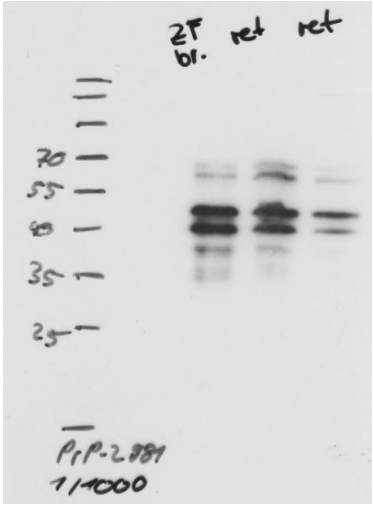

Figure 9.6 Characterization of the zebrafish PrP-2 pAb 981 in WB. The pAb 981 against zebrafish PrP-2 shows several bands in WB analysis of zebrafish brain (br.) and retina (ret.) lysates. The predicted size of zebrafish PrP-2 is ~70 kDa. Most prominent bands appear between 50 and 40 kDa, depending on the degree of protein degradation and the experimental conditions.

9.7. Chapter 5.3.1: Analysis of PrP-2 expression upon ONS in zebrafish RGCs

(Re-) arrangement of PrP-2 and its optic nerve lesion-induced up-regulation

Figure 9.7 below shows the confocal scan of the zebrafish RGC layer. The single planes of the confocal Z-stack are displayed. They illustrate the reorganization and accumulation of PrP-2 upon ONL from a ring-shaped, membranous pattern into big, diffuse clusters, probably in specialized signaling rafts at the cell surface and maybe also in cytoplasmic signaling vesicles. After ONL, zebrafish RGCs survived and stayed intact during the preparation, as demonstrated by the Dapi staining of the nuclei.

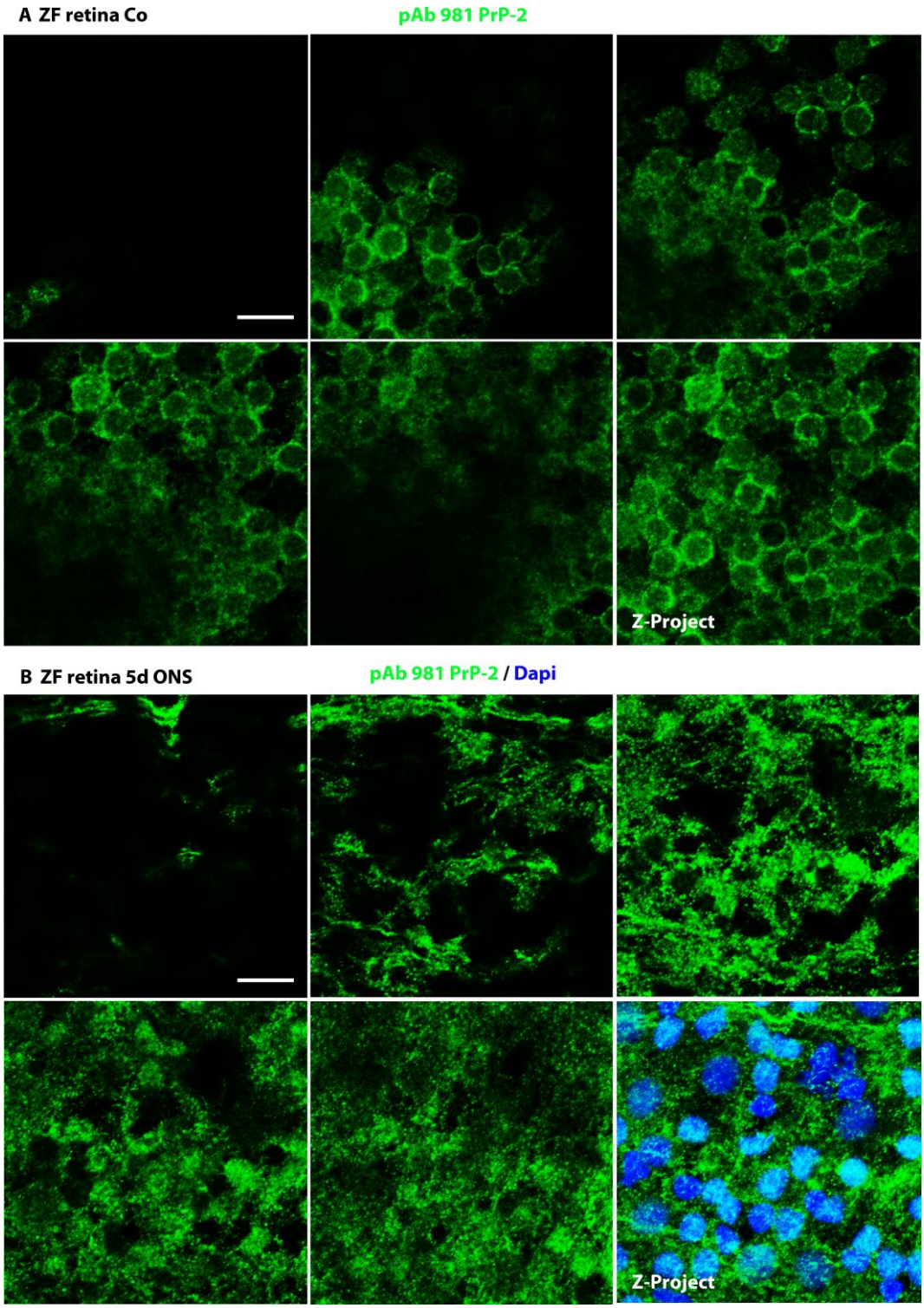

Figure 9.7 Characterization of the pAb PrP-2 981 pattern in zebrafish retinae. A. Control retina. Immunostaining of PFA-fixed tissue shows a circular, membranous pattern of PrP-2 in RGCs throughout all confocal stacks.PrP-2 accumulates at cell-cell-contacts. **B.** Upon ONL, PrP-2 becomes quantitatively increased and reorganized in the cell bodies in big protein clusters (PrP-2 green, Dapi blue). Scale bars: 25 µm. Images collected at 1.21 µm intervals in a depth of 8.46 µm for **A** and at 1.05 µm intervals in a depth of 7.35 µm for

Figure 5.3.1 G: IHC: PrP-2 fluorescence intensity quantification

Zebrafish retinae	Co, fluorescence intensity (AU)	5d ONS, fluorescence intensity (AU)
Exp. 1	19.075	30.959
	20.606	60.553
Exp. 2	18.808	69.848
	19.147	62.066
Exp.3	20.598	53.289
	14.131	61.035
Mean ± SEM	**18.728 ± 974**	**56.292 ± 5.503**
%	**100**	**300,6**
N retinae	**6**	**6**

Unpaired, two-tailed t-test

Column B	5d ONS
vs.	vs,
Column A	Co
Unpaired t test	
P value	<0,0001
P value summary	****
Significantly different (P < 0.05)?	Yes
One- or two-tailed P value?	Two-tailed
t, df	t=6,721 df=10
How big is the difference?	
Mean ± SEM of column A	18728 ± 974, n=6
Mean ± SEM of column B	56292 ± 5503, n=6
Difference between means	37564 ± 5589
95% confidence interval	25112 to 50016
R squared (eta squared)	0,8188
F test to compare variances	
F, DFn, Dfd	31,92, 5, 5
P value	0,0017
P value summary	**
Significantly different (P < 0.05)?	Yes

Welch`s test (unequal variances t-test)

Column B	5d ONS
vs.	vs,
Column A	Co
Unpaired t test with Welch's correction	
P value	0,0009
P value summary	***
Significantly different (P < 0.05)?	Yes
One- or two-tailed P value?	Two-tailed
Welch-corrected t, df	t=6,721 df=5,313
How big is the difference?	
Mean ± SEM of column A	18728 ± 974, n=6
Mean ± SEM of column B	56292 ± 5503, n=6
Difference between means	37564 ± 5589
95% confidence interval	23449 to 51679
R squared (eta squared)	0,8948
F test to compare variances	
F, DFn, Dfd	31,92, 5, 5
P value	0,0017
P value summary	**
Significantly different (P < 0.05)?	Yes

Figure 5.3.1 H: PrP-2 protein density quantification in WBs

Zebrafish retinae	Control, protein density (AU), normalized to α-tubulin	5d ONS, protein density (AU), normalized to α-tubulin
Exp. 1	61.407	102.266

9.8. Chapter 5.3.2: MO-mediated knockdown of PrP-2, quantification of protein levels in zebrafish RGCs

Figure 5.3.2. D: IHC, PrP-2 protein fluorescence intensity quantification in zebrafish retinae

Zebrafish retinae	Control MO 140 µM, fluorescence intensity (AU)	PrP-2 MO 1 140 µM, fluorescence intensity (AU)	PrP-2 MO 2 140 µM, fluorescence intensity (AU)
Exp. 1	37.645	--	--
	46.374	--	--
	45.002	--	--
	52.121	--	--
	34.423	--	--
	--	--	--
Exp. 2	42.844	32.143	--
	39.743	43.502	--
	49.921	23.966	--
	--	21.436	--
	--	26.297	--
	--	27.093	--
Exp. 3	27.746	26.001	--
	31.220	24.889	--
	23.033	14.619	--
	28.307	20.203	--
	28.046	23.389	--
Exp. 4	--	14.697	20.170
	--	12.334	16.241
	--	13.300	20.876
	--	16.232	21.420
	--	9.491	--
	--	9.944	--
Mean ± SEM	**37.417 ± 2.611**	**21.149 ± 2.138**	**19.677 ± 1.173**
%	**100**	**56,4**	**52,6**
N retinae	**13**	**17**	**4**

One-way ANOVA

ANOVA summary					
F	14,72				
P value	<0,0001				
P value summary	****				
Significant diff. among means (P < 0.05)?	Yes				
R square	0,487				
Brown-Forsythe test					
F (DFn, DFd)	2,861 (2, 31)				
P value	0,0724				
P value summary	ns				
Are SDs significantly different (P < 0.05)?	No				
Bartlett's test					
Bartlett's statistic (corrected)	4,878				
P value	0,0872				
P value summary	ns				
Are SDs significantly different (P < 0.05)?	No				
ANOVA table	SS	DF	MS	F (DFn, DFd)	P value
Treatment (between columns)	2205922456	2	1102961228	F (2, 31) = 14,72	P<0,0001
Residual (within columns)	2323395042	31	74948227		
Total	4529317498	33			
Data summary					
Number of treatments (columns)	3				
Number of values (total)	34				

Follow-up multiple comparison between means

Number of families	1							
Number of comparisons per family	3							
Alpha	0,05							
Tukey's multiple comparisons test	Mean Diff,	95,00% CI of diff,	Significant?	Summary	Adjusted P Value			
Co Mo vs. PrP-2 Mo 1	16268	8418 to 24119	Yes	****	<0,0001	A-B		
Co Mo vs. PrP-2 Mo 2	17741	5558 to 29923	Yes	**	0,0032	A-C		
PrP-2 Mo 1 vs. PrP-2 Mo 2	1472	-10368 to 13313	No	ns	0,9498	B-C		
Test details	Mean 1	Mean 2	Mean Diff,	SE of diff,	n1	n2	q	DF
Co Mo vs. PrP-2 Mo 1	37417	21149	16268	3190	13	17	7,213	31
Co Mo vs. PrP-2 Mo 2	37417	19677	17741	4950	13	4	5,068	31
PrP-2 Mo 1 vs. PrP-2 Mo 2	21149	19677	1472	4811	17	4	0,4328	31

9.9. Chapter 5.4: The neuronal role of PrP-2

Figure 5.4.1.1 C: Knockdown of PrP-2 *in vitro* impairs neurite outgrowth of zebrafish RGCs

Cultured primary RGCs	Morpholino (µM)	$\bar{x}$ axon length (µm)	%	N neurons
Exp. 1	Co MO (2)	202	100	41
	PrP-2 MO 1 (0,5)	147,6	73,1	104
	PrP-2 MO 2, (0,5)	167,5	82,9	111
	PrP-2 MO 1&2 (0,5)	156,5	77,5	71
Exp. 2	Co MO (2)	170,0	100	79
	PrP-2 MO 1 (1)	118,1	69,5	54
	PrP-2 MO 2 (1)	137,4	80,2	67
Exp. 3	Co MO (2)	253,4	100	196
	PrP-2 MO 1 (1)	161,3	63,7	147
	PrP-2 MO 2 (1)	190,1	75	142
	PrP-2 MO 1&2 (1)	194,4	76,7	144
	PrP-2 MO 2 (2)	168,3	66,4	133
	PrP-2 MO 1&2 (2)	158,6	62,6	123
Exp. 4	Co MO (2)	353,7	100	291
	PrP-2 MO 1 (1)	263,5	74,5	268
	PrP-2 MO 2 (1)	271,3	76,7	196
	PrP-2 MO 1&2 (1)	266,6	75,4	223
	PrP-2 MO 1 (2)	246,8	69,8	297
	PrP-2 MO 2 (2)	267,2	75,5	191
	PrP-2 MO 1&2 (2)	275,0	77,7	237

Morpholino (µM)	Mean ± SEM (normalized)	N neurons	N experiments
Co MO (2)	**--**	**607**	**4**
PrP-2 MO 1 (0,5)	**73,7**	**104**	**1**
PrP-2 MO 2 (0,5)	**82,9**	**111**	**1**
PrP-2 MO 1&2 (0,5)	**77,5**	**71**	**1**
PrP-2 MO 1 (1)	**69,1 ± 3,092**	**469**	**3**
PrP-2 MO 2 (1)	**77,43 ± 1,641**	**405**	**3**
PrP-2 MO 1&2 (1)	**75,85 ± 0,75**	**367**	**2**
PrP-2 MO 1 (2)	**69,8**	**297**	**1**
PrP-2 MO 2 (2)	**70,9 ± 4,5**	**324**	**2**
PrP-2 MO 1&2 (2)	**70,1 ± 7,6**	**360**	**2**

Two-way ANOVA between grouped data, concentrations and PrP-2 morpholino sequences 1, 2 or 1&2

	MO concentration (µM)	CO MO	PrP-2 MO 1			PrP-2 MO 2			PrP-2 MO 1&2	
0,5 µM	0,5	100	73,1			82,9			77,5	
1 µM	1	100	69,5	63,7	74,5	80,2	75	76,7	76,7	75,4
2 µM	2	100	69,8			66,4	75,5		62,6	77,7

Table Analyzed	axon length grouped %				
Two-way ANOVA	Ordinary				
Alpha	0,05				
Source of Variation	% of total variation	P value	P value summary	Significant?	
Interaction	2,687	0,9130	ns	No	
MO conc.Factor	3,278	0,3750	ns	No	
MO group Factor	75,09	0,0013	**	Yes	
ANOVA table	SS	DF	MS	F (DFn, DFd)	P value
Interaction	60,64	6	10,11	F (6, 7) = 0,3093	P=0,9130
MO conc.Factor	73,99	2	37	F (2, 7) = 1,132	P=0,3750
MO group Factor	1695	3	565	F (3, 7) = 17,29	P=0,0013
Residual	228,7	7	32,68		
Number of missing values	17				

Follow-up test to compare means

Within each row, compare columns (simple effects within rows)								
Number of families	3							
Number of comparisons per family	6							
Alpha	0,05							
Tukey's multiple comparisons test	Mean Diff,	95,00% CI of diff,	Significant?	Summary	Adjusted P Value			
0,5 µM								
CO MO vs. PrP-2 MO 1	26,9	0,1399 to 53,66	Yes	*	0,0489			
CO MO vs. PrP-2 MO 2	17,1	-9,66 to 43,86	No	ns	0,2367			
CO MO vs. PrP-2 MO 1&2	22,5	-4,26 to 49,26	No	ns	0,0995			
PrP-2 MO 1 vs. PrP-2 MO 2	-9,8	-36,56 to 16,96	No	ns	0,6391			
PrP-2 MO 1 vs. PrP-2 MO 1&2	-4,4	-31,16 to 22,36	No	ns	0,9452			
PrP-2 MO 2 vs. PrP-2 MO 1&2	5,4	-21,36 to 32,16	No	ns	0,9059			
1 µM								
CO MO vs. PrP-2 MO 1	30,77	8,917 to 52,62	Yes	**	0,0096			
CO MO vs. PrP-2 MO 2	22,7	0,8505 to 44,55	Yes	*	0,0424			
CO MO vs. PrP-2 MO 1&2	23,95	0,7751 to 47,12	Yes	*	0,0434			
PrP-2 MO 1 vs. PrP-2 MO 2	-8,067	-23,52 to 7,383	No	ns	0,3778			
PrP-2 MO 1 vs. PrP-2 MO 1&2	-6,817	-24,09 to 10,46	No	ns	0,5874			
PrP-2 MO 2 vs. PrP-2 MO 1&2	1,25	-16,02 to 18,52	No	ns	0,9947			
2 µM								
CO MO vs. PrP-2 MO 1	30,2	3,44 to 56,96	Yes	*	0,0291			
CO MO vs. PrP-2 MO 2	29,05	5,875 to 52,22	Yes	*	0,0175			
CO MO vs. PrP-2 MO 1&2	29,85	6,675 to 53,02	Yes	*	0,0153			
PrP-2 MO 1 vs. PrP-2 MO 2	-1,15	-24,32 to 22,02	No	ns	0,9983			
PrP-2 MO 1 vs. PrP-2 MO 1&2	-0,35	-23,52 to 22,82	No	ns	>0,9999			
PrP-2 MO 2 vs. PrP-2 MO 1&2	0,8	-18,12 to 19,72	No	ns	0,9989			
Test details	Mean 1	Mean 2	Mean Diff,	SE of diff,	N1	N2	q	DF
0,5 µM								
CO MO vs. PrP-2 MO 1	100	73,1	26,9	8,084	1	1	4,706	7
CO MO vs. PrP-2 MO 2	100	82,9	17,1	8,084	1	1	2,991	7
CO MO vs. PrP-2 MO 1&2	100	77,5	22,5	8,084	1	1	3,936	7
PrP-2 MO 1 vs. PrP-2 MO 2	73,1	82,9	-9,8	8,084	1	1	1,714	7
PrP-2 MO 1 vs. PrP-2 MO 1&2	73,1	77,5	-4,4	8,084	1	1	0,7697	7
PrP-2 MO 2 vs. PrP-2 MO 1&2	82,9	77,5	5,4	8,084	1	1	0,9446	7
1 µM								

CO MO vs. PrP-2 MO 1	100	69,23	30,77	6,601	1	3	6,592	7
CO MO vs. PrP-2 MO 2	100	77,3	22,7	6,601	1	3	4,863	7
CO MO vs. PrP-2 MO 1&2	100	76,05	23,95	7,001	1	2	4,838	7
PrP-2 MO 1 vs. PrP-2 MO 2	69,23	77,3	-8,067	4,667	3	3	2,444	7
PrP-2 MO 1 vs. PrP-2 MO 1&2	69,23	76,05	-6,817	5,218	3	2	1,847	7
PrP-2 MO 2 vs. PrP-2 MO 1&2	77,3	76,05	1,25	5,218	3	2	0,3388	7
2 µM								
CO MO vs. PrP-2 MO 1	100	69,8	30,2	8,084	1	1	5,283	7
CO MO vs. PrP-2 MO 2	100	70,95	29,05	7,001	1	2	5,868	7
CO MO vs. PrP-2 MO 1&2	100	70,15	29,85	7,001	1	2	6,03	7
PrP-2 MO 1 vs. PrP-2 MO 2	69,8	70,95	-1,15	7,001	1	2	0,2323	7
PrP-2 MO 1 vs. PrP-2 MO 1&2	69,8	70,15	-0,35	7,001	1	2	0,0707	7
PrP-2 MO 2 vs. PrP-2 MO 1&2	70,95	70,15	0,8	5,716	2	2	0,1979	7

Correlation

	MO concentration (µM) vs. CO MO	MO concentration (µM) vs. PrP-2 MO 1	MO concentration (µM) vs. PrP-2 MO 2	MO concentration (µM) vs. PrP-2 MO 1&2
Pearson r	Horizontal line			
r		-0,6601	-0,9882	-0,9893
95% confidence interval				
R squared		0,4357	0,9765	0,9788
P value				
P (two-tailed)		0,5410	0,0980	0,0930
P value summary		ns	ns	ns
Significant? (alpha = 0.05)		No	No	No
Number of XY Pairs	3	3	3	3

Figure 5.4.1.2 B: Knockdown of PrP-2 impairs axonal outgrowth of zebrafish retinal explants *in vitro*

Cultured retinal explants	Co MO, 70 µM, 1 dic, $\bar{x}$ axons / explant	Co MO, 70 µM, 2 dic, $\bar{x}$ axons / explant	PrP-2 MO 1, 70 µM, 1 dic, $\bar{x}$ axons / explant	PrP-2 MO 1, 70 µM, 2 dic, $\bar{x}$ axons / explant	PrP-2 MO 2, 70 µM, 1 dic, $\bar{x}$ axons / explant	PrP-2 MO 2, 70 µM, 2 dic, $\bar{x}$ axons / explant
Exp. 1	30,2	60,6	--	--	11,3	29,5
Exp. 2	39,6	65,5	15	38,1	--	--
Exp. 3	58	--	25,9	--	23,3	--
Mean ± SEM	**42,6**	**63,05**	**20,45**	**38,1**	**17,3**	**29,5**
%	**100**	**100**	**48**	**60,4**	**40,6**	**46,8**
N expl.	**126**		**89**		**95**	

Cultured retinal explants	Co MO, 140 µM, 1 dic, $\bar{x}$ axons / explant	Co MO, 140 µM, 2 dic, $\bar{x}$ axons / explant	PrP-2 MO 1, 140 µM, 1 dic, $\bar{x}$ axons / explant	PrP-2 MO 1, 140 µM, 2 dic, $\bar{x}$ axons / explant	PrP-2 MO 2, 140 µM, 1 dic, $\bar{x}$ axons / explant	PrP-2 MO 2, 140 µM, 2 dic, $\bar{x}$ axons / explant
Exp. 1	23,7	51,5	6,3	21,9	2,1	10,2
Exp. 2	61,3	85,2	3,5	16,8	4,7	13,3
Mean ± SEM	**42,5**	**68,35**	**4,9**	**19,35**	**3,4**	**11,75**
%	**100**	**100**	**11,5**	**28,3**	**8**	**17,2**
N expl.	**64**		**79**		**68**	

Two-way ANOVA between groups 70 and 140 µM of control and PrP-2 morpholino sequences 1 and 2

Table Analyzed	raw grouped				
Two-way ANOVA	Ordinary				
Alpha	0,05				
Source of Variation	% of total variation	P value	P value summary	Significant?	
Interaction	4,66	<0,0001	****	Yes	
MO conc. Factor	11,09	<0,0001	****	Yes	
MO group Factor	43,92	<0,0001	****	Yes	
ANOVA table	SS	DF	MS	F (DFn, DFd)	P value
Interaction	18657	4	4664	F (4, 506) = 13,58	P<0,0001
MO conc. Factor	44399	2	22199	F (2, 506) = 64,63	P<0,0001
MO group Factor	175849	2	87924	F (2, 506) = 256	P<0,0001
Residual	173802	506	343,5		
Number of missing values	205				

Follow-up test to compare means

Compare cell means regardless of rows and columns					
Number of families	1				
Number of comparisons per family	36				
Alpha	0,05				
Sidak's multiple comparisons test	Mean Diff,	95,00% CI of diff,	Significant?	Summary	Adjusted P Value
70 µM 1 dic:Co MO vs. 70 µM 1 dic:**PrP-2 MO 1**	26,79	14,11 to 39,48	Yes	****	<0,0001
70 µM 1 dic:Co MO vs. 70 µM 1 dic:PrP-2 MO 2	30,17	17,49 to 42,86	Yes	****	<0,0001
70 µM 1 dic:Co MO vs. 140µM 1dic:Co MO	12,69	1,702 to 23,67	Yes	**	0,0084
70 µM 1 dic:Co MO vs. 140µM 1dic:**PrP-2 MO 1**	48,5	38,03 to 58,97	Yes	****	<0,0001
70 µM 1 dic:Co MO vs. 140µM 1dic:PrP-2 MO 2	49,93	39,1 to 60,77	Yes	****	<0,0001
70 µM 1 dic:Co MO vs. 140 µM 2 dic:Co MO	-25,26	-38,65 to -11,86	Yes	****	<0,0001
70 µM 1 dic:Co MO vs. 140 µM 2 dic:**PrP-2 MO 1**	34,16	23,6 to 44,71	Yes	****	<0,0001
70 µM 1 dic:Co MO vs. 140 µM 2 dic:PrP-2 MO 2	41,45	30,58 to 52,32	Yes	****	<0,0001
70 µM 1 dic:**PrP-2 MO 1** vs. 70 µM 1 dic:PrP-2 MO 2	3,378	-10,44 to 17,2	No	ns	>0,9999
70 µM 1 dic:**PrP-2 MO 1** vs. 140µM 1dic:Co MO	-14,11	-26,39 to -1,832	Yes	**	0,0090
70 µM 1 dic:**PrP-2 MO 1** vs. 140µM 1dic:**PrP-2 MO 1**	21,7	9,885 to 33,52	Yes	****	<0,0001
70 µM 1 dic:**PrP-2 MO 1** vs. 140µM 1dic:PrP-2 MO 2	23,14	10,99 to 35,28	Yes	****	<0,0001
70 µM 1 dic:**PrP-2 MO 1** vs. 140 µM 2 dic:Co MO	-52,05	-66,52 to -37,58	Yes	****	<0,0001
70 µM 1 dic:**PrP-2 MO 1** vs. 140 µM 2 dic:**PrP-2 MO 1**	7,361	-4,53 to 19,25	No	ns	0,8274
70 µM 1 dic:**PrP-2 MO 1** vs. 140 µM 2 dic:PrP-2 MO 2	14,65	2,479 to 26,83	Yes	**	0,0046
70 µM 1 dic:PrP-2 MO 2 vs. 140µM 1dic:Co MO	-17,49	-29,76 to -5,21	Yes	***	0,0002
70 µM 1 dic:PrP-2 MO 2 vs. 140µM 1dic:**PrP-2 MO 1**	18,32	6,506 to 30,14	Yes	****	<0,0001
70 µM 1 dic:PrP-2 MO 2 vs. 140µM 1dic:PrP-2 MO 2	19,76	7,617 to 31,9	Yes	****	<0,0001
70 µM 1 dic:PrP-2 MO 2 vs. 140 µM 2 dic:Co MO	-55,43	-69,9 to -40,95	Yes	****	<0,0001
70 µM 1 dic:PrP-2 MO 2 vs. 140 µM 2 dic:**PrP-2 MO 1**	3,982	-7,909 to 15,87	No	ns	>0,9999
70 µM 1 dic:PrP-2 MO 2 vs. 140 µM 2 dic:PrP-2 MO 2	11,28	-0,8998 to 23,45	No	ns	0,1062
140µM 1dic:Co MO vs. 140µM 1dic:**PrP-2 MO 1**	35,81	25,84 to 45,78	Yes	****	<0,0001
140µM 1dic:Co MO vs. 140µM 1dic:PrP-2 MO 2	37,25	26,89 to 47,6	Yes	****	<0,0001
140µM 1dic:Co MO vs. 140 µM 2 dic:Co MO	-37,94	-50,95 to -24,93	Yes	****	<0,0001
140µM 1dic:Co MO vs. 140 µM 2 dic:**PrP-2 MO 1**	21,47	11,41 to 31,52	Yes	****	<0,0001
140µM 1dic:Co MO vs. 140 µM 2 dic:PrP-2 MO 2	28,76	18,37 to 39,15	Yes	****	<0,0001
140µM 1dic:**PrP-2 MO 1** vs. 140µM 1dic:PrP-2 MO 2	1,435	-8,37 to 11,24	No	ns	>0,9999
140µM 1dic:**PrP-2 MO 1** vs. 140 µM 2 dic:Co MO	-73,75	-86,33 to -61,18	Yes	****	<0,0001
140µM 1dic:**PrP-2 MO 1** vs. 140 µM 2 dic:**PrP-2 MO 1**	-14,34	-23,83 to -4,852	Yes	****	<0,0001
140µM 1dic:**PrP-2 MO 1** vs. 140 µM 2 dic:PrP-2 MO 2	-7,049	-16,89 to 2,795	No	ns	0,5518
140µM 1dic:PrP-2 MO 2 vs. 140 µM 2 dic:Co MO	-75,19	-88,07 to -62,31	Yes	****	<0,0001
140µM 1dic:PrP-2 MO 2 vs. 140 µM 2 dic:**PrP-2 MO 1**	-15,78	-25,67 to -5,886	Yes	****	<0,0001
140µM 1dic:PrP-2 MO 2 vs. 140 µM 2 dic:PrP-2 MO 2	-8,484	-18,72 to 1,748	No	ns	0,2531
140 µM 2 dic:Co MO vs. 140 µM 2 dic:**PrP-2 MO 1**	59,41	46,77 to 72,06	Yes	****	<0,0001
140 µM 2 dic:Co MO vs. 140 µM 2 dic:PrP-2 MO 2	66,7	53,79 to 79,62	Yes	****	<0,0001
140 µM 2 dic:**PrP-2 MO 1** vs. 140 µM 2 dic:PrP-2 MO 2	7,293	-2,638 to 17,22	No	ns	0,4965

Figure 5.4.2: Knockdown of PrP-2 *in vivo* impairs SFK signaling of zebrafish RGCs

Figure 5.4.2. B: SFK protein density quantification in WB of zebrafish retinae

Zebrafish retinae		PrP-2, protein density (AU), norm. to a-actin	totSrc, protein density (AU), norm. to a-actin	pSrc, protein density (AU), norm. to a-actin
Exp. 1	Co MO 140 µM	27.743.978	35.334.484	19.864.037
	PrP-2 MO 1 140 µM	2.235.230,01	8.913.832,21	8.105.999,63
%		**30,1**	**66,3**	**11**
Exp. 2	Co MO 140 µM	53.944.789	31.469.685	54.675.182
	PrP-2 MO 1 140 µM	16.224.740,1	20.860.902,6	6.020.322,12
%		**8,1**	**25,2**	**40,8**
Mean ± SEM (normalized)		**19,1 ± 11**	**45,75 ± 20,55**	**25,9 ± 14,9**

One-way ANOVA

P value	<0,0001				
P value summary	****				
Are SDs significantly different (P < 0.05)?	Yes				
Bartlett's test					
Bartlett's statistic (corrected)					
P value					
P value summary					
Are SDs significantly different (P < 0.05)?					
ANOVA table	SS	DF	MS	F (DFn, DFd)	P value
Treatment (between columns)	8065	3	2688	F (3, 4) = 7,025	P=0,0451
Residual (within columns)	1531	4	382,7		
Total	9595	7			
Data summary					
Number of treatments (columns)	4				
Number of values (total)	8				

Follow-up multiple comparison between control and other groups

Number of families	1							
Number of comparisons per family	3							
Alpha	0,05							
Dunnett's multiple comparisons test	Mean Diff,	95,00% CI of diff,	Significant?	Summary	Adjusted P Value	A-?		
Co MO vs. PrP-2 MO PrP-2	80,9	10,13 to 151,7	Yes	*	0,0325	B	PrP-2 MO PrP-2	
Co MO vs. PrP-2 MO totSrc	54,25	-16,52 to 125	No	ns	0,1091	C	PrP-2 MO totSrc	
Co MO vs. PrP-2 MO pSrc	74,1	3,33 to 144,9	Yes	*	0,0432	D	PrP-2 MO pSrc	
Test details	Mean 1	Mean 2	Mean Diff,	SE of diff,	n1	n2	q	DF
Co MO vs. PrP-2 MO PrP-2	100	19,1	80,9	19,56	2	2	4,136	4
Co MO vs. PrP-2 MO totSrc	100	45,75	54,25	19,56	2	2	2,773	4
Co MO vs. PrP-2 MO pSrc	100	25,9	74,1	19,56	2	2	3,788	4

9.10. Chapter 5.5: Potential interactions of Thy-1 and PrP in hippocampal neurons

Figure 5.5 B.1 & B.2: Quantification of localized Thy-1 and PrP clusters

Primary data to Figure 5.5 B.1 and B.2 are contained in the laboratory book, protocol and stored electronic data of my consolidation course student Josephine Brandes.

Figure 5.5 C: SiRNA-mediated knockdown of PrP, Thy-1 or Thy-1 and PrP impairs neurite outgrowth

Primary hippocampal neurons	SiCo (100 pmol) $\bar{x}$ axon length (µm)	SiPrP (100 pmol) $\bar{x}$ axon length (µm)	SiThy-1 (100 pmol) $\bar{x}$ axon length (µm)	SiThy-1 & PrP (100 pmol) $\bar{x}$ axon length (µm)
Exp. 1	250,5	206,3	191,4	261
Exp. 2	569,6	424,0	374,6	472,2
Exp. 3	309,7	212,0	260,9	266,9
Mean	**376,6**	**280,8**	**275,6**	**333,4**
Mean (normalized) ± SEM	**100**	**74,6 ± 5,352**	**73 ± 4,028**	**88,5 ± 1,65**
N neurons	**184**	**148**	**107**	**118**

One-sample t-test: column statistics of axon lengths, %

	Co siRNA	Thy-1 siRNA	PrP siRNA	Thy-1 & PrP siRNA
Number of values	3	3	3	2
Minimum	100	65,77	68,45	82,9
25% Percentile	100	65,77	68,45	82,9
Median	100	76,41	74,44	84,55
75% Percentile	100	84,24	82,36	86,2
Maximum	100	84,24	82,36	86,2
Mean	100	75,47	75,08	84,55
Std. Deviation	0	9,271	6,977	2,333
Std. Error of Mean	0	5,352	4,028	1,65
Lower 95% CI of mean	100	52,44	57,75	63,58
Upper 95% CI of mean	100	98,5	92,42	105,5
Sum	300	226,4	225,3	169,1
One sample t test	Sample difference has zero SD			
Theoretical mean		100	100	100
Actual mean		75,47	75,08	84,55
Discrepancy		-24,53	-24,92	-15,45
95% CI of discrepancy		-47,56 to -1,497	-42,25 to -7,584	-36,42 to 5,515
t, df		t=4,582 df=2	t=6,185 df=2	t=9,364 df=1
P value (two tailed)		0,0445	0,0252	0,0677
Significant (alpha=0.05)?		Yes	Yes	No

Figure 5.5 E: Thy-1 protein level, wild type vs. PrP-knockout, fluorescence intensity quantification

Primary hippocampal neurons	Wild type, $\bar{x}$ fluorescence intensity Thy-1 (AU)	PrP-knockout, $\bar{x}$ fluorescence intensity Thy-1 (AU)
Exp.1	38,7	42,8
N neurons	**30**	**30**
%	**100**	**110,6**

PART II RTN4b

9.11. Chapter 5.7: Expression of RTN4b in zebrafish RGCs, specificity of the pAb RTN4b K1121

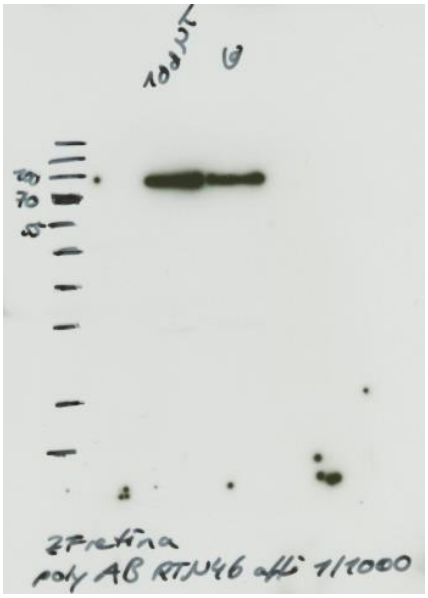

Figure 9.11 Characterization of the zebrafish RTN4b pAb K1121 in WB. The pAb K1121 shows a specific band in WB of zebrafish retina lysates at the predicted molecular mass of zebrafish RTN4b (~90 kDa), which increases after ONL.

9.12. Chapter 5.7.1: Analysis of RTN4b expression upon ONL in zebrafish RGCs

RTN4b expression, immunohistochemical (IHC) analysis

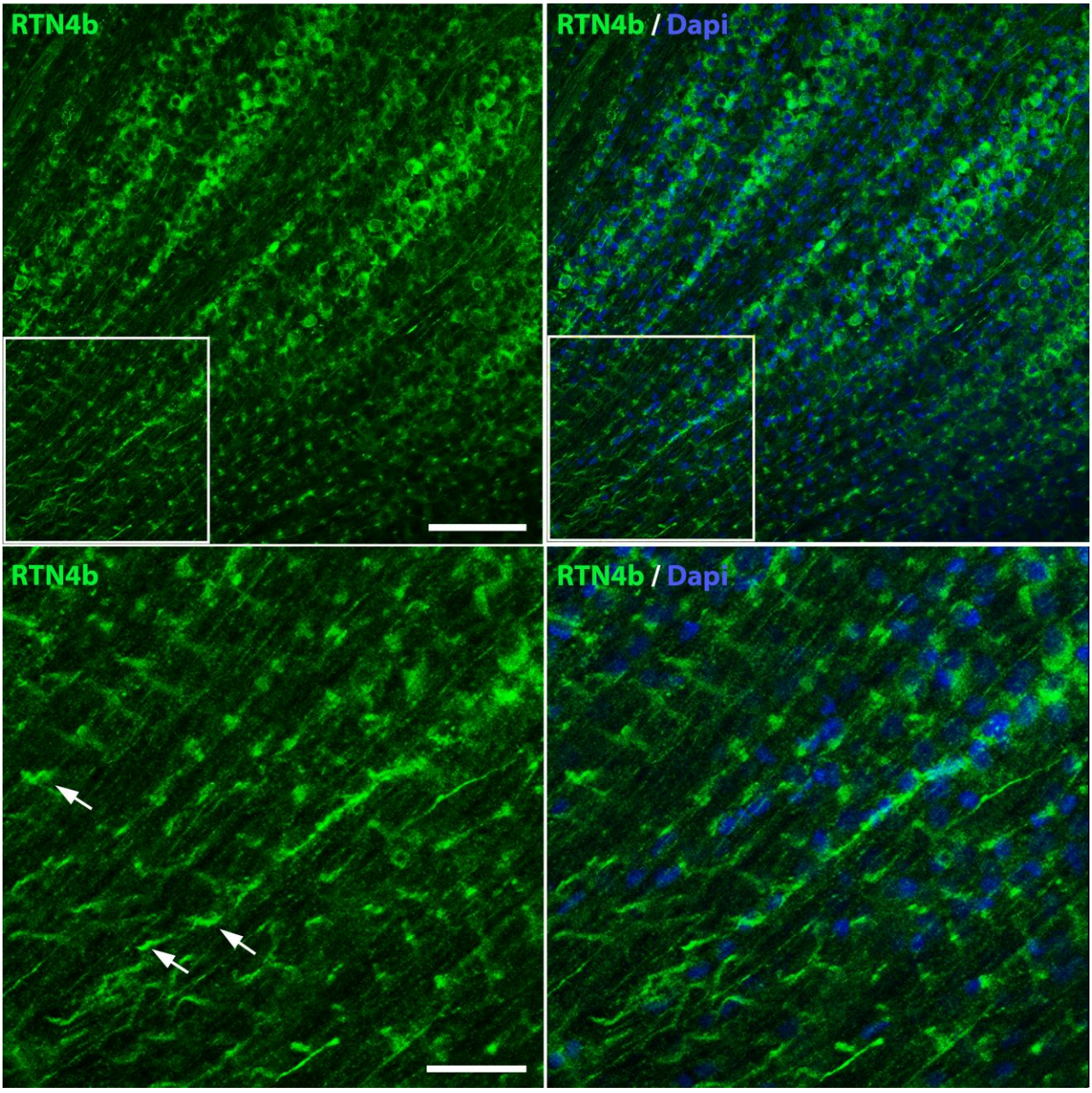

Figure 9.12.1 RTN4b expression in the zebrafish retina. The pAb K1121 shows a ubiquitous, strong expression of RTN4b in retinal ganglion cells, 5 days after optic nerve lesion. In the center, near to the optic disc, Müller glia endfeet become labeled between the axon fascicles (arrows in the magnification picture below) and are also RTN4b positive (RTN4b green, Dapi blue). This would have to be confirmed further by using specific Müller glia marker like Kir4.1 and Kir2 or rhophilin (Roesch et al., 2008). Scale bars: upper image 50 µm, lower image 15 µm.

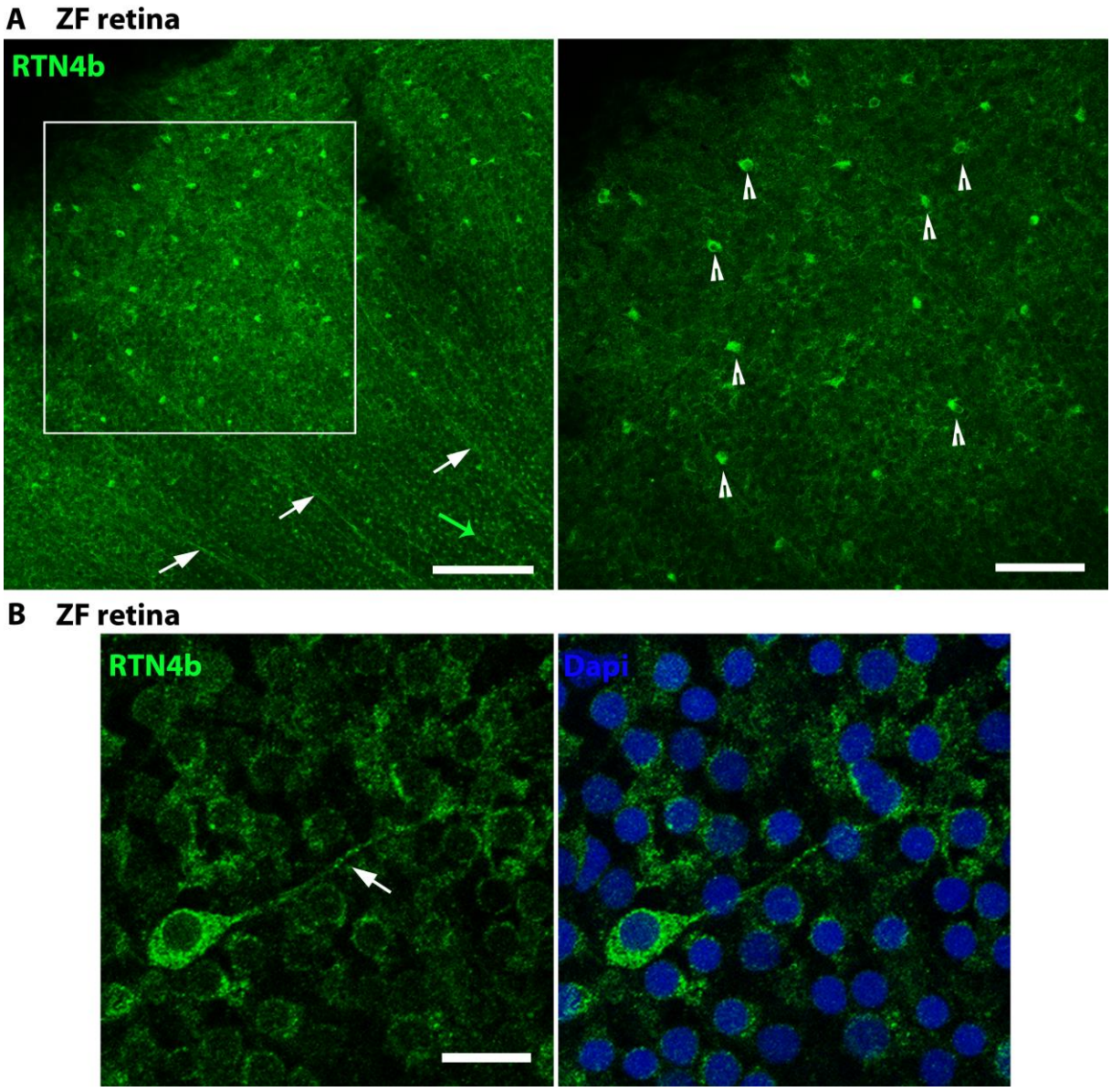

Figure 9.12.2 RTN4b expression in the zebrafish retina. A. The pAb K1121 shows a ubiquitous expression of RTN4b in the untreated zebrafish retina. Axon fascicles are weakly stained (arrows in the left image). Some RGCs in between display a stronger labeling for RTN4b (arrowheads in the right image). Towards the optic disc (green arrow), Müller glia endfeet are also labeled between the axon fascicles (as described above in Figure 9.12.1). Scale bars: left image 100 µm, right image 50 µm. **B.** Close-up of a retinal ganglion cell, which shows a strong intracellular and axonal expression of RTN4b (RTN4b green, Dapi blue). Scale bar: 20 µm.

Pattern of RTN4b in retinal ganglion cells and its optic nerve lesion-induced up-regulation

Figure 9.12.3 below shows the confocal scan of the zebrafish RGC layer. The single planes of the confocal Z-stack are displayed.

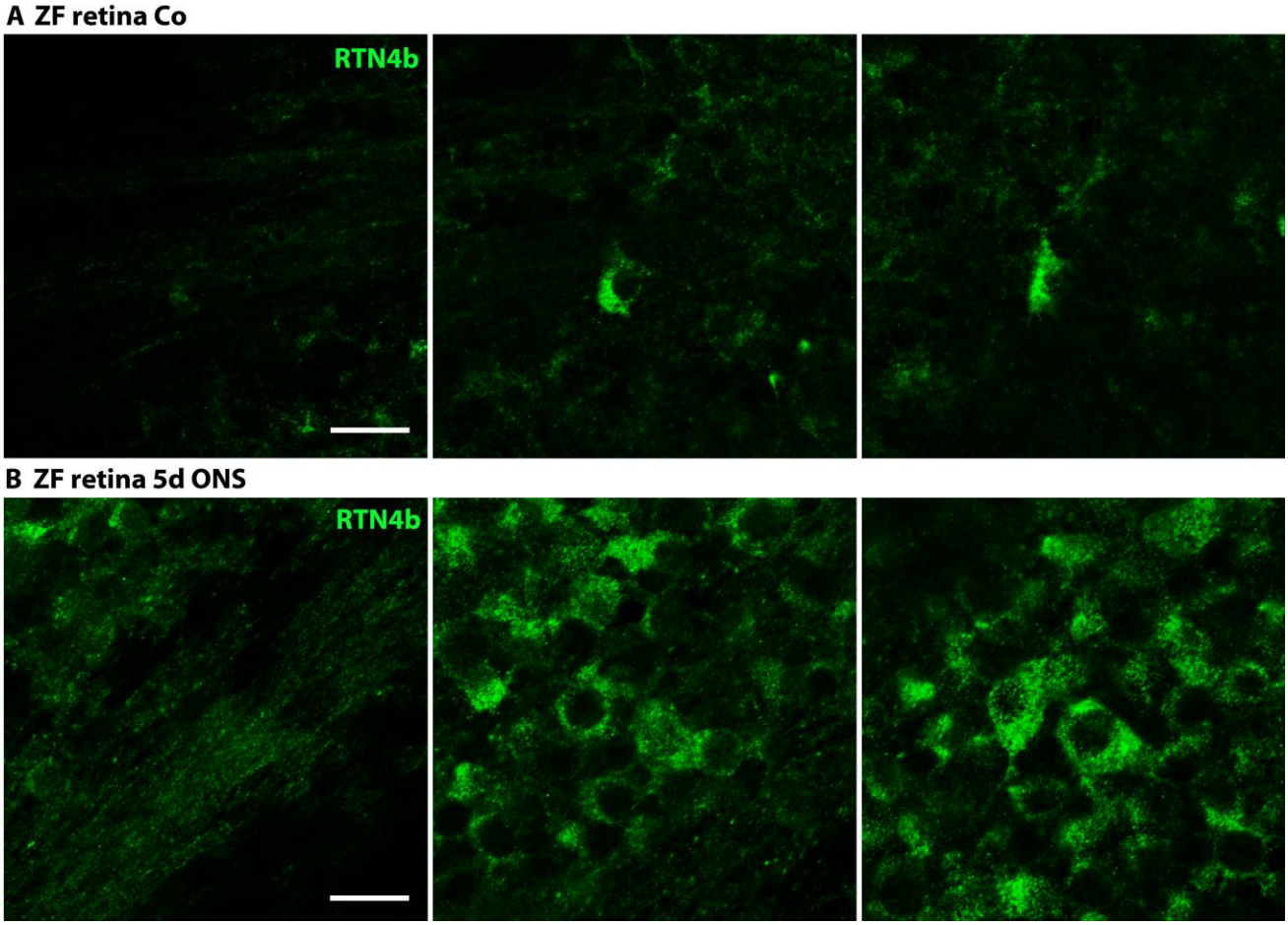

Figure 9.12.3 Characterization/pattern of the zebrafish RTN4b pAb K1121 throughout confocal z-stacks of retinal ganglion cells (RGCs). A. Control retina. Immunostaining of fixed and permeabilized tissue shows a weak intracellular distribution in a grainy pattern for RTN4b throughout confocal z-stacks. The vast majority of cells are labeled weakly, with some RGCs in between expressing more protein (as described in Figure 9.12.2). Axons are labeled weakly. **B.** After optic nerve lesion intracellular RTN4b increases and it becomes strongly expressed by all RGCs and their axons. Cell bodies of RGCs are enlarged after optic nerve lesion. Scale bars: 25 µm. Images collected at 1.6 µm intervals in a depth of 4.79 µm for **A** and at 1.6 µm intervals in a depth of 6.38 µm for **B**.

Figure 5.7.1 E: IHC: RTN4b fluorescence intensity quantification

Zebrafish retinae	5d Control, fluorescence intensity (AU)	5d ONS, fluorescence intensity (AU)	10d Co, fluorescence intensity (AU)	10d ONS, fluorescence intensity (AU)
Exp. 1	51.711	77.938	--	--
	35.081	21.278	--	--
	15.564	23.755	--	--
	17.602	18.596	--	--
	10.524	19.772	--	--
	16.602	20.374	--	--
	9.051	--	--	--
Exp. 2	--	--	55.857	112.142
	--	--	54.467	76.254
	--	--	24.560	50.160
	--	--	33.304	30.566
	--	--	13.340	21.367
	--	--	9.895	15.288
	--	--	--	29.396
	--	--	--	17.144
	--	--	--	29.772
Mean ± SEM	**22.305 ± 5860**	**30.286 ± 9557**	**31.904 ± 8099**	**42.454 ± 10772**
%	**100**	**136**	**100**	**133**
N retinae	**7**	**6**	**6**	**9**

One-way ANOVA

ANOVA summary					
F	0,9105				
P value	0,4506				
P value summary	ns				
Significant diff. among means (P < 0.05)?	No				
R square	0,1022				
Brown-Forsythe test					
F (DFn, DFd)	0,4678 (3, 24)				
P value	0,7075				
P value summary	ns				
Are SDs significantly different (P < 0.05)?	No				
Bartlett's test					
Bartlett's statistic (corrected)	3,534				
P value	0,3163				
P value summary	ns				
Are SDs significantly different (P < 0.05)?	No				
ANOVA table	SS	DF	MS	F (DFn, DFd)	P value
Treatment (between columns)	1650855437	3	550285146	F (3, 24) = 0,9105	P=0,4506
Residual (within columns)	14504347882	24	604347828		
Total	16155203319	27			

Figure 5.7.1 F: RTN4b protein density quantification in WBs of zebrafish retinae

Zebrafish retinae	5d Control, protein density (AU), normalized to α-tubulin	5d ONS, protein density (AU), normalized to α-tubulin
Exp. 1	36.551.070	56.423.593
%	**100**	**154**

9.13. Chapter 5.7.2: Knockdown of RTN4b impairs axonal outgrowth of zebrafish retinal explants *in vitro*

Figure 5.7.2 B:

Cultured retinal explants	Control MO, 70 µM, 1 dic, $\bar{x}$ axons / explant	RTN4b MO 1, 70 µM, 1 dic, $\bar{x}$ axons / explant
Exp. 1	39,5	13,1
Mean ± SEM	**39,49 ± 2,437, n=41**	**13,13 ± 2,091, n=38**
%	**100**	**33,25**
N explants	**41**	**38**

Cultured retinal explants	Control MO, 140 µM, 1 dic, $\bar{x}$ axons / explant	Control MO, 140 µM, 2 dic, $\bar{x}$ axons / explant	RTN4b MO 1, 140 µM, 1 dic, $\bar{x}$ axons / explant	RTN4b MO 1, 140 µM, 2 dic, $\bar{x}$ axons / explant
Exp. 1	38,5	77,1	8,9	40,9
Mean ± SEM	**38,51 ± 2,403**	**77,08 ± 3,036**	**8,912 ± 1,615**	**40,88 ± 3,059**
%	**100**	**100**	**23,1**	**53**
N explants	**39**		**34**	

Two-way ANOVA between groups 70 and 140 µM of control and RTN4b morpholino sequence 1

Table Analyzed	axon number raw grouped				
Two-way ANOVA	Ordinary				
Alpha	0,05				
Source of Variation	% of total variation	P value	P value summary	Significant?	
Interaction	0,5397	0,1467	ns	No	
Row Factor	32,67	<0,0001	****	Yes	
Column Factor	29,5	<0,0001	****	Yes	
ANOVA table	SS	DF	MS	F (DFn, DFd)	P value
Interaction	996,1	2	498	F (2, 228) = 1,936	P=0,1467
Row Factor	60300	2	30150	F (2, 228) = 117,2	P<0,0001
Column Factor	54442	1	54442	F (1, 228) = 211,6	P<0,0001
Residual	58660	228	257,3		
Number of missing values	54				

Follow-up multiple comparison between means

Compare cell means regardless of rows and columns								
Number of families	1							
Number of comparisons per family	15							
Alpha	0,05							
Tukey's multiple comparisons test	Mean Diff,	95,00% CI of diff,	Significant?	Summary	Adjusted P Value			
70 µM 1 dic:Co Mo 140 µM 2d vs. 70 µM 1 dic:RTN4b MO1	26,36	15,98 to 36,74	Yes	****	<0,0001			
70 µM 1 dic:Co Mo 140 µM 2d vs. 140 µM 1 dic:Co Mo 140 µM 2d	0,975	-9,337 to 11,29	No	ns	0,9998			
70 µM 1 dic:Co Mo 140 µM 2d vs. 140 µM 1 dic:RTN4b MO1	30,58	19,88 to 41,27	Yes	****	<0,0001			
70 µM 1 dic:Co Mo 140 µM 2d vs. 140 µM 2 dic:Co Mo 140 µM 2d	-37,6	-47,4 to -27,79	Yes	****	<0,0001			
70 µM 1 dic:Co Mo 140 µM 2d vs. 140 µM 2 dic:RTN4b MO1	-1,395	-12,09 to 9,299	No	ns	0,9990			
70 µM 1 dic:RTN4b MO1 vs. 140 µM 1 dic:Co Mo 140 µM 2d	-25,38	-35,89 to -14,87	Yes	****	<0,0001			
70 µM 1 dic:RTN4b MO1 vs. 140 µM 1 dic:RTN4b MO1	4,22	-6,663 to 15,1	No	ns	0,8751			
70 µM 1 dic:RTN4b MO1 vs. 140 µM 2 dic:Co Mo 140 µM 2d	-63,95	-73,96 to -53,94	Yes	****	<0,0001			
70 µM 1 dic:RTN4b MO1 vs. 140 µM 2 dic:RTN4b MO1	-27,75	-38,63 to -16,87	Yes	****	<0,0001			
140 µM 1 dic:Co Mo 140 µM 2d vs. 140 µM 1 dic:RTN4b MO1	29,6	18,78 to 40,42	Yes	****	<0,0001			
140 µM 1 dic:Co Mo 140 µM 2d vs. 140 µM 2 dic:Co Mo 140 µM 2d	-38,57	-48,51 to -28,63	Yes	****	<0,0001			
140 µM 1 dic:Co Mo 140 µM 2d vs. 140 µM 2 dic:RTN4b MO1	-2,37	-13,19 to 8,447	No	ns	0,9887			
140 µM 1 dic:RTN4b MO1 vs. 140 µM 2 dic:Co Mo 140 µM 2d	-68,17	-78,51 to -57,84	Yes	****	<0,0001			
140 µM 1 dic:RTN4b MO1 vs. 140 µM 2 dic:RTN4b MO1	-31,97	-43,15 to -20,79	Yes	****	<0,0001			
140 µM 2 dic:Co Mo 140 µM 2d vs. 140 µM 2 dic:RTN4b MO1	36,2	25,87 to 46,53	Yes	****	<0,0001			
Test details	Mean 1	Mean 2	Mean Diff,	SE of diff,	N1	N2	q	DF
70 µM 1 dic:Co Mo 140 µM 2d vs. 70 µM 1 dic:RTN4b MO1	39,49	13,13	26,36	3,612	41	38	10,32	228
70 µM 1 dic:Co Mo 140 µM 2d vs. 140 µM 1 dic:Co Mo 140 µM 2d	39,49	38,51	0,975	3,588	41	39	0,3843	228
70 µM 1 dic:Co Mo 140 µM 2d vs. 140 µM 1 dic:RTN4b MO1	39,49	8,912	30,58	3,721	41	34	11,62	228
70 µM 1 dic:Co Mo 140 µM 2d vs. 140 µM 2 dic:Co Mo 140 µM 2d	39,49	77,08	-37,6	3,411	41	48	15,59	228
70 µM 1 dic:Co Mo 140 µM 2d vs. 140 µM 2 dic:RTN4b MO1	39,49	40,88	-1,395	3,721	41	34	0,5301	228
70 µM 1 dic:RTN4b MO1 vs. 140 µM 1 dic:Co Mo 140 µM 2d	13,13	38,51	-25,38	3,656	38	39	9,818	228
70 µM 1 dic:RTN4b MO1 vs. 140 µM 1 dic:RTN4b MO1	13,13	8,912	4,22	3,787	38	34	1,576	228
70 µM 1 dic:RTN4b MO1 vs. 140 µM 2 dic:Co Mo 140 µM 2d	13,13	77,08	-63,95	3,483	38	48	25,97	228
70 µM 1 dic:RTN4b MO1 vs. 140 µM 2 dic:RTN4b MO1	13,13	40,88	-27,75	3,787	38	34	10,36	228
140 µM 1 dic:Co Mo 140 µM 2d vs. 140 µM 1 dic:RTN4b MO1	38,51	8,912	29,6	3,764	39	34	11,12	228
140 µM 1 dic:Co Mo 140 µM 2d vs. 140 µM 2 dic:Co Mo 140 µM 2d	38,51	77,08	-38,57	3,458	39	48	15,77	228
140 µM 1 dic:Co Mo 140 µM 2d vs. 140 µM 2 dic:RTN4b MO1	38,51	40,88	-2,37	3,764	39	34	0,8904	228

140 µM 1 dic:RTN4b MO1 vs. 140 µM 2 dic:Co Mo 140 µM 2d	8,912	77,08	-68,17	3,595	34	48	26,81	228
140 µM 1 dic:RTN4b MO1 vs. 140 µM 2 dic:RTN4b MO1	8,912	40,88	-31,97	3,89	34	34	11,62	228
140 µM 2 dic:Co Mo 140 µM 2d vs. 140 µM 2 dic:RTN4b MO1	77,08	40,88	36,2	3,595	48	34	14,24	228

9.14. Chapter 5.8: Inhibitory substrate properties of different Nogo-A (RTN4b) M1-4 peptides, tested on zebrafish and mammalian neurons

Figure 5.8.1.1 D: Rat and zebrafish RTN4b inhibit, mutated rat M1-4 D/A permits differentiation of RGCs *in vitro*

Primary ZF RGCs	Substrate (200 nmol)	total neurons	undifferentiated neurons	undifferentiated neurons, %
Exp. 1	**GST**	138	28	**20,3**
	Rat RTN4b M1-4	50	15	**30,0**
	Rat RTN4b M1-4 D/A	--	--	--
	ZF RTN4b M1-4	--	--	--
Exp. 2	**GST**	80	13	**16,3**
	Rat RTN4b M1-4	137	104	**75,9**
	Rat RTN4b M1-4 D/A	54	10	**18,5**
	ZF RTN4b M1-4	--	--	
Exp. 3	**GST**	84	11	**13,1**
	Rat RTN4b M1-4	96	31	**32,3**
	Rat RTN4b M1-4 D/A	--	--	**--**
	ZF RTN4b M1-4	134	50	**37,3**
	GST	**Rat RTN4b M1-4**	**Rat RTN4b M1-4 D/A**	**ZF RTN4b M1-4**
$\bar{x}$ **% of undiff. neurons**	**16,6**	**46,1**	**18,5**	**37,3**

One-way ANOVA

Table Analyzed	amount of undifferentiated cells, column %				
Data sets analyzed	A : GST 200 nmol	B : Rat M1-4 200 nmol	C : Rat M1-4 D/A 200 nmol	D : ZF M-14 200 nmol	
ANOVA summary					
F	1,466				
P value	0,3502				
P value summary	ns				
Significant diff. among means (P < 0.05)?	No				
R square	0,5237				
Brown-Forsythe test					
F (DFn, DFd)					
P value					
P value summary					
Are SDs significantly different (P < 0.05)?					
Bartlett's test					
Bartlett's statistic (corrected)					
P value					
P value summary					
Are SDs significantly different (P < 0.05)?					
ANOVA table	SS	DF	MS	F (DFn, DFd)	P value
Treatment (between columns)	1500	3	499,9	F (3, 4) = 1,466	P=0,3502
Residual (within columns)	1364	4	340,9		
Total	2863	7			
Data summary					
Number of treatments (columns)	4				
Number of values (total)	8				

Figure 5.8.1.1 E & F: Rat and zebrafish RTN4b inhibit, mutated rat M1-4 D/A permits outgrowth of zebrafish RGCss *in vitro*

Cultured primary RGCs	**GST (200 nmol) $\bar{x}$ axon length (µm)**	**Rat RTN4b M1-4, (200 nmol) $\bar{x}$ axon length (µm)**	**Rat RTN4b M1-4 D/A (200 nmol), $\bar{x}$ axon length (µm)**	**ZF RTN4b M1-4 (200 nmol) $\bar{x}$ axon length (µm)**
Exp. 1	228,6	134,1	--	--
Exp. 2	251,1	128,3	271,3	--
Exp. 3	310,5	212,7	--	189,7
Mean ± SEM	**258,5 ± 14,26**	**171 ± 14,77**	**271,3 ± 44,39**	**189,7 ± 17,05**
%	**100**	**59,4**	**108,1**	**61,6**
N neurons	**250**	**133**	**44**	**84**

One-way ANOVA

Table Analyzed	axon length,µM,raw column				
Data sets analyzed	A : Data Set-A	B : Data Set-B	C : Data Set-C	D : Data Set-D	
ANOVA summary					
F	6,591				
P value	0,0002				
P value summary	***				
Significant diff. among means (P < 0.05)?	Yes				
R square	0,03753				
Brown-Forsythe test					
F (DFn, DFd)	2,082 (3, 507)				
P value	0,1016				
P value summary	ns				
Are SDs significantly different (P < 0.05)?	No				
Bartlett's test					
Bartlett's statistic (corrected)	37,07				
P value	<0,0001				
P value summary	****				
Are SDs significantly different (P < 0.05)?	Yes				
ANOVA table	SS	DF	MS	F (DFn, DFd)	P value
Treatment (between columns)	867631	3	289210	F (3, 507) = 6,591	P=0,0002
Residual (within columns)	22247989	507	43882		
Total	23115620	510			
Data summary					
Number of treatments (columns)	4				
Number of values (total)	511				

Follow-up multiple comparison of means

Number of families	1							
Number of comparisons per family	6							
Alpha	0,05							
Tukey's multiple comparisons test	Mean Diff,	95,00% CI of diff,	Significant?	Summary	Adjusted P Value			
Column A vs. Column B	87,51	29,56 to 145,5	Yes	***	0,0006	A-B		
Column A vs. Column C	-12,78	-101 to 75,5	No	ns	0,9823	A-C		
Column A vs. Column D	68,86	0,7625 to 137	Yes	*	0,0463	A-D		
Column B vs. Column C	-100,3	-194,2 to -6,381	Yes	*	0,0310	B-C		
Column B vs. Column D	-18,65	-93,9 to 56,6	No	ns	0,9194	B-D		
Column C vs. Column D	81,63	-18,85 to 182,1	No	ns	0,1564	C-D		
Test details	Mean 1	Mean 2	Mean Diff,	SE of diff,	n1	n2	q	DF
Column A vs. Column B	258,5	171	87,51	22,48	250	133	5,505	507
Column A vs. Column C	258,5	271,3	-12,78	34,25	250	44	0,5276	507
Column A vs. Column D	258,5	189,7	68,86	26,42	250	84	3,686	507
Column B vs. Column C	171	271,3	-100,3	36,43	133	44	3,893	507
Column B vs. Column D	171	189,7	-18,65	29,19	133	84	0,9035	507
Column C vs. Column D	271,3	189,7	81,63	38,98	44	84	2,961	507

Figure 5.8.1.2 B: Rat M1-4 and zebrafish M1-4 inhibit, mutated rat M1-4 D/A permits outgrowth of zebrafish retinal explants *in vitro*

Cultured primary RGCs	**GST (200 nmol) $\bar{x}$ axon / explant**	**Rat RTN4b M1-4, (200 nmol) $\bar{x}$ axon / explant**	**Rat RTN4b M1-4 D/A (200 nmol), $\bar{x}$ axon / explant**	**ZF RTN4b M1-4 (200 nmol) $\bar{x}$ axon / explant**
Exp. 1	28,1	6,8	--	8,5
Exp. 2	23,1	1	23,7	4,6
Exp. 3	13,2	3,4	15,1	1,5
Exp. 4	21,9	0,5	17,2	0,4
Mean ± SEM	**21,6**	**2,9**	**18,7**	**3,8**
%	**100**	**13,4**	**87**	**17,6**
N explants	**51**	**39**	**38**	**39**

One-way ANOVA

Table Analyzed	number of axons raw column				
Data sets analyzed	A : GST	B : Rat M 1-4	C : Rat M 1-4 D/A	D : ZF M 1-4	
ANOVA summary					
F	17,82				
P value	<0,0001				
P value summary	****				
Significant diff. among means (P < 0.05)?	Yes				
R square	0,2224				
Brown-Forsythe test					
F (DFn, DFd)	8,335 (3, 187)				
P value	<0,0001				
P value summary	****				
Are SDs significantly different (P < 0.05)?	Yes				
Bartlett's test					
Bartlett's statistic (corrected)	119,4				
P value	<0,0001				
P value summary	****				
Are SDs significantly different (P < 0.05)?	Yes				
ANOVA table	SS	DF	MS	F (DFn, DFd)	P value
Treatment (between columns)	12783	3	4261	F (3, 187) = 17,82	P<0,0001
Residual (within columns)	44706	187	239,1		
Total	57489	190			
Data summary					
Number of treatments (columns)	4				
Number of values (total)	191				

Follow-up multiple comparison of means

Number of families	1							
Number of comparisons per family	6							
Alpha	0,05							
Tukey's multiple comparisons test	Mean Diff,	95,00% CI of diff,	Significant?	Summary	Adjusted P Value			
GST vs. Rat M 1-4	17,79	9,877 to 25,7	Yes	****	<0,0001	A-B		
GST vs. Rat M 1-4 D/A	2,928	-5,053 to 10,91	No	ns	0,7773	A-C		
GST vs. ZF M 1-4	17,17	9,261 to 25,09	Yes	****	<0,0001	A-D		
Rat M 1-4 vs. Rat M 1-4 D/A	-14,86	-24 to -5,725	Yes	***	0,0002	B-C		
Rat M 1-4 vs. ZF M 1-4	-0,6154	-9,692 to 8,461	No	ns	0,9981	B-D		
Rat M 1-4 D/A vs. ZF M 1-4	14,25	5,11 to 23,38	Yes	***	0,0004	C-D		
Test details	Mean 1	Mean 2	Mean Diff,	SE of diff,	n1	n2	q	DF
GST vs. Rat M 1-4	20,53	2,744	17,79	3,052	75	39	8,242	187
GST vs. Rat M 1-4 D/A	20,53	17,61	2,928	3,079	75	38	1,345	187
GST vs. ZF M 1-4	20,53	3,359	17,17	3,052	75	39	7,957	187
Rat M 1-4 vs. Rat M 1-4 D/A	2,744	17,61	-14,86	3,524	39	38	5,963	187
Rat M 1-4 vs. ZF M 1-4	2,744	3,359	-0,6154	3,501	39	39	0,2486	187
Rat M 1-4 D/A vs. ZF M 1-4	17,61	3,359	14,25	3,524	38	39	5,717	187

Figure 5.8.2 B & C: Rat M1-4 and zebrafish M1-4 inhibit, mutated rat M1-4 D/A permits spreading of neuron-like rat PC12 cells *in vitro*

Cultured PC12 cells	**GST (200 nmol), $\bar{x}$ perimeter (µm)**	**Rat RTN4b M1-4 (200 nmol), $\bar{x}$ perimeter (µm)**	**Rat RTN4b M1-4 D/A (200 nmol), $\bar{x}$ perimeter (µm)**	**ZF RTN4b M1-4 (200 nmol), $\bar{x}$ perimeter (µm)**
Exp. 1	636,1	424,9	616,8	--
Exp. 2	1601,7	838,8	1586,2	--
Exp. 3	887,6	515,8	--	699,2
Mean ± SEM	**1116 ± 37,83**	**642,2 ± 22,06**	**1159 ± 45,88**	**699,2 ± 42,74**
%	**100**	**57,6**	**103,9**	**62,7**
N	**448**	**466**	**313**	**85**

One-way ANOVAs

Table Analyzed	cell perimeter (µM) raw column				
Data sets analyzed	A : GST	B : Rat M4	C : ZF M4		
ANOVA summary					
F	30,08				
P value	<0,0001				
P value summary	****				
Significant diff. among means (P < 0.05)?	Yes				
R square	0,1718				
Brown-Forsythe test					
F (DFn, DFd)	2,934 (2, 290)				
P value	0,0548				
P value summary	ns				
Are SDs significantly different (P < 0.05)?	No				
Bartlett's test					
Bartlett's statistic (corrected)	7,605				
P value	0,0223				
P value summary	*				
Are SDs significantly different (P < 0.05)?	Yes				
ANOVA table	SS	DF	MS	F (DFn, DFd)	P value
Treatment (between columns)	7145208	2	3572604	F (2, 290) = 30,08	P<0,0001
Residual (within columns)	34440283	290	118760		
Total	41585491	292			
Data summary					
Number of treatments (columns)	3				
Number of values (total)	293				

Table Analyzed	cell perimeter (µm) raw column				
Data sets analyzed	A : GST	B : M4	C : M4 D/A		
ANOVA summary					
F	53,77				
P value	<0,0001				
P value summary	****				
Significant diff. among means (P < 0.05)?	Yes				
R square	0,09571				
Brown-Forsythe test					
F (DFn, DFd)	33,01 (2, 1016)				
P value	<0,0001				
P value summary	****				
Are SDs significantly different (P < 0.05)?	Yes				
Bartlett's test					
Bartlett's statistic (corrected)	115,3				
P value	<0,0001				
P value summary	****				
Are SDs significantly different (P < 0.05)?	Yes				
ANOVA table	SS	DF	MS	F (DFn, DFd)	P value
Treatment (between columns)	59942483	2	29971241	F (2, 1016) = 53,77	P<0,0001
Residual (within columns)	566360625	1016	557442		
Total	626303108	1018			
Data summary					
Number of treatments (columns)	3				
Number of values (total)	1019				

Follow-up multiple comparison of means

Number of families	1							
Number of comparisons per family	3							
Alpha	0,05							
Tukey's multiple comparisons test	Mean Diff,	95,00% CI of diff,	Significant?	Summary	Adjusted P Value			
GST vs. M4	520	387,9 to 652,1	Yes	****	<0,0001	A-B		
GST vs. M4 D/A	35,31	-102,6 to 173,2	No	ns	0,8195	A-C		
M4 vs. M4 D/A	-484,7	-619,1 to -350,3	Yes	****	<0,0001	B-C		
Test details	Mean 1	Mean 2	Mean Diff,	SE of diff,	n1	n2	q	DF
GST vs. M4	1194	674,1	520	56,28	334	372	13,07	1016
GST vs. M4 D/A	1194	1159	35,31	58,74	334	313	0,8502	1016
M4 vs. M4 D/A	674,1	1159	-484,7	57,27	372	313	11,97	1016

Record of contributions

If not stated otherwise, the experiments shown in this thesis were planned and performed by myself or under my direct supervision. The corresponding primary data and statistical evaluation are listed in chapter 9. Synopsis of primary data.

Contributions from students under my supervision:

- Master student Sarah Henrich investigated in her master thesis "Thy-1-induced and reggie-mediated signaling" the association of the signaling molecules Src, ERK and cofilin to reggie in primary mouse hippocampal neurons upon siRNA-mediated Thy-1 knockdown. She analyzed axonal outgrowth of primary hippocampal neurons upon Thy-1 knockdown or overexpression and performed reggie rescue experiments after loss-of Thy-1. Furthermore, she took part in the characterization of CAD cells for further biochemical analysis (see Figs. 5.2.4. and 5.6.).
- Bachelor student Julia Henkelmann joined in her bachelor thesis "Characterization of a monoclonal antibody against zebrafish Thy-1" the screening of monoclonal antibodies specific for zebrafish Thy-1 (see Figs. 5.1.3 and 5.1.6.).
- Consolidation course student J. Brandes contributed to the measurements in Fig. 5.5 by quantifying the co-localization of Thy-1 and PrP after antibody-mediated clustering in mouse hippocampal cell (see Fig. 5.5 A, B.1 and B.2).
- M. Sc. Stefan Strütt quantified PC12 cells growing on different rat and zebrafish RTN4b substrates in spreading assays (see Fig. 5.8.2.) as part of a HiWi assignment.

Contributions from scientific collaborations:

- During the course of my PhD thesis I collaborated closely with Dr. V. Bodrikov, who was a postdoc in the group and a good colleague and personal friend of mine. Dr. V. Bodrikov joined the group as an expert in mouse primary cell culture. Together we established the primary culture of zebrafish RGCs. Regarding fish RGCs (single cells and explants), I isolated the retinae, and in the majority of the experiments Dr. Bodrikov cultured the cells. I performed transfections (*in vivo* or *in vitro*) and the immunocyto- / histochemistry or biochemistry. I also performed microscopy experiments, the image analysis and the statistical evaluation.
  Dr. Bodrikov also kindly provided primary mouse hippocampal cultures and performed several transfections with siRNA or EGFP constructs. This contribution concerns the results shown in Figs. 5.2.3 and 5.5. Dr. Bodrikov also collaborated to part II of my thesis by coating coverslips with the different RTN4b substrates and culturing fish RGCs/explants (as described above) and PC12 cells for the outgrowth and spreading assays shown in chapter 5.8 (Figs. 5.8.1.1, 5.8.1.2, 5.8.2).

- Prof. Dr. E. Málaga-Trillo injected zebrafish embryos in the Thy-1 morpholino-mediated knockdown experiments. He advised me in performing the immunostainings and acquired the microscopy images shown in Figs. 5.1.5.1 and 5.1.5.2.

Danksagung

Bei Frau Prof. Dr. C.A.O. Stürmer bedanke ich mich für die Möglichkeit auf diesem aktuellen und spannenden Gebiet der Neurowissenschaften zu forschen. Vielen Dank für die Einführung in dieses faszinierende Thema und die Bereitstellung der Sachmittel sowie eines Laborplatzes.

Ich möchte mich bei Prof. Dr. M. Gröttrup, Prof. Dr. A. Bürkle, Prof. Dr. E. May und Prof. Dr. D. Legler für die Begutachtung meiner Arbeit und die große Unterstützung als mein Promotionskomitee bedanken. Vielen Dank an Prof. Dr. Elisa May für die fachliche Unterstützung, sowie die Korrektur und Betreuung meiner schriftlichen Arbeit. Herrn Prof. G. Galizia danke ich ebenfalls für die intensive Betreuung und Korrektur beim Verfassen meiner schriftlichen Arbeit.

Prof. Dr. E. Málaga-Trillo möchte ich herzlich für die enorme Zeit und Energie danken, die er in meine Arbeit investierte. Danke für die tatkräftige Unterstützung bei molekularbiologischen, biochemischen und zebrafisch-embryologischen Aufgaben. Vielen Dank für die die zahlreichen effizienten und wissenschaftlichen Diskussionen, die konstruktive, technische und theoretische Führung und das Korrekturlesen.
Vielen Dank an Dr. G. Solis für die Starthilfe im Labor bei Klonierungsarbeiten und biochemischen Fragen.
Dr. V. Bodrikov danke ich für seine Hilfe und Mitarbeit während der Etablierung und Herstellung von primären Zellkulturen von Zebrafisch- und Mausneuronen. Die zahlreichen Diskussionen waren stets hilfreich und konstruktiv.
Herzlichen Dank an Ulrike Binkle und Marianne Wiechers für die technische Unterstützung im Labor und bei der Herstellung der Zebrafisch-Antikörper. Vielen Dank an Anette-Yvonne Loos für die Pflege und Bereitstellung der Zebrafische.

Bei Dr. A. Matuszak möchte ich mich ganz herzlich für den herzlichen Beistand und die intensive Begleitung bedanken. Herzlichen Dank an die Mitarbeiter des Referats für Gleichstellung und Familienförderung, Frau Marion Wölki und Frau Tanja Edelhäußer, für die finanzielle Unterstützung.

Herzlichen Dank an Herrn Prof. Dr. G. Maret für den großen Einsatz und die außerordentlichen Bemühungen als Ombudsmann.

Bei meinen lieben Kollegen Nikola, Franziska, Emily, Yvonne, Alejo, Gonzalo, Vsevolod und Ed möchte ich mich für die schöne gemeinsame Zeit in Konstanz bedanken.

Zuletzt möchte ich noch meine große Dankbarkeit gegenüber meiner Familie ausdrücken, die mich immer ermutigt und unterstützt hat und stets für mich da war, wenn ich tatkräftige Hilfe gebraucht, oder Rat gesucht habe.